Loughborough University

Enhanced Electrochromic Performance of Nickel Oxide-Based Ceramic Precursor Films

By

Muhammad Z Sialvi

A Doctoral Thesis

Submitted in Partial Fulfilment of the Requirements

for the Award of

Doctor of Philosophy

of Loughborough University.

Contents

Acknowledgments

Abstract

An electrochromic (EC) material is able to change colour under the influence of an electric potential. The development of energy efficient "smart windows" for architectural applications is at present the subject of intense research for both economic and environmental reasons. Thus there is now a considerable research effort to develop smart windows with natural colour switching properties, i.e. shades of grey. In this regard, a promising metal oxide with a brown-black anodic colouring state is NiO or 'hydrated nickel oxide' (also called nickel 'hydroxide', $Ni(OH)_2$). The present work outlines the preparation and optimisation of EC nickel oxide-based ceramic precursor films onto various conducting substrates towards smart window applications.

The literature review chapter outlines the different methods used for generating ceramic materials, a review of electrochromism and history of nickel oxide-based EC materials are also provided. Thins films have been deposited by an electrochemical cathodic deposition and by aerosol assisted chemical vapour deposition (AACVD) technique.

For hydrated NiO films prepared by electrochemical cathodic deposition, various deposition factors at small-scale area (30 x 7 mm) have been investigated in order to optimise the films' properties towards EC applications. With deposition on fluorine-doped tin oxide (SnO_2:F, FTO) on glass, use of nickel nitrate (0.01 mol dm^{-3}) solution at an applied current of -0.2 mA (-0.1 mA cm^{-2}) for 800 s was optimal for preparing uniform deposits with a porous interconnecting flake-like structure, which is generally regarded as favourable for the intercalation/deintercalation of hydroxide ions during redox cycling. The as-deposited hydrated NiO films showed excellent transmittance modulation ($\Delta\%T$ = 83.2 at 432 nm), with average colouration efficiency (CE) of 29.6 $cm^2 C^{-1}$ and low response times. However, after 50 voltammetric cycles, the cycle life was found to fade by 17.2% from charge measurements, and 28.8 % from *in-situ* transmittance spectra measurements.

In an attempt to prepare films with improved durability, AACVD has been used for the first time in the preparation of thin-film EC nickel(II) oxide (NiO). The as-deposited

films were confirmed to be cubic NiO from analysis of powder X-ray diffraction data, with an optical band gap that decreased from 3.61 to 3.48 eV with an increase in film thickness (in the range 330–820 nm). The EC properties of the films were investigated as a function of film thickness, following 50, 100 and 500 conditioning oxidative voltammetric cycles in aqueous KOH (0.1 mol dm^{-3}). Light modulation of the films increased with the number of conditioning cycles. EC response times were < 10 s and generally longer for the colouration than the bleaching process. The films showed excellent stability when tested for up to 10000 colour/bleach cycles.

Using a calculation method based on the integration of experimental spectral power distributions derived from *in-situ* visible region spectra over the CIE 1931 colour-matching functions, the colour stimuli of the NiO-based films, and the changes that take place on reversibly switching between the 'bleached' and coloured forms have been calculated. Films prepared by both deposition techniques gave positive a^* and b^* values to produce orange. However, in combination with low L^* values, the films were perceived as brown-grey.

Hydrated NiO prepared via electrochemical cathodic deposition suffers from two well-known limitations; firstly, it shows catalytic properties towards the oxygen evolution reaction (OER), which is a process very close to the Ni(II)/Ni(III) redox process. Secondly, hydrated NiO shows poor cycling durability in alkaline solution. The co-deposition of single or bimetallic additives is an effective way to overcome these problems. Electrochemical studies revealed that the combination of cobalt (10%) with lanthanum (5%) was found to be the optimal composition for preparing hydrated NiO films with improved film durability.

Finally, the emphasis of this work was on scale-up of deposition. Therefore, optimised deposition conditions from small scale (3.0 x 0.7 cm) have been used to successfully deposit films on two different sized large-area (10 x 7.5 and 30 x 30 cm) conducting substrates.

List of symbols, abbreviations and acronyms

$\%Y_L$	percentage luminance
A	ampere and the rate constant for nucleation
at.%	atomic percentage
c	speed of light
E	potential
E_O	anodic peak potential
E_R	cathodic peal potential
h	Planck constant
hv	photon energy
K_{sp}	solubility product constant
N(t)	number density
N_0	the total number of sites where nuclei can form
Q	charge density
q_f	Faradaic charge density
R_a	surface roughness average
T	temperature
t	time
T_b	transmittance of 'bleached' form
t_b	switching times for 'bleaching'
T_c	transmittance of coloured form
t_c	switching times for colouration
T_s	solar transmittance
v	frequency
V	voltage
Wt%	weight percentage
x	chromaticity coordinate
y	chromaticity coordinate
$\Delta\%T$	change in transmittance between the 'bleached' and coloured forms
ΔA	change in absorbance
η	colouration efficiency
λ	wavelength (nanometres, nm)

λ_d	dominant wavelength
λ_{max}	wavelength of the maximum of the absorption band, (nanometres, nm)
$\Omega / \square^{-1}$	ohms per square
τ	response time

AACVD	aerosol assisted chemical vapour deposition
Abs	absorbance
AFM	atomic force microscopy
Ag/Ag$^+$	silver wire pseudo reference electrode
BASi	Bio Analytical Systems Inc
CE	colouration efficiency (centimetres square per coulomb, $cm^2\ C^{-1}$)
CE	counter electrode
CIE	Commission Internationale de l'Eclairage
CR	contrast ratio
CVD	chemical vapour deposition
CVs	cyclic voltammograms
EC	electrochromic
ECD	electrochromic device
ED	electroless deposition
EDS	energy dispersive X-ray spectroscopy elemental analysis
EQCN	electrochemical quartz crystal nanobalance
FEGSEM	high resolution field emission gun scanning electron microscope
FTO	Fluorine-doped tin oxide (SnO_2:F)
HER	hydrogen evolution reaction
ICDD PDF	International Centre for Diffraction Data Powder Diffraction File
ITO	Tin-doped indium oxide (In_2O_3(Sn))
LbL	electrostatic layer-by-layer assembly
NiO	hydrated nickel(II) oxide
OER	oxygen evolution reaction
PAH	poly(allylamine hydrochloride)
PEDOT:PSS	poly(3,4-ethylenedioxythiophene) doped with poly(styrenesulfonate)
RE	reference electrode
SCE	saturated calomel electrode. The potential is 242 mV vs. the standard hydrogen electrode. The electrolyte is potassium chloride (saturated)

SEM	scanning electron microscope
TA	thiazine compound
TCO	transparent conducting oxide
UV-vis	ultraviolet-visible
VDUs	visual-display units
WE	working electrode
XRD	x-ray diffraction

1. Introduction

In his 1961 paper,[1] Platt stated that "theoretical considerations suggest that the absorption and emission spectra of certain dyes may be shifted by hundreds of angstroms upon application of a strong electric field". He suggested that this effect could "be called "electrochromism" in analogy to "thermochromism" and "photochromism" which describe changes of colour produced by heat and light". Although this was the first use of the term "electrochromism", the effect Platt described is quite different to the modern definition given by Monk, Mortimer and Rosseinsky,[2] as a "a change, evocation, or bleaching, of colour as effected by an electron-transfer (redox) process or by sufficient electric potential". In order for a material to have electrochromic (EC) properties, it requires the generation of different visible region electronic absorption bands on switching between redox states.[3] Colour change associated with EC materials is commonly between a transparent ('bleached') state and a coloured state, or between two coloured states. In cases where more than two redox states are electrochemically available the EC material may exhibit several colours and be termed polyelectrochromic.[4]

The major driving force for innovation in EC materials falls within two broad, overlapping categories according to the mode of operation: electrochromic devices (ECDs) operating by transmission (smart windows) or by reflection (mirrors). Proposed applications of EC materials include optical information and storage, anti-glare car rear-view mirrors, sunglasses and protective eyewear for the military. From these applications, probably the most significant success has been that of Gentex Corporation's self-darkening rear-view mirrors now operating in several million cars.[5] More recently, they have been able to advance the technology towards windows for passenger aircraft (discussed in chapter 2, section 8.3). EC materials for smart windows and other applications are judged on specific key parameters, as potential materials for commercial applications. These include; materials with a high contrast ratio, colouration efficiency, (absorbance change/charge injected per unit area), cycle life, response time and write-erase efficiency (% of originally formed colouration that may be subsequently electro-bleached).

1. Introduction

A simple two-electrode ECD is shown in figure 1.1. An ECD is essentially a rechargeable battery in which a suitable solid or liquid electrolyte (ion conductor) separates the EC material from a charge balancing counter electrode. The process of charging and discharging the electrochemical cell with an applied potential of a few volts results in the EC material changing colour and after the resulting pulse of current has decayed and the colour change has been effected, the new redox state persists, with little or no input of power, in the so-called 'memory effect'. The EC electrode, in both the reflective and transmission modes consists of a glass or plastic slide coated with an electrically conducting film such as tin-doped indium oxide (ITO) on one side, onto which a primary EC material (a typical example being tungsten oxide (WO_3)) is deposited. On the other side of the ion conductor, a film acting as a ion storage, or ideally a secondary EC material (a typical example being nickel oxide (NiO)) with complementary EC properties to those of the primary EC material is deposited onto a second electrically conducting film to complete the basic features of an operating ECD. For applications that are designed to operate in the reflective mode, the counter electrode can be of any material with a suitable reversible redox reaction. On the other hand, for variable light transmission devices (smart windows) the counter electrode substrate must also be transparent, i.e. mostly ITO, with the chemical species being either colourless in both its redox forms or EC in a complementary mode to the primary EC material. In any case, the most important component or the heart of the device is often the primary EC material and the aim of this work will be to prepare and optimise EC hydrated NiO as a potential primary EC material towards smart window applications.
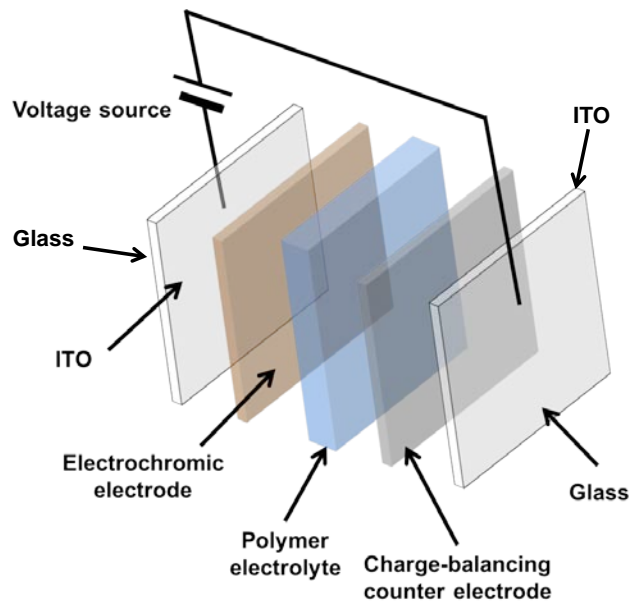
Figure 1.1. Schematic diagram showing different layers of a solid-state ECD suitable for a transmissive light-modulation application.

1.1. Smart windows

A large portion of the world's energy is used for heating, cooling and lighting of buildings. The US alone spends 25.3 billion dollars a year on air conditioning (U.S. energy information administration).[6] A major reason for such high expenditure is that windows allow a lot of solar energy to enter the building as visible light and invisible infrared radiation. In order to combat this problem, air conditioning is used to make the indoor working environment more comfortable. In recent years, a new class of windows has received a lot of attention as a means to achieve energy efficiency in buildings. Dynamic tintable or so-called smart windows are able to change transmittance so light is only let in when someone is present in the room. When the room is empty the coloured form of the device can preclude much solar radiation. Therefore, in relation to sustainability needs and minimising the negative environmental impact, smart window technology may lead to drastic reduction in energy consumption of highly glazed buildings by reducing cooling loads, heating loads and the demand for electric lighting,[7] as well as improving indoor comfort due to less glare and thermal discomfort.[8]

The development of smart windows for architectural applications is at present the subject of intense research, as it's become evident that the appeal of smart windows is both economic and environmental. Thus there is now a considerable research effort to develop smart windows with natural colour switching properties, i.e. shades of grey. In this regard, a promising metal oxide with a brown-black anodic colouring state is NiO or 'hydrated nickel oxide' (also called nickel 'hydroxide', $Ni(OH)_2$). Ceramic precursor films based on NiO combine a reasonable cost with excellent EC properties. However, the choice of preparative routes and deposition parameters are key to obtaining films with desired morphologies and engineering properties.

1.2. Thin film formation

The main focus of this thesis is on the precipitation of NiO-based ceramic materials onto transparent conducting substrates for EC smart window applications. Two different deposition techniques will have been used to immobilise the films. Firstly, hydrated NiO thin films were deposited by electrochemical cathodic deposition, in which nickel nitrate solution is used to grow the films galvanostatically. Precipitation takes place because of the increase of interfacial pH, due to the electrochemical reduction of NO_3^- anions to generate OH^- (equation 1.1 and 1.2). Due to this chemical reaction at the electrode/electrolyte interface the formation of sufficient (or excess) OH^- ions occur. As more OH^- is electrogenerated, and the pH increases, the amount of hydrated NiO species present at the electrode will exceed its solubility limits and precipitation will occur.

$NO_3^- + 7\ H_2O + 8e^- \rightarrow NH_4^+ + 10\ OH^-$ $\qquad E^o = -0.12$ V (SHE) $\qquad\qquad$ (1.1)

$2\ OH^- + Ni^{2+} \rightarrow Ni(OH)_2$ $\qquad\qquad\qquad\qquad\qquad\qquad\qquad\qquad\qquad\qquad\quad$ (1.2)
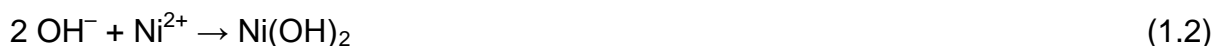
Secondly, porous NiO films have been prepared using an aerosol assisted chemical vapour deposition (AACVD) method. The AACVD method involves the atomisation of precursor solution into fine aerosol droplets. Subsequently, the droplets are directed towards a heated zone, where the solvent is rapidly evaporated, and the chemical precursors undergo decomposition and /or chemical reactions near or on a heated conducting substrate to form the desired film.[9]

1.3. Aims

The first aim of this work was the immobilisation of EC NiO-based thin films onto transparent conducting substrates electrochemically and by AACVD methods. For the films prepared by an electrochemical cathodic deposition, the effect of deposition conditions such as deposition current, time of deposition, concentration of nickel nitrate and the use of different transparent conducting substrates was investigated in order to optimise the deposition of EC hydrated NiO. For the AACVD films, the effect of deposition time and continuous voltammetric cycling in aqueous KOH (0.1 mol dm^{-3}) were investigated with the aim of enhancing the films' EC properties. The second aim was to characterise the films' EC performance parameters such as colouration efficiency, cycle life and response times. Furthermore, the *in-situ* visible region spectra were also used to generate chromaticity data from an earlier established Microsoft® Excel® spreadsheet[10] for the accurate calculation of CIE (Commission Internationale de l'Eclairage)[11] 1931 *xy* chromaticity coordinates and luminance data.

The third aim was to enhance the already promising EC properties of the hydrated NiO films by incorporating other metals into the active material. The effects of additives on the chromaticity data were also investigated.

Finally, the emphasis of this work was on scale-up of deposition. Therefore, optimised deposition conditions from small scale (5 x 0.7 cm) were used to deposit films on two different large scale (10 x 7.5 and 30 x 30 cm) conducting substrates towards smart window applications.

1.4. References

[1]   Platt, J. R. Electrochromism, a possible change of color producible in dyes by an electric field. *J. Chem. Phys.*, **34**, 1961, 862-3.

[2]   Monk, P. M. S., Mortimer, R. J. and Rosseinsky, D. R. *Electrochromism and Electrochromic Devices*, Cambridge Univ Press, Cambridge, 2007.

1. Introduction

[3]   Monk, P. M. S., Mortimer, R. J. and Rosseinsky, D. R. *Electrochromism: Fundamentals and Applications*, VCH, Weinheim, 1995.

[4]   Mortimer, R. J. Electrochromic materials. *Chem. Soc. Rev.*, **26**, 1997, 147-56.

[5]   Byker, H. J., Gentex Corporation. Single-compartment, self-erasing, solution-phase electrochromic devices, solution for use therein and uses thereof. US Patent 0,240,226, 1996.

[6]   http://www.eia.gov/emeu/recs/recs2005/c&e/detailed_tables2005c&e.html. Table AC4. Total expenditures for air-conditioning by equipment type, 2005 (accessed 25 April 2013).

[7]   Baetens, R., Jelle, B. P. and Gustavsen, A. Properties, requirements and possibilities of smart windows for dynamic daylight and solar energy control in buildings: A state-of-the-art review. *Sol. Energy Mater. Sol. Cells*,. **94**, 2010, 87-105.

[8]   Niklasson, G. A. and Granqvist, C. G. Electrochromics for smart windows: thin films of tungsten oxide and nickel oxide, and devices based on these. *J. Mater. Chem.*, **17**, 2007, 127-56.

[9]   Hou, X. and Choy, K. L. Processing and applications of aerosol-assisted chemical vapor deposition. *Chem. Vap. Deposition.*, **12**, 2006, 583-96.

[10]   Mortimer, R. J., Varley, T. S. Quantification of colour stimuli through the calculation of CIE chromaticity coordinates and luminance data for application to *in situ* colorimetry studies of electrochromic materials, *Displays*, **32**, 2011, 35-44.

[11]   Wyszecki, G. and Stiles, W. S. *Color Science: Concepts and Methods, Quantitative Data and Formulae*, 2nd ed., John Wiley and Sons, New York, 1982.

2. Literature review

In this chapter a review of relevant literature is undertaken. Firstly, a review of the different ceramic processing and fabrication methods will be outlined. A brief history of electrochromism, electrode reaction and the generation of colour will then be given, followed by a more detailed account of the properties/parameters of electrochromic (EC) materials and their commercial application. Finally, literature on NiO-based films as an EC material will be surveyed.

2.1. Ceramics

Ceramics have been the subject of many studies covering a wide range of materials. In recent times, particular attempts have been made to divide ceramics into two categories: traditional ceramics and advanced ceramics. Within the last 50 years interest has been focused on advanced ceramics, which are often high purity oxides with tailored morphology and stoichiometry, that are employed in areas of engineering, electronics and medicine. This is evident by the increasing number of journals, publications and conferences aimed at this particular type of material. The increasing use of ceramics in these areas has resulted in many studies to improve the properties and reliability of such materials. Within these studies it has been identified that improvements can be achieved by paying particular attention to the fabrication process. A comprehensive review of the different ceramic processing and fabrication methods has been written by Rahaman.[1]

2.2. Importance of ceramics

Traditional ceramics have been developed and used since the time of the earliest civilisation. The earliest ceramics were pottery, and clay based refractories; including kiln linings.

Over the years, ceramics have been used for architectural applications such as ceramic bricks, cements and concrete. More recently, much of the focus has shifted towards a new class of ceramics termed advanced ceramics.[2,3] Examples include coatings for corrosion protection,[4] electronic devices such as semiconductors and resistors. Other applications include gas and humidity sensors[5-8] bioceramics used for artificial hip joints, jaw bone reconstruction and dental implants. These are only a few of the many applications for ceramics and due to the increasing usage of such materials there are still enormous demands for improving their engineering properties. The desired properties required for a particular application can be achieved through controlling the microstructures of the ceramic body at the processing stage.

2.3. Ceramic fabrication processes

Figure 2.1 summaries the many different methods for generating ceramic materials. Each method will fabricate its desired ceramic product by controlling the degree of purity and homogeneity of the material. All fabrication methods use suitable starting materials for the production of the desired shape and microstructures such as films and fibres.

The following review of the different fabrication processes to date has been separated into three categories according to the use of the starting material: gaseous, liquid or solid phases. These methods will be compared with alternative processes such as electroless deposition, hydrothermal methods and electrochemical deposition techniques. The emphasis will be on the advantages and disadvantages of each process, as well as showing how well suited each method is for producing thin ceramic precursor films for EC applications.

Electrochemical techniques

- Reactions which consume H^+ ions
  $H^+ + e^- \rightarrow H_{ads}$ or H_{abs}
- Electrolysis of water
  $2H_2O + 2e^- \rightarrow H_2 + 2OH^-$
- Nitrate reduction reaction
  $NO_3^- + 7H_2O + 8e^- \rightarrow NH_4^+ + 10\ OH^-$
- Synthesis takes place at the electrode-electrolyte interface by applying a current.
- Quick method with good control of film microstructure and materials immobilised directly onto substrate.

Sol-gel process

- Two processes: using a sol produces particulate gel, using a solution produces polymeric gel.
- Can produce high purity materials.
- Fairly expensive starting materials and time consuming process.

Fabrication from powders

- Assembly of fine divided solids (powders) by applying heat.
- Two processes: melt casting and sintering of powders.
- Produces high purity materials with great uniformity.
- Defects within samples may be formed in processing stage, which affects the engineering properties.

Ceramic fabrication processes

Vapour deposition

- Chemical vapour deposition (CVD).
- Substrate exposed to volatile precursor(s), which react and/or decompose to form desired products.
- Can coat large areas (mass production).
- Very low deposition rates.

Electrostatic layer-by-layer technique

- Assembly through electrostatic interactions.
- Growth of different charged species (cationic and anionic) leads to formation of multilayer structure.
- Easy and inexpensive process, which allows the incorporation of various materials within the film.
- Time consuming process for multilayer formation.

Electroless deposition

- Films produced without the use of counter electrodes or an external power source, however oxidising agent is required.
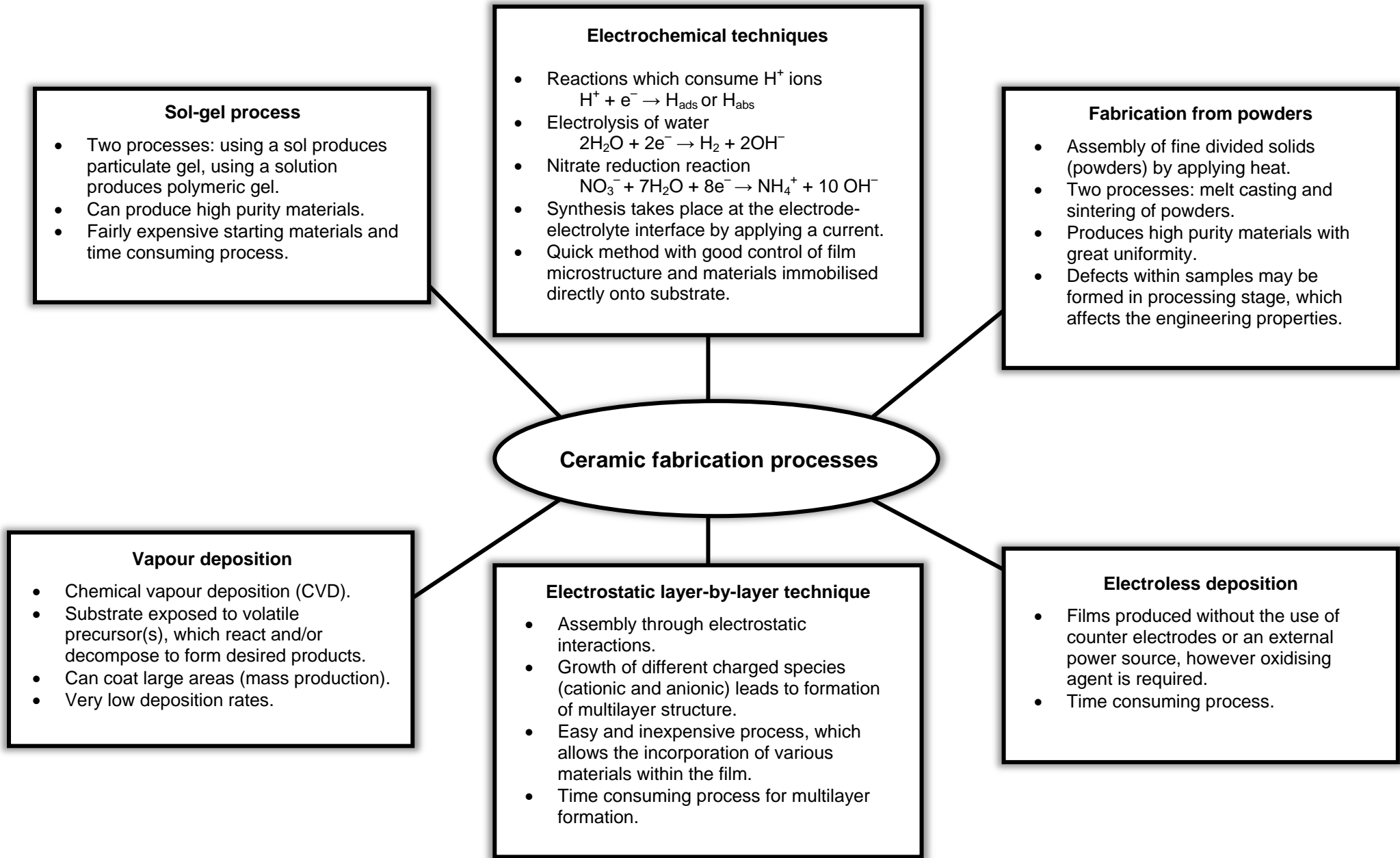- Time consuming process.

Figure 2.1. Summary of the different fabrication processes for ceramic materials.

9

2.3.1. Gas-phase reactions

The most well-known and most widely used gas-phase reaction method is chemical vapour deposition (CVD). It is an established process by which reactive molecules in the gas phase are transported to a surface at which they chemically react to form solid films.[9,10] Materials deposited using this process include metals, ceramics, and semiconductors used for many applications such as coatings, films for electronic devices and optical fibres. The advantages of this technique include the ability to deposit adherent films onto large and complicated shapes/areas for mass production, with thickness from as little as 0.1 μm up to several centimetres can be achieved by prolonging the deposition process. The desired morphology of the deposit can be achieved by careful control of process variables. These variables include the flow rate of the reactant gases, the nature of the flow rate of any carrier gases, the pressure in the reaction vessel, and the temperature of the substrate. Disadvantages include very low deposition rates, development of microstructures with large columnar grains, which limits the formation of thin films and coatings, and the use of high temperatures.

The EC properties of NiO thin films prepared by CVD have been investigated by Maruyama and Arai.[11] In this study, transparent NiO films were deposited onto fluorine doped tin oxide (FTO) conductive substrate using nickel acetylacetonate as the precursor and air as the carrier gas. Films produced showed good adhesion to the substrate with large changes in optical transmittance. Colouration efficiency (CE) was also calculated to show the amount of electrochrome which may be coloured by one absorbance unit per unit charge and a value of 44 cm^2/C was achieved.

2.3.2. Liquid precursor methods

Liquid precursor methods convert solutions of metal compounds into a solid body. An example of this is the sol-gel process, where a solution of metal compounds or a suspension of very fine particles in a liquid is converted into a highly viscous mass such as simple or complex oxides.[12,13] There are two different sol-gel processes (figure 2.2), depending on if a sol or a solution is used. Using a sol produces a

network of gelled material consisting of colloidal particles. A solution produces a network of polymer chains of metal-organic compounds (such as metal alkoxides) by hydrolysis and condensation reactions. There are many advantages of using sol-gel processes, such as use of low temperatures, and production of materials with high purity and good chemical homogeneity. However, the disadvantages include fairly expensive starting materials, time consuming process and problems with drying the material.
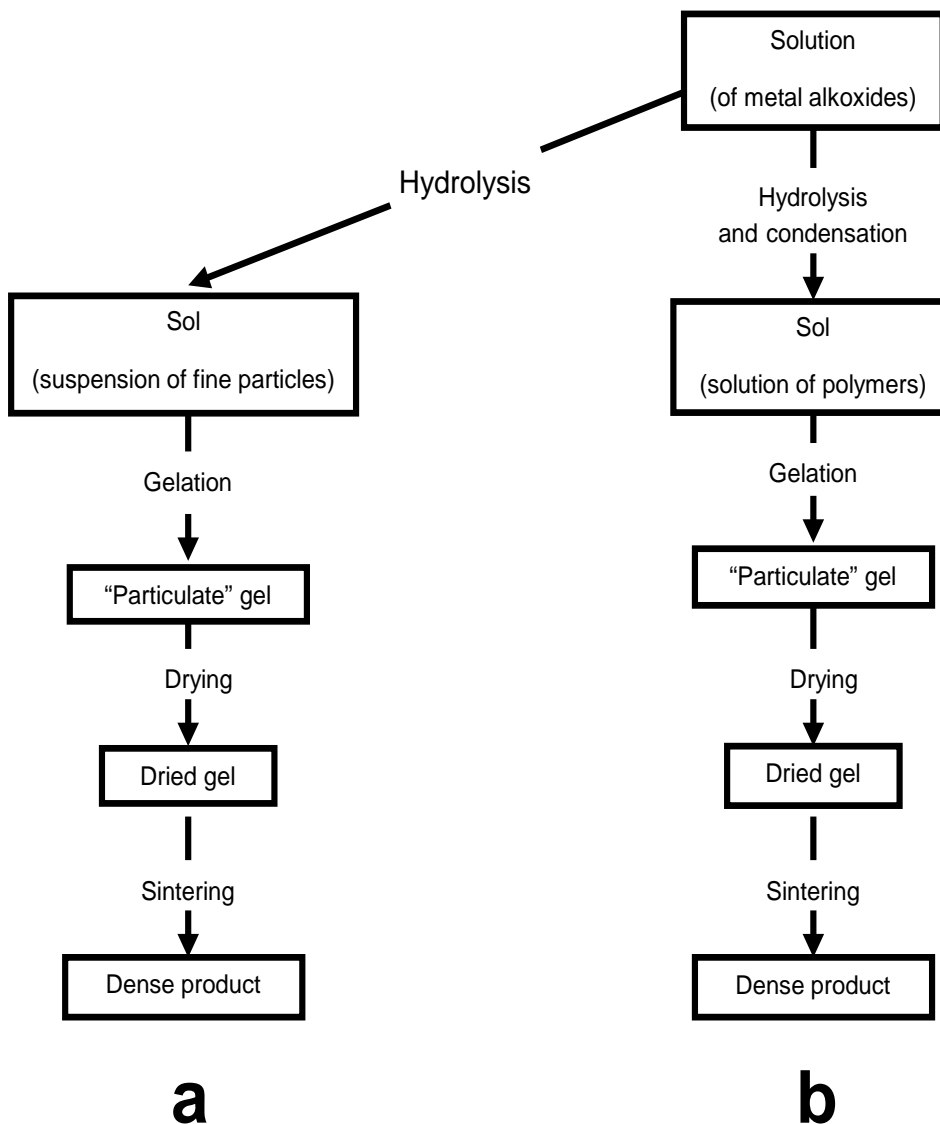

Figure 2.2. Basic flowcharts for sol-gel processing using (a) a suspension of fine particles and (b) a solution. Diagram redrawn from.[1]

Sharma *et al.*[14] used sol-gel methods to investigate the EC properties of hydrated NiO. The outcome of this work was that the preparation of dip-coated films produced by the sol-gel method was strongly dependent on the reaction parameters, e.g. solvent, polymer and heat treatment. Film thickness, as well as the EC effect decreased with increasing temperature and heating time. This method for producing hydrated NiO was a time consuming process, as it took more than four hours to produce the gel, which then required a further step to immobilise the ceramic material onto conducting SnO_2 coated glass for analysis.

2.3.3. Fabrication from powders

This process involves the assembly of finely divided solids (powders) by applying heat. There are two fabrication methods using powders: melt casting and sintering of compacted powders.

Melt casting is the simplest of the two methods and involves melting a mixture of powders, which is followed by several methods, including casting, rolling, pressing, blowing, and spinning in order to achieve the desired shape. However, this method suffers from uncontrolled grain growth, which effects the properties of the ceramic (e.g. low strength). It is also very difficult to obtain a melt as ceramics often have high melting points or even decompose prior to melting. Therefore, for these reasons melt casting is limited to the fabrication of glasses.

Sintering of compacted powders is a route which is more suited for the production of polycrystalline ceramics. This process involves the consolidation of a mass of fine particles (i.e. a powder) to form a porous, shaped article (also referred to as a green body or powder compact), which is then sintered (i.e. heated) to produce a dense product (figure 2.3).[1]

This method can suffer from defects within the sample in the processing stage, which is further enhanced in the sintering stage. Consequently, affecting the microstructure (e.g. density, grain size and producing cracks), which affects the engineering

properties of the material. Using this method to produce EC films could possibly affect the uniformity and the thickness of the film.
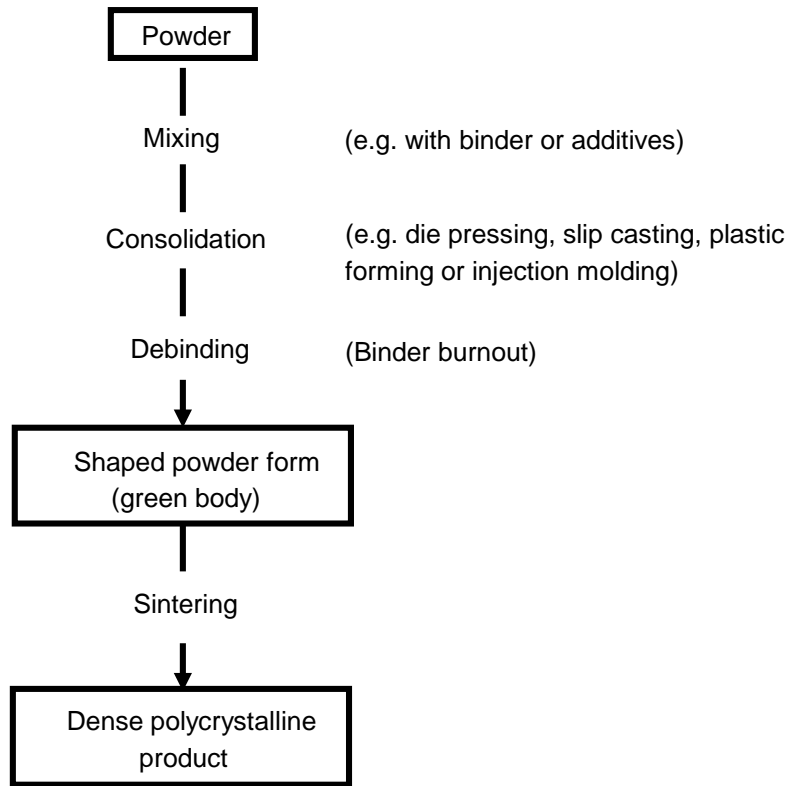
Figure 2.3. Basic flowcharts for the production of polycrystalline ceramics by sintering of consolidated powders. Diagram redrawn from.[1]

2.3.4. Electroless deposition (ED)

It is well known that electroless deposition (ED) of ceramic thin films evolved from electroless plating of thin metal films. A general review of ED as well as other techniques using low temperature aqueous solutions was written by Niesen and De Guire[15]. These authors outlined three characteristics which distinguish electroless plating:

- A change in the oxidation state of the metal cation (dissolved in aqueous solution) to an insoluble state (which in electroless plating is the neutral metallic state);

- The participation of the deposition surface (the substrate and, later, the film) in the redox process, usually as a path for transfer of electrons from the site of an oxidation to the site of a reduction;
- The need for catalysis to initiate and sustain the process.

It was also noted that films are produced without the use of a counter electrode nor connections to an external electrical power source. However, in order for a electrochemical reaction to take place a suitable oxidising agent must be present.

Kamath *et al.* used an ED method for hydrated NiO synthesis through the complexation-precipitation route[16]. These authors used a Ni(NO$_3$)$_2$ (0.1 mol dm^{-3}) solution which was added to tri-sodium citrate and KOH (0.1 mol dm^{-3}) was added drop wise to raise the pH to 11.6. This produced a precipitate over a period of one week. Cyclic voltammetry studies showed that the electroless hydrated NiO showed a higher coulombic efficiency (>90%), a more anodic reversible potential and a higher degree of reversibility as compared to conventionally prepared electrosynthesised hydrated NiO. Disadvantage of using this method is the amount of time taken to produce the material. The experimental details that it took 18h before a voluminous floating precipitate was produced. This was further left for a week until the precipitate settled and used for analysis.

2.3.5. Hydrothermal methods

Hydrothermal methods are suited to the manufacture of ceramic powders and involve heating reactants such as metal salts, oxides and hydroxides in water at temperatures and pressures up to around 300 ⁰C and 100 MPa[3]. This can produce sub-micron ceramic particulates of controlled size and shape.

Insoluble metal hydroxide ceramic precursor can be precipitated by controlled addition of hydroxyl species from aqueous metal salt solutions (equation 2.1).

$$M^{z+}(aq) + zOH^-(aq) \leftrightarrow M(OH)_z(s) \tag{2.1}$$

On the other hand, at elevated temperatures hydrolysis leads to the deprotonation of bound water, which generates hydroxide ligands (equation 2.2).

$$[M(H_2O)_x]^{z+} \rightarrow [M(H_2O)_{x-y}(OH)_y]^{(z-y)+} + yH^+ \quad\quad\quad (2.2)$$
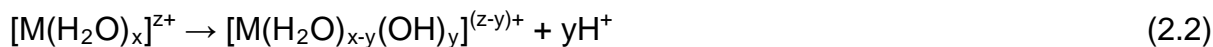
For both methods, variation of temperature, pressure and solution concentration can control particle size and morphology of the ceramic precursor. Therefore, producing single and homogeneous mixed oxide powders from relatively cheap starting materials. A disadvantage of using this method for generating films for EC applications is that in order to electrochemically analyse the film it must be immobilised onto a suitable substrate. As the material produced is in powder form it will require a further step to achieve this.

A hydrothermal method was used by Zhang *et al.* to synthesise hydrated NiO nanocrystalline thin films for the application as a catalyst precursor[17]. They produced hexagonal β-phase hydrated NiO sheets with a mean diameter of about 80 nm, and a thickness of 15 nm. For this study the hydrothermal temperature was an important influence on the growth and the morphology of the film. The optimum hydrothermal conditions for producing thin films were found to be 170 °C for two hours. In comparison to other methods, they found the hydrothermal method ideal for processing very fine nanocrystalline thin films with high purity, controlled stoichiometry, high quality, narrow particle size distribution, controlled morphology, and high crystallinity. However, the extra step needed to immobilise the film onto the substrate by heating in a autoclave between 100-300°C and 1.8-11 MPa pressure for several hours is a major disadvantage.

2.3.6. Electrochemical routes

Electrosynthetic techniques have been used for many decades for the synthesis of ceramic thin films and coatings, nanoparticulate materials, and metastable phases. A comprehensive review of the different electrosynthetic techniques has been written by Therese *et al.*[18]

2. Literature review

Electrochemical synthesis takes place at the electrode-electrolyte interface by applying a electric current between two or more electrodes in an electrolyte solution. Experiments carried out using electrochemical routes are simple, quick and the instruments are inexpensive and readily available.

The electrodeposition of metal hydroxide has been carried out for a number of years. For example in 1974 Pickett[19] carried out work for the electro-precipitation of hydrated NiO on the surface of a nickel plate, a process now known as the Air Force. Later research by Pickett and Maloy[20] further developed this process by co-precipitating with cobalt. Their method involved applying a constant current density which was sufficient to decompose the supporting electrolyte to liberate hydroxide ions. The hydroxide ions reacted with Ni^{2+} to precipitate hydrated NiO within the pores of the nickel plate. Co-precipitation with cobalt increased the potential range thereby allowing charging to occur at less positive potentials and minimising oxygen evolution.

There are various electrosynthetic techniques employed for the synthesis of ceramic materials. These include electromigration of reactant species and electrolysis of fused salts for producing polycrystalline powders and single crystals for the applications of battery electrodes. Electrogeneration of base by cathodic reduction and anodic oxidation are techniques used for producing coatings, films and powders for the synthesis of electrode materials for secondary cells, fabrication of hydroxide films and synthesis of compounds with a high oxidation state. Finally, there is pulse current synthesis used for the production of layer-by-layer films and coatings of composites and solid solutions. Some of these techniques are summarised below, in more detail.
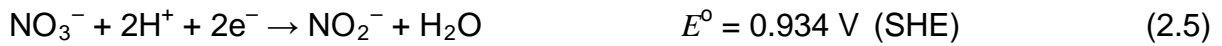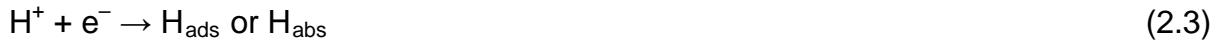
2.3.6.1.   Electrogeneration of Base

Electrogeneration of base is a technique widely used for ceramic material synthesis. This can be achieved by passing an electric current through a metal salt solution, which causes a pH increase at the electrode-electrolyte interface and depending on the metal deposition potential, may compete with the metal ion reduction reaction to

deposit the metal at the cathode or for more positive potential reactions deposit in the form of a hydroxide. Depending on the potential, choice of anion and the pH of the solution three different reactions may take place.

1) Reactions which consume H^+ ions

$$H^+ + e^- \rightarrow H_{ads} \text{ or } H_{abs} \tag{2.3}$$

$$2H^+ + 2e^- \rightarrow H_2 \qquad\qquad E^o = 0.0 \text{ V (SHE)} \tag{2.4}$$

$$NO_3^- + 2H^+ + 2e^- \rightarrow NO_2^- + H_2O \qquad\qquad E^o = 0.934 \text{ V (SHE)} \tag{2.5}$$

$$NO_3^- + 10H^+ + 8e^- \rightarrow NH_4^+ + 3H_2O \tag{2.6}$$

2) Electrolysis of water

$$2H_2O + 2e^- \rightarrow H_2 + 2OH^- \qquad\qquad E^o = -0.828 \text{ V (SHE)} \tag{2.7}$$

3) Anion (nitrate reduction reactions)

$$NO_3^- + H_2O + 2e^- \rightarrow NO^- + 2OH^- \qquad\qquad E^o = 0.01 \text{ V (SHE)} \tag{2.8}$$

Out of the three, electrolysis of water is the most widely used reaction for the electrogeneration of base. Mitchell *et al.*[6] used electrolysis of aqueous non-dischargeable metal salt solutions for the generation of aluminium hydroxide films at a hydrogen sorbing palladium electrode for the manufacture of humidity sensing materials.

A nitrate reduction reaction to generate base was used by Monk *et al.*[21-23] to deposit mixed metal oxides for EC applications. The oxides in these studies included CoO, FeO, MoO_3, NiO and WO_3. Mixed metal oxides included cobalt (doped with Cr, Fe, Mn, Ni, W or Zn oxides). Their studies showed that by co-depositing with other oxides they were able to tune the EC colour formed for a particular metal oxide, as well as improving the ionic conductivity by increasing the chemical diffusion coefficient.

2.3.6.2. Anodic oxidation

For this method, a metal ion in a lower oxidation state is oxidised to a higher oxidation state anodically by choosing the pH of the electrolyte in such a way that the lower oxidation state is stable whereas the higher oxidation state readily under goes hydrolysis. This results in the formation of a metal oxide or hydroxide. This technique is suited to the synthesis of compounds with metal ions in unusual high oxidation states. Examples include stabilisation of Fe(IV), Co(IV), Ni(IV), or Cu(III). Applications of materials produced using this method include magnetic devices, electrode materials and ECDs. Monk *et al.*[24] used anodic oxidation to deposit films of EC tungsten oxide containing additional metal oxides. They found that co-depositing tungsten oxide with other metal oxides showed different cyclic voltammetry, ac impedance behaviour and uv-vis spectra.

2.3.6.3. Pulse current synthesis

Simultaneous deposition of two metal ions (such as Ni^{2+} and Mn^{2+}) can be achieved by the use of alternating currents. This is possible by the pulsed electrolysis of a mixed metal nitrate solution where the working electrode is alternately polarised anodically then cathodically for a length of time. This can result in the formation of a layer-by-layer composite of hydrated NiO and hydrated MnO or a single mixed single phase solid composition depending on the level of frequency applied.

2.4. History of electrochromism

A more comprehensive review of the history of electrochromism has been presented elsewhere.[25-27] As mentioned previously, Platt first coined the term electrochromism in 1961. However, the process of redox-colouration chemistry dates back to as early as 1815 when Berzelius showed that pure WO_3 (which is pale yellow) changed colour on reduction when warmed under a flow of dry hydrogen gas.[28] A later paper by Wöhler[29] extended this study to a chemical reduction reaction with sodium metal. In 1842 Sir John Frederick William Herschel was the first to introduce the use of

Prussian blue redox–colouration process for photochromic colour change involving electron transfer.[30] Herschel's method 'cyanotype' produced photographs and diagrams by generating Prussian blue $KFe^{III}[Fe^{II}(CN)_6](s)$ from moist paper pre-impregnated with ferric ammonium citrate and potassium ferricyanide, forming yellow Prussian brown $Fe^{3+}[Fe(CN)_6]^{3-}$ or $Fe^{III}[Fe^{III}(CN)_6]$.

Twentieth century developments lead to the first known suggestion of an ECD. A London patent of 1929[31] describes the electrogeneration of molecular iodine from iodide ions. They formed I_2 then effected the chemical oxidation of a dye precursor to form a bright colour change. A year later, Kobosew and Nekrassow[32] demonstrated the first colour change involving the electrochemical reduction of a solid, tungsten trioxide (equation 2.10).

$$WO_3 \text{ (s)} + x(H^+ + e^-) \rightarrow H_xWO_3 \text{ (s)} \tag{2.10}$$
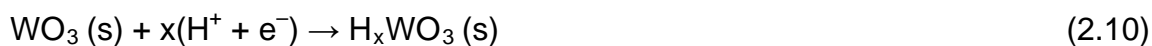
A later paper by Brimm *et al.*[33] extended the work of Kobosew and Nekrassow to effect reversible colour changes, for $Na_x WO_3$ immersed in aqueous acid. The first use of organic viologen for ECD dates back to the early 1970s when a Dutch division of Philips utilised an aqueous organic viologen, heptyl viologen as the bromide salt for commercial applications.[34,35] At much the same time, numerous other authors worked on devices based on heptyl viologens. In 1969, like Philips, Imperial Chemical Industries first analysed the response of heptyl viologen in water but quickly changed to the larger viologen cyanophenyl paraquat, which showed a higher colouration efficiency (η).[36] Barclay's group at Independent Business Machines,[37] and Texas Instruments[38] in Dallas were the other groups investigating devices based on heptyl viologen. However, none of these studies attracted further attention and due to this reason most workers now consider the work of Deb in 1969 as the first suggestion of an ECD. He formed EC colour by applying an electric field of 10^4 V cm^{-1} across a thin film of dry tungsten trioxide deposited on quartz under vacuum. The term 'electrophotography' was used to describe the effect where a film of WO_3 was exposed to open air rather than immersed in ion-containing electrolyte solutions, suggesting that the mobile counter cation might have come from simultaneous ionisation of interstitial and/ or adsorbed water.[39]

A superior EC effect was demonstrated in 1971 by Blanc and Staebler.[40] They applied electrodes to the opposing faces of doped, crystalline $SrTiO_3$ and observed an EC colour move into the crystal from the two electrodes. However, their work required the crystal to be heated to *ca.* 200 °C, which would not be viable for commercial device formation. A year later, Beegle developed a display of WO_3 having identical counter and working electrode, with an intervening opaque layer.[41] Despite the different number of studies into EC materials, most workers nowadays cite Deb's later paper[42] from 1973, as the true birth of EC technology. In recent published work, it is often said that this paper describes the first 'true' ECD, with a film of WO_3 immersed in an ion-containing electrolyte. From here on a surge in published work based on WO_3 indicated its promising EC properties towards device formation. In 1974, Green and Richman[43] in London proposed a system based on WO_3 in which the mobile ion was Ag^+. A year later, Faughnan *et al.*[44] of the RCA Laboratories in Princeton, New Jersey reported WO_3 undergoing reversible EC colour change while immersed in aqueous sulphuric acid. Their work provided detailed analysis of the speed of colour change in terms of Butler-Volmer electrode dynamics, establishing a pioneering model of electro-bleaching[45] and electro-colouration.[46]

In 1978, Mohapatra[47] of the Bell Laboratories in New Jersey was the first to publish work based on the reversible electro-insertion of lithium ions (equation 2.11).

$$WO_3 \text{ (s)} + x(Li^+ \text{ (aq)} + e^-) \rightarrow Li_x WO_3 \text{ (s)}. \qquad (2.11)$$
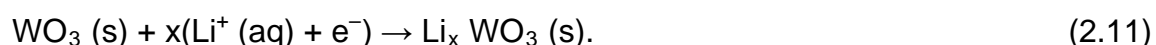
During this period, research into electrochromism of organic material also increased. In 1974, Parker and co-workers[48] showed the preparation of methoxybiphenyl species, the electrogenerated radical cations of which are intensely coloured. In 1979 and 1980, Kaufman and co-workers[49,50] of IBM (in New York) published the first report of an EC polymer comprising an alkyl-chain backbone with pendant electroactive species. In 1979, Diaz and co-workers[51] outlined the first account of an EC conducting polymer, which involved the synthesis of thin-film poly(pyrrole).

2.5. Electrode reaction investigated

The present work describes the role of EC hydrated NiO as an 'electroactive' species which can undergo an electron release, i.e. 'oxidation', (equation 2.12), or electron uptake, i.e. 'reduction', (equation 2.13) in a redox reaction that takes place at an electrode. In most cases, an electrode will consist of a metal or especially in electrochromism, an adequately conductive semiconductor often deposited as a thin film on glass, with external connections, in contact with an electroactive material.

$$Ni(OH)_2 \rightarrow NiOOH + H^+ + e^- \hspace{3cm} (2.12)$$
$$NiOOH + H^+ + e^- \rightarrow Ni(OH)_2 \hspace{3cm} (2.13)$$

An electoactive material may be an atom or ion, a molecule or radical, sometimes multiply bonded in a solid film and for a successful electron transfer to take place it must be in contact with the electrode. It may be in solution – solvated and/or complexed – in which case it must approach sufficiently closely to the electrode substrate and undergo the adjustment that contribute to the (sometimes low) activation energy accompanying electron transfer. In other systems, the electroactive material may be a solid or dispersed within a sold matrix, in which case that proportion of the electrochrome physically in contact with the electrode substrate undergoes the redox reaction most rapidly, the remainder of the electroactive material less so.[25] In the case of EC hydrated NiO, a solid film is deposited onto the surface of the electrode substrate and electron transfer takes place by increasing the anodic potential which reduces the energy barrier for oxidation of Ni(II) to Ni(III). Thus, weakening the OH bond and increasing the mobility of the proton. At anodic oxidation potentials charge transfer takes place and Ni(II) is oxidised to Ni(III), while a proton is released from the OH group. The diffusing proton reacts with OH⁻ ions at the electrode/ electrolyte interface to form water.

2.6. Generation of colour

The particular part of a system that causes colour is termed a chromophore. Colour is observed when chromophores absorb photons from part of the spectrum and the

colour seen is complementary to that absorbed. For example, if a material absorbs red on illumination with white light then the colour reflected or observed is blue. EC materials switch from the bleached to the coloured state by simultaneous ion (usually H^+ or Li^+) and electron injection or ejection. As a result of this injection or ejection, colour centres are formed in the material. Light absorption enables electrons to be promoted between quantised (i.e. wave-mechanically allowed) energy levels, such as the ground and first excited states.[25] The wavelength of light absorbed, λ, is related to the magnitude of the energy gap E between these levels according to the Planck relation (equation 2.14).

$$E = hv = hc / \lambda \qquad\qquad (2.14)$$

Where v is the frequency, h is the Planck constant and c the speed of light in vacuo. The magnitude of E thus relates to the colour since, when λ is the wavelength at the maximum (usually designated as λ_{max}) of the absorption band observed in the spectrum of a chromophore, its position in the spectrum clearly governs the observed colour.[25]

All materials will undergo change of spectra on redox change. This is due to electroactive species comprising different number of electrons before and after electron-transfer reaction, so different redox states necessarily exhibit different spectroscopic transitions and hence will require different energies E for electron promotion between the ground and excited state.[25]

Most EC applications such as displays require materials to be reversible and show a markedly different colour change from one state to the other. This means that the absorption band of one redox state should be in the visible region while the other in the ultraviolet (UV). However, there are cases where EC materials show a colour change for two redox states in the UV or near infrared region and in these cases suitable spectrometry methods are used to identify the spectral change. For NiO-based EC materials the main effect takes place in the UV and VIS spectra, where the colour changes observed are transparent for the reduced form (hydrated NiO) to a neutral brown-grey colour for the oxidised form (NiOOH).

2.7. Electrochromic types and parameters defining their operation

In order for an EC material or ECD to be identified as a potential candidate for the commercial market, their operations are judged using specific properties or parameters. These formulated factors allow comparisons between different devices and materials.

2.7.1. Electrochromic type

As described by Chang *et al.*[52], the type of electrochrome used in an ECD governs the kinetic behaviour demonstrated. There are three types of electrochrome styled as I, II and III. A type I electrochrome is soluble, and remains in solution all times during the redox process. An example of a type I electrochrome is methyl viologen (1,1′-dimethyl-4,4′-bipyridilium - **I)** in water (equation 2.15).

$$MV^{2+}_{(aq)} + e^- \rightarrow MV^{+\bullet}_{(aq)} \qquad\qquad (2.15)$$
colourless   blue

2X⁻

I
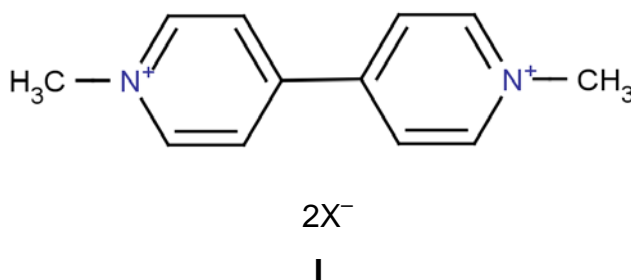
The most common car mirrors manufactured by Gentex operate by type I electrochromism.[53] In the Gentex mirror, an ITO/glass and a reflective metallic electrodes are separated by a solution containing two electrochromes.

Type II electrochromes are soluble in their colourless state but following electron transfer form a coloured solid on the surface of the electrode. A good example of a type II electrochrome is heptyl viologen (1,1′-di-heptyl-4,4′-bipyridilium - **II)**, which is pale yellow in aqueous solution (HV^{2+} dication dibromide) but forms a layer of deeply

coloured radical cation salt on reduction. A two-step process is involved during reduction, first an electron transfer reaction (equation 2.16) and subsequent precipitation (equation 2.17).

$$HV^{2+} + e^- \rightarrow HV^{+\bullet} \tag{2.16}$$

$$HV^{+\bullet} + X^- \rightarrow HV^{+\bullet}\, X^- \tag{2.17}$$

$$2X^-$$

II
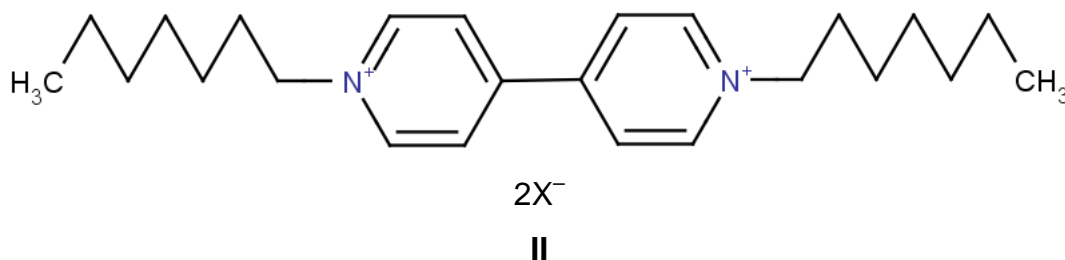
Type III electrochromes are permanently insoluble thin films and are most commonly employed for display purposes. All inorganic electrochromes (including hydrated NiO) are examples of type III electrochromes. Electrically conducting polymers derived from thiophenes,[54] anilines[55] or pyrroles[56] represent type III ECDs with organic electrochromes.

2.7.2. Contrast ratio

The contrast ratio CR is a commonly employed measure denoting the intensity of colour formed electrochemically (equation 2.18).

$$CR = \left(\frac{R_o}{R_x}\right) \tag{2.18}$$

Where R_x is the intensity of light reflected diffusely through the coloured state of a display, and R_o is the intensity reflected similarly but from a non-shiny white card.[57] CR is best quoted at a specific wavelength and is commonly expressed as a ratio such as 7:1. For devices and display applications a high CR value is desirable, a low CR value of less than 3 would be impossible to be observed by eye. For a NiO-based device a CR of 10:1 is quoted by Mathew *et al.*[58] for the cell WO_3|electrolyte|NiO.

2.7.3. Response time τ

Response time is the time required for an ECD to change from its bleached to the coloured state (or vice versa). Quoted values of response time are often unreliable due to the lack of consistency in the reporting of response-time data and in the use of different criteria in determining the value. In some cases, response time may represent the time required for some fraction of the colour (arbitrary or defined) to form, or in other examples it may relate to the time required for an amount of charge (again arbitrary or defined) to be consumed in forming a colour at the working electrode.[25]

EC materials for smart window applications require a slow colour change (response), as rapid changes in the indoor environment may result in workers feeling ill due to the lack of time needed for the eye to accommodate the conditions.[59] For smart windows the time for going between clear and dark states depends on the size of the window, and anything between ten seconds and a few minutes can be regarded as typical. For a WO_3 and NiO-based ECD a response time for the colouration and bleached states is quoted as 180s and 60s respectively by Kullman *et al.*[60]

On the other hand, applications such as display devices are required to show a more rapid response. An example of fast responsive polymers based on poly(3,4-alkylenedioxythiophene) 'PEDOT' (IV) have been investigated by Reynolds and co-workers.[61] These authors showed that polymer films with thickness *ca.* 300 nm could be fully switched between the reduced and oxidised forms in 0.8-2.2 s. Furthermore, an even faster responsive ECD based on the viologen bis(2-phosphonoethyl)-4,4′-bipyridilium (V) was described as 'ultrafast', due to its rapid response time of 250 ms.[35]

2.7.4. Write–erase efficiency

The write-erase efficiency is the fraction (usually expressed as a percentage) of the originally formed colouration which may be subsequently electrobleached. For successful ECDs the efficiency must approach 100%, which is a major test of design

and construction. The write-erase efficiency of type I EC materials will be low, since type I electrochromes are very soluble in water in their dicationic and radical-cation states and time for diffusion to and from the electrode must be accounted for. Type II and III electrochromes do not have this problem, since between the write and erase part of the colouration process the coloured form of the electrochrome is not lost from the electrode by diffusion.[25] The write-erase efficiency of type I aqueous MV electrochromes can be improved by a process called 'derivatisation', where the material is directly attached to the electrode and as a result retarding the rate at which the solution-phase radical-cation product of electron transfer diffuses away from the electrode and into the bulk solution.[62] A second method used to improve this effect is by employing polymeric electrolytes to immobilise the electrochrome to the electrode.[63] A third approach is to use a colourless methoxyfluorenes in acetonitrile[64] solution which precipitates onto the electrode on electron transfer.

2.7.5. Cycle life

Cycle life is an important property for a commercially successful ECD as it is an experimental measure of the durability. The cycle life of an ECD represents the number of write-erase cycles that can be performed before any significant degradation.

Maximising of the cycle life is an important objective and a successful device will typically stipulate a minimum of 100,000 cycles. Good quality stability data will involve cycles greater than τ, known as 'deep' cycles. On the other hand, cycle life measurements less than τ, known as 'shallow' cycles are less valued for devices. Degradation of EC NiO films upon redox cycling was investigated by Zhao *et al.*[65] It was shown by cyclic voltammetry that both anodic and cathodic peak areas decreased as the cycles increased, indicating that the amount of charge injected and extracted during EC reaction was reduced. They concluded that after 4000 cycles the relative capacity of co-deposited NiO with Cu remained over 40%. In another study, Vidotti and Córdoba de Torresi[66] examined the stability of Ni, Co, and Cd(OH)$_2$ nanoparticles immobilised by electrophoretic deposition. Their study showed that

after the electrode was submitted to repetitive EC cycling (colouration and bleaching) for over 1 hour of cycling less than 1% absorbance was lost.

2.7.6. Power consumption

ECDs are known to consume power during write or erase cycles and not between them. This retention of colour is known as the 'memory effect'. For example the intense colour of a sample of viologen radical cation remains undimmed for many months in the absence of a chemical oxidising agent, such as molecular oxygen.[35] However, to date a perfect battery with infinite shelf life has not yet been invented and any ECD (all of which follow battery operation) will eventually fade unless the colour is renewed by further charging.[25] The power consumed is a function of the amount of colour formed and removed at an electrode during the redox process, and usually expressed as charge in relation to another parameter (e.g. contrast ratio). Lee and Joo[67] fabricated an EC material based on Ni-W oxide by a reactive sputtering method. They observed that charge transfer resistance, which has been known to be very high for NiO becomes significantly low with the addition of tungsten, hence, leading to decreased power consumption and a possible increase in operating lifetime, both which are important in practical applications.

2.7.7. Colouration efficiency η

Colouration efficiency is the amount of electrochrome which may be coloured by one absorbance unit per unit charge and is almost always expressed as the magnitude of the absorbance being determined at the wavelength maximum λ_{max}. The colouration efficiency η is defined according to equation 2.19.

$$Abs = \eta\,Q \tag{2.19}$$

Where *Abs* is the absorbance formed by passing a charge density of *Q*. A graph of *Abs* against *Q* accurately gives η as the gradient. It is well known that for an ECD to be efficient it must show a maximised η.

Colouration efficiencies based on hydrous NiO have been quoted by Carpenter *et al.*[68] They were able to deposit adherent, uniform thin films by a cathodically electrodeposited method with η = 50 cm^2/C. A later paper by Vidotti *et al.*[69] improved the η to 80.3 cm^2/C at 457nm. Their method immobilised sonochemically synthesised Ni(OH)$_2$ nanoparticles for application in EC electrodes. More recently, Dalavi and co-workers used a chemical bath deposition technique to immobilise nanoporous NiO thin films with η = 95 cm^2/C.[70]

2.8. Applications of electrochromic materials

As previously mentioned, EC materials fall within two broad, overlapping categories according to the mode of operation: ECDs operating by transmission (smart windows) or by reflection (mirrors). In recent years, there has been a huge surge in the number of studies towards EC materials. This is also evident from the high number of patents which have been filed to describe the various commercially viable applications. In this section, the most common applications of ECDs will be outlined.

2.8.1. Smart windows

The term 'smart window' was first described in 1985 by Svensson and Granqvist as windows that electrochemically change in transmittance.[71] Their work considered coatings of crystalline WO$_3$ which is still the most studied and well-known EC material. The WO$_3$ EC phenomenon can be represented by the simple reaction in equation 2.20.

$$WO_3 + xM^+ + xe^- \leftrightarrow M_xWO_3 \qquad\qquad (2.20)$$

(transparent)   (deep blue)

Where M$^+$ can be H$^+$, Li$^+$, Na$^+$, or K$^+$, $0 < x > 1$. WO$_3$ exhibits an intense blue colour change, however doping the oxide with molybdenum (Mo) provides a more neutral colour suited towards window application. An example of transmittance regulation in an ECD based on WO$_3$ is shown in figure. 2.4.[72] This study highlighted that WO$_3$

films deposited using this method possessed excellent modulation to the visible light and the maximum average transmittance modulation of 70.06% was successfully reached.
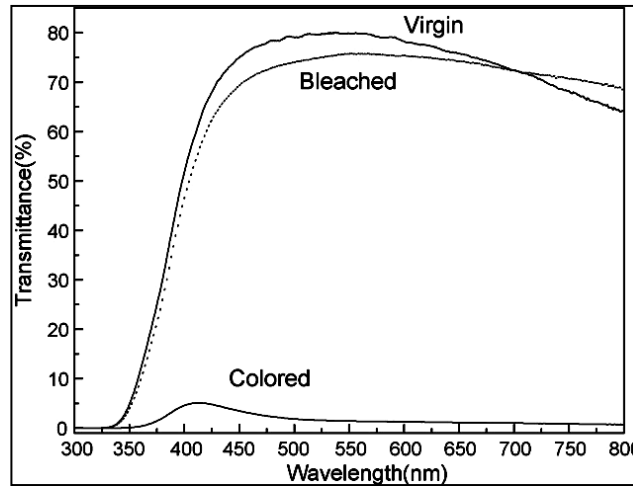

Figure 2.4. Spectral transmittance of three-layer WO$_3$ film prepared by dip coating-pyrolysis. Figure taken from.[72]

The application and construction of EC windows based on WO$_3$ has often been reviewed.[73,74] The developments of smart windows for architectural applications are at present the subject of intense research, as it has become evident that the appeal of smart windows is both economic and environmental. Therefore, over the last two decades there has been much activity to develop WO$_3$ based ECDs with wide modulation range, high durability (high number of performed colouring/bleaching cycles) and relatively fast switching times. Some examples are highlighted in Table 2.1.

Table 2.1. Data for WO_3-based ECD found in literature showing materials, sample size, modulation range, the performed number of colouring/bleaching cycles and the switching time for colouration and bleaching $t_{c/b}$. Figure redrawn from.[75]

ECD	Modulation range T (−)	cycles	Switching time $t_{c/b}$ (s)	Reference
WO₃-based construction				
G|ITO|WO₃|PVB:LiClO₄|CeTiO$_x$|ITO|G	T_{sol} 0.73–0.045	16×10³	60	Schlotter *et al.*[76]
	T_{vis} 0.81–0.07			
WO₃|NiO-based construction				
G|ITO|WO₃|PMMA-PC-Li⁺|NiO|ITO|G		10⁴	–	Lechner and Thomas[77]
G|ITO|WO₃|ZrP·xH₂O|ZrO₂|NiO|ITO|G	T_{vis} 0.74–0.38	–	60	Azens *et al.*[78]
	T_{sol} 0.53–0.25			Karlsson and Roos[79]
G|SnO₂|WO₃|PVDF-Li⁺|NiO:Li|SnO₂|G	T_{vis} 0.75–0.02	–	–	Michalak *et al.*[80]
G|ITO|WO₃|Ta₂O₅|NiO|ITO|G	T_{vis} 0.73–0.18	10⁵	–	Nagai *et al.*[81]
	T_{sol} 0.55–0.11			
G|SnO₂|WO₃|PEO/PEGMA:Li⁺|NiO:Li|SnO₂|G	T_{vis} 0.70–0.27	–	120	Penissi *et al.*[82]
G/P|ITO|WO₃|ZrP|ZrO₂|NiO|ITO|G/P	T_{vis} 0.75–0.14	10³	180/60	Kullman *et al.*[83]
P|ITO|WO₃|PMMA-PPG-Li⁺|NiO|ITO|P	T_{550} 0.70–0.35	5×10³	200	Granqvist *et al.*[84]
G|FTO|WO₃|P-3|NiO|FTO|G	T_{vis} 0.58–0.06	10³	2	Zelazowska[85]
WO₃|IrO₂-based construction				
G/P|ITO|WO₃|Ta₂O₅|IrO₂|ITO	T_{550} 0.70–0.18	3.5×10⁴	–	O'Brien *et al.*[86]
WO₃|Polymer-based construction				
G|ITO|WO₃|PAMPS|PANI|ITO|G	T_{sol} 0.74–0.35	–	11/11	Jelle and Hagen[87]
G|ITO|WO₃|PAMPS|PB|PANI|ITO|G	T_{sol} 0.73–0.23	4×10³	34/23	Jelle and Hagen[87]
G|ITO|WO₃|PAMPS|PB|PANI|ITO|G (another version)	T_{sol} 0.64–0.08	–	300/100	Jelle and Hagen[88]
G|SnO₂|WO₃|PVSA:PVP:H⁺|PB|SnO₂|G	T_{550} 0.72–0.06	2×10⁴	30	Ho[89]
G|ITO|WO₃|PAMPS:L|PANI-CSA|AR|ZnSe|AR	R_{1200} 0.65–0.22	900	9	Topart and Hourquebie[90]
P|ITO|WO₃:H₂O|PVDF-HFP-Li⁺|PANI|ITO|P	T_{800} 0.12–0.02	–	–	Marcel and Tarascon[91]

Research into non-tungsten oxide EC material for smart windows is found to be rare. This is mainly due to rather poor EC properties found with other materials, in particular the durability of these devices is found to be incompatible with commercial applications. Most of the non-tungsten based research is focused on niobium oxide-based ECDs and polymer-based devices. Examples include the work by Heusing *et al.*[92] (in 2006) on pure and doped niobium oxide layers which change their colour by insertion of Li⁺ ions from transparent to brown, grey or blue. Their study highlighted the colouration efficiency of a large ECD (30 x 40 cm) to be 27cm²/C, which is very low when compared to a WO_3-based ECD. Lock *et al.*[93] investigated a polymer-based ECD of poly-3,4-ethylenedioxythiophene (PEDOT) coated on ITO plastic substrate via a chemical vapour deposition (CVD) technique. Films produced using this technique showed a colour contrast of 45% at 566 nm, however the stability of the device was found to be 85% over 150 cycles.

2.8.2. Electrochromic car mirrors

While the application of EC materials is ever growing, the outstanding success to date is that of the Gentex Corporation, who produce self-darkening rear-view interior car mirrors (figure. 2.5 (b))[94] currently operating on several million cars, including Audi, Bentley, BMW, and Volkswagen. The mode of EC rear-view mirrors can be explained with reference to the schematic diagram in figure 2.5 (a) where an optically absorbing EC material over the reflective surface decreases the intensity of the incident beam. As a result, the reflected emergent beam is not as dazzling to the driver's eyes thereby alleviating discomfort.
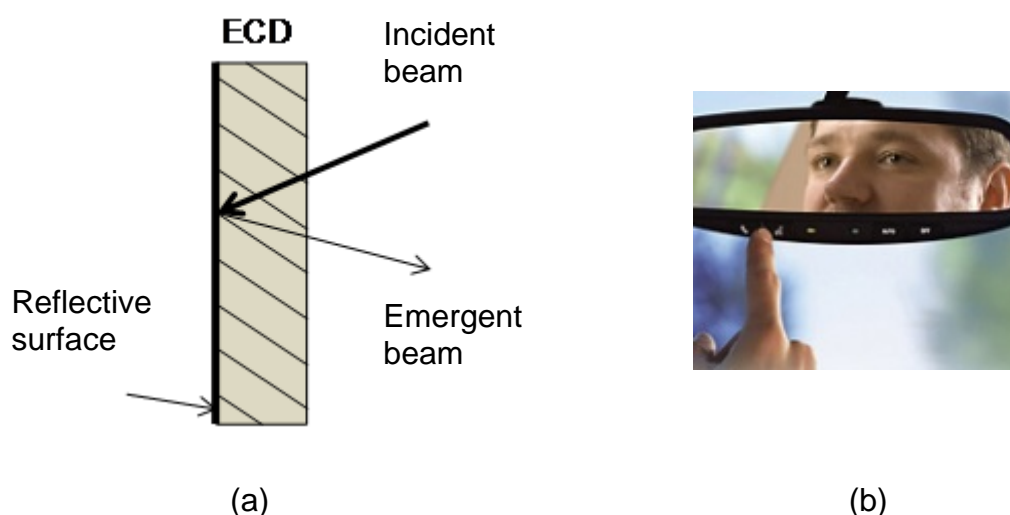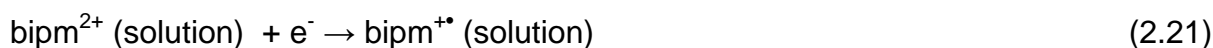

(a) (b)

Figure 2.5. (a) Schematic diagram of an ECD operating in reflective mode. The reflective surface is made of polished platinum or platinum-based alloy. (b) A Gentex self-darkening rear-view mirror.[94]

Undoubtedly, the world's most successful EC mirror is the Gentex Night-Vision System,[53] which makes up over 90% of all self-darkening mirrors sales. The Gentex device involves two EC materials, a viologen species (bipyridilium, $bipm^{2+}$) and phenothiazine which is a thiazine (TA) compound. The reflective surface is typically a metallic electrode with an ITO-coated glass as the front electrode. In operation, the colour formed is an intense blue-green and equation 2.21 and 2.22 illustrates the colour-forming reactions.

$$bipm^{2+} \text{ (solution)} + e^- \rightarrow bipm^{+\bullet} \text{ (solution)} \qquad (2.21)$$

$$TA \text{ (solution)} \rightarrow TA^{+\bullet} \text{ (solution)} + e^- \qquad\qquad (2.22)$$

2.8.3. Aircraft windows

After the success of EC car mirrors, Gentex has expanded its product line by creating the world's first interactive windows for use in commercial and business aircraft. In December 2005, Gentex signed an agreement with PPG Aerospace and Boeing to install EC windows in the new long-range Boeing 787 aircraft, known as the 'Dreamliner'. These dimmable windows allow cabins to be switched from a bright, clear state to an extreme dark state, or to a comfortable intermediate level in between, all at the touch of a button.[95] The windows are also 25% greater in area as compared to the usual and the control panel allows passenger to achieve the desired level of darkening (figure. 2.6 (a and b).). The technology of smart windows for aircrafts applications is relatively new therefore details into the EC system involved have yet to be revealed.

(a)   (b)

Figure 2.6. (a) EC windows installed in the new Boeing Dreamliner. (b) A window-seat controller which allows the passenger to activate the system and change the amount of visible light entering the cabin.[95]

2.8.4. Other applications

Other applications include ECD visors and sunglasses operating in a transmittance mode. In 1981, Nikon was the first to market EC sunglasses, termed 'variable-opacity lens filter.[96] Due to the manual operation to achieve the colour change, EC sunglasses are not able to compete with the now available photochromic lenses that

darken automatically. As a result, research into EC sunglasses is limited when compared to other EC applications.

ECDs operating as displays have been proposed for flat-panel displays for applications such as television and visual-display units (VDUs). The advantage of ECDs is that most possess the memory effect. This means that once images are formed, very little or no additional input power is required. This highly attractive feature is useful for shutters and displays that do not require updating too often. Examples include: electronic books/newspapers, transport terminal displays and advertising boards. However, due to the insufficient response time, low cycle lives and the technical problem of potential drop associated with the semiconductive electrode substrate, their application is restricted to televisions and VDU screens.

Investigation into EC paper was proposed by Talmay in 1942, where 'electrolytic writing paper' consisting of paper pre-impregnated with particulate MoO_3 and WO_3 was used to form an image following reduction at an inert-metal electrode acting as a pen.[97,98] Other EC materials have also been considered for such an application. Examples include viologens[99,100] Prussian blue[99,100] and the metal oxide MoO_3 and WO_3.[100] More recently, Tehrani *et al.* (in 2006) used a organic EC systems based on, poly(3,4-ethylenedioxythiophene) doped with poly(styrenesulfonate) (PEDOT:PSS) towards roll-to-roll production of polymer based EC display on flexible substrate. A year later, Andersson *et al.*[101] extended this study to improve the fill factor from 29% to 42% and increased the effective area of display from 42% to 65% by adding an extra layer of PEDOT:PSS on the counter electrode.

2.9. Electrochromic nickel oxide

NiO is the most commonly used anodic oxide-based EC material. It is able to change from a transparent to a neutral coloured state upon extraction of protons or insertion of OH^- ions. EC materials based on NiO have been less widely studied than WO_3, however due to their reasonable cost and excellent EC properties, the research has accelerated significantly in recent years. In this section, a brief history of NiO as an

EC material will be outlined. Also, the redox process involved with NiO will be discussed in detail.

2.9.1. History of electrochromic NiO-based materials

NiO-based materials have been researched extensively as the active material in batteries[102-105] for over 40 years but it was not until 1979 when its EC properties were investigated. McIntyre *et al.*[106] found that EC films of NiO can be deposited by cycling the potential of a nickel electrode in an alkaline electrolyte (1.0 mol dm^{-3} KOH) and by electrodeposition. Their results showed that during colouration the film changes from transparent to a dark bronze colour with a reflective contrast ratio of 100:1 and coloration and bleaching times of 50 ms and 19 ms respectively. A later paper by Lampert *et al.* (in 1986) extended this study to look at the 'chemical and optical properties of EC NiO films'.[107] This paper was probably the first to identify the potential application of EC NiO towards large-scale optical shutters, information displays and automotive and aerospace glazing. These authors concluded that the solar transmittance (*T*s) can be switched from *T*s(bleached) = 0.73 to *T*s(coloured) = 0.35 for films with a thickness of about 500 Å.

The same authors further examined the EC effect of hydrated NiO in 1987[108] and they concluded that by using cyclic voltammetry the switching of the films is controlled by the diffusion of protons, and OH⁻ plays a role in the reaction mechanism.

Probably the first study to construct an ECD based on hydrated NiO was Yu and Lampert (in 1989).[109] The structure of their device consisted of up to five distinct layers (figure. 2.7). The layers consisted of a transparent conductive substrate (tin oxide coated glass), an EC material (NiO, working electrode), a polymeric ion conductor (which can also serve as a lamination material), an EC material (counter electrode), and another transparent conductive substrate. The colouration or bleaching effect was carried out by applying a low potential (1-3 V) between the working and counter electrodes.
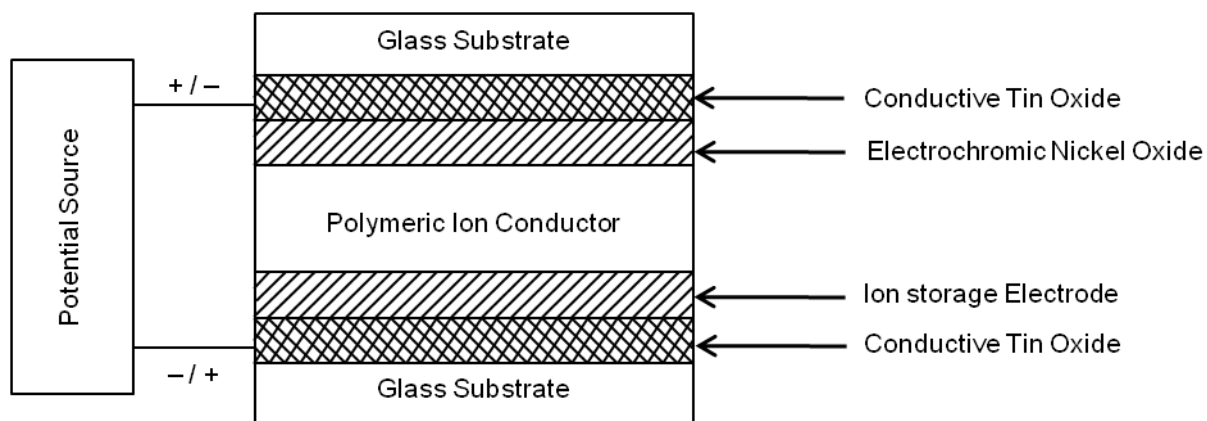
Figure 2.7. Schematic of a symmetric ECD utilising a polymer ion conductor as a laminator layer. Diagram redrawn from.[109]

In the same year, Passerini *et al.*[110] published a paper which outlined that NiO may be used in conjunction with WO_3 in an ECD for window applications. Their communication reported preliminary data taken for a device using WO_3 as the primary EC material and NiO as the secondary EC material with an intermediate solid electrolyte of poly(ethylene oxide) doped with lithium perchlorate, $(PEO)_8LiCLO_4$. Initial results showed good durability of 1000 voltage pulses and colouration and bleaching switching times of about 10 seconds. A little later, in 1994, Cantão *et al.* also examined a similar device system but with different electrolytes. They used TiO_x and TaO_x electrolytes to show the EC behaviour of all-solid state devices. In the reflective mode the devices showed chemically compatible, the films were adherent and produced reflectance changes as large as 90% .[111]

The use of NiO as a secondary EC material has continued to attract attention due to the material exhibiting a neutral colour change upon extraction of protons or insertion of OH^- ions. To date, the majority of the ECDs have focused on using NiO as a secondary electrochrome on the counter electrode with another primary EC material on the working electrode. In most cases, the partner EC material used is WO_3.[77-85] However, in some cases poly(pyrrole),[112] poly(thiophene),[113] or poly(methylthiophene)[113] have also been investigated.

2.10. References

[1]   Rahaman, M. N. *Ceramic Processing*, USA, CRC Press, 2007.

[2]   McColm, I. J. and Clark, N. J. *Forming, Shaping and Working of High-performance Ceramics*, Glasgow, Blackie and Son Ltd, 1988.

[3]   Segal, D. *Chemical Synthesis of Advanced Ceramic Materials*, Cambridge University Press, Cambridge, Book 1 of the "Chemistry of Solid State Materials" Series, 1989.

[4]   Tiwari, A., Zhu, J., Hibara, L. H. The Development of low-temperature Hardening Silicone Ceramer Coatings for the Corrosion Protection of Metals. *Surf. Coat. Technol.*, **202**, 2008, 4620-35.

[5]   Mitchell, P. J., Wilcox, G. D. An electrochemical route to pre-shaped ceramic bodies. *Nature.*, **357**, 1992, 396-97.

[6]   Mitchell, P. J., Mortimer, R. J., Wallace, A. Evaluation of a cathodically precipitated aluminium hydroxide film at a hydrogen-sorbing palladium electrode as a humidity sensor. *J. Chem. Soc., Faraday Trans.*, **94**, 1998, 2423-28.

[7]   Mortimer, R. J., Mayes, R. J., Dann, S. E. Metal and mixed metal (oxy)-hydroxide ceramic precursor materials prepared by cathodically-induced precipitation using a hydrogen-sorbing palladium electrode. *Mater. Lett.*, **61**, 2007, 5121-25.

[8]   Mortimer, R. J., Mayes, R. Characterisation and humidity-sensing properties of aluminium (oxy)-hdroxide films prepared by cathodically induced precipitation. *Sens. Actuators, B.*, **127**, 2007, 124-32.

[9]   Person, H. O. *Handbook Of Chemical Vapor Deposition (CVD): Principles, Technology, and Applications*, Noyes, Park Ridges, NJ, 1992.

[10]   Hitchman, M. L. and Jensen, K. F. *Chemical Vapor Deposition: Principles and Applications*, Academic Press, London, 1993.

[11]   Maruyama, T. and Arai, S. The electrochromic properties of nickel oxide thin films prepared by chemical vapour deposition. *Sol. Energy Mater. Sol. Cells.*, **30**, 1993, 257-62.

[12]   Brinker, C. J. and Scherer, G. W. *Sol-Gel Science*, Academic Press, New York, 1990.

[13] Klein, L. C. *Sol-Gel Technology for Thin Films, Fibers, Performs, Electronics and Specialty Shapes*, Noyes Publications, Park Ridge, NJ, 1988.

[14] Sharma, P. K., Fantini, M. C. A. and Gorenstein, A. Synthesis, characterization and electrochromic properties of NiO_xH_y thin films prepared by a sol-gel method. *Solid State Ionics.* **113-115**, 1998, 457-63.

[15] Niesen, T. P., De Guire, M. R. Review: Deposition of ceramic thin films at low temperatures from aqueous solutions. *J. Electroceram.*, **6**, 2001, 169-207.

[16] Kamath, P. V., Subbanna, G. N. Electroless nickel hydroxide: synthesis and characterization. *J. Appl. Electrochem.,* **22**, 1992, 478-82.

[17] Zhang, E., Tang, Y., Zhang, Y., Gue, C., Yang, L. Hydrothermal synthesis of β-nickel hydroxide nanocrystalline thin film and growth of oriented carbon nanofibers. *Mater. Res. Bull.,* **44**, 2009, 1765-70.

[18] Therese, G. H. A. and Kamath, P.V. Electrochemical synthesis of metal oxides and hydroxides. *Chem. Mater.,* **12**, 2000, 1195-204.

[19] Pickett, D. F. Preparation of nickel electrodes. U.S. Pat. 3,827,911, 1974.

[20] Pickett, D. F., Maloy, J. T. Microelectrode studies of electrochemically coprecipitated cobalt hydroxide in nickel hydroxide electrodes. *J. Electrochem. Soc.*, **125**, 1978, 1026-32.

[21] Monk, P. M. S., Chester, S. L., Higham, D. S., Partridge, R. D. Electrodeposition of cobalt oxide doped with additional metal oxides. *Electrochim. Acta*, **39**, 1994, 2277-84.

[22] Monk, P. M. S., Ayub, S. Solid-state properties of thin films electrochromic cobalt-nickel oxide. *Solid State Ionics*, **99**, 1997, 115-24.

[23] Monk, P. M. S., Akhter, S. P., Boutevin, J., Duffield, J. R. Towards the tailoring of electrochromic bands of metal-oxide mixtures. *Electrochim. Acta*, **46**, 2001, 2091-96.

[24] Monk, P. M. S., Chester, S. L. Electro-deposition of films of electrochromic tungsten oxide containing additional metal oxides. *Electrochim. Acta*, **38**, 1993, 1521-26.

[25] Monk, P. M. S., Mortimer, R. J. and Rosseinsky, D. R. *Electrochromism and Electrochromic Devices*, Cambridge Univ Press, Cambridge, 2007.

[26] Granqvist, G. C. *Handbook of Inorganic Electrochromic Materials*. Amsterdam, Elsevier, 1995.

[27] Byker, H. J. Commercial developments in electrochromics. *Proc. Electrochem. Soc.*, **94-2**, 1994, 1-13.

[28] Berzelius, J. J. Afhandlingar I fysik. *Kemi Och Mineralogie*, **4**, 1815, 293, as cited in ref. 26.

[29] F. Wöhler. *Ann. Phys.*, **2**, 1824, 350, as cited in ref. 26.

[30] See the article 'True Blue (cyanotype) part 2: blue history' by Peter Marshall, available [online] at photography.about.com/library/weekly6/aa061801b.htm, as cited in ref. 25.

[31] Smith, F.H., British Patent, 328,017, 1929.

[32] Kobosew, N. and Nekrassow, N. I. Bildung freier wasserstoffatome bei kathodenpolarisation der metalle. *Z. Electrochem.*, **36**, 1930, 529.

[33] Brimm, E. O., Brantley, J. C., Lorenz, J. H. and Jellinek, M. H. *J. Am. Chem. Socl.*, **73**, 1951, 5427.

[34] Philips Electronic and Associated Industries Ltd. Image display apparatus. British Patent 1,302,000, 4 Jan 1973. [The patent was first filed on 24th June 1971.]

[35] Schoot, C. J., Ponjée, J. J., van Dam, H. T., van Doorn, R. A. and Bolwijn, P. T. New electrochromic memory display. *Appl. Phys. Lett.*, **23**, 1973, 64-5.

[36] Short, G. D. and Thomas, L. Radiation sensitive materials containing nitrogenous cationic materials, British Patent 1,310,813, published 21 March 1973. [The patent was first filed on 28 May 1969.]

[37] Barclay, D. J., Bird, C. L., Kirkman, D. K., Martin, D. H. and Moth, F. T. An integrated electrochromic data display, SID 80 Digest, 1980, abstract 12.2, 124.

[38] Jasinski, R. J. N-Heptylviologen radical cation films on transparent oxide electrodes. *J. Electrochem. Soc.*, **125**, 1978, 1619-23.

[39] Deb, S. K. A novel electrophotographic system, *Appl. Opti.*, **Suppl.3**, 1969, 192-5.

[40] Blanc, J. and Staebler, D. L. Electrocoloration in $SrTiO_3$: vacancy drift and oxidation-reduction of transition metals. *Phys. Rev. B.*, **4**, 1971, 3548-57.

[41] Beegle, L. C. Electrochromic device having identical display and counter electrodes. US Patent 3,704,057, 28 November 1972.

[42] Deb, S. K. Optical and photoelectric properties and colour centres in thin films of tungsten oxide. *Philos. Mag.*, **27**, 1973, 801-22.

[43]   Green, M. and Richman, D. A solid state electrochromic cell–the RbAg$_4$I$_5$/WO$_3$ system. *Thin Solid Films*, **24**, 1974, S45-6.

[44]   Faughnan, B. W., Crandall, R. S. and Heyman, P. M. Electrochromism in WO$_3$ amorphous films. *RCA Rev.*, **36**, 1975, 177-97.

[45]   Faughnan, B. W., Crandall, R. S. and Lampert, M. A. Model for the bleaching of WO$_3$ electrochromic films by an electric field. *Appl. Phys. Lett.*, **27**, 1975, 275-7.

[46]   Crandall, R. S. and Faughnan, B. W. Dynamics of coloration of amorphous electrochromic films of WO$_3$ at low voltages. *Appl. Phys. Lett.*, **28**, 1976, 95-7.

[47]   Mohapatra, S. K. Electrochromism in WO$_3$. *J. Electrochem. Soc.*, **285**, 1978, 284-8.

[48]   Ronlán, A., Coleman, J., Hammerich, O. and Parker, V. D. Anodic oxidation of methoxybiphenyls: the effect of the biphenyl linkage on aromatic cation radical and dication stability. *J. Am. Chem. Soc.*, **96**, 1974, 845-9.

[49]   Kaufman, F. B., Schroeder, A. H., Engler, E. M. and Patel, V. V. Polymer-modified electrodes: a new class of electrochromic materials. *Appl. Phys. Lett.*, **36**, 1980, 422-5.

[50]   Kaufman, F. B. and Engler, E. M. Solid-state spectroelectrochemistry of cross-linked donor bound polymer films. *J. Am. Chem. Soc.*, **101**, 1979, 547-9.

[51]   Kanazawa, K. K., Diaz, A. F., Geiss, R. H., Gill, W. D., Kwak, J. F., Logan, J. A., Rabolt, J. F. and Street, G. B. 'Organic metals': polypyrrole, a stable synthetic 'metallic' polymer. *J. Chem. Soc., Chem. Commun.*, 1979, 854-5.

[52]   Chang, I. F., Gilbert, B. L. and Sun, T. I. Electrochemichromic systems for display applications. *J. Electrochem. Soc.* **122**, 1975, 955-62.

[53]   Byker, H. J., Gentex Corporation. Single-compartment, self-erasing, solution-phase electrochromic devices, solution for use therein and uses thereof. US Patent 0,240,226, 1996.

[54]   Ma, C., Zheng, J., Yang, S., Zhu, D., Bin, Y. and Xu, C. Electrochromic kinetics of nanostructured poly(3,4-(2,2-dimethylpropylenedioxy)thiophene) film on plastic substrate. *Org. Electron.* **12**, 2011, 980-7.

[55]   Montazami, R., Jain, V. and Heflin, J. R. High contrast asymmetric solid state electrochromic devices based on layer-by-layer deposition of polyaniline and poly(aniline sulfonic acid). *Electrochim. Acta*, **56**, 2010, 990-4.

[56]   da Silva, A. J. C., Ribeiro Nogueira, F. A., Tonholo, J. and Ribeiro, A. S. Dual-type electrochromic device based on polypyrrole and polythiophene derivatives. *Sol. Energy Mater. Sol. Cells*, **95**, 2011, 2255-9.

[57]   Faughnan, B. W. and Crandall, R. S. Electrochromic devices based on WO_3 in Pankove J. L. (ed), Display Devices, Berlin, Springer-Verlag, 1980, pp. 181-211.

[58]   Mathew, J. G. H., Sapers, S. P., Cumbo, M. J., O'Brien, N. A., Sargent, R. B., Raksha, V. P., Lahaderne, R. B. and Hichwa, B. P. Large area electrochromics for architectural applications. *J. Non-Cryst. Solid*, **218**, 1997, 342-6.

[59]   Granqvist, C. G. Smart windows and intelligent glass façades. *Smart Materials Bulletin*, **2002**, 2002, 9-10.

[60]   Kullma, L., Azens, A., Vaivars, G. and Granqvist, C. G. Electrochromic devices incorporating Cr oxide and Ni oxide films: A comparison. *Solar Energy*, **68**, 2000, 517-22.

[61]   Welsh, D. M., Kumar, A., Morvant, M. C. and Reynolds, J. R. Fast electrochromic polymer based on new poly(3,4-alkylenedioxythiophene) derivatives. *Synth. Met.*, **102**, 1999, 967-8.

[62]   Dominey, R. N., Lewis, T. J. and Wrighton, M. S. Synthesis and characterization of a benzylviologen surface-derivatizing reagent. N,N'-Bis[p-(trimethoxysilyl)benzyl]-4,4'-bipyridinium dichloride. *J. Phys. Chem*, **87**, 1983, 5345-54.

[63]   Bookbinder, D. C. and Wrighton, M. S. Electrochromic Polymers Covalently Anchored to Electrode Surfaces. Optical and Electrochemical Properties of a Viologen-Based Polymer. *J. Electrochem. Soc*, **130**, 1983, 1080-7.

[64]   Grant, B., Clecak, N. J., Oxsen, M., Jaffe, A. and Keller, G. S. Study of the electrochromism of methoxyfluorene compounds. *J. Org. Chem.*, **45**, 1980, 702-5.

[65]   Zhao, L., Su, G., Liu, W., Cao, L., Wang, J., Dong, Z. and Song, M. Optical and electrochemical properties of Cu-doped NiO films prepared by electrochemical deposition. *Appl. Surf. Sci*, **257**, 2011, 3974-9.

[66]   Vidotti, M. and Córdoba de Torresi, S. I. Electrostatic layer-by-layer and electrophoretic deposition as methods for electrochromic nanoparticle immobilization. *Electrochim. Acta.*, **54**, 2009, 2800-4.

[67] Lee, S. H. and Joo, S. K. Electrochromic behavior of Ni-W oxide electrodes.Sol. *Energy Mater. Sol. cells.*, **39**, 1995, 155-66.

[68] Carpenter, M. K., Conell, R. S. and Corrigan, D. A. The electrochromic properties of hydrous nickel oxide. *Sol. Energy Mater.*, **16**, 1987, 333-46.

[69] Vidotti, M., van Greco, C., Ponzio, E. A and Córdoba de Torresi, S. I. Sonochemically synthesized $Ni(OH)_2$ and $Co(OH)_2$ nanoparticles and their application in electrochromic electrodes. *Electrochem. Commun.*, **8**, 2006, 554-60.

[70] Dalavi, D. S., Suryavanshi, M. J., Patil, D. S., Mali, S. S., Moholkar, A. V., Kalagi, S. S., Vanalkar, S. A., Kang, S. R., Kim, J. H. and Patil, P. S. Nanoporous nickel oxide thin films and its improved electrochromic performance: Effect of thickness. *Appl. Surf. Sci.*, **257**, 2011, 2647-56.

[71] Svensson, J. S. E. M. and Granqvist, C. G. Electrochromic coatings for 'smart windows'. *Sol. Energy Mater.*, **12**, 1985, 391-402.

[72] Yang, H., Shang, F., Gao, L. and Han, H. Structure, electrochromic and optical properties of WO_3 films prepared by dip coating-pyrolysis. *Appl. Surf. Sci.*, **257**, 2007, 5553-57.

[73] Niklasson, G. A. and Granqvist, C. G. Electrochromics for smart windows: thin films of tungsten oxide and nickel oxide, and devices based on these. *J. Mater. Chem.*, **17**, 2007, 127-56.

[74] Granqvist, C. G. Electrochromic tungsten oxide films: Review of progress 1993-1998. *Sol. Energy Mater. Sol. Cells.*, **60**, 2000, 201-262.

[75] Baetens, R., Jelle, B. P. and Gustavsen, A. Properties, requirements and possibilities of smart windows for dynamic daylight and solar energy control in buildings: A state-of-the-art review. *Sol. Energy Mater. Sol. Cells,*. **94**, 2010, 87-105.

[76] Schlotter, P., Baur, G., Scmidt R. and Weinberg, U. Laminated electrochromic device for smart windows. In: Wittwer W. and Granqvist, C.G. Editors, Optical Materials Technology for Energy Efficiency and Solar Energy Conversion, vol. XIII (1994), pp. 351–362

[77] Lechner R. and Thomas, L. K. All solid state electrochromic devices on glass and polymeric foils. *Sol. Energy Mater. Sol. Cells.*, **54**, 1998, 139-46.

[78] Azens, A., Kullman, L., Vaivars, G., Nordberg H. and Granqvist, C. G. Sputter-deposited nickel oxide for electrochromic applications. *Solid State Ionics*, **113**, 1998, 449-56.

[79] Karlsson J. and Roos, A. Angle-resolved optical characterisation of an electrochromic device. *Sol. Energy*, **68**, 2000, 493-7.

[80] Michalak, F., von Rottkay, K., Richardson, T., Slack J. and Rubin, M. Electrochromic lithium nickel oxide thin films by RF-sputtering from a $LiNiO_2$ target. *Electrochim. Acta*. **44**, 1999, 3085-92.

[81] Nagai, J., McMeeking G. D. and Saitoh, Y. Durability of electrochromic glazing. *Sol. Energy Mater. Sol. Cells.*, **56**, 2009, 3090-19.

[82] Penissi, A., Simone, F., Barletta, G., Di Marco, G. and Lanza, M. Preliminary test of a large electrochromic window. *Electrochim. Acta*, **44**, 1999, 3237-32.

[83] Kullman, L., Azens, A., Vaivars, G. and Granqvist, C. G. Electrochromic devices incorporating Cr oxide and Ni oxide films: a comparison. *Sol. Energy*, **68**, 2000, 517-22.

[84] Granqvist, C. G., Avendaño, E. and Azens, A. Electrochromic coatings and devices: survey of some recent advances. *Thin Solid Films*, **442**, 2003, 201-11.

[85] Zelazowska E. and Rysiakiewicz-Pasek, E. WO_3-based electrochromic system with hybrid organic–inorganic gel electrolytes. *J. Non-Cryst. Solids*, **354**, 2008, 4500-05.

[86] O'Brien, N. A., Gordon, J., Mathew, H. and Hichwa, B.P. Electrochromic coatings—applications and manufacturing issues. *Thin Solid Films*, **345**, 1999, 312-18.

[87] Jelle, B. P. and Hagen, G. Transmission spectra of an electrochromic window based on polyaniline, Prussian Blue and tungsten oxide. *J. Electrochem. Soc.*, **140**, 1993, 3560-64.

[88] Jelle, B. P. and Hagen, G. Solar modulation in an electrochromic window using polyaniline, prussian blue and tungsten oxide. In: Ho K. C. and MacArthur, A. Editors, Proceedings of the Second Symposium on Electrochromic Materials vol. 2, The Electrochemical Society, Pennington, NJ (1994), pp. 324–338.

[89] Ho, K. C. Cycling and at-rest stabilities of a complementary electrochromic device based on tungsten oxide and prussian blue thin films. *Electrochim. Acta*, **44**, 1999, 3227-35.

[90] Topart, P. and Hourquebie, P. Infrared switching electroemissive devices based on highly conducting polymers. *Thin Solid Films*, **352**, 1999, 243-8.

[91] Marcel, C. and Tarascon, J. -M. An all-plastic $WO_3 \cdot H_2O$/polyaniline electrochromic device. *Solid State Ionics*, **143**, 2001, 89-101.

[92] Heusing, S., Sun, D. -L., Otero-Anaya, J. and Aegerter, M. A. Grey, brown and blue coloring sol–gel electrochromic devices, *Thin Solid Films,* **502**, 2006, 240-5.

[93] Lock, J. P., Luthkenhaus, J. L., Zacharia, N. S., Im, S. G., Hammond, P. T. and Gleason, K. K. Electrochemical investigation of PEDOT films deposited via CVD for electrochromic applications. *Synth. Met.*, **157**, 2007, 894-8.

[94] http://www.gentex.com/automotive/products/driver-safety (accessed 25 April 2013).

[95] http://www.gentex.com/aerospace (accessed 45 April 2013).

[96] www.nikon.co.jp/main/eng/porfolio/about/history/corporate_history.htm; as cited in ref. 25.

[97] Talmay, P. Electrolytic recording. US Patent 2,319,765, 1943.

[98] Talmay, P. Electrolytic recording paper. US Patent 2,281,013, 1942.

[99] Rosseinsky, D. R. and Monk, J. L. Thin layer electrochemistry in a paper matrix: electrochromography of Prussian blue and two bipyridilium systems. *J. Electroanal. Chem.*, **270**, 1989, 473-8.

[100] Monk, P. M. S., Delage, F. and Costa Vieira, S. M. Electrochromic paper: utility of electrochromes incorporated in paper. *Electrochim. Acta*, **46**, 2001, 2195-202.

[101] Andersson, P., Forchheimer, R., Tehrani, P. and Berggren, M. Printable All-Organic Electrochromic Active-Matrix Displays. *Adv. Funct. Mater.* **17**, 2007, 3074-82.

[102] Jayashree, R. S. and Kamath, P. V. Layered double hydroxide of Ni with Cr and Mn as candidate electrode materials for alkaline secondary cells. *J. Power Sources*, **107**, 2002, 120-124.

[103] Freitas, M. Nickel hydroxide powder for $NiO \cdot OH/Ni(OH)_2$ electrodes of the alkaline batteries. *J. Power Sources*, **93**, 2001, 163-73.

[104] Gifford, P., Adams, J., Corrigan, D. and Venkatesan, S. Development of advanced nickel/metal hydride batteries for electric and hybrid vehicles. *J. Power Sources*, **80**, 1999, 157-63.

[105] Dixit, M., Kamath, P. V. and Gopalakrishnan J. Zinc-Substituted α-Nickel Hydroxide as an Electrode Material for Alkaline Secondary Cells. *J. Electrochem. Soc.* **146**, 1999, 79-82.

[106] McIntyre, J. D. E., Peck, W. F. and Schwartz, G. P. Electronic Materials Conf, Abstract D-4, 1979.

[107] Lampert, C. M., Omstead, T. R. and Yu, P. C. Chemical and optical properties of electrochromic nickel oxide films. *Sol. Energy Mater.*, **14**, 1986, 161-174.

[108] Yu, P. C., Nazri, G. and Lampert, C. M. Spectroscopic and electrochemical studies of electrochromic hydrated nickel oxide films. Sol. Energy. Mater., 16, 1987, 1-17.

[109] Yu, P. C. and Lampert, C. M. In-situ spectroscopic studies of electrochromic hydrated nickel oxide films. *Sol. Energy Mater.*, **19**, 1989, 1-16.

[110] Passerini, S., Scrosati, B., Gorenstein. A., Andersson, A. M. and Granqvist, C. G. An electrochromic window based on $LixWO_3/(PEO)_8LiClO_4/NiO$. *J.Electrochem. Soc.*, **136**, 1989, 3394-5.

[111] Cantão, M. P., Lourenço, A., Gorenstein, A., Córdoba de Torresi, S. I. and Torresi. R. M. Inorganic oxide solid state electrochromic devices. *Mater. Sci. Eng., B*, **26**, 1994, 157-61.

[112] Avino, C., Panero, S. and Scrosati, B. An electrochromic window based on a modified polypyrrole/nickel oxide combination. *J. Mater. Chem.*, *3*, 1993, 1259-6.

[113] Arbizzani, C., Mastragostine, M., Passerini, S., Pillegi, R. and Scrosati, B. An electrochromic window based on polymethyl thiophene and nickel oxide electrodes. *Electrochim. Acta.*, **36**, 1991, 837-40.

3. Experimental

This chapter outlines the experimental arrangements and procedures used for work presented in this thesis. Any experimental techniques introduced by previous authors will be cited accordingly within the relevant sections.

3.1 Chemicals used

Ammonium hydroxide	NH_4OH	Fisher Scientific (S.G = 0.88, 35% NH_3)
Boric acid	BH_3O_3	Fluka (>99.5%)
Cadmium nitrate tetrahydrate	$Cd(NO_3)_2.4H_2O$	Acros Organics (99+%)
Cerium nitrate hexahydrate	$Ce(NO_3)_3.6H_2O$	BDH (98)
Cobalt nitrate hexahydrate	$Co(NO_3)_2.6H_2O$	Aldrich (98%)
Copper nitrate trihydrate	$Cu(NO_3)_2.3H_2O$	Fisher Scientific (>99.5%)
Hydrochloric acid	HCl	Fisher Scientific (S.G = 1.16, 32%)
Isopropyl alcohol	$(CH_3)_2CHOH$	Fisher Scientific (99.5%)
Lanthanum nitrate hexahydrate	$La(NO_3)_3.6H_2O$	Alfa Aesar (99.9%)
Nickel nitrate hexahydrate	$Ni(NO_3)_2.6H_2O$	Acros Organics (99%)
Nickel acetylacetonate	$C_{10}H_{14}NiO_4$	Aldrich (95%)
Nickel chloride	$NiCl_2$	Aldrich (98%)
Nickel sulphate hexahydrate	$NiSO_4.6H_2O$	Fisher Scientific (>98%)
Nitric acid	HNO_3	Fisher Scientific (70%)
N,N-dimethylaminoethanol	$C_4H_{11}NO$	Fluka (98%)
Potassium hydroxide	KOH	Fisher Scientific (>85%)
Poly(allylamine hydrochloride)	$(C_3H_8ClN)_n$	Aldrich (Average Mw ≈ 58,000)
Sulphuric acid	H_2SO_4	Aldrich (95-98%)

3.2 Instrumentation

All electrochemical techniques including cyclic voltammetry, chronoamperometry and chronopotentiometry (galvanostatic) were carried out using a Princeton Applied Research potentiostat/galvanostat 263A. Software used was PowerSuite version 2.10.5 with PowerCV version 2.10.5. A second, Sycopel AEW2 electrochemical workstation was also used for some experimental measurements.

For layer-by-layer (LbL) deposition technique, metal hydroxide nanoparticles were synthesised by employing a Misonix S-4000 ultrasonic processor/sonicator with a standard ½" diameter tapped horn and irradiating the solution with a high intensity ultrasound radiation. Figure 3.1 shows the sonicator which consists of a generator, convertor and a horn.

Figure 3.1. Photograph showing a Misonix S-4000 ultrasonic processor/sonicator (image taken from the Misonix, Inc operation manual).

In situ visible region spectra were recorded using a Hewlett Packard 8452A diode array spectrophotometer.

A Thurlby PL310 waveform generator was used as a power supply to electrochemically clean the working electrodes. Substrate conductance and resistance was measured using a Jandel HM20 4-point universal probe.

Once the experiments were completed all data were tabulated and plotted by transferring to Microsoft® Excel® 2010 or Origin® version 6.1 software.

3.3 Electrodes

In order to prepare thin films for different experimental purposes, a wide range of electrodes types were used. For nitrate reduction and metallic nickel investigations, a glassy carbon (surface area = 0.0707 cm^2), a gold (0.0201 cm^2) and a platinum (0.0201 cm^2) electrodes were used which were purchased from Bio Analytical Systems Inc (BASi) (figure. 3.2).
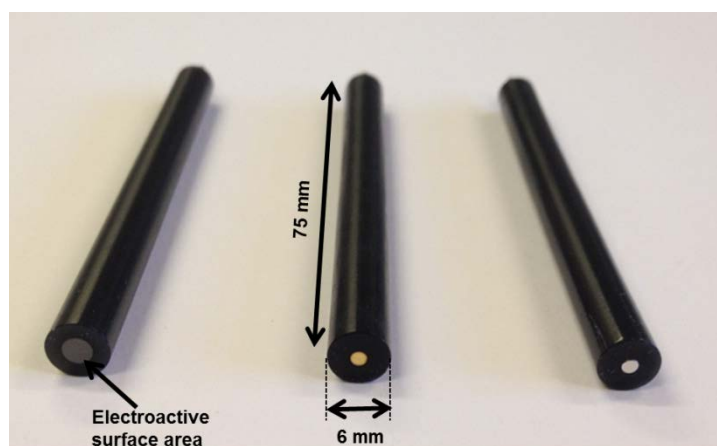
Figure 3.2. Photograph showing the three BASi disk electrodes (left to right, glassy carbon, gold, and platinum). Electroactive surface area is 0.0707 cm^2 for glassy carbon and 0.0201 cm^2 for gold and platinum.

Two different optically transparent conductive substrates were used for preparing nickel oxide-based precursor films for electrochromic (EC) studies. Fluorine-doped tin oxide (SnO$_2$:F, FTO) on glass (30 x 30 cm, NSG TEC^{TM} C15, R$_s$ 14 Ω / □$^{-1}$) were received as gift from Pilkington Group limited. For small scale experiments, the 30 x 30 cm FTO/glass plates were cut to 50 x 7 mm size samples using an Inland Scoreone glass cutter and glass pliers (figure 3.3). Tin-doped indium oxide (In$_2$O$_3$(Sn), ITO) on glass, (50 x 7 mm, CB-50IN-CUV, R$_s$ 5-15 Ω / □$^{-1}$) purchased from Delta Technologies were also used as substrates for depositing and analysing the EC materials. For large-scale deposition trials, two different sized FTO/glass

3. Experimental

(10 x 7.5 and 30 x 30 cm) substrates were used which were also obtained from Pilkington Group limited.
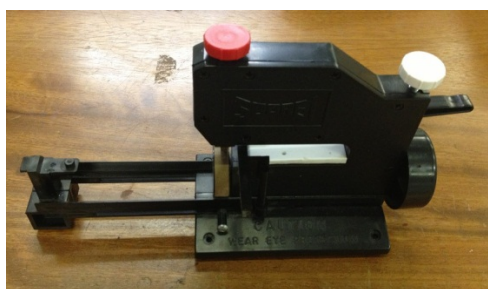

(a)   (b)

Figure 3.3. Photographs showing (a) Inland Scoreone cutter used to score the FTO/glass plate. (b) Glass pliers used to carefully break the glass into appropriate size.

Figure 3.4 shows the two types of flag electrodes made from platinum (20 x 20 mm) or palladium (50 x 50 mm) foil which were used to prepare films for XRD analysis. The deposited films were dried in air, before carefully scraping the surface to generate powdered material for XRD experiments.
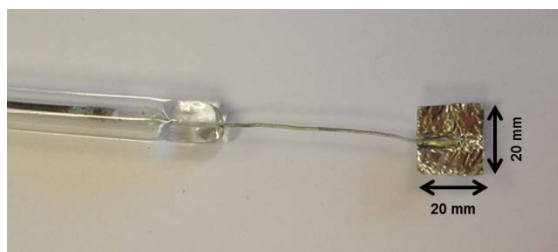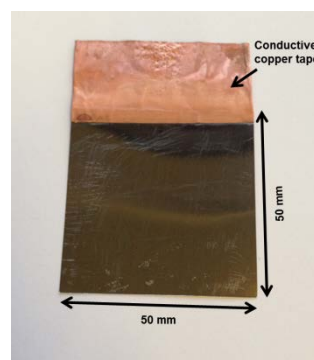
(a)   (b)

Figure 3.4. Photographs showing (a) Platinum flag electrode. (b) Palladium foil electrode.

A platinised titanium counter electrode (figure 3.5) was used for all electrochemical measurements. For small-scale experiments an alternative platinum mesh-flag style (Aldrich, 99.9%) counter electrode was also used, where the flag was approximately 20 x 10 mm. Both counter electrodes were cleaned by dipping in concentrated sulphuric acid and flame treated to remove impurities.
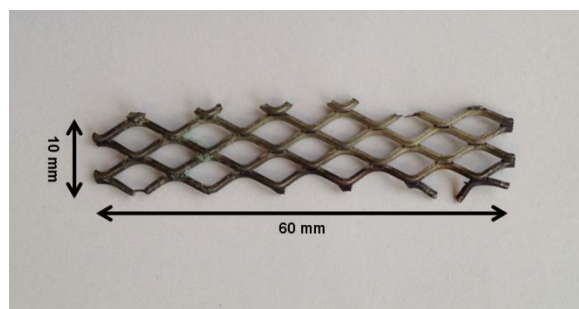
Figure 3.5. Photograph showing a platinised titanium counter electrode.

For all small and large-scale experiments, a saturated calomel (Hg/Hg$_2$Cl$_2$, SCE) reference electrode (figure 3.6 (a)) purchased from Sentek was used. For *in situ* spectroelectrochemistry measurements a silver (Ag/Ag$^+$) wire pseudo reference electrode (figure 3.6 (b)) was used within a standard 1 cm pathlength UV-vis plastic cuvette.
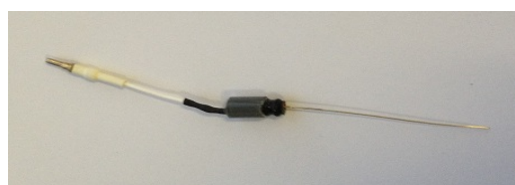
(a)   (b)

Figure 3.6. Photographs showing (a) Sentek saturated calomel reference electrode with a ceramic frit and 120 x120 mm dimensions. (b) 50 mm length silver wire pseudo reference electrode adapted from a BASi Ag/AgCl reference electrode.

3.3.1. Electrode cleaning

Prior to any experimental investigation, ITO/glass and FTO/glass substrates required several cleaning steps to remove any impurities on the surface. The conductive substrates were first rinsed with Milli-Q$^®$ deionised water (18.2 MΩ cm) then sonicated in each of the following solutions for 10 minutes: Propan-2-ol, acetone and ethanol. Once the thin films were deposited, they were removed from the conducting substrates by dipping in HCl (1.5 mol dm^{-3}) solution and rinsing with deionised water. This would allow the substrate to be re-used as the deposited films were dissolved without removing or affecting the conductive layer.

Platinum and palladium flag electrodes were cleaned electrochemically by anodising then cathodising for 1 minute in 0.5 mol dm^{-3} sulphuric acid. A current of 100 mA was applied in both directions using a Thurlby PL310 waveform generator. This method was followed by flame treating the electrode to remove any deposited film and contaminants from the surface.

3.4 Electrochemical arrangements

For small scale experiments, a simple electrochemical cell arrangement was used with the compartment containing all three electrodes during measurements (figure 3.7). Prior to measurements, the three electrode terminals were abraded to ensure good electrical contact.
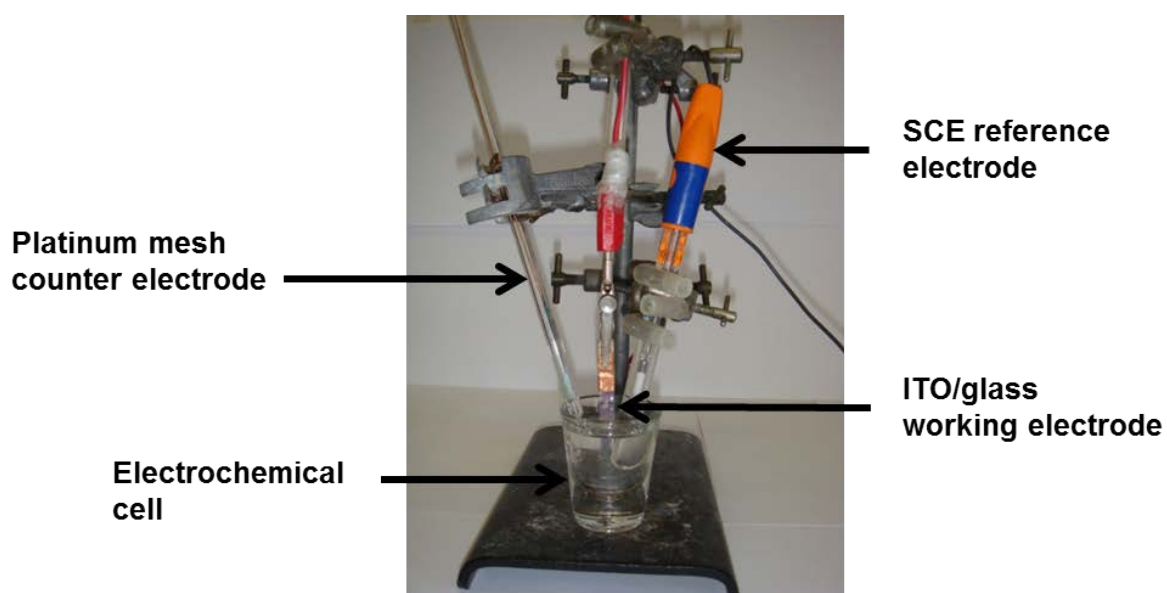
Figure 3.7. Image showing a one compartment electrochemical cell used for all small-scale experiments. The electrochemical cell had a diameter of 5 cm at the top and 2 cm at the base.

For large-scale experiments two custom glass tanks (35 x 35 x 5 cm) were manufactured by Quorn & Loughborough Glass (figure 3.8). The one compartment glass tanks were used to deposit thins films on 30 x 30 cm FTO/glass conductive substrates. Large-scale electrochemical arrangements consisted of two FTO/glass substrates (one working electrode and one counter electrode) and a SCE (reference electrode). One glass tank was used to deposit the film and the other for cycling

experiments. The tanks were cleaned with concentrated nitric acid and then rinsed with Milli-Q® deionised water (18.2 MΩ cm) before all experimentation.

Figure 3.8. Image showing a one compartment electrochemical tank used for all large-scale experiments. The tank dimensions were 35 x 35 x 5 cm.

In order to optimise film uniformity, the working and counter electrodes were held parallel, 10 mm apart within the cell (figure 3.9). Prior to film preparation, adhesive copper tape was applied to the top 20 mm of each conducting substrate for a uniform electrical contact.

(a) (b)
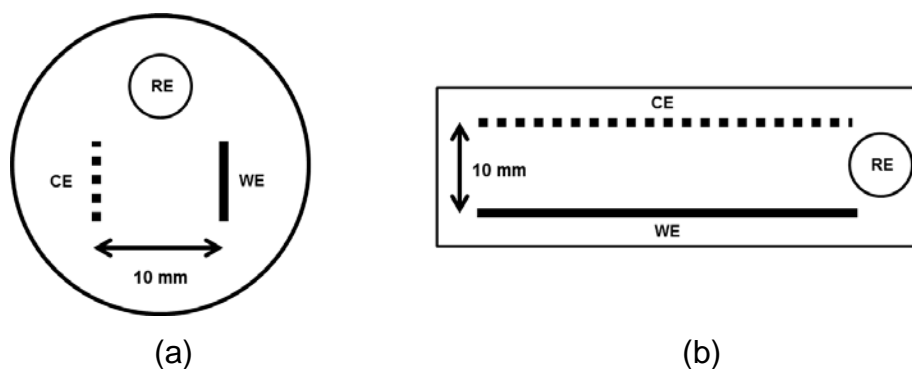
Figure 3.9. Overhead view of cell arrangement showing reference electrode (RE), counter electrode (CE) and working electrode (WE). (a) Small scale cell (5 cm diameter). (b) Large scale custom tank (35 x 5 cm dimensions).

3.5 Film characterisation

Various characterisation techniques were used to study the chemistry, morphology and structural properties of the deposited films. In this section, the experimental procedure for each technique is outlined.

3.5.1. Scanning electron microscopy

Scanning electron microscopy (SEM) was used to investigate the film chemistry, morphology and uniformity. The SEM used was a Leo 1530 Field Emission Gun Scanning Electron Microscope system with an energy dispersive X-ray spectroscopy (EDS) elemental analysis system. Nickel oxide-based films were deposited onto conducting glass using a range of deposition techniques. Before analysis the deposited films were washed with distilled water, dried in air and then mounted on SEM stubs using conducting silver paint. Samples were coated with a thin layer of gold to improve the conductivity of the films. A Polaron Emitech SC7604 sputter coater was used.

3.5.2. Atomic force microscopy

Atomic force microscopy (AFM) was used to study film morphology and average surface roughness. A Veeco Explorer system was used. Films were formed on different conducting substrates and submitted for analysis. The imaging was carried out in Tapping Mode (TM-AFM) using a high resonant frequency (HRF) at approximately 300 kHz - silicon probe. The scan frequency was 2 Hz.

The average surface roughness of the conductive substrates and the deposited films were also determined by AFM analysis. The average roughness was calculated as the mean value of the surface height ($\bar{Z}$) relative to the centre plane, which was determined by equating the volumes enclosed by the image of the surface above and below the plane (equation 3.1)[1]. Where (N) is the number of points in the sample area.

$$R_{avg} = \sum_{n=1}^{N} \frac{|Z_n - \bar{Z}|}{N} \qquad (3.1)$$

3.5.3. X-ray diffraction

Powder X-ray diffraction (XRD) data were collected to determine/identify the different phases of nickel oxide-based materials. A Bruker D8 Advance Powder Diffractometer fitted with a PSD detector operating with monochromated Cu Kα1 radiation (1.5406Å). X-ray data were collected of films deposited onto conducting substrates and of powders scraped from the substrate.

For electrochemical cathodic deposition, films were formed on a platinum or palladium flags by applying a current of -0.2 mA for 10 hours. The precipitate was then dried in air and the thin film was removed from the substrate to accumulate powder for XRD experiment. Powdered material was prepared by grinding in a pestle and mortar before placing in a plastic sample holder for analysis. Room temperature XRD patterns were collected in the 2θ range of 5° to 70°.

Thin films on conducting glass were also prepared for XRD analysis using electrochemical and aerosol assisted chemical vapour deposition (AACVD) techniques. Prior to collecting the data, the samples were mounted on perspex flat sample holders and data were collected for a 2θ range of 5 - 80° using a 0.00147° 2θ step.

All data collected were compared against patterns from the International Centre for Diffraction Data (ICDD) Powder Diffraction File (PDF).

3.6 Film formation

Nickel oxide-based thin films were deposited onto various electrodes by three different deposition techniques. The experimental procedures for each of these methods are outlined in this section.

3.6.1. Electrochemical cathodic deposition

Electrochemically hydrated NiO thin films were deposited by electrochemical cathodic deposition, in which aqueous nickel nitrate (0.01 mol dm^{-3}) solution was used to grow the films galvanostatically, according to the method of Carpenter *et al.*[2] Films were deposited using a chronopotentiometry technique (figure 3.10), where a fixed current density was applied and the potential versus time (seconds) was monitored. Co-deposited films were prepared using a mixed nitrate solution with a total metal concentration of 0.01 mol dm^{-3}. For single additive films, the deposition solution consisted of nickel nitrate (0.009 mol dm^{-3}) and the additive metal nitrate (0.001 mol dm^{-3}). For bimetallic additives, deposition solution consisted of nickel nitrate (0.0085 mol dm^{-3}), first additive metal nitrate (0.001 mol dm^{-3}) and second additive (0.0005 mol dm^{-3}). After depositing the film, it was washed with distilled water then immersed in KOH (0.1 mol dm^{-3}) for EC performance analysis.
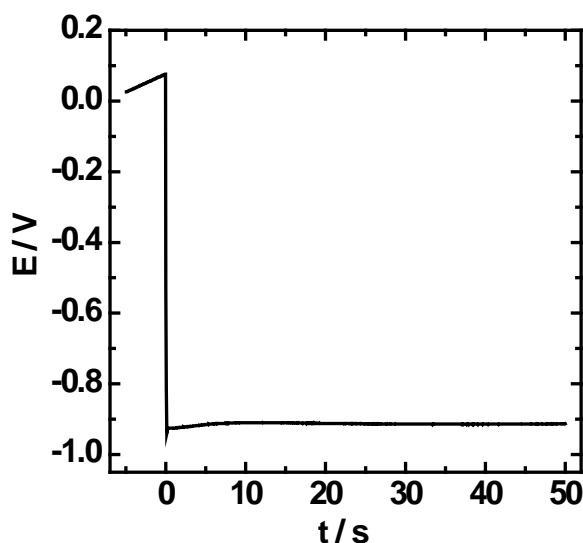
Figure 3.10. Potential-time transient for hydrated NiO film formation on ITO/glass. Deposition solution 0.01 mol dm^{-3} Ni(NO$_3$)$_2$, current -0.2 mA (-0.1 mA cm^{-2}), deposition time 50 seconds.

3.6.2. Aerosol assisted chemical vapour deposition (AACVD)

Nickel (II) acetylacetonate (0.05 mol dm^{-3}) was used as the source material for preparing NiO thin films. Precursor solution was prepared by heating and stirring

nickel acetylacetonate and 1 cm^3 of N,N-dimethylaminoethanol in toluene for 30 min then allowing the solution to cool to room temperature. The precursor solution was then placed above the piezoelectric modulator of an ultrasonic humidifier to atomise the solution into fine aerosol droplets. A schematic drawing of the AACVD with a two chamber configuration is illustrated in figure 3.11.

Using air as a carrier gas, the aerosol droplets were first transferred at a flow rate of 0.21 dm^3 min^{-1} into the first chamber where any large particles were separated and held. A second carrier gas (air) at a flow rate of 2.34 dm^3 min^{-1} was then used to direct the small particles towards the heated substrate, where they underwent evaporation, decomposition and chemical reaction to synthesise the desired films. The flow rate was controlled by a L1X linear flow meter. The substrate was heated to 450°C (FTO/glass is found to be stable to >1000°C) by placing it on a temperature controlled hot plate. Films were deposited for 10, 15 and 20 min and are abbreviated as NiO(10 min), NiO(15 min) and NiO(20 min) respectively.
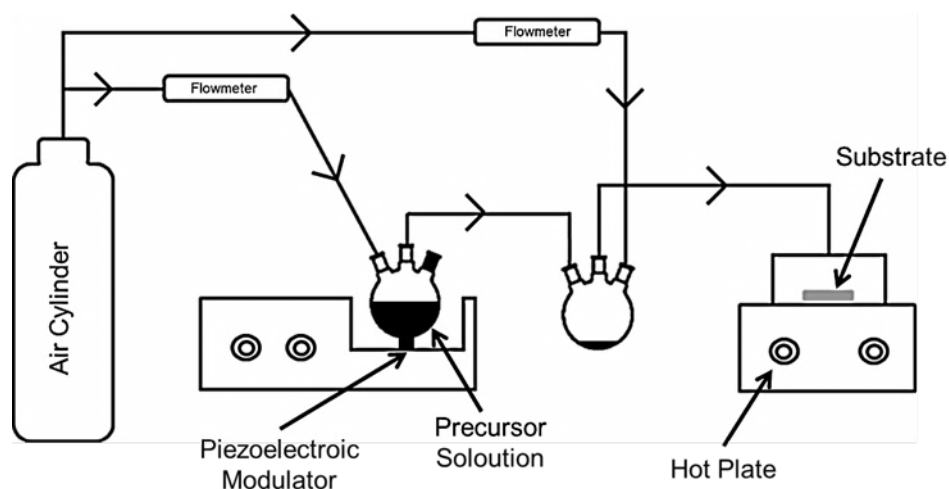

Figure 3.11. Schematic diagram of the experimental AACVD apparatus.

3.6.3. Electrostatic layer-by-layer (LbL) assembly

Layer-by-layer (LbL) assembly was conducted through electrostatic interactions, where the growth of different charged species (cationic and anionic species) leads to the formation of a multilayer structure.[3] Hydrated NiO nanoparticles were synthesised by mixing 10 cm^3 of nickel nitrate (0.01 mol dm^{-3}) aqueous solution with

200 μl of NH_4OH (1 mol dm^{-3}) in a sonication flask. A nanoparticle suspension was obtained by employing a direct immersion titanium horn immersed 1 cm into the mixture and irradiated with high intensity ultrasound radiation for 5 min. The resulting nanoparticle suspension was used as the anionic layer during LbL deposition.

Multilayer structure of hydrated NiO was deposited, by dipping the ITO/glass into a solution of Poly(allylamine hydrochloride) (PAH) (0.5 mol dm^{-3}) for 5 mins. The ITO/glass was then rinsed with deionised water and dried with N_2 gas. It was then placed in a hydrated NiO nanoparticles solution for 5 mins, washed and dried again. Multiple bilayers were created by repeating these steps (figure 3.12).
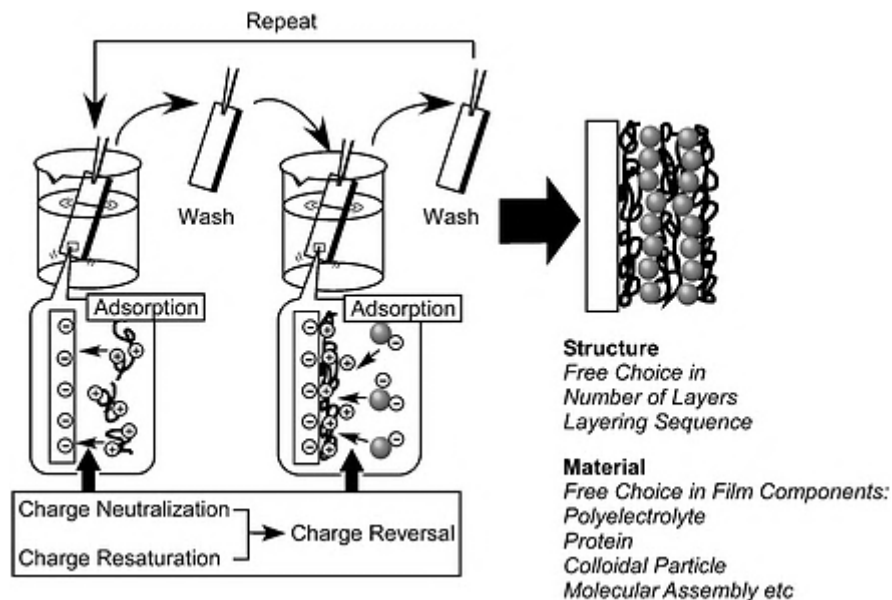
Figure 3.12. Schematic showing a layer-by-layer assembly through electrostatic interaction. Figure taken from.[4]

3.7 References

[1]   Boussu, K., Van der Bruggen, B., Volodin, A., Snauwaert, J., Van Haesendonck, C and Vandecasteele, C. Roughness and hydrophobicity studies of nanofiltration membranes using different modes of AFM. *J. Colloid Interface Sci.* **289**, 632-38.

3. Experimental

[2]   Carpenter, M. K., Conell, R. S. and Corrigan, D. A. The electrochromic properties of hydrous nickel oxide. *Sol. Energy Mater.*, **16**, 1987, 333-46.

[3]   Vidotti, M. and Córdoba de Torresi, S. I. Electrostatic layer-by-layer and electrophoretic deposition as methods for electrochromic nanoparticle immobilization. *Electrochim. Acta.*, **54**, 2009, 2800-4.

[4]   Ariga, K., Hill, J. P. and Ji, Q. Layer-by-layer assembly as a versatile bottom-up nanofabrication technique for exploratory research and realistic application. *Phys. Chem. Chem. Phys.*, **9**, 2007, 2319-40.

4. Preparation and optimisation of electrochromic nickel oxide-based thin films

4.1. Introduction

The most widely used methods for preparing electrochromic (EC) NiO-based ceramic thin films include sputtering,[1-3] electron-beam deposition[4] and thermal vacuum evaporation,[5] although these physical methods require expensive equipment. Other chemical methods such as sol-gel,[6] chemical bath[7] and hydrothermal deposition techniques[8] have also been investigated. Many of the methods described often use an extra step (extremely capital and energy intensive) to immobilise the material onto the substrate. This step can be eliminated by using electrochemical routes or an aerosol-assisted chemical vapour deposition (AACVD) technique, as the product is deposited directly onto the electrode in the form of a thin film. Furthermore, other methods have limited film composition control which can affect the film microstructure, resulting in the formation of products with undesired grains/thickness and strength. Using electrochemical routes, this problem can be easily overcome, as using varying bath compositions, controlling the current and potential applied through the cell you are able to synthesise ceramic materials with precise microstructures and engineering properties. In the case of the AACVD technique, low cost, high deposition rates and the ability to operate under varied environments at low pressure, or even in open atmosphere, make AACVD an ideal process for mass production.

This chapter will outline the preparation and optimisation of NiO-based film deposited by an electrochemical cathodic deposition and by an AACVD technique. Section 4.3 will highlight the effect of using different nickel salt baths on the nitrate reduction reaction for the deposition of hydrated NiO ($Ni(OH)_2$) thin films and to investigate at what potentials metallic nickel competes with hydrated NiO formation. The effect of deposition conditions such as deposition current, time of deposition, concentration of nickel nitrate and the use of different transparent conducting substrates will be

discussed in order to optimise the deposition of EC hydrated NiO. Section 4.6 will outline the preparation of NiO thin films by the AACVD technique, with the aim of enhancing the films' EC properties. Throughout the chapter, the emphasis will be on optimising two specific factors which are highly important to the functioning of EC smart windows; firstly, EC film uniformity which is important for any display application, as devices must show uniform colour change; secondly, the durability or the cycle life which is represented by the number of write-erase cycles that can be performed before any significant degradation. Finally, throughout the chapter various surface characterisation techniques which have been performed on the films will investigate the film structure, morphology and composition.

4.2. Hydrated NiO film preparation by electrochemical cathodic deposition

Preparation of ceramic thin films based on hydrated NiO was initiated according to the method of Carpenter *et al.*[9] Electrochemical cathodic deposition was achieved by applying a suitable electric current between two or more electrodes separated by a metal nitrate electrolyte. In general, precipitation takes place because of the increase of interfacial pH at the electrode/electrolyte interface, due to the electrochemical reduction of nitrate anions to generate hydroxide ions. As more hydroxide is electrogenerated, and the pH increases, the amount of metal hydroxide species present at the electrode will exceed its solubility limits and precipitation will occur (figure 4.1).

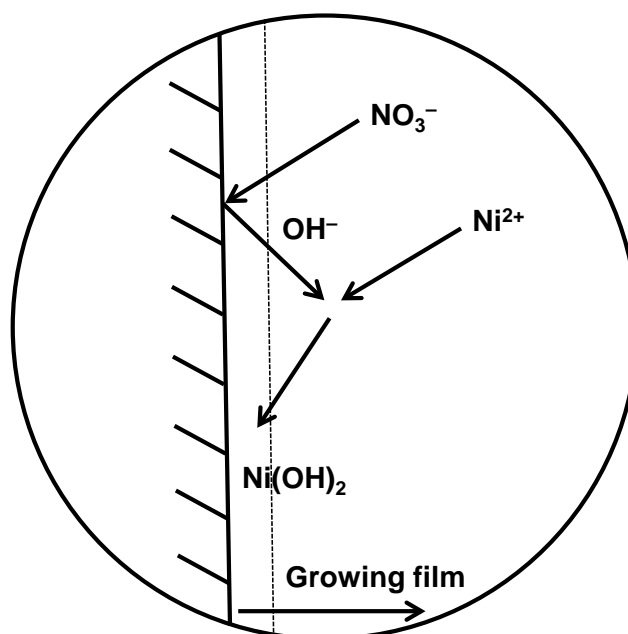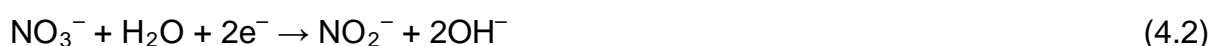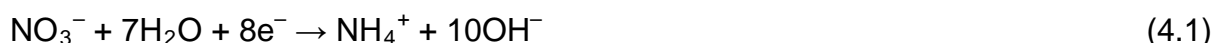# 4. Preparation and optimisation of electrochromic nickel oxide-based thin films

Figure 4.1. Schematic representation of the electrochemical cathodic precipitation of hydrated NiO. Diagram adapted from.[10]

The electrode deposition mechanism and the exact nature of the cathodic reaction have been investigated in detail. Most researchers have proposed that the deposition was due to an electrochemically induced pH change which resulted in the production of ammonium ions, according to equation 4.1.[11-14] On the other hand, others have postulated a nitrate reduction to nitrite (equation 4.2).[15,16] Although these reactions have different overall cathode reactions, the primary product is the generation of hydroxide ions which react further with Ni^{2+} to precipitate hydrated NiO directly onto the substrate according to equation 4.3.

$$NO_3^- + 7H_2O + 8e^- \rightarrow NH_4^+ + 10OH^- \tag{4.1}$$
$$NO_3^- + H_2O + 2e^- \rightarrow NO_2^- + 2OH^- \tag{4.2}$$
$$2OH^- + Ni^{2+} \rightarrow Ni(OH)_2 \tag{4.3}$$

4.3. Hydrated NiO deposition using $Ni(NO_3)_2$, $NiCl_2$ and $NiSO_4$

As previously mentioned, electrogeneration of hydroxide ions at the electrode occurs through the process of nitrate ion reduction. However, depending on the pH of the bath, choice of cathode material and deposition potential, the generation of

60

hydroxide ions may compete with the metal ion reduction reaction (equation 4.4). The process of nickel electroplating to obtain coatings for anti-corrosion[17] and decorative[18] applications is a well-known process in industry. However, for EC application the deposition of nickel presents a possible problem as it restricts the amount of active EC hydrated NiO from being deposited onto the substrate. Therefore, in this section, different nickel salt solutions were used to prepare hydrated NiO films, with the use of cyclic voltammetry (CV) and chronoamperometry techniques to determine the potentials at which metallic nickel competes with the hydrated NiO formation.

$$Ni^{2+} + 2e \rightarrow Ni \tag{4.4}$$

Figure 4.2 shows the potential-time transient for the deposition of hydrated NiO thin films on tin-doped indium oxide on glass (ITO/glass) using 0.01 mol dm^{-3} nickel nitrate, chloride and sulphate solutions. From the plot it is seen that when a fixed current density (-0.1 mA cm^{-2}) is driven, the working electrode potential moves to a value that can sustain that current. In this case, the deposition of hydrated NiO on ITO/glass takes place between -0.75 and -1.00 V vs. SCE. Having deposited the film, it was then transferred to an electrochemical cell containing aqueous KOH (0.1 mol dm^{-3}) electrolyte for electrochemical characterisation. Figure 4.3 (a) shows typical CVs of the hydrated NiO/oxy-hydroxide (NiOOH) redox process, one anodic peak (A_1), responsible for the oxidation (colouration) and one cathodic peak (A_2), for the reduction ('bleaching') process being observed. An increase in anodic current after +0.60 V (B) corresponds to the beginning of the oxygen evolution reaction (OER).

On comparison, the potential-time behaviour between the three different solutions is very similar (figure 4.2). However, on subsequent electrochemical cycling in KOH (0.1 mol dm^{-3}) electrolyte, the amount of electroactive material on the ITO/glass substrate varies as indicated by the different anodic and cathodic peak currents (figure 4.3 (a)). Film thickness was also measured by using the Faradaic charge density (q_f) for the oxidation and reduction process obtained by integrating the current-potential data between 0.2 to 0.5 V. Values of 3.46, 1.42 and 1.51 mC cm^{-2}, corresponding to approximately 15, 6 and 7 equivalent monolayers of hydrated NiO

were measured for films deposited using nickel nitrate, chloride and sulphate solutions, respectively.[†] The deposition of hydrated NiO films from chloride and sulphate baths show lower deposition efficiencies due to the absence of a nitrate reduction reaction. In the chloride and sulphate baths, the main source of hydroxide ions is the hydrogen evolution reaction (HER) (equation 4.5).[19] Figure 4.3 (b), (c) and (d) represents CVs for the hydrated NiO films in KOH (0.1 mol dm^{-3}) electrolyte recorded at different scan rates (5 - 150 mV s^{-1}). The anodic (insert in figure 4.3 (b), (c) and (d)) and cathodic peak currents increase with scan rate with a square root dependency, signifying the dominance of a diffusion process (figure 4.4 (b)), a typical response for a thin film which has been reported elsewhere.[16]

$$2H_2O + 2e^- \rightarrow H_2 + 2OH^- \tag{4.5}$$

Figure 4.4 (a) shows the CVs for a platinum flag electrode recorded in nickel nitrate, chloride and sulphate solutions at 50 mV s^{-1}. The CV recorded for nickel nitrate showed a cathodic peak (A) between 0.2 and -0.1 V which is a characteristic of the nitrate reduction process to generate base[16] (equation 4.1 or 4.2). For CVs recorded in the chloride and sulphate baths, this peak was absent to confirm that hydrated NiO formation in this case was primarily due to hydroxide ions formed via the HER. The effects of scan rate (20 to 200 mV s^{-1}) for a platinum flag electrode recorded in all three solutions are also reported (figure 4.4 (b), (c) and (d)). With nickel nitrate showing a diffusion controlled process for the cathodic nitrate reduction process, as indicated by a linear increase in the cathodic peak (between 0.2 and -0.1 V) currents with square root of scan rate (figure 4.4 (b) insert).[16] CVs recorded at different scan rates in nickel chloride and sulphate solutions, again lacked the characteristics for the nitrate reduction process, even at fast scan rates.

[†] From the hydrated NiO crystallographic data, an equivalent monolayer is about 1.4 x 10^{-9} mol cm^{-2}. By assuming a surface roughness factor for ITO/glass[20] of 1.6 and one-electron process between Ni(II)/Ni(III), this corresponds to a q_f value of approximately 0.224 mC cm^{-2}.
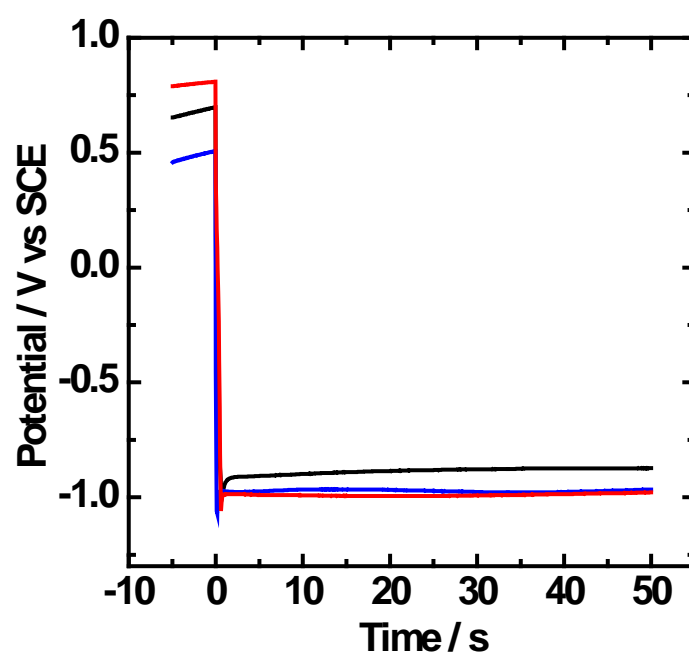
Figure 4.2. Potential-time transients for electrochemical cathodic deposition of hydrated NiO film on ITO/glass (electrode surface area = 30 x 7 mm) from 0.01 mol dm^{-3} solutions, with a current of -0.2 mA for 50 s. Deposition using nickel nitrate (—), nickel chloride (—) and nickel sulphate (—).
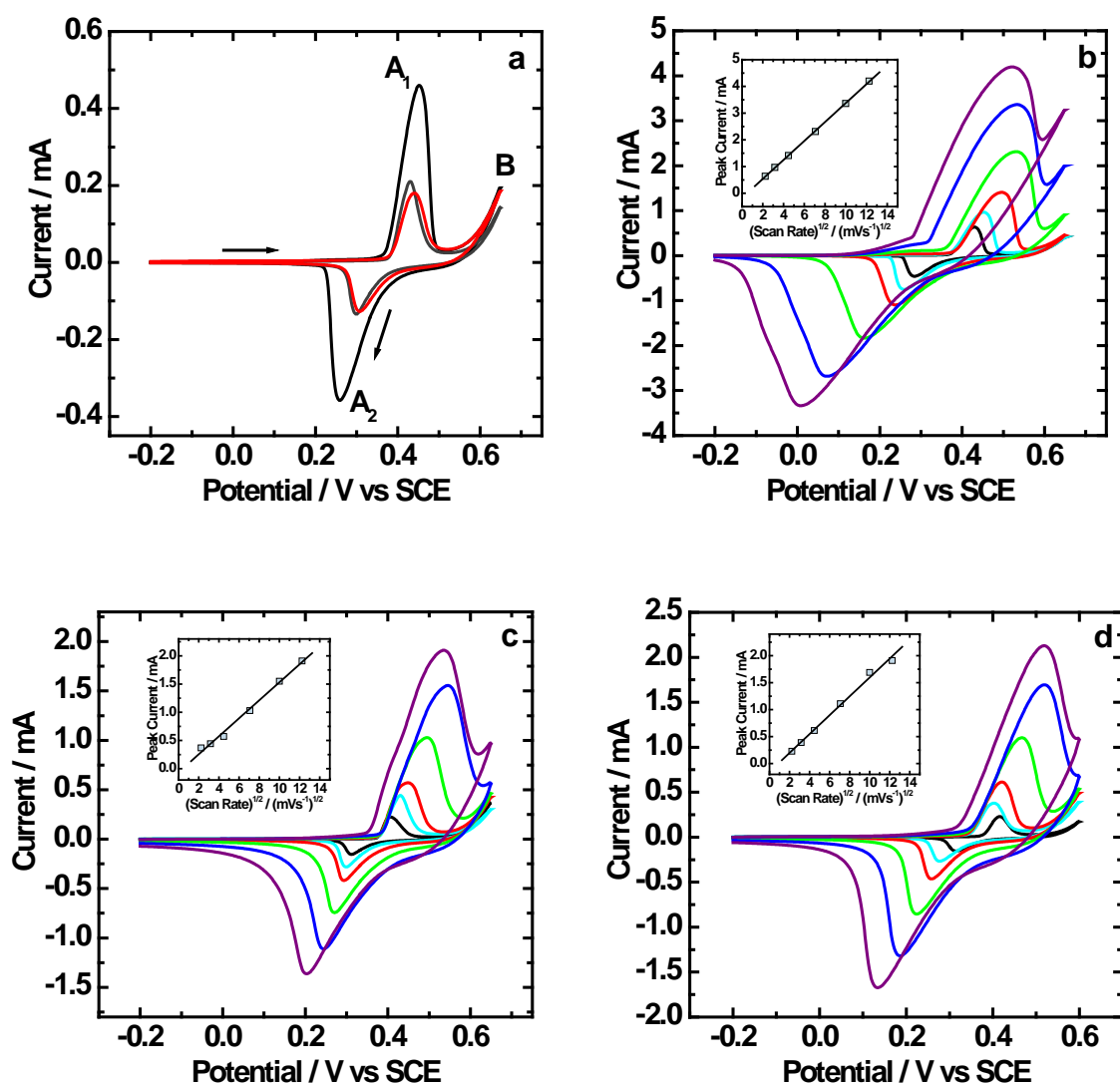
Figure 4.3. CVs for the oxidation and reduction process for the as-deposited hydrated NiO films deposited on ITO/glass from 0.01 mol dm^{-3} solutions of nickel nitrate (——), nickel chloride (——) and nickel sulphate (——) solutions followed by cycling in aqueous KOH (0.1 mol dm^{-3}) electrolyte at 10 mV s^{-1} (a) . CVs for the as-deposited hydrated NiO film on ITO/glass cycled in aqueous KOH (0.1 mol dm^{-3}) electrolyte at 5 (——), 10 (——), 20 (——), 50 (——), 100 (——) and 150 mV s^{-1} (——) deposited from 0.01 mol dm^{-3} solutions of nickel nitrate (b), nickel chloride (c) and nickel sulphate (d). The potential range was -0.20 V → +0.65 V → -0.20 V vs. SCE. The arrows in (a) indicate the direction of potential scan. Inserts in (b), (c) and (d) illustrate the anodic peak current vs. square roots of scan rate for 5, 10, 20, 50, 100 and 150 mV s^{-1}.

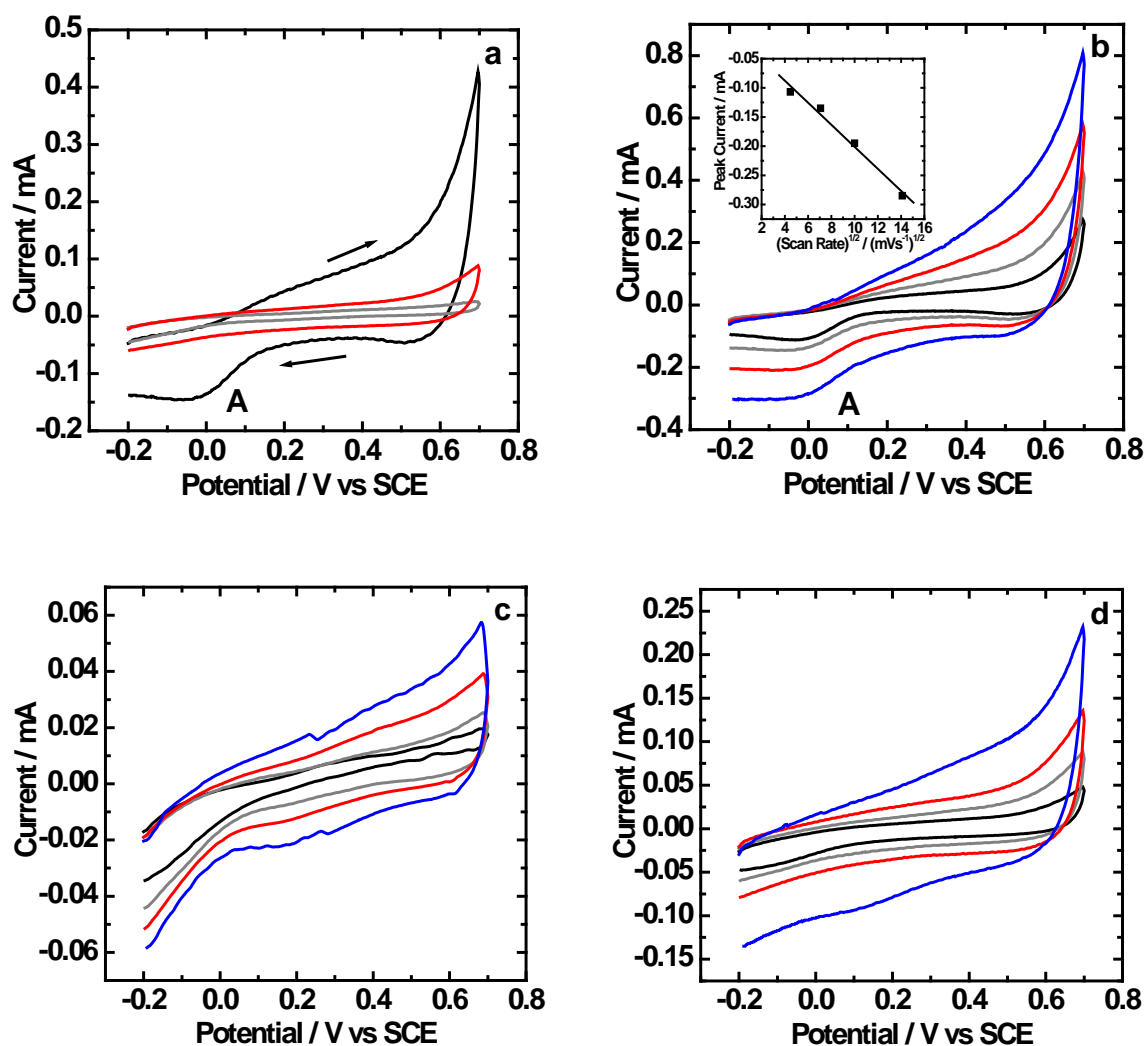# 4. Preparation and optimisation of electrochromic nickel oxide-based thin films

Figure 4.4. CVs for a platinum flag electrode (surface area = 20 x 20 mm) in 0.1 mol dm^{-3} nickel nitrate (——), nickel chloride (——) and nickel sulphate (——) at a scan rate of 50 mV s^{-1} (a), CVs at scan rates of 20 (——), 50 (——), 100 (——) and 200 mV s^{-1} (——) for a platinum flag electrode in nickel nitrate (0.1 mol dm^{-3}) (b), nickel chloride (c) and nickel sulphate (d). The potential range was -0.20 V → +0.70 V → -0.20 V vs. SCE. The arrows in (a) indicate the direction of potential scan. Insert in (b) illustrates the cathodic peak current vs. square roots of scan rate for 20- 200 mV s^{-1}.

Figure 4.5 shows photographs of the hydrated NiO films in the 'bleached' and coloured state for films deposited using nickel nitrate, chloride and sulphate solutions. The as-deposited films (figure 4.5 (photographs a)) prepared from all three nickel salt solutions showed contrasting film transparency and appearance. The as-deposited film prepared from nickel nitrate solution appeared fully transparent. On the other hand, the as-deposited films prepared by nickel chloride and sulphate solutions showed areas with patches of silver coloured deposits, typical of nickel

appearance. Upon potential switching by CV, the films were oxidised to the oxy-hydroxide form with the fully coloured state being formed (figure 4.5 (photographs b)). Comparing the coloured photographs showed that the film deposited from nickel nitrate produced a uniform brown-grey colouration but films from nickel chloride and sulphate showed a mixture of brown-grey coloured areas responsible for the oxidation of hydrated NiO together with the patches of the deposited nickel. These observations confirm that in the case of preparing films by nickel chloride and sulphate baths, a mixture of hydrated NiO and nickel deposition takes place, to produce non-uniform films.
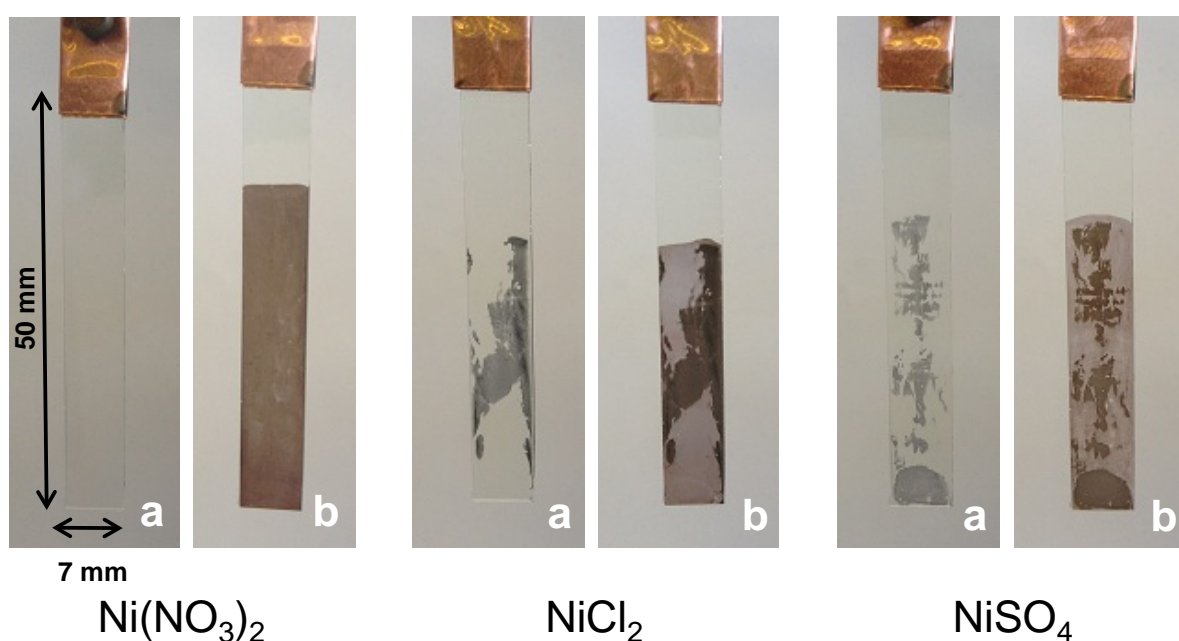
Figure 4.5. Photographs of hydrated NiO films deposited from different nickel salt solutions of 0.01 mol dm^{-3} concentrations. (a) As-deposited hydrated NiO films and (b) NiOOH film (film switched to the coloured state by cyclic voltammetry between –0.20 to +0.60 V vs. SCE at 10 mV s^{-1}, and then removal at +0.60 V). Films were deposited on the lower 30 mm length of each 7 mm width ITO/glass at an applied current of -0.2 mA for 500 s.

To examine the film surface morphology, micrographs were produced by a high resolution field emission gun scanning electron microscope (FEGSEM). The surface morphology of ITO/glass was typically of a smooth appearance (figure 4.6 (a)) and for hydrated NiO film on ITO/glass, a uniform open porous structure of interconnected flakes (figure 4.6 (b)), with a morphology in close agreement with that found by Carpenter *et al.*[9] Energy dispersive X-ray spectroscopy (EDS) elemental

analysis was also carried out to examine the film composition. In the case of films prepared from nickel nitrate solution, EDS elemental analysis confirmed the presence of nickel and oxygen as elements present in a hydrated NiO film. The presence of indium, tin, oxygen and silicon were due to the ITO/glass substrate. Prior to analysing, the films were coated with a thin layer of gold to improve their conductivity.
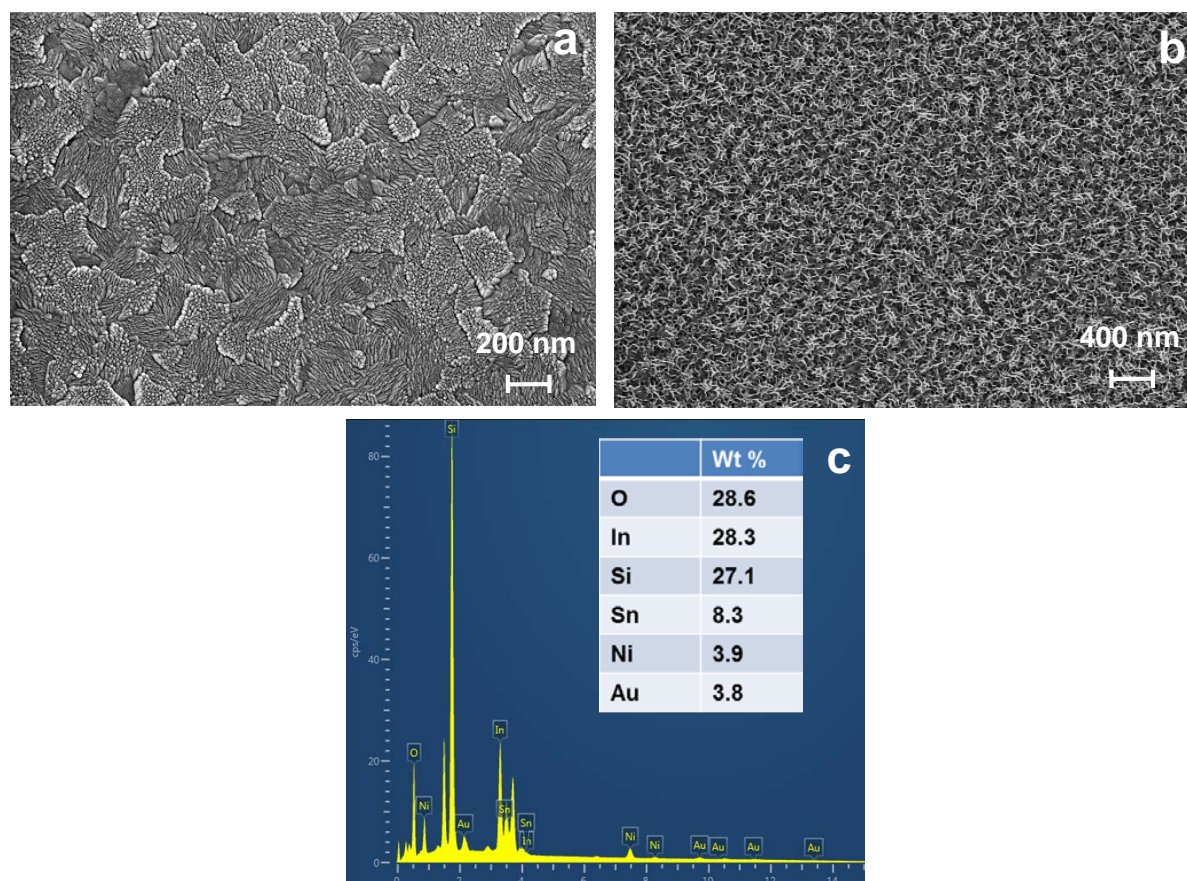

	Wt %
O	28.6
In	28.3
Si	27.1
Sn	8.3
Ni	3.9
Au	3.8

Figure 4.6. High resolution field emission gun scanning electron microscope (FEGSEM) images showing the surface of a bare ITO/glass substrate (a) and a hydrated NiO film deposited on ITO/glass using nickel nitrate (0.01 mol dm^{-3}) solution at an applied current of -0.2 mA for 500 s (b). An energy dispersive X-ray spectroscopy (EDS) analysis showing the chemical composition (Wt %) of the hydrated NiO film taken from (b).

Figures 4.7 (a) and 4.8 (a) shows the FEGSEM micrographs for films deposited using nickel chloride and sulphate baths, respectively. From the micrographs, it can be seen that using these two baths produced coexisting states with different areas of film morphology. The interconnecting flakes were representative of the hydrated NiO

phase and the nickel deposition being observed as the distribution of scattered granules with an average particle size of 500 nm. Furthermore, EDS elemental analysis (figures 4.7 and 4.8 (b) and (c)) at the two different states also confirmed that the higher weight percentage (Wt %) of nickel at the location of the granules was due to the presence of metallic nickel electrodeposition. These observations confirm that the non-uniform appearance for films prepared from nickel chloride and sulphate baths is due to the parallel formation of hydrated NiO and metallic nickel (figure 4.5).

The effect of applied potential on the formation of hydrated NiO and nickel electrodeposition was also investigated. Figure 4.9 and table 4.1 show the current-time behaviour and the corresponding FEGSEM micrographs for films deposited at different applied potential onto ITO/glass substrates from nickel nitrate, chloride and sulphate baths. In the case of films prepared from nickel nitrate, at applied potentials of between -0.5 and -0.8 V vs. SCE, the formation of hydrated NiO is induced. This is due to the basic environment (increasing pH) being created by the HER and nitrate reduction process at the electrode/electrolyte interface. The mechanism for nickel electrodeposition starts to coexist with hydrated NiO from -0.9 V, as indicated by the increase in current (figure 4.9 (a)) between 50 and 500 s and the FEGSEM micrograph (table 4.1), with the occurrence of a few nickel nucleation sites. Similarly for films prepared using nickel chloride, at potentials more positive than -0.8 V, the deposition of hydrated NiO with interconnecting flakes was observed. However, from -0.9 V, nickel deposition begins to coexist at the onset of HER and Ni^{2+}/Ni^{0} reactions running in parallel. The steady state increase in current (figure 4.9 (b)) after 50 s and the nucleation-growth of nickel nodules (1 μm) (table 4.1) at the surface of the film confirms the coexistence of both states. Finally, for films deposited using the nickel sulphate bath, the Ni^{2+}/Ni^{0} reactions begins to compete from an applied potential of -0.8 V (figure 4.9 (c)), with nickel deposition being observed from the micrographs at this potential (table 4.1).
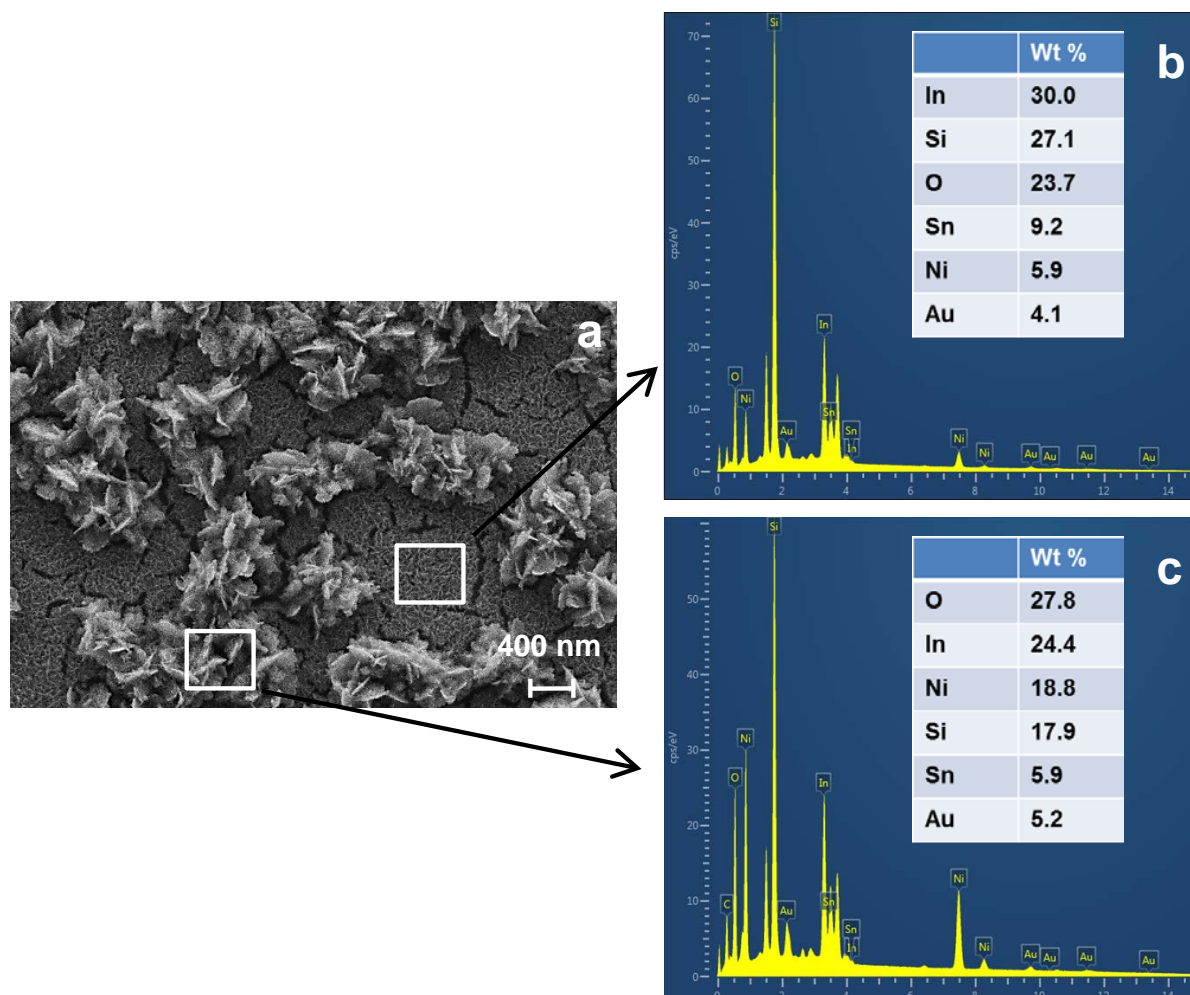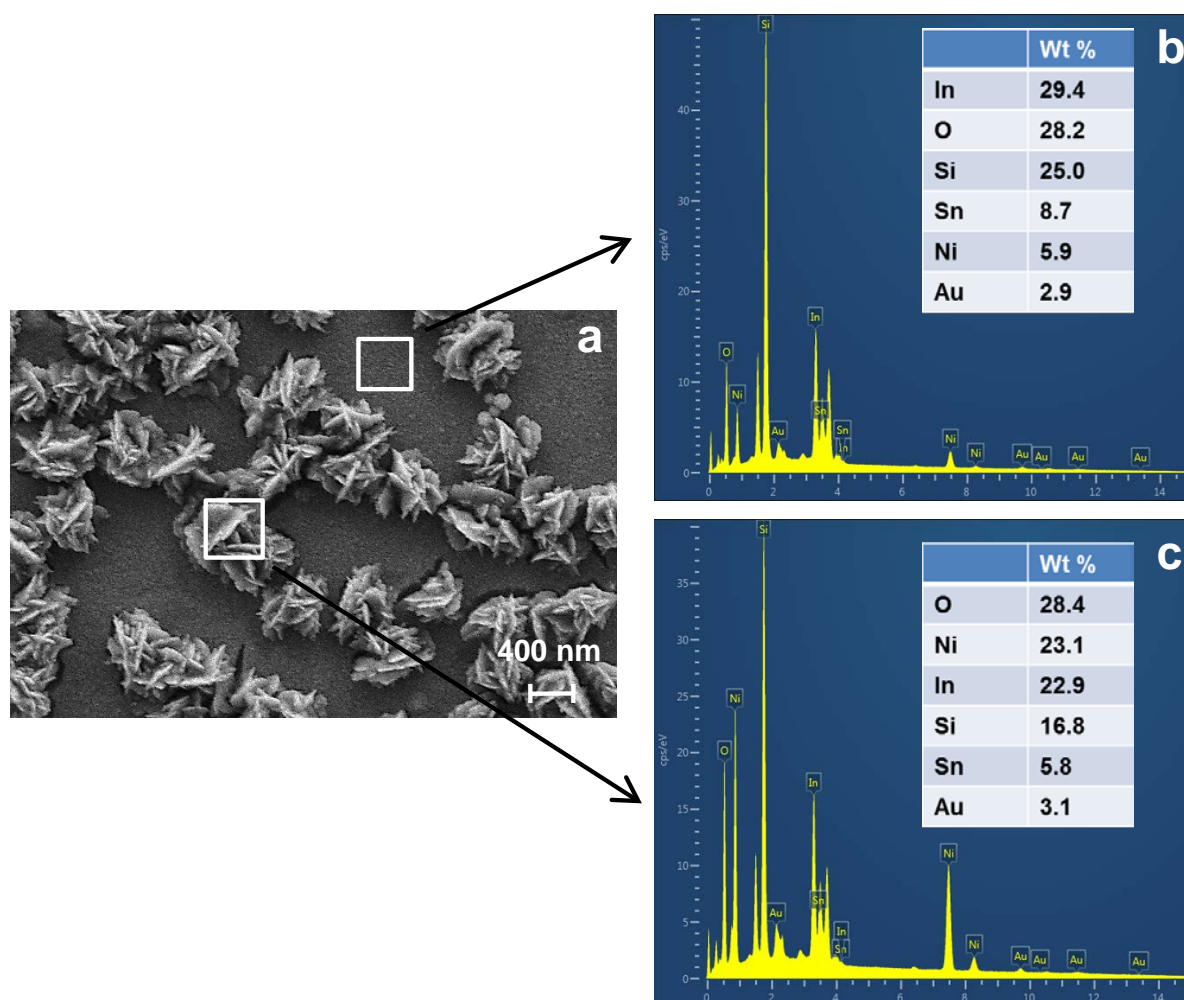
Figure 4.7. High resolution field emission gun scanning electron microscope (FEGSEM) image showing the surface of a hydrated NiO film deposited on ITO/glass using nickel chloride (0.01 mol dm^{-3}) solutions at an applied current of -0.2 mA for 500 s (a). An energy dispersive X-ray spectroscopy (EDS) analysis showing the chemical composition (Wt %) of the hydrated NiO film taken at two different points on the SEM micrograph (a), at a hydrate NiO film site (b) and at a nickel nucleation-growth site (c).

Figure 4.8. High resolution field emission gun scanning electron microscope (FEGSEM) image showing the surface of a hydrated NiO film deposited on ITO/glass using nickel sulphate (0.01 mol dm^{-3}) solutions at an applied current of -0.2 mA for 500 s (a). An energy dispersive X-ray spectroscopy (EDS) analysis showing the chemical composition (Wt %) of the hydrated NiO film taken at two different points on the SEM micrograph (a), at a hydrate NiO film site (b) and at a nickel nucleation-growth site (c).
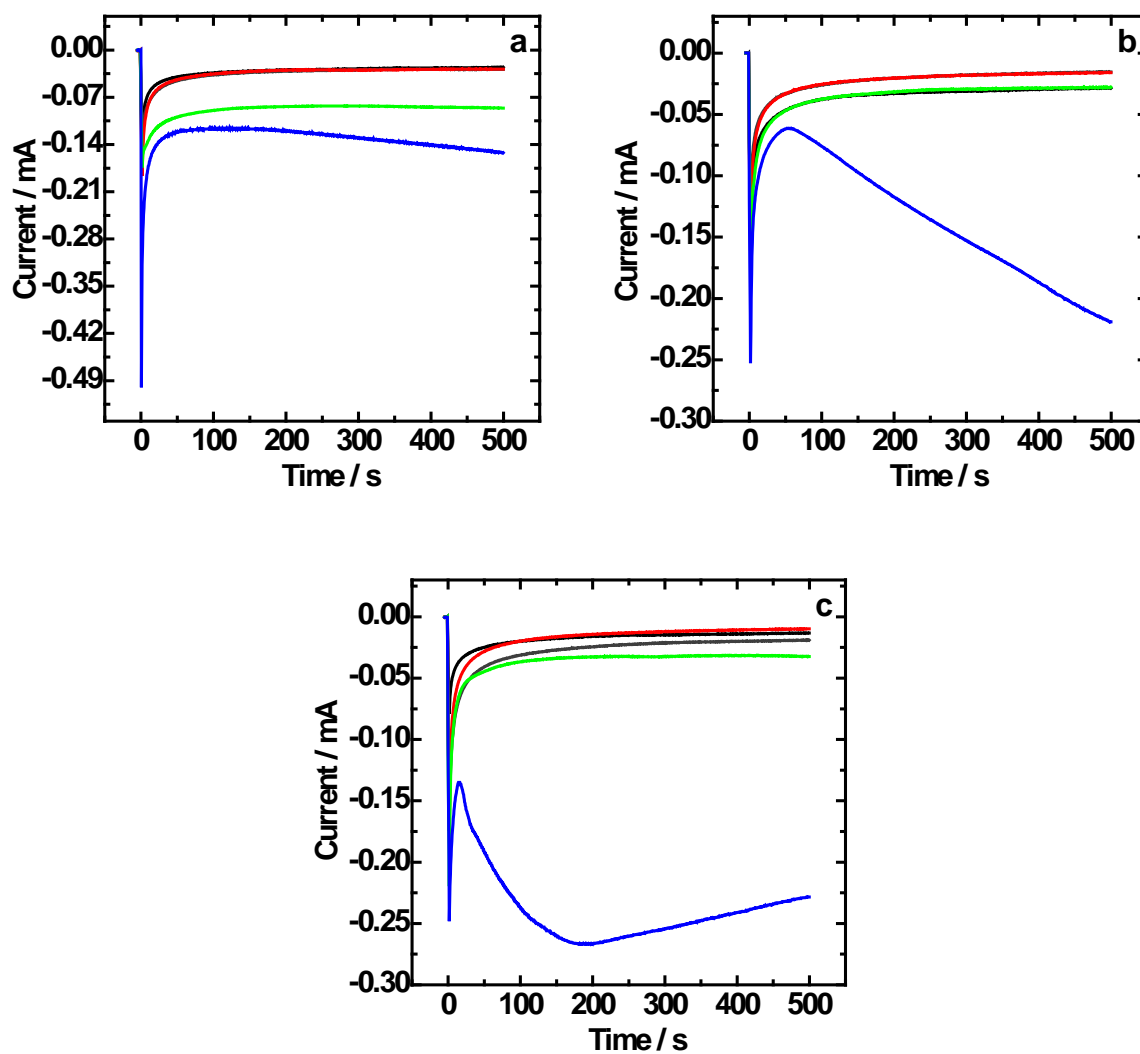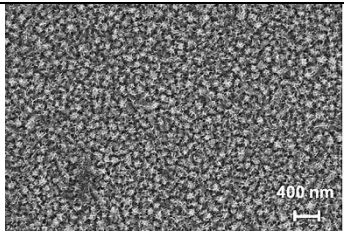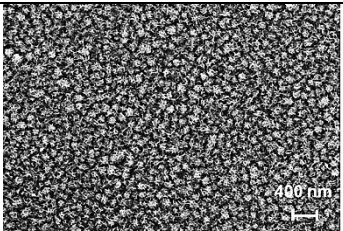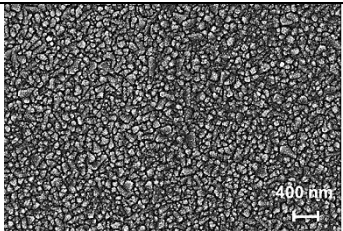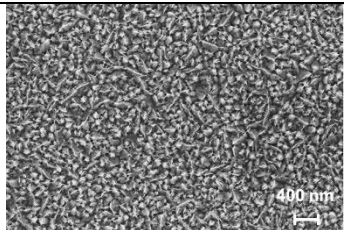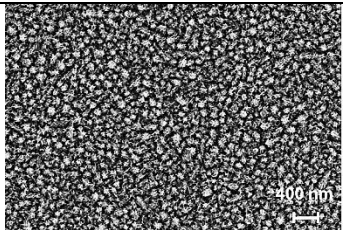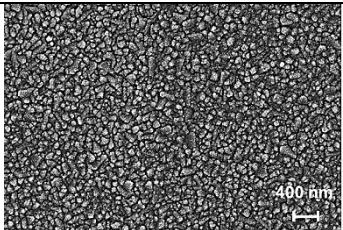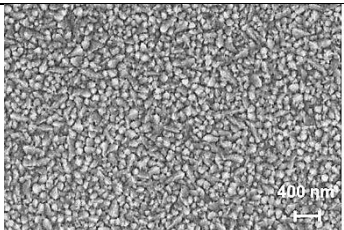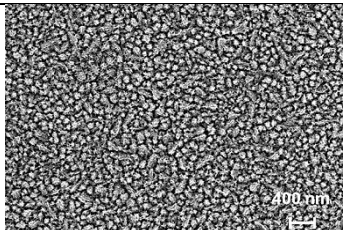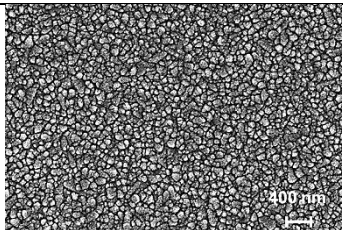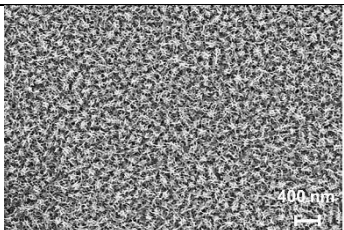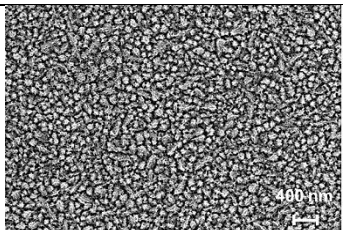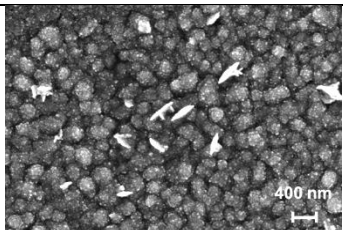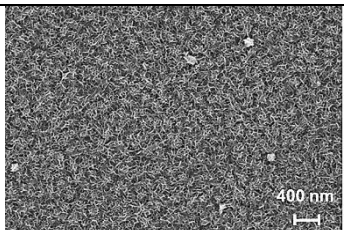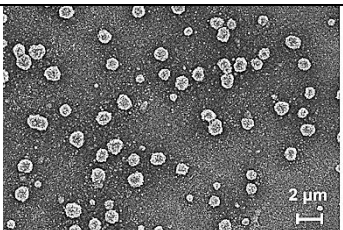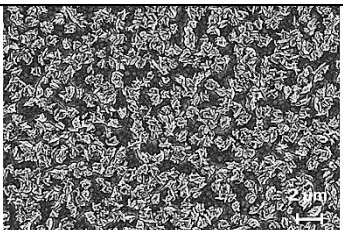
Figure 4.9. Current-time transients for the electrochemical cathodic deposition of hydrated NiO films from 0.01 mol dm^{-3} solution of nickel nitrate (a), nickel chloride (b) and nickel sulphate (c) at applied potentials of -0.5 (——), -0.6 (——), -0.7 (——), -0.8 (——) and -0.9 V (——) for 500 s.

Table 4.1. High resolution field emission gun scanning electron microscope (FEGSEM) images showing the surface of hydrated NiO films deposited on ITO/glass using 0.01 mol dm^{-3} solutions of nickel nitrate, chloride and sulphate at applied potentials of -0.5, -0.6, -0.7, -0.8 and -0.9 V for 500 s.

Deposition potential (V) vs. SCE	Ni(NO$_3$)$_2$ (0.01 mol dm^{-3})	NiCl$_2$ (0.01 mol dm^{-3})	NiSO$_4$ (0.01 mol dm^{-3})
-0.5			
-0.6			
-0.7			
-0.8			
-0.9			

4.3.1. Metallic nickel deposition

This section outlines the effect of different bath compositions for the electrodeposition of nickel. Before discussing any experimental results, it is important to understand the two independent processes that occur during nucleation-growth.[21] The first process involves several stages towards the formation and growth of a single nucleus of the metal, known as nucleation. These stages include:

- Transport of solvated metal ions through the solution to the electrode surface.
- Electron transfer
- Partial or complete loss of the solvation sheath to form an adatom.
- Surface diffusion of adatoms.
- Clustering of the adatoms to form a nucleus of sufficient size for it to be stable.
- Growth of the nucleus by incorporation of adatoms at favourable sites in the lattice structure of the metal.

The second process includes further important stages in the progress of crystal growth, as outlined below:

- Formation of nuclei.
- Growth of each isolated centre.
- Overlap of the expanding centres.
- Formation of a continuous layer over the whole cathode surface.
- Thickening of the complete layer.

In the case of nickel deposition on inert substrates (e.g. gold or glassy carbon), nickel atoms are initially deposited onto which the individual crystals of nickel will grow. This process approach is based on a widely used first order rate expression for nucleation (equation 4.6).[22]

$$N(t) = N_0 \{1 - \exp(-At)\} \tag{4.6}$$

4. Preparation and optimisation of electrochromic nickel oxide-based thin films

Where N(t) is the number density, N_0 is the total number of sites where nuclei can form and A is the rate constant for nucleation.

Figure 4.10 shows a set of CVs recorded using a Au working electrode in nickel nitrate, chloride and sulphate solutions for the deposition and stripping of nickel. For nickel nitrate electrolyte (figure 4.10 (a)), the potential range was 0.60 V → -0.70 V → 0.60 V vs. SCE. A predominant cathodic current attributed to the HER was produced between -0.40 and -0.70 V with bubbling being observed at the electrode surface. After completing the cycle, there was no indication of nickel deposit on the surface of the Au electrode, also the CV (figure 4.10 (a)) produced did not show any characteristics for the deposition and stripping process. In the case of nickel chloride and sulphate electrolytes (figure 4.10 (b)), the potential range was 0.60 V → -1.10 V → 0.60 V vs. SCE, two cathodic and one anodic peaks were produced. Peak A_1 was again was due to the HER, however, previous studies have also suggested that the large negative current is due to the onset of simultaneous nickel deposition and HER.[23] Peak A_2 in the region of -0.70 V and peak B in the region of -0.40 V was due to the deposition and stripping of nickel, respectively.
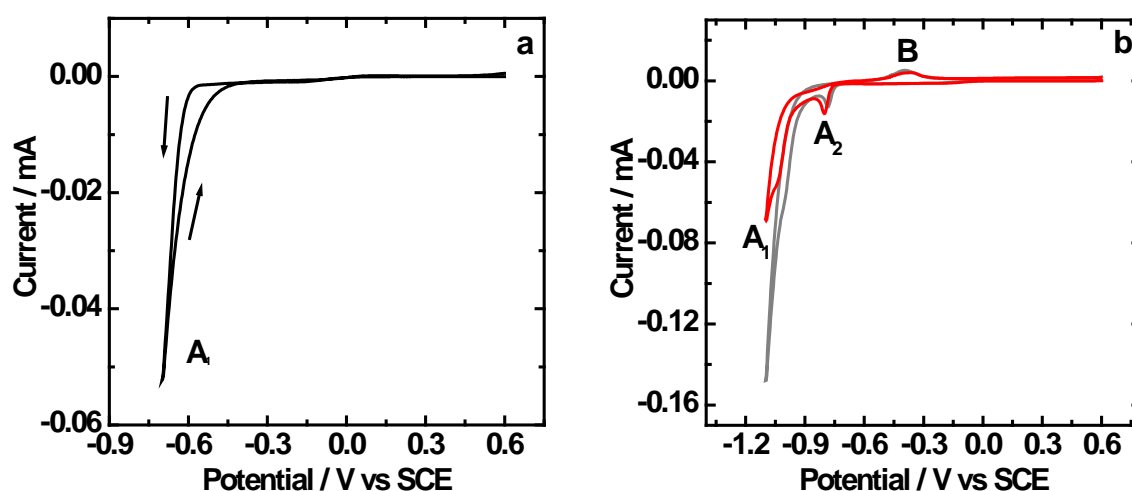
Figure 4.10. CVs for a gold BASi electrode (surface area = 0.0201 cm^2) in 0.1 mol dm^{-3} solutions of nickel nitrate (a), nickel chloride (——) and nickel sulphate (——) (b) electrolyte at a scan rate of 10 mV s^{-1}. The arrows in (a) indicate the direction of potential scan.

For comparison, figure 4.11 shows typical examples for the deposition and stripping of zinc and copper metal. One cathodic peak for the deposition and one anodic peak

for the stripping process can been seen clearly from the voltammograms. Stopping the CV just after the deposition potentials produced a silver shiny and red-brown deposit for both zinc (-1.30 V) and copper (-0.30 V), respectively. In an attempt to achieve nickel nucleation-growth process, these experimental conditions were repeated using different concentrations of $NiSO_4$ in K_2SO_4 (0.5 mol dm^{-3}) electrolyte on a glassy carbon electrode. Similarly to the zinc and copper, a sharp cathodic peak was observed for the deposition process (figure 4.12). However, the anodic stripping peak which corresponds to the amount of material deposited on the electrode during the forward sweep was absent. Furthermore, stopping the CV just after the deposition potential (-1.15 V) did not show any signs of nickel nucleation.
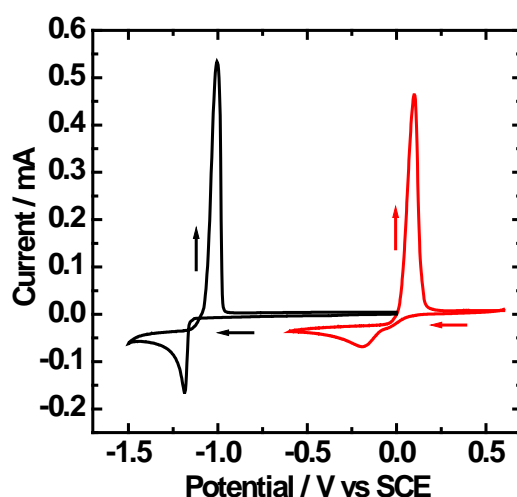
Figure 4.11. CVs for metal deposition and stripping on a glassy carbon BASi electrode. Zinc deposition using $ZnSO_4$ (10 mmol dm^{-3}) in K_2SO_4 (0.5 mol dm^{-3}) electrolyte (——) and copper deposition using $CuSO_4$ (10 mmol dm^{-3}) in K_2SO_4 (0.5 mol dm^{-3}) electrolyte (——) at a scan rate of 50 mV s^{-1}. The potential range for zinc deposition was 0.00 V → -1.50 V → 0.00 V vs. SCE and for copper deposition was 0.60 V → -0.60 V → 0.60 V vs. SCE. The arrows indicate the direction of potential scan.

When compared to the electrodeposition of zinc and copper, the process of nickel deposition is found to be more complex, with simultaneous hydrogen evolution playing a key role towards inhibiting the deposition process. Previous studies have discussed the influence of bath composition on improving the rate of deposition. In particular, the role of boric acid, which is shown to be an important component for facilitating deposition by acting as a catalyst to lower the overpotential of nickel

deposition.[24] Another study has also suggested that the buffering action of boric acid by reducing the pH near the electrode-electrolyte interface prevents the precipitation of hydrated NiO and increases the efficiency of nickel deposition.[25] A commercially available method used in the electroplating industry for nickel electrodeposition is the Watts-type plating bath.[26] figure 4.13 (a) shows a CV for a glassy carbon electrode cycled in a Watts bath composition. Two distinct peaks were observed, one during the cathodic scan and one on reversal for the anodic scan for the deposition and stripping process respectively. Additionally, upon stopping the scan just after the deposition potential (-1.10 V) changed the appearance of the uncoated glassy carbon (figure 4.13 (b)) from a black to a bright silver colour (figure 4.13 (c)), to confirm the successful nickel deposition.

Another simple technique to establish nucleation-growth by triangular scans of potential was described by Fletcher *et al.*[27] In this study, the authors showed that this treatment can be applied in two cases, namely rate control by interfacial kinetics and rate control by hemispherical diffusion. It was concluded that for both cases a current maximum should occur on reverse scans of triangular scans of potentials, known as nucleation loops. This technique was used to examine the nickel nucleation-growth using nickel chloride in boric acid on a glassy carbon electrode. Figure 4.14 shows the presence of a nucleation loop, characterised in this case as an irreversible growth.[27]

4. Preparation and optimisation of electrochromic nickel oxide-based thin films
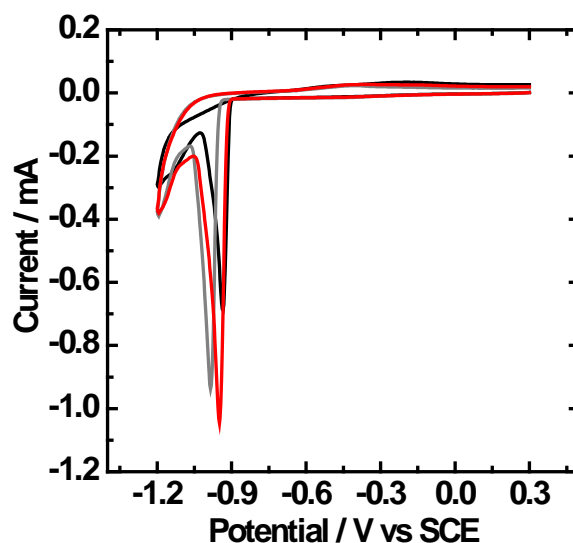
Figure 4.12. CVs for nickel deposition from different concentrations of $NiSO_4$ on a glassy carbon BASi electrode at a scan rate of 50 mV s^{-1}. $NiSO_4$ (20 mmol dm^{-3}) in K_2SO_4 (0.5 mol dm^{-3}) electrolyte (——), $NiSO_4$ (30 mmol dm^{-3}) in K_2SO_4 (0.5 mol dm^{-3}) electrolyte (——) and $NiSO_4$ (40 mmol dm^{-3}) in K_2SO_4 (0.5 mol dm^{-3}) electrolyte (——). The potential range was 0.30 V $\rightarrow$ -1.20 V $\rightarrow$ 0.30 V vs. SCE.
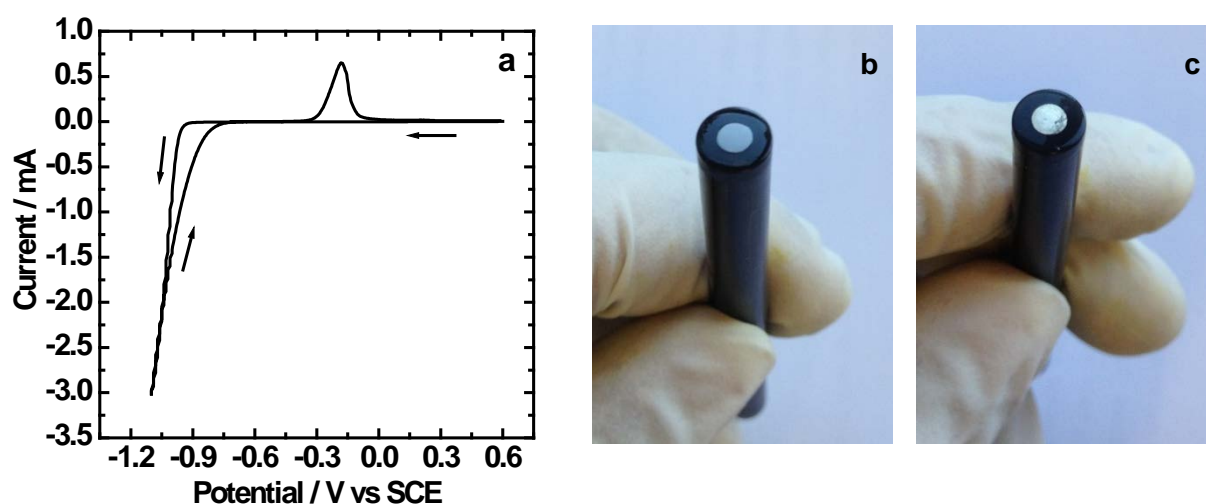
Figure 4.13. CVs for nickel deposition using a Watts electroplating bath (($NiSO_4$ (0.85 mol dm^{-3}), $NiCl_2$ (0.15 mol dm^{-3}) and H_3BO_3 (0.55 mol dm^{-3})) on a BASi glassy carbon electrode at 50 mV s^{-1} (a). Photographs showing uncoated electrode (b) and electrode coated with a bright nickel deposit (deposit achieved by cyclic voltammetry between 0.60 to -1.10 V vs. SCE at 50 mV s^{-1}, and then removal at -1.10 V) (c). The arrows in (a) indicate the direction of potential scan.

4. Preparation and optimisation of electrochromic nickel oxide-based thin films
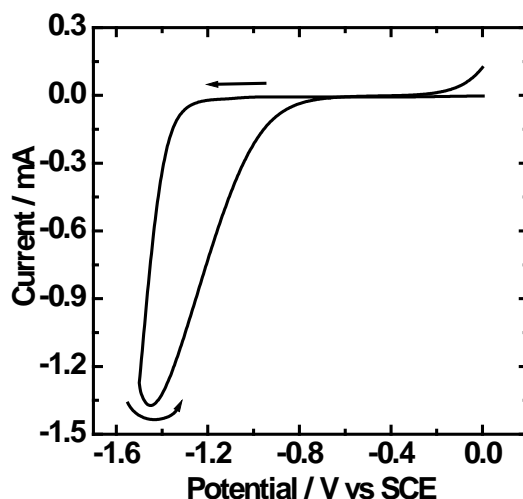
Figure 4.14. CVs for nickel deposition using $NiCl_2$ (1.00 mol dm^{-3}) in H_3BO_3 (0.70 mol dm^{-3}) (b) at 100 mV s^{-1} on a BASi glassy carbon electrode. The arrows indicate the direction of potential scan.

4.4. Optimisation of hydrated NiO films prepared by electrochemical cathodic deposition

Optimisation of deposition conditions and the subsequent cycling in basic (KOH) electrolyte of hydrated NiO films have been the subject of previous studies.[13, 28-30] Streinz et al.[28] utilised an electrochemical quartz crystal nanobalance (EQCN) to measure the mass of hydrated NiO films prepared from nickel nitrate solutions. They looked at the effect of deposition time, applied current and nickel nitrate concentration on the electrochemical deposition rate. Their results showed that the deposited mass increased proportionally with both time and current. However, the rate of deposition was significantly reduced when depositing hydrated NiO films from high nickel nitrate concentration (above 0.1 mol dm^{-3}) baths. It was concluded that at high concentrations the utilisation efficiency of the hydroxide ions was significantly less than 100 % (approximately 20%) and the formation of an alternative soluble cluster ion complex $[Ni_4(OH)_4]^{4+}$ was favoured, which diffused away from the reaction interface before deposition could occur. Subbaiah and co-workers[29] also considered the effects of applied current density on the particle size for battery applications. They found the grain size to increase with increasing current density. To date, there is no apparent work on the effect of different deposition conditions towards optimising the film uniformity and durability. Therefore, in this section, the

78

4. Preparation and optimisation of electrochromic nickel oxide-based thin films

effect of a number of deposition factors, including deposition current, time, nickel nitrate concentration and use of different transparent conducting substrates will be discussed, with the aim of producing uniform and durable deposits.

4.4.1. Effect of fixed current

Figure 4.15 (a) and (b) shows the effect of applied currents on the CVs and the corresponding visible region absorbance spectra (oxidised brown-grey coloured) of the as-deposited hydrated NiO films. For films deposited between -0.1 and -0.4 mA (-0.05 and -0.2 mA cm^{-2}), an increase in both the peak currents and the absorbance of the oxidised state was observed. Similar results were also reported by Streinz *et al.*[28] who found that the deposition rate increased proportionally with applied current. This relationship can be expressed by considering equations 4.1 and 4.2. As the number of hydroxide ions generated is related to the number of electrons available therefore, using Faraday's law the number of electrons available can be directly related to the applied deposition charge.

Figure 4.16 shows the photographs of the oxidised (coloured) and the reduced ('bleached') states as well as the FEGSEM images of the hydrated NiO films deposited onto ITO/glass. Films deposited at low applied currents (-0.1 to -0.4 mA) showed a uniform brown-grey colouration upon switching in KOH (0.1 mol dm^{-3}) electrolyte. From the FEGSEM images, it can be seen that the surface morphologies of the films showed a typical open porous structure of interconnected flakes which is similar to that reported by Carpenter *et al.*[9] This porous nature of the film allows the facilitation of hydroxide ions insertion/extraction thus leading to enhanced reversible EC performance.

Films prepared at an applied current of -0.8 mA showed an irreversible response (figure 4.15 (a)), with reduced peak currents and a lower absorbance value than those deposited at -0.2 and -0.4 mA (insert figure 4.15 (b)). Furthermore, the photographs in figure 4.16 showed the colouration state to be present both after the oxidation and reduction process. This irreversible behaviour can be explained by analysing the surface morphology of the as-deposited film (figure 4.16, FEGSEM

4. Preparation and optimisation of electrochromic nickel oxide-based thin films

image (d)). At high deposition current, the surface of the film appears non-porous with a grainier morphological nature which would reduce the efficiency of the hydroxide insertion/extraction process. Hence resulting in an irreversible redox system with reduced EC performance.
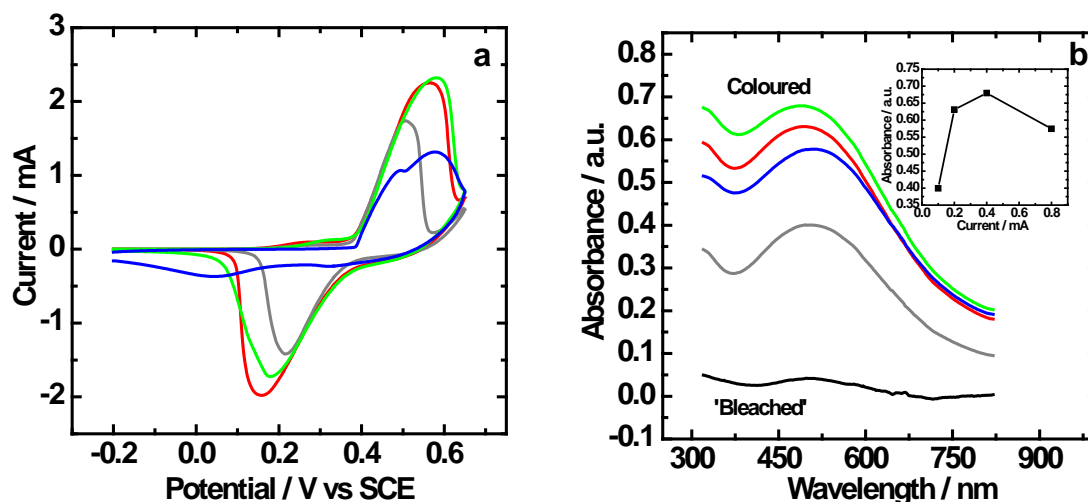
Figure 4.15. CVs for the oxidation and reduction process for the as-deposited hydrated NiO films deposited on ITO/glass from 0.01 mol dm^{-3} solution of nickel nitrate at -0.1 mA (——), -0.2 mA (——), -0.4 mA (——) and -0.8 mA (——) for 300 s followed by cycling in aqueous KOH (0.1 mol dm^{-3}) electrolyte at 10 mV s^{-1} (a). The potential range was -0.20 V → +0.65 V → -0.20 V vs. SCE. Visible region absorbance spectra of the as-deposited hydrated NiO in the 'bleached' state (——) (which was similar for all the films deposited at different currents) and coloured (brown-grey) state of films deposited at -0.1 mA (——), -0.2 mA (——), -0.4 mA (——) and -0.8 mA (——) (b). Coloured UV-vis spectra were recorded after oxidising (-0.20 V → +0.65 V vs. SCE) the films then removing them from the KOH electrolyte and measuring the absorbance against a blank ITO/glass. Inserts in (b) illustrate the absorbance at maxima (λ_{max} = 490 nm) vs. applied currents.

-0.1 mA 300 s   **-0.2 mA 300 s**   **-0.4 mA 300 s**   **-0.8 mA 300 s**
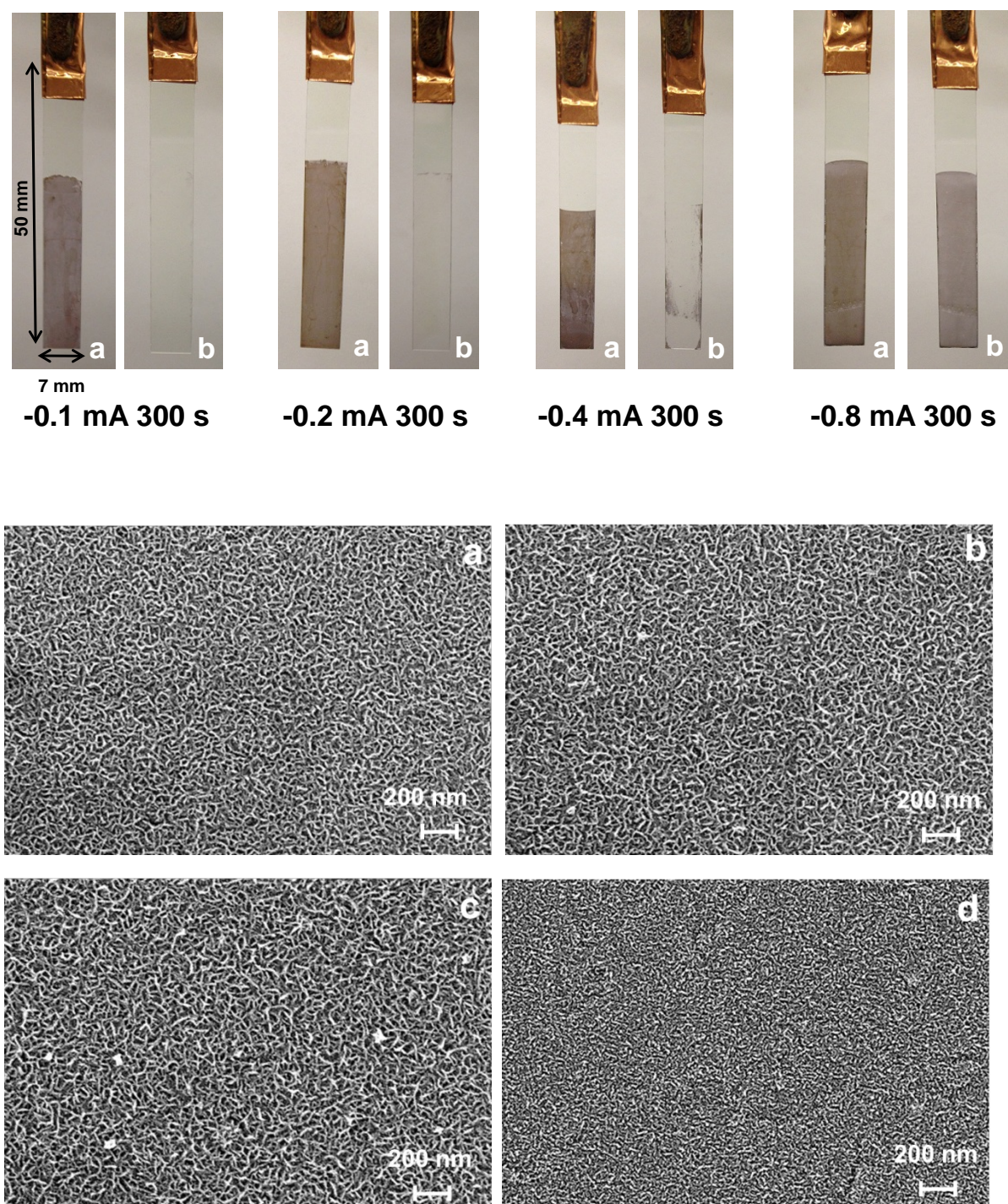
Figure 4.16. Above: Photographs of hydrated NiO films deposited from nickel nitrate solutions (0.01 mol dm^{-3}) at different applied currents for 300 s. (a) NiOOH film (film switched to the coloured state by cyclic voltammetry between –0.20 to +0.65 V vs. SCE at 10 mV s^{-1}, and then removed at +0.65 V) and (b) reduced hydrated NiO film. Films were deposited on the lower 30 mm length of each 7 mm width ITO/glass. Below: High resolution field emission gun scanning electron microscope (FEGSEM) images showing the surface of the hydrated NiO films deposited on ITO/glass from nickel nitrate (0.01 mol dm^{-3}) solution at applied currents of -0.1 mA (a), -0.2 mA (b), -0.4 mA (c) and -0.8 mA (d) for 300 s.

4. Preparation and optimisation of electrochromic nickel oxide-based thin films

4.4.2. Effect of deposition time

Figure 4.17 (a) and (b) shows the effect of deposition time on the CVs and the corresponding visible region absorbance spectra (oxidised brown-grey coloured) of the as-deposited hydrated NiO films. The anodic and cathodic peak currents and the absorbance increased linearly (insert figure 4.17 (b)) with an increase in deposition time, with more electroactive material being deposited. Furthermore, photographs of the oxidised (coloured) state show an increased tone of uniform colour change to the brown-grey form with increasing deposition time (figure 4.18 pictures (a)). The films deposited for 100 and 400 s showed a completely reversible response, with full transparency being achieved after film reduction (figure 4.18 pictures (b)). However, in the case of film deposited for 800 s, the film still showed signs of brown-grey colouration at the edge of the ITO/glass substrate.

In an attempt to establish the film thickness, cross-sectional FEGSEM images were taken of the samples. However, as the films were very thin, the FEGSEM instrument was not able to produce suitable focused images down to the required magnification. Therefore, film thickness was calculated using Faraday's law by integrating the current under the oxidation peak (figure 4.17 (a)). Calculated film thicknesses were approximately 17, 52 and 82.5 nm for hydrated NiO films deposited at -0.2 mA for 100, 400 and 800 s, respectively. An illustrative calculation is shown for hydrated NiO film deposited on ITO/glass at -0.2 mA for 800 s.

The moles of hydrated NiO was:

$$\frac{charge/number\ of\ electrons\ in\ process}{Faraday's\ constant} = \frac{70.52 \times 10^{-3}/1}{96485} = 7.3 \times 10^{-7}\ mol \qquad (4.7)$$

The mass of hydrated NiO was:

$$mass = moles \times M_r = 7.3 \times 10^{-7} \times 92.70808 = 6.8 \times 10^{-5}g \qquad (4.8)$$

ITO/glass surface area = 2.1 cm^2

4. Preparation and optimisation of electrochromic nickel oxide-based thin films

$$\frac{6.8 \times 10^{-5}}{2.1} = 3.3 \times 10^{-5} \ g \ cm^{-2} = 0.033 \times 10^{-3} \ mg \ cm^{-2}$$

Hydrated NiO density = 4 g/cm^3

$$\frac{mass}{volume} = \frac{0.033 \times 10^{-3}}{4} = 8.25 \times 10^{-6} \ cm = 8.25 \times 10^{-8} \ m = 82.5 \ nm \qquad (4.9)$$

Figure 4.18 also shows the surface morphologies of the deposited films. From the FEGSEM images, it can be seen that with increasing deposition time the films' porosity also increased with the interconnecting flake-like structure growing vertically.
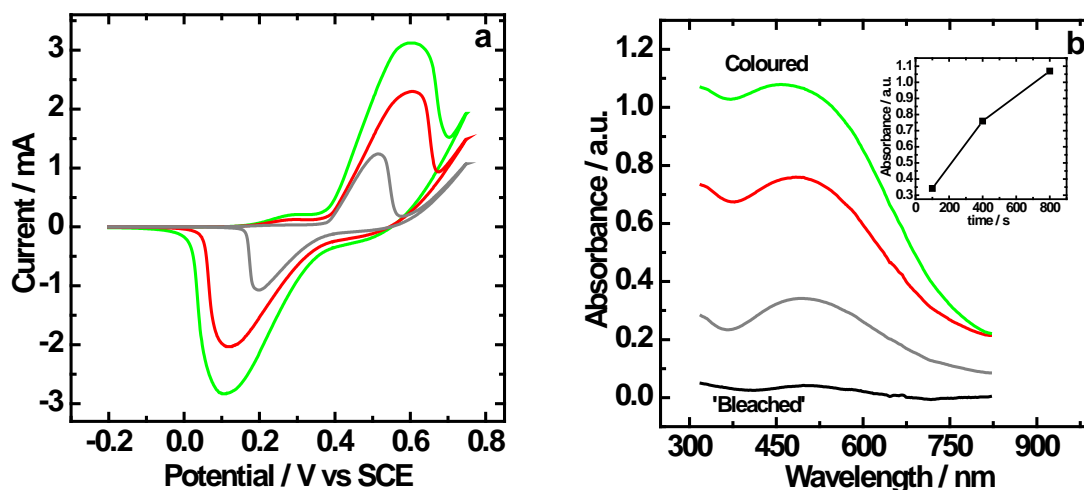
Figure 4.17. CVs for the oxidation and reduction process for the as-deposited hydrated NiO films deposited on ITO/glass from 0.01 mol dm^{-3} solution of nickel nitrate at -0.2 mA for 100 s (——), 400 s (——) and 800 s (——) followed by cycling in aqueous KOH (0.1 mol dm^{-3}) electrolyte at 10 mV s^{-1} (a). The potential range was -0.20 V → +0.75 V → -0.20 V vs. SCE. Visible region absorbance spectra of the as-deposited hydrated NiO in the 'bleached' state (——) (which was similar for all the films deposited at different currents) and coloured (brown-grey) state of films deposited at -0.1 mA for 100 s (——), 400 s (——) and 800 s (——). Coloured UV-vis spectra were recorded after oxidising (-0.20 V → +0.75 V vs. SCE) the films then removing from the KOH electrolyte and measuring the absorbance against a blank ITO/glass. Inserts in (b) illustrate the absorbance at maxima (λ_{max} = 490 nm) vs. different deposition times.

4. Preparation and optimisation of electrochromic nickel oxide-based thin films
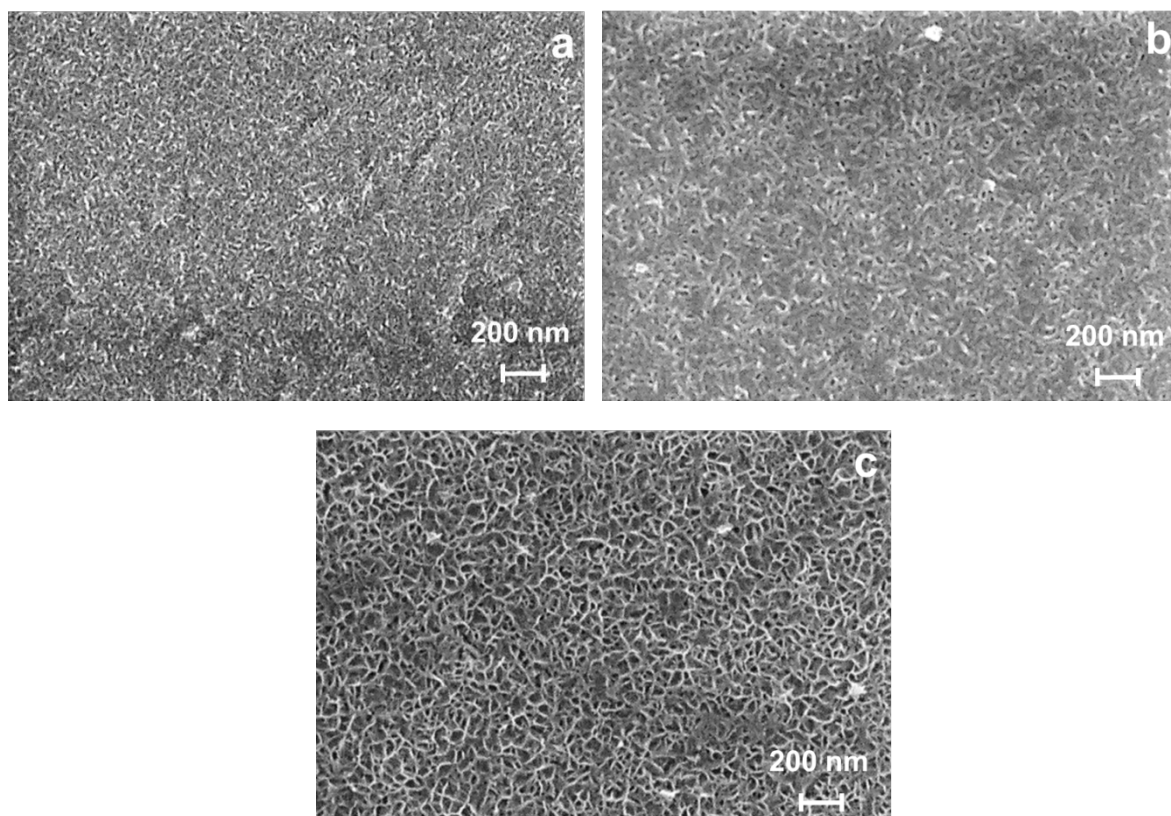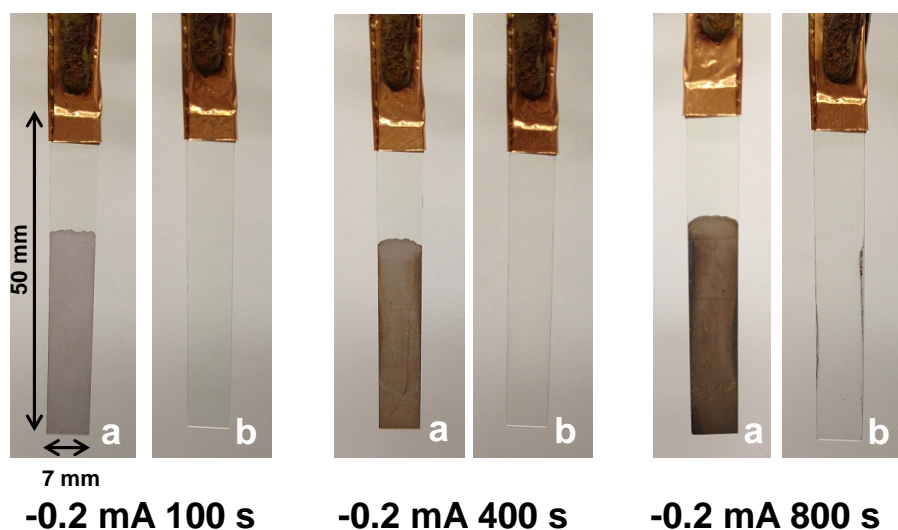
Figure 4.18. Above: Photographs of hydrated NiO films deposited from nickel nitrate solutions (0.01 mol dm^{-3}) at different applied current of -0.2 mA at different times. (a) NiOOH film (film switched to the coloured state by cyclic voltammetry between –0.20 to +0.75 V vs. SCE at 10 mV s^{-1}, and then removal at +0.75 V) and (b) reduced hydrated NiO film. Films were deposited on the lower 30 mm length of each 7 mm width ITO/glass. Below: High resolution field emission gun scanning electron microscope (FEGSEM) images showing the surface of the hydrated NiO films deposited on ITO/glass from nickel nitrate (0.01 mol dm^{-3}) solution at applied current of -0.2 mA for 100 s (a), 400 s (b) and 800 s (c).

4.4.3. Effect of nickel nitrate concentration

The effect of different nickel nitrate concentration on the deposition of hydrated NiO films can be seen in figure 4.19. From the CVs, it can be seen that peak currents for the oxidation and reduction redox processes increase as the nickel nitrate concentration increases (0.005 to 0.05 mol dm^{-3}). However, the visible region absorbance value is maximum for the film deposited using 0.01 mol dm^{-3} concentration solution (figure 4.19 (b)). At the higher concentration of 0.1 mol dm^{-3} the deposition efficiency is reduced and the redox process becomes less reversible. Similar observations were also reported by Streinz *et al.*[28] they found that the deposition efficiency decreased as the nickel nitrate concentration increased above 0.1 mol dm^{-3}. They concluded that at high concentrations the formation of a soluble cluster ion complex $[Ni_4(OH)_4]^{4+}$ hindered the precipitation of hydrated NiO due to the complex diffusing away from the electrode back into the bulk solution, however, they did not present evidence of the existence of this complex.

Films deposited from low concentration solutions (0.005 and 0.01 mol dm^{-3}) showed better uniformity than those prepared from 0.05 and 0.1 mol dm^{-3} (photographs in figure 4.20). Furthermore, at higher concentrations the films became irreversible with brown-grey colouration still being observed.

Investigation into the stability (drop in charge after the 2nd voltammetric cycle) of hydrated NiO films prepared from different concentrations of nickel nitrate solution was carried out by calculating the percentage drop in charge (C) as outlined below:

$$\% \text{ drop in charge} = \frac{maximum\ C\ of\ cycle\ 2}{maximum\ C\ of\ cycle\ 1} \times 100 \qquad (4.10)$$

The calculated drop in charge after two successive colouration/bleaching cycles in KOH electrolyte was 0.48, 1.93, 5.3 and 33.9 % for hydrated NiO film deposited from 0.005, 0.01, 0.05 and 0.1 mol dm^{-3}, respectively. The relationship between drop in charge and concentration of deposition bath can be considered further by examining the films' surface morphologies (FEGSEM images figure 4.20). From the images it can be seen that at low concentrations, the morphology is consistent with those of

4. Preparation and optimisation of electrochromic nickel oxide-based thin films

the interconnecting porous, flake like structure. However, at high concentration a contrasting morphology was observed. The scattered clusters of hydrated NiO particles appear less porous, which agrees with the lack of reversibility shown in photographs in figure 4.20. Also, the low stability after two colouration/bleaching cycles would suggest that at high concentration, the possible formation of soluble cluster ion complex takes place, which delaminates away from the surface of the ITO/glass during redox cycling in KOH electrolyte.
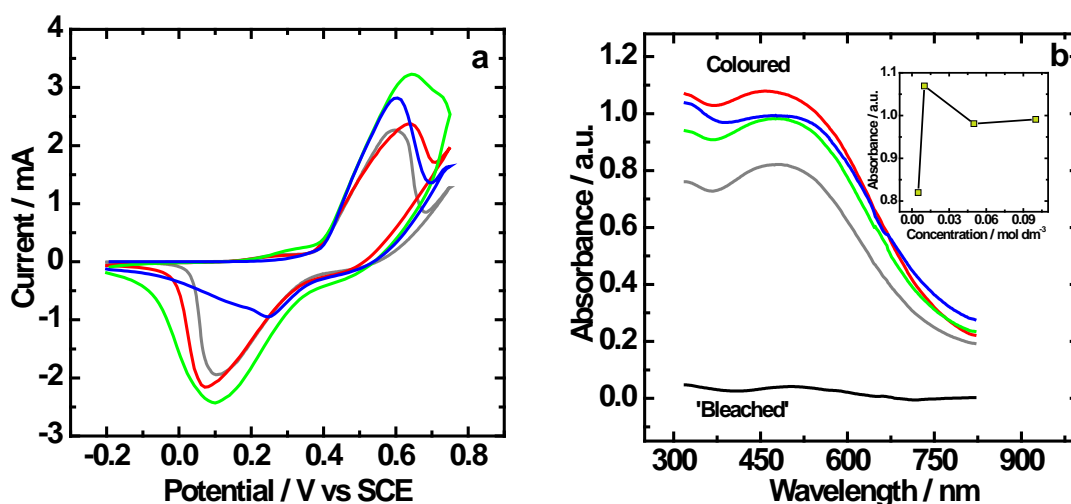
Figure 4.19. CVs for the oxidation and reduction processes for the as-deposited hydrated NiO films deposited on ITO/glass at -0.2 mA for 800 s from nickel nitrate concentrations of 0.005 (——), 0.01 (——), 0.05 (——) and 0.1 mol dm^{-3} (——) followed by cycling in aqueous KOH (0.1 mol dm^{-3}) electrolyte at 10 mV s^{-1} (a). The potential range was -0.20 V $\rightarrow$ +0.75 V $\rightarrow$ -0.20 V vs. SCE. Visible region absorbance spectra of the as-deposited hydrated NiO in the 'bleached' state (——) (which was similar for all the films deposited at different currents) and coloured (brown-grey) state of films deposited from 0.005 (——), 0.01 (——), 0.05 (——) and 0.1 mol dm^{-3} (——) (b). Coloured UV-vis spectra were recorded after oxidising (-0.20 V $\rightarrow$ +0.75 V vs. SCE) the films then removing from the KOH electrolyte and measuring the absorbance against a blank ITO/glass. Inserts in (b) illustrate the absorbance at maxima (λ_{max} = 490 nm) vs. different nickel nitrate concentrations.

4. Preparation and optimisation of electrochromic nickel oxide-based thin films
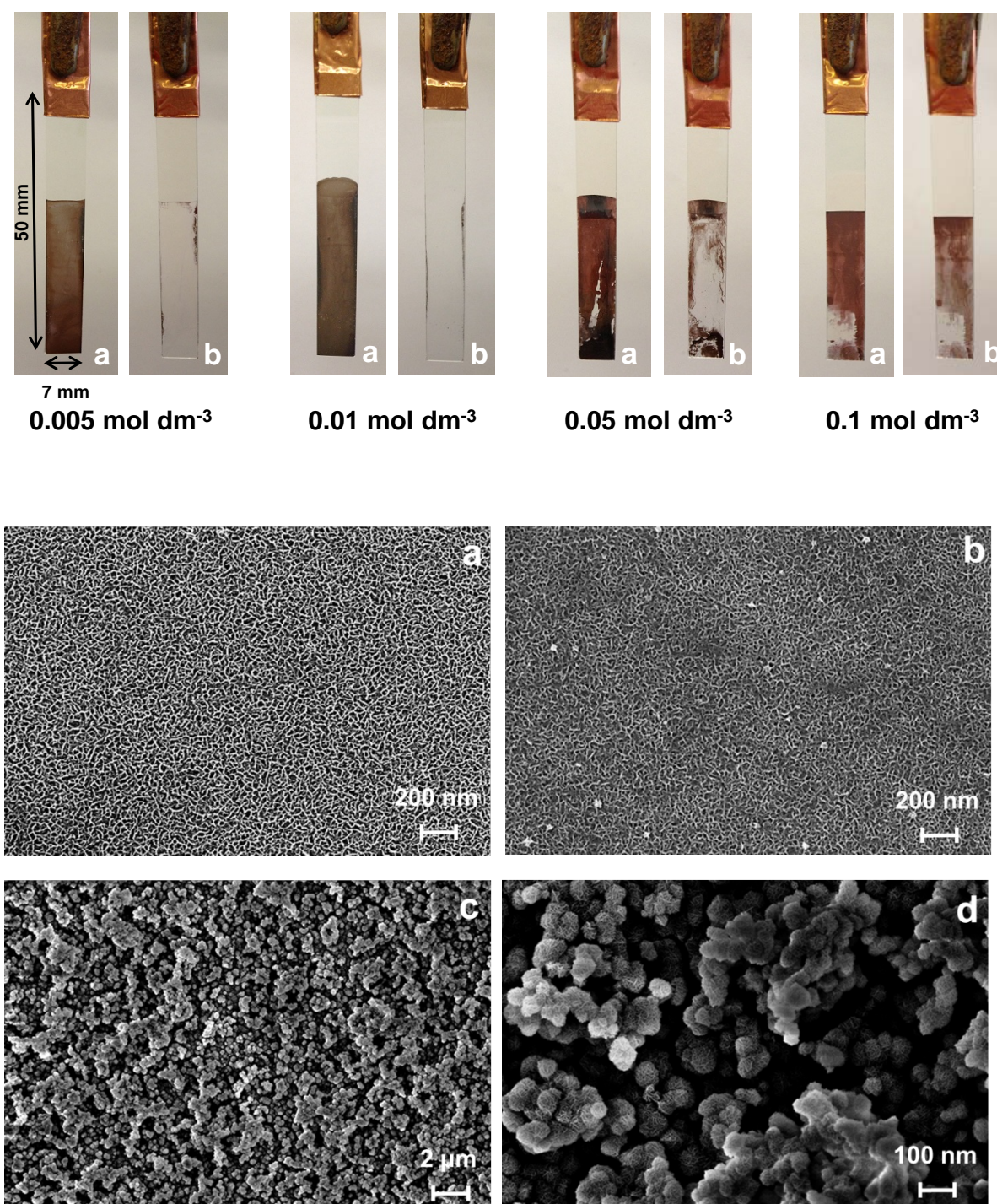
Figure 4.20. Above: Photographs of the hydrated NiO films deposited from different concentration of nickel nitrate solutions at an applied current of -0.2 mA for 800 s. (a) NiOOH film (film switched to the coloured state by cyclic voltammetry between –0.20 to +0.75 V vs. SCE at 10 mV s^{-1}, and then removed at +0.75 V) and (b) reduced hydrated NiO film. Films were deposited on the lower 30 mm length of each 7 mm width ITO/glass. Below: High resolution field emission gun scanning electron microscope (FEGSEM) images showing the surface of the hydrated NiO films deposited on ITO/glass from nickel nitrate concentrations of 0.005 (a), 0.01 (b), 0.05 (c) and 0.1 (d) at an applied current of -0.2 mA for 800 s.

4.4.4. Effect of different transparent conducting oxide (TCO) substrates

The use of transparent conducting oxide (TCO) semiconductors is essential for most optoelectronic device applications such as flat panels and smart windows. The most widely used and available TCO's are tin-doped indium oxide ($In_2O_3(Sn)$, ITO) on glass or fluorine-doped tin oxide (SnO_2:F, FTO) on glass. Historically, the more dominant of the two has been ITO/glass, due to its high demand and use in hand-held smart devices and flat panel displays.[31,32] On the other hand, the architectural use towards energy-efficient smart windows has often involved deposition on FTO/glass, due to its efficiency in preventing radiative heat loss[33] and high optical and electrical properties.

More recently, it has become apparent that due to the high demand for ITO transparent electrodes in the past six years the price of indium has increased from around US $100 to nearly $1000 per kilogram.[34] Furthermore, due to its short supply it has been predicted that indium, a silvery metal produced as a by-product of zinc mining could become scarce within the next 10 years. Due to these reasons, there has been a surge in recent developments to produce alternative TCO's with low resistivity. A detailed survey of these potential TCO's can be found elsewhere.[32]

In this section, a comparative study of ITO and FTO/glass is discussed, with the aim of examining the durability of the deposited hydrated NiO film during continuous redox cycling in KOH electrolyte.

Figure 4.21 (a) and (b) shows the stability of hydrated NiO films deposited on both ITO and FTO/glass substrates over 50 colouration/bleaching cycles, respectively. From the CVs it can be seen that the film stability is much greater on FTO/glass than ITO/glass, as indicated by the reduction in both the oxidation and reduction peak currents on continuous cycling of the latter. Furthermore, figure 4.21 (c) and table 4.2 shows the film degradation to be 95.3 and 26.8 % on ITO/glass and FTO/glass, respectively. This trend can be further considered by examining the AFM images of the as-deposited and films after 50 cycles. The imaging was carried out in Tapping Mode (TM-AFM) using a high resonant frequency (HRF) at approximately 300 kHz -

silicon probe. The scan frequency was 2 Hz. From the images it is clear that the morphology of the film after 50 cycles appears to change considerably on ITO/glass (figure 4.22 (a)). The film after 50 cycles shows a smoother surface when compared to the 1st cycle which indicates that the film has delaminated away from the surface or re-dissolved into the electrolyte. On FTO/glass the film morphology for both the 1st and the 50th cycle show similar morphology indicating that the film is still adherent (figure 4.22 (b)).
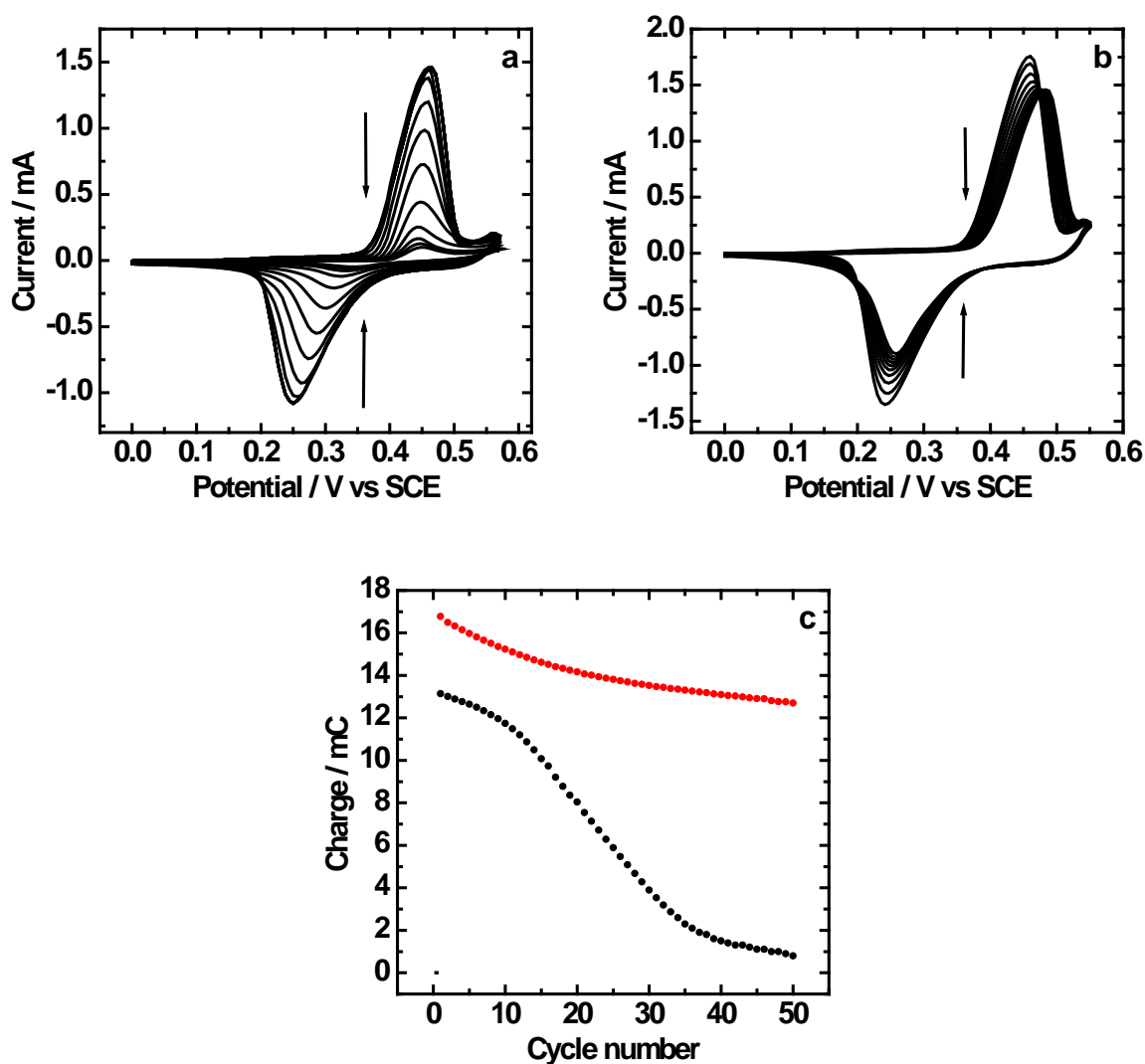
Figure 4.21. CVs showing the durability of the as-deposited hydrated NiO films prepared at an applied current of -0.6 mA for 50 s on ITO/glass (a) and FTO/glass (b) then cycled in aqueous KOH (0.1 mol dm^{-3}). The potential range was –0.20 V → +0.55 V → –0.20 V vs. SCE for 50 cycles at the scan rate of 10 mV s^{-1}. Every 10th CV is shown in figures (a) and (b). Charge vs. cycle number for hydrated NiO film prepared on ITO/glass (——) and FTO/glass (——) (c). The arrows in (a) and (b) indicate film degradation on increasing cycle number.

4. Preparation and optimisation of electrochromic nickel oxide-based thin films

Table 4.2. Percentage drop in charge after 50 successive colouration/bleaching cycles in KOH electrolyte. Hydrated NiO films were deposited on ITO/glass or FTO/glass from nickel nitrate (0.01 mol dm^{-3}) solution by applying a current of -0.6 mA for 50 s.

TCO substrate	Drop in charge (%) film 1	Drop in charge (%) film 2	Drop in charge (%) film 3	Average Drop in charge (%)
ITO/glass	95.2	96.1	94.7	95.3
FTO/glass	26.5	27.1	26.8	26.8

The improved durability on FTO/glass can be explained with reference to AFM images of the bare TCO's on glass (figure 4.23 (a)). From the images it can be seen that FTO/glass has a higher surface roughness average (Ra = 14.5 nm) than ITO/glass (Ra = 3.6 nm). As a result, the deposition of hydrated NiO particles takes place deep into the grooves and pores of the FTO conducting film and during cycling the amount of film delaminated from the surface is reduced.
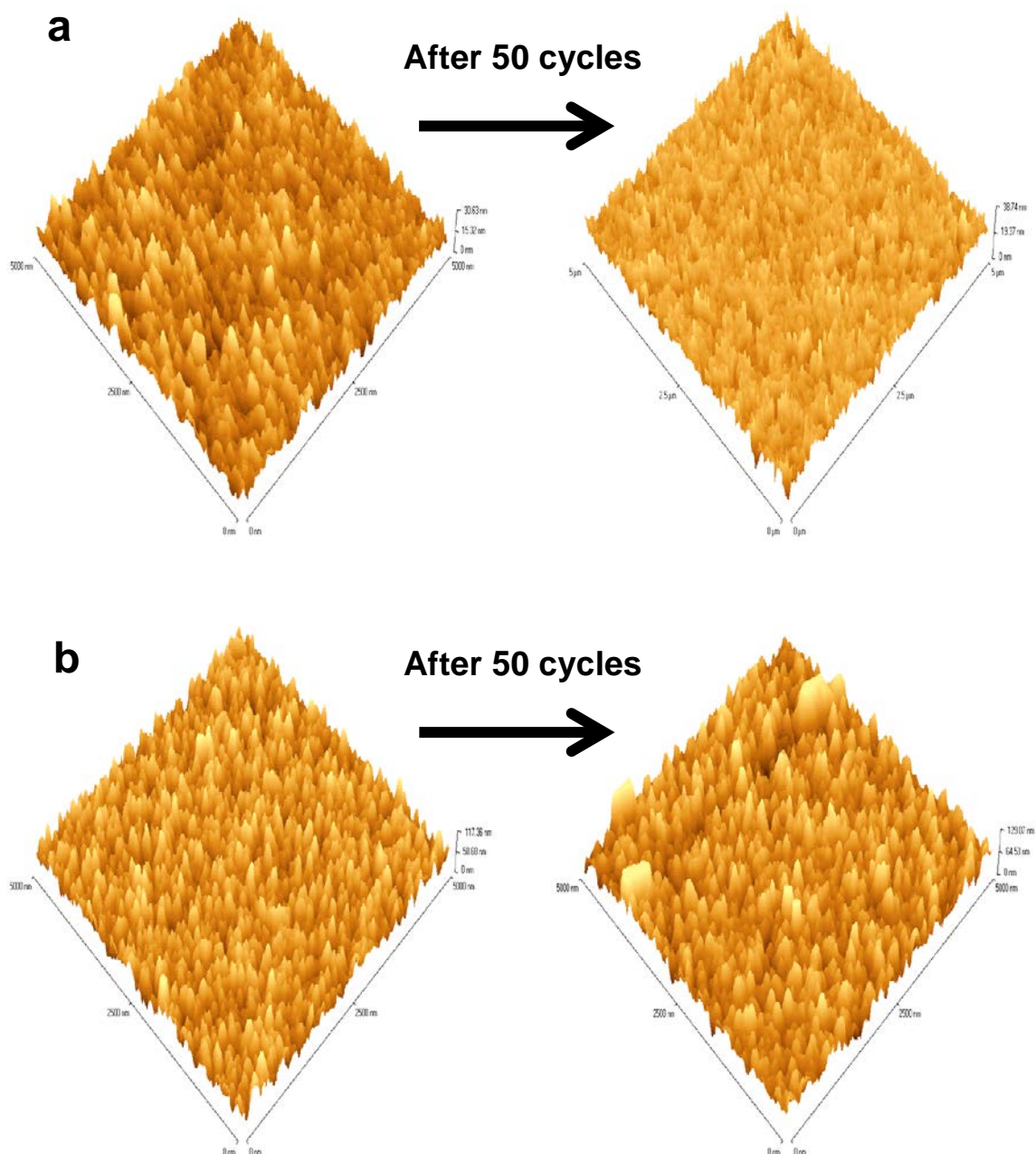
Figure 4.22. Atomic force microscopy (AFM) images showing the surface morphology of the as-deposited film and after cycling 50 times in aqueous KOH (0.1 mol dm^{-3}). Hydrated NiO films prepared at applied current of -0.6 mA for 50 s on ITO/glass (a) and FTO/glass (b). The image space for all four samples was identical, however, the scale of the AFM image in (a) after 50 cycles is given in microns.
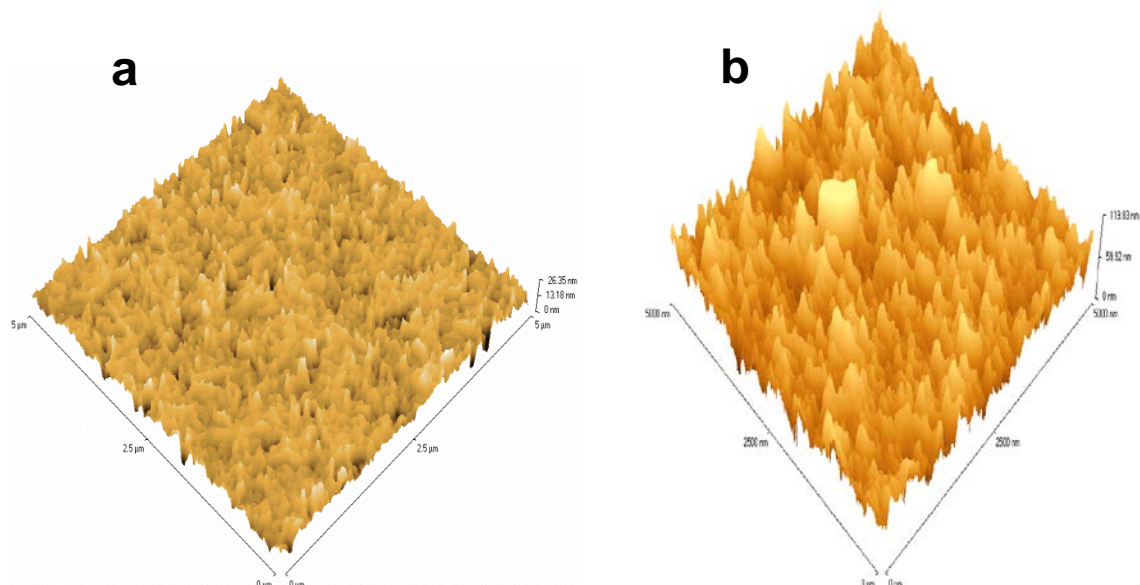
Figure 4.23. Atomic force microscopy (AFM) images showing the surface morphology and the Ra values of the bare ITO/glass (Ra = 3.6 nm) (a) and FTO/glass (Ra = 14.5 nm) (b). The image space of samples (a) and (b) were identical, however, the scale of the AFM image in (a) is given in microns.

4.4.5. Substrate pre-treatment

Another technique which has been employed elsewhere[35,36] is to anodically polarise the conducting substrate in KOH (1.0 mol dm^{-3}) solution prior to film deposition. This pre-treatment is said to be necessary for the formation of a uniform and adherent film. Figure 4.24 shows films of hydrated NiO deposited onto FTO/glass without and with pre-treatment. From the images it is observed that deposition without any pre-treatment (figure 4.24 (a)) produces patchy and non-uniform film. On the other hand, deposition following pre-treatment significantly improves the uniformity of the film (figure 4.24 (b)). As a result of this observation all consequent films were grown after pre-treatment at small and large scale.

4. Preparation and optimisation of electrochromic nickel oxide-based thin films
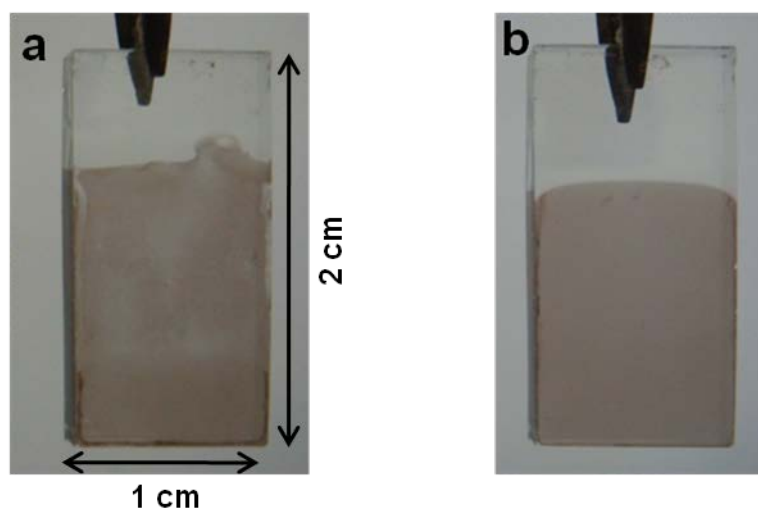
Figure 4.24. Photographs of films deposited at -0.6 mA cm^{-2} for 50s on FTO/glass without polarisation (a) and with polarisation (b) at 2 mA cm^{-2} for 30s in KOH (1.0 mol dm^{-3}) solution.

4.4.6. Crystalline phase of the as-deposited hydrated NiO films

Figure 4.25 (a) shows the powder XRD patterns for hydrated NiO films deposited on ITO and FTO/glass. In both cases, the XRD patterns are characteristic for the ITO/glass (International Centre for Diffraction Data (ICDD) Powder Diffraction File (PDF) 89-4596) and FTO/glass (41-1445), with the hydrated NiO films being of an amorphous nature. These results are in agreement with those obtained by Garcia-Miquel et al.[37] who prepared their NiO thin films onto conducting glass by a sol-gel technique. They found the NiO films to be predominantly amorphous. In an attempt to improve the crystallinity, numerous samples of different thickness were prepared onto both ITO/glass and FTO/glass, however the XRD patterns were still of an amorphous nature.

XRD patterns where then recorded on hydrated NiO powder which was obtained by scraping away the film deposited onto a palladium foil electrode (50 x 50 mm) from nickel nitrate (0.01 mol dm^{-3}) solution at an applied current of -0.2 mA for 10 hours. This process was repeated until enough powder was accumulated. The XRD pattern recorded on this sample is shown in figure 4.25 (b), which can be assigned to a typical alpha-phase jamborite NiO (25-1363) and is consistent with the XRD analysis

4. Preparation and optimisation of electrochromic nickel oxide-based thin films

by Wohlfahrt-Mehrens *et al.*[38] who also prepared their film by an electrochemical cathodic deposition technique.
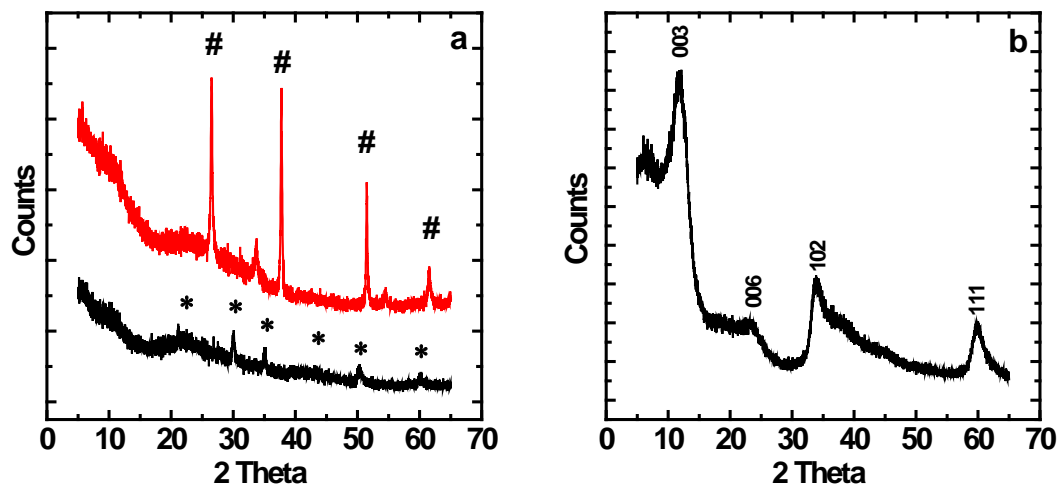
Figure 4.25. (a) Powder XRD patterns for hydrated NiO film deposited from nickel nitrate (0.01 mol dm^{-3}) solution at an applied current of -0.2 mA for 800 s on ITO/glass (*shows the reflections due to ITO) (——) and FTO/glass (#shows reflections due to FTO) (——). (b) XRD patterns for hydrated NiO powder accumulated by scraping the film away from a palladium foil electrode (50 x 50 mm). Film deposited from nickel nitrate (0.01 mol dm^{-3}) solution at an applied current of -0.2 mA for 10 hours.

4.5. NiO film preparation by aerosol-assisted chemical vapour deposition (AACVD)

Chemical vapour deposition (CVD) is a well-established technique which involves homogeneous and heterogeneous chemical reaction of gaseous species leading to the formation of powders or films. The process has been used to deposit a wide range of materials, including metals, films and coatings for semiconductors, optoelectronics, energy conversion devices and refractory ceramic materials used for hard coatings and corrosion protection. Advantages of the CVD technique include the ability to produce highly pure materials with structural control at atomic or nanometre scales and the ability to scale up the process for large area coatings on flat or complex shape engineering components. However, the main problems associated with this technique are the difficulty of depositing multicomponent

4. Preparation and optimisation of electrochromic nickel oxide-based thin films

materials with well controlled stoichiometry and the lack of volatile precursor availability.

As a variant of the conventional CVD process, the aerosol-assisted chemical vapour deposition (AACVD) method does not require volatile precursors, but simply soluble in a given solvent. When compared to the CVD method, the AACVD route presents various advantages:[39-43]

- a wide choice and availability of precursors for high quality CVD products at low cost, which is a critical issue for mass production.
- simplification of the delivery and vaporisation of precursor via the generation of a precursor aerosol.
- high deposition rate, which may be obtained from a high mass-transport rate of the precursor, and the possible improvements of precursor selection.
- a more flexible reaction environment, since the AACVD can be operated under low pressure, atmospheric pressure, or even in an open atmosphere.
- simplification of the synthesis of multicomponent products with precise stoichiometric control.

The AACVD method involves the atomisation of precursor solution into sub-micrometre-sized aerosol droplets. The droplets are subsequently transported using an inert or reactive carrier gas into a heating zone, where the solvent is rapidly evaporated, and the chemical precursors undergo decomposition and/or chemical reaction near or on a heated substrate to form the desired films.[44] A schematic of the deposition mechanism is shown in figure 4.26.

For thin film formation, a suitable solvent with high solubility, low vapour pressure and low viscosity is used to prepare the starting precursor.[45] A wide range of starting materials can be used, these include; pure liquid, single-source precursor, a mixture of several liquid chemicals or can be prepared by dissolving solid or liquid chemicals. Aerosol generators for the atomisation of the starting precursor solution can be ultrasonic, pneumatic aerosol jet or electrostatic aerosol atomisation. The most common of the three is ultrasonic aerosol generation which uses a piezoelectric

transducer to apply a high-frequency electric field. This causes the transducer to vibrate and instigates the formation of fine droplets.[46]
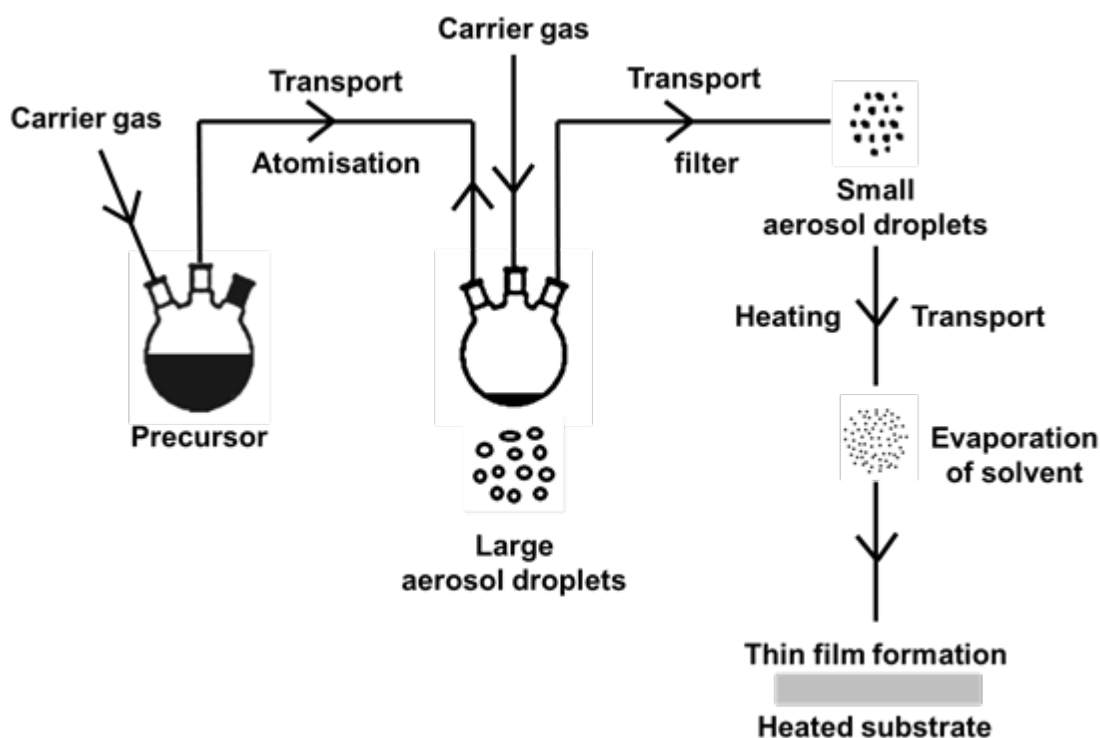
Figure 4.26. Schematic diagram showing the AACVD deposition mechanism. Diagram adapted from.[39]

4.5.1. Crystalline phases identified, film morphology and optical absorption of the as-deposited NiO films

Figure 4.27 shows the powder XRD patterns for NiO films prepared using the AACVD technique on FTO/glass at different deposition times. The reflections at 37.3°, 43.3° and 62.9° 2Ө can be assigned to cubic NiO (International Centre for Diffraction Data (ICDD) Powder Diffraction File (PDF) 47-1049). The NiO phase is stable and its formation is independent of the film thickness. The intensity of the NiO reflections suggests preferred orientation of the films, as the (111) reflection is more intense than the (200). In a randomly oriented sample of NiO, the (200) reflection should be the most intense.

4. Preparation and optimisation of electrochromic nickel oxide-based thin films

Figure 4.28 shows photographs of the AACVD as-deposited NiO films at the three deposition times, with SEM images shown in figure 4.29. Uniform NiO films cover the FTO/glass substrate surface and exhibit a nano-scale morphology of octahedral-like grains. The cross-sectional SEM images (inserts in figure 4.29) show that film thickness increases with deposition time.

Figure 4.30 shows the optical absorption spectra for the as-deposited films recorded in the wavelength range 330–820 nm (3.75–1.51 eV). The data were analysed using a classical relation for near edge optical absorption in semiconductor materials.[47] Analysing the variation of $(\alpha h\nu)^2$ vs. photon energy ($h\nu$) in eV for NiO films suggests a direct interband transition. The band gaps were 3.61, 3.53 and 3.48 eV for the NiO(10 min), NiO(15 min) and NiO(20 min) films, respectively. These direct band energy values are in good agreement with literature values for NiO thin films grown from electrodeposited nickel sulphide followed by thermal oxidation.[48] The slight decrease in band gap with increasing film thickness is attributed to an increase in grain size (figure 4.29).
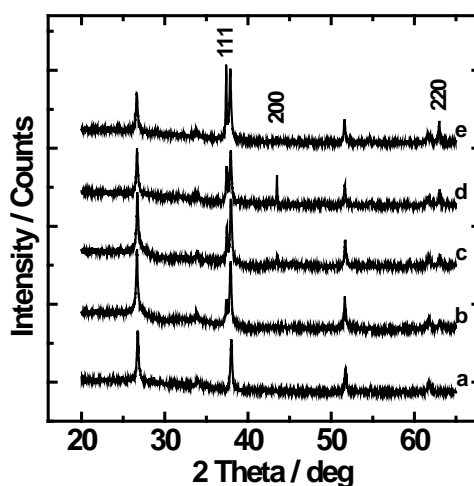
Figure 4.27. Powder XRD patterns for: (a) FTO/glass, (b) NiO(10 min), (c) NiO(15 min), (d) NiO(20 min) and (e) NiO(20 min) after 3500 oxidative conditioning voltammetric cycles in aqueous KOH (0.1 mol dm^{-3}).
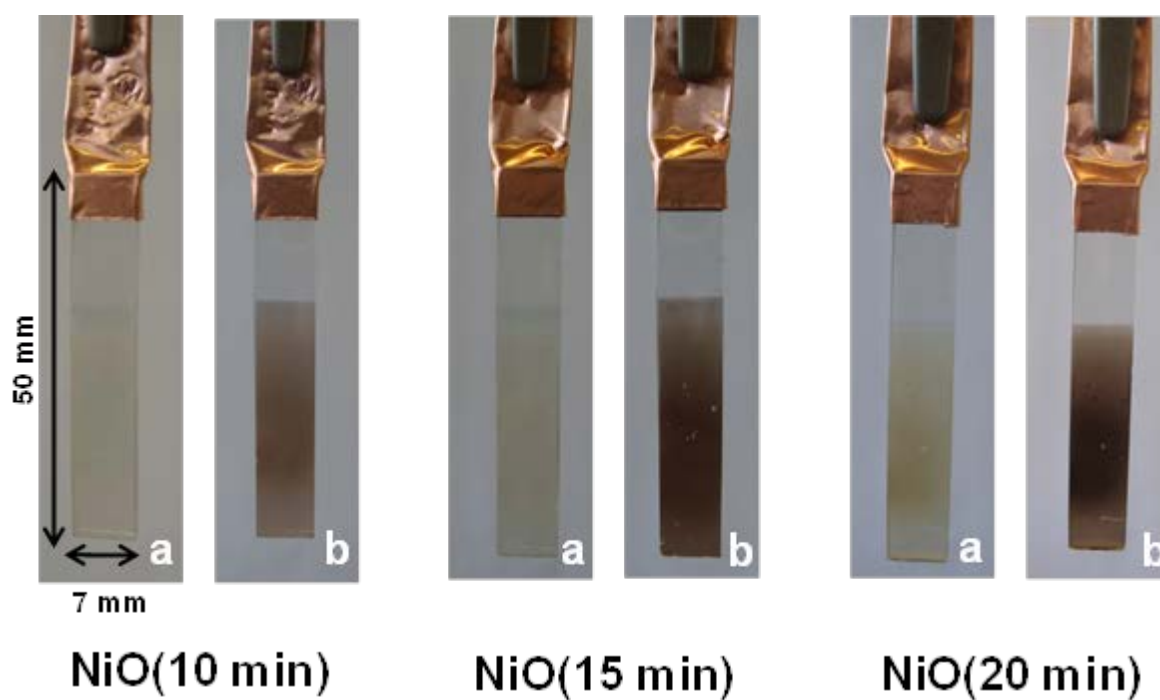
Figure 4.28. Photographs of (a) as deposited NiO films and (b) NiOOH films (following 3500 cycles –0.50 to +0.70 V vs. SCE at 50 mV s⁻¹, and then removal at +0.70 V). Each film was deposited on the lower 30 mm length of each 7 mm width FTO/glass). Although the as-deposited (pictures a) films appear grey in the pictures, by eye they appear light green.
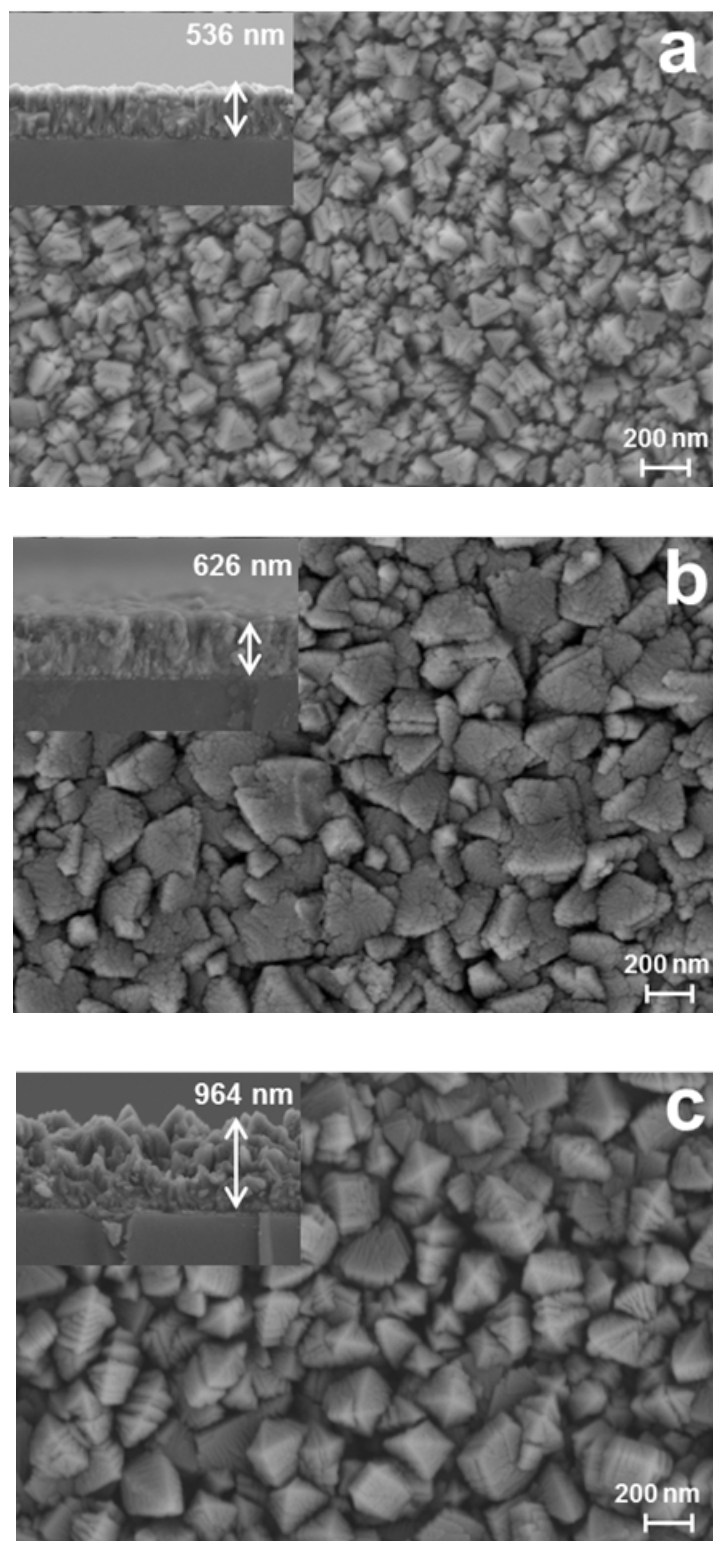
Figure 4.29. SEM images of NiO films deposited on FTO/glass for three deposition times: (a) NiO(10 min), (b) NiO(15 min) and (c) NiO(20 min). Inserts illustrate the cross sectional images.

4. Preparation and optimisation of electrochromic nickel oxide-based thin films
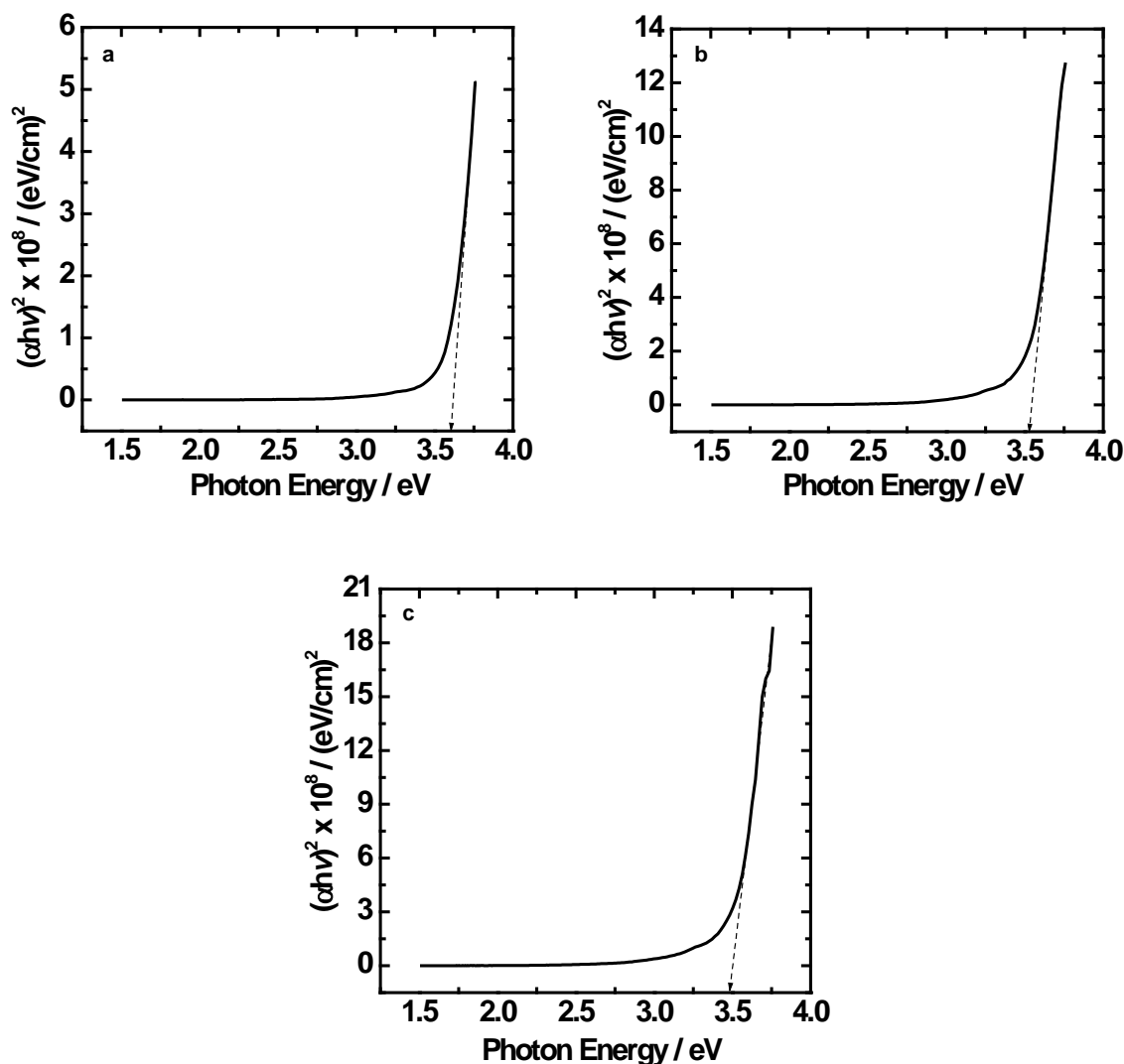
Figure 4.30. Optical absorption spectra of $(\alpha h v)^2$ vs. photon energy ($h v$) for films deposited on FTO/glass: (a) NiO(10 min), (b) NiO(15 min) and (c) NiO(20 min).

4.5.2. Transformation of the surface morphology of the AACVD prepared NiO films during electrochemical cycling in aqueous KOH (0.1 mol dm^{-3}) electrolyte.

Figure 4.31 shows an example of CVs in aqueous KOH (0.1 mol dm^{-3}) electrolyte commencing with, in this case, an as-deposited NiO(15 min) film. From the plot it can be seen that during the first 50 cycles, a continuous increase in capacity under the oxidation and reduction process takes place. This process is known as the so called activation period and has been reported for NiO films prepared by sol-gel,[37] and pulsed laser-deposition.[49-51] Furthermore, because of this activation process, on

continuous oxidative voltammetric cycling, the octahedral-like grains of as-deposited NiO (figure 4.32 (a)) transform to an open porous structure of interconnected flakes (figure 4.32 (b)). Such a porous interconnecting structure will enhance the intercalation/deintercalation of hydroxide ions (equation (4.11), a simplified form of the redox process)) during electrochemical cycling, thus leading to enhanced EC performance. Similar porous morphologies have been previously reported in the literature for NiO-based films prepared by chemical bath deposition methods.[7, 52]

$$NiO + OH^- \rightleftharpoons NiOOH + e^- \hspace{4cm} (4.11)$$
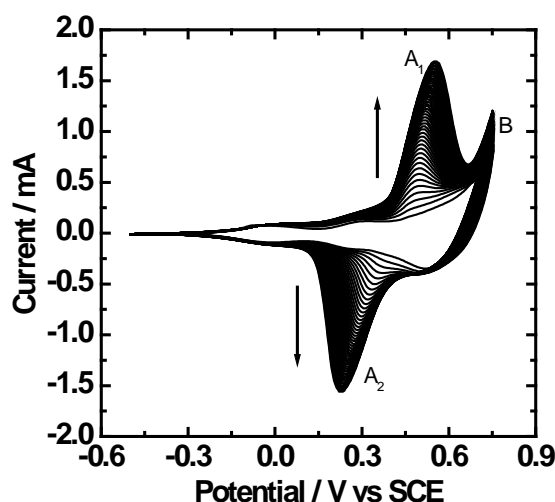
Figure 4.31. CVs starting from the as-deposited NiO(15 min) film in aqueous KOH (0.1 mol dm^{-3}). The potential range was −0.50 V → +0.70 V → −0.50 V vs. SCE for 50 cycles at the scan rate of 50 mV s^{-1}.

The electrochemically generated porous NiO is EC and oxidatively switches (Equation (4.11)), from a 'bleached' (transmissive light green) state to the coloured nickel oxyhydroxide (NiOOH) (deep brown - for photographs see figure 4.28) state. On continuous cycling, this process of morphology transformation is enhanced as the peak currents gradually increase with cycle number (figure 4.31).

The two broad redox peaks in the CVs (figure 4.31) are associated with the colouration and bleaching process for NiO,[53] one anodic peak (A$_1$), responsible for the oxidation and one cathodic peak (A$_2$), for the reduction process. For all sets of such CVs, an increase in anodic current after +0.60 V (B) is observed which

corresponds to the beginning of the oxygen evolution reaction (OER). These CV features are similar to those obtained for NiO thin films initially prepared by electrodeposition[9] and chemical bath deposition[54] techniques. The anodic and cathodic peak currents increase (figure 4.33) with an increase in deposition time, with more electroactive material being available. XRD data collected on this sample showed NiO still to be present (figure 4.27(e)), but the relative intensities were now different to the original deposited film, with the (200) reflection especially reduced in intensity. This agrees with the morphology changes shown in the SEM images (figure 4.32).
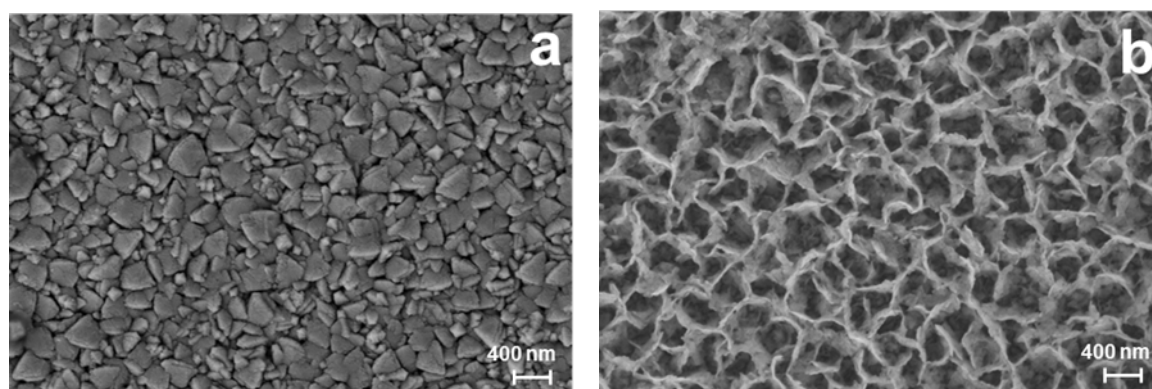
Figure 4.32. SEM images of NiO(15 min) films deposited on FTO/glass: (a) as-deposited and (b) following 3500 electrochemical cycles in aqueous KOH (0.1 mol dm^{-3}).
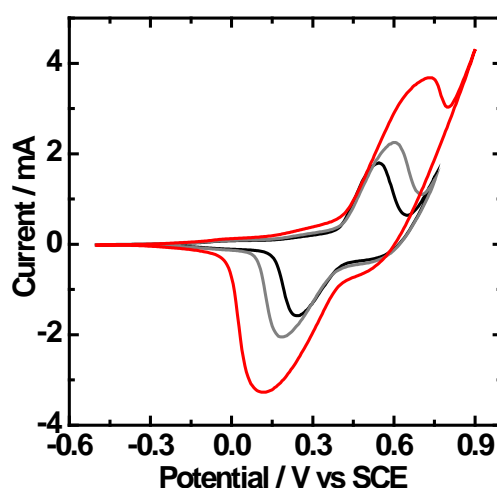
Figure 4.33. The 100th CV (at 50 mV s^{-1}) in aqueous KOH (0.1 mol dm^{-3}) of films prepared from as-deposited NiO(10 min) (——), NiO(15 min) (——) and NiO(20 min) (——).

4.6. Conclusion

This chapter described the formation of hydrated NiO (Ni(OH)$_2$) films by an electrochemical cathodic deposition technique. The effect of different nickel salt solutions on depositing hydrated NiO films was examined. It was established that deposition using nickel nitrate solution produced films with a uniform porous interconnecting flake-like structure. Such morphology is generally regarded as favourable for the intercalation/deintercalation of hydroxide ions during redox cycling. In the case of deposition from nickel chloride and sulphate solutions, the coexistance of hydrated NiO and metalic nickel produced a non-uniform deposit. The effect of different bath composition for the electrodeposition of nickel was also examined. The deposition of nickel was found to be a complex process, with simultaneous hydrogen evolution playing a key role towards inhibiting the deposition process. The use of boric acid and a commercially available Watts bath composition was found to increase the efficiency of nickel deposition.

Various deposition factors were investigated in order to optimise the preparation of electrochromic (EC) hydrated NiO films. With deposition on FTO/glass using nickel nitrate (0.01 mol dm^{-2}) solution at an applied current of -0.2 mA for 800 s being optimal for preparing uniform and durable deposits.

Finally, aerosol-assisted chemical vapor deposition (AACVD) was used for the preparation of nickel(II) oxide (NiO) thin films. The as-deposited films were confirmed to be cubic NiO from analysis of powder X-ray diffraction data, with an optical band gap that decreased from 3.61 to 3.48 eV with an increase in film thickness (in the range 500-1000 nm). The as-deposited films had an octahedral-like grain structure. On oxidative voltammetric cycling in aqueous KOH (0.1 mol dm^{-3}) electrolyte the morphology gradually changed to an open porous NiO structure.

4. Preparation and optimisation of electrochromic nickel oxide-based thin films

4.7. References

[1]   Xu, Y. Z., Qiu, M. Q., Qiu, S. C., Dai, J., Cao, G. J., He, H. H. and Wang, J. Y. Electrochromism of NiO_xH_y films grown by DC sputtering. *Sol. Energy Mater. Sol. Cells*, **45**, 1997, 105-13.

[2]   Yueyan, S., Zhiyang, Z. and Xiaoji, Y. Electrochromic properties of NiO_xH_y thin films. *Sol. Energy Mater. Sol. Cells*, **71**, 2002, 51-59.

[3]   Conell, R. S., Corrigan, D. A. and Powell, B. R. The electrochromic properties of sputtered nickel oxide films, *Sol. Energy Mater. Sol. Cells*, **25**, 1992, 301-13.

[4]   Agrawal, A., Habibi, H. R., Agrawal, R. K., Cronin, J. P., Roberts, D. M., Caron-Papowich, R. and Lampert, C. M. Effect of deposition pressure on the microstructure and electrochromic properties of electron-beam-evaporated nickel oxide films. *Thin Solid Films*, **221**, 1992, 239-53.

[5]   Scarminio, J., Urbano, B., Gardes, J. and Gorenstien, A. Electrochromism in nickel oxide films obtained by thermal decomposition. *J. Mater. Sci. Lett.*, **11**, 1992, 562-63.

[6]   Sharma, P. K., Fantini, M. C. and Gorenstein, A. Synthesis, characterization and electrochromic properties of NiOxHy thin films prepared by a sol-gel method. *Solid State Ionics*, **113-115**, 1998, 457-63.

[7]   Dalavi, D. S., Suryavanshi, M. J., Patil, D. S., Mali, S. S., Moholkar, A. V., Kalagi, S. S., Vanalkar, S. A., Kang, S. R., Kim, J. H. and Patil, P. S. Nanoporous nickel oxide thin films and its improved electrochromic performance: Effect of thickness. *Appl. Surf. Sci.*, **257**, 2011, 2647-56.

[8]   Zhang, E., Tang, Y., Zhang, Y., Gue, C. and Yang, L. Hydrothermal synthesis of β-nickel hydroxide nanocrystalline thin film and growth of oriented carbon nanofibers. *Mater. Res. Bull.*, **44**, 2009, 1765-70.

[9]   Carpenter, M. K., Conell, R. S. and Corrigan, D. A. The electrochromic properties of hydrous nickel oxide. *Sol. Energy Mater.*, **16**, 1987, 333-46.

[10]   Murthy, M., Nagarajan, G. S., Weidner J. W. and Van Zee. J. W. A model for the galvanostatic deposition of nickel hydroxide. *J. Electrochem. Soc.*, **143**, 1996, 2319-27.

[11]   Provazi, K., Giz, M. J., Dall'Antonia, L. H. and Córdoba de-Torresi S. I. The effect of Cd, Co, and Zn as additives on nickel hydroxide opto-electrochemical behavior. *J. Power Sources*, **102**, 2001, 224-32.

[12]   Córdoba de-Torresi S. I. The effect of manganese addition on nickel hydroxide electrodes with emphasis on its electrochromic properties. *Electrochim. Acta*, **40**, 1995, 1101-7.

[13]   Streinz, C. C., Motupally, S. and Weidner, J. W. The effect of temperature and ethanol on the deposition of nickel hydroxide films. *J. Electrochem. Soc.*, **142**, 1995, 4051-56.

[14]   Desilvestro, J. Corrigan, D. A. and Weaver, M. J. Characterization of redox states of nickel hydroxide film electrodes by in situ surface raman spectroscopy. *J. Electrochem. Soc.*, **135**, 1988, 885-92.

[15]   Law, H. H. and Sapjeta, J. A novel substrate for nickel-cadmium batteries. *J. Electrochem. Soc.*, **135**, 10, 1988, 2418-22.

[16]   Jayashree, R. S. and Kamath, P. V. Nickel hydroxide electrodeposition from nickel nitrate solutions: mechanistic studies. *J. Power Sources*, **93**, 2001, 273-78.

[17]   Hsu, H. and Yang. T. Improvement of corrosion resistance of AZ91D magnesium alloy by nickel plating. *Procedia Engineering*, **36**, 2012, 279-84.

[18]   Bazzaoui, M., Martins, J. I., Bazzaoui, E. A. and Albourine. A. Environmentally friendly process for nickel electroplating of ABS. *Appl. Surf. Sci.*, **258**, 2012, 7968-75.

[19]   Therese, G. H. A and Kamath. P. V. Cathodic reduction of different metal salt solutions Part I: synthesis of metal hydroxides by electrogeneration of base. *J. Appl. Electrochem.*, **28**, 1998, 539-43.

[20]   Carolus, M. D., Bernasek, S. L. and Schwartz, J. Measuring the surface roughness of sputtered coatings by microgravimetry. *Langmuir*, **21**, 2005**,** 4236-39.

[21]   Pletcher, D. *A first course in electrode processes*, The Electrochemical Consultancy, England, 1991.

[22]   Heerman, L. and Tarallo, A. Theory of the chronoamperometric transient for electrochemical nucleation with diffusion-controlled growth. *J. Electroanal. Chem.*, **470**, 1999, 70-6.

[23] Möller, F. A., Kintrup, J., Lachenwitzer, A., Magnussen, O. M. and Behm, R. J. In situ STM study of the electrodeposition and anodic dissolution of ultrathin epitaxial Ni films on Au(111). *Phys. Rev. B: Condens. Matter*, **56**, 1997, 12506-18.

[24] Hoare. J. P. Boric acid as a catalyst in nickel plating solutions. *J. Electrochem. Soc.*, **134**, 1987, 3102-3.

[25] Ji, J., Cooper, W. C., Dreisinger, D. B. and Peters, E. Surface pH measurements during nickel electrodeposition. *J. Appl. Electrochem.*, **25**, 1995, 642-50.

[26] Ibrahim, M. A. M. Black nickel electrodeposition from a modified Watts bath. *J. Appl. Electrochem.*, **36**, 2006, 295-301.

[27] Fletcher, S., Halliday, C. S., Gates, D., Westcott, M., Lwin, T. and Nelson, G. The response of some nucleation/growth processes to triangular scans of potential. *J. Electroanal. Chem. Interfacial Electrochem.*, **159**, 1983, 267-85.

[28] Streinz, C. C., Hartman, A. P., Motupally, S. and Weidner, J. W. The effects of current and nickel nitrate concentration of the deposition of nickel hydroxide films. *J. Electrochem. Soc.* **142**, 1995, 1084-89.

[29] Subbaiah, T., Mallick, S. C., Mishra, K. G., Sanjay, K. and Das, R. P. Electrochemical precipitation of nickel hydroxide. *J. Power Sources*, **112**, 2002, 562-9.

[30] Kalu, E. E., Nwoga, T. T., Srinivasan, V. and Weidner, J. W. Cyclic voltammetric studies of the effects of time and temperature on the capacitance of electrochemically deposited nickel hydroxide. *J. Power Sources*, **92**, 2001, 163-7.

[31] Granqvist, C. G., Azens, A., Hjelm, A., Kullman, L., Niklasson, G. A., Rönnow, D., Strømme Mattsson, M., Veszelei, M. and Vaivars, G. Recent advances in electrochromics for smart windows applications. *Sol. Energy*, **63**, 1998, 199-216.

[32] Minami, T. Transparent conducting oxide semiconductors for transparent electrodes. *Semicond. Sci. Technol.*, **20**, 2005, S35-44.

[33] Ginley, D. S. and Bright, C. Transparent conducting oxides. *MRS Bull.*, **25**, 2000, 15-18.

[34] Baetens, R., Jelle, B. P. and Gustavsen, A. Properties, requirements and possibilities of smart windows for dynamic daylight and solar energy control in

4. Preparation and optimisation of electrochromic nickel oxide-based thin films

buildings: A state-of-the-art review. *Sol. Energy Mater. Sol. Cells, 94*, 2010, 87-105.

[35] Wu, M., Yang, C. and Wang, M. Morphological and structural studies of nanoporous nickel oxide films fabricated by anodic electrochemical deposition techniques. *Electrochim. Acta*, **54**, 2008, 155-61.

[36] Srinivasan, V. and Weidner, J. An electrochemical route for making porous nickel oxide electrochemical capacitors. *J. Electrochem. Soc.*, **144**, 1997, L210-13.

[37] Garcia-Miquel, J. L., Zhang, Q., Allen, S. J., Rougier, A., Blyr, A., Davies, H. O., Jones, A. C., Leedham, T. J., Williams, P. A. and Impey, S. A. Nickel oxide sol–gel films from nickel diacetate for electrochromic applications. *Thin Solid Films*, **424**, 2003, 165-70.

[38] Wohlfahrt-Mehrens, M., Oesten, R., Wilde, P. and Huggins. R. A. The mechanism of electrodeposition and operation of Ni(OH)$_2$ layers. *Solid State Ionics*, **86-88**, 1996, 841-7.

[39] Choy, K. L. Chemical vapour deposition of coatings. *Prog. Mater Sci.*, **48**, 2003, 57-170.

[40] Tahir, A. A., Ehsan, M. A., Mazhar, M., Wijayantha, K. G. U., Zeller, M. and Hunter, A. D. Photoelectrochemical and photoresponsive properties of Bi$_2$S$_3$ nanotube and nanoparticle thin films. *Chem. Mater.*, **22**, 2010, 5084-92.

[41] Dharmadasa, R., Tahir, A. A. and Wijayantha, K. G. U. Single step growth and characterization of zinc oxide, tin oxide, and composite (Zn$_x$Sn$_{1-x}$O$_y$) nanoplate and nanocolumn electrodes. *J. Am. Ceram. Soc.*, **94**, 2011, 3540-46.

[42] Tahir, A. A. and Wijayantha, K. G. U. Photoelectrochemical water splitting at nanostructured ZnFe$_2$O$_4$ electrodes. *J. Photochem. Photobiol., A*, **216**, 2010, 119-25.

[43] Bloor, L. G., Manzi, J., Binions, R., Parkin, I. P., Pugh, D., Afonja, A., Blackman, C. S., Sathasivam, S. and Carmalt, C. J. Tantalum and titanium doped In$_2$O$_3$ thin films by aerosol-assisted chemical vapor deposition and their gas sensing properties. *Chem. Mater.*, **24**, 2012, 2864-71.

[44] Hou, X. and Choy, K. L. Processing and applications of aerosol-assisted chemical vapor deposition. *Chem. Vap. Deposition*, **12**, 2006, 583-96.

[45] Hubert-Pfalzgraf, L. G. and Guillon, H. Trends in precursor design for conventional and aerosol-assisted CVD of high-T_c superconductors. *Appl. Organomet. Chem.*, **12**, 1998, 221-36.

[46] Choy, K. L. *Handbook of nanostructured materials and nanotechnology, vol. 1: synthesis and processing* (Ed: H. S. Nalwa), Academic Press, San Diego, 2000.

[47] Kawar, R. K., Chigare, P. S. and Patil, P. S. Substrate temperature dependent structural, optical and electrical properties of spray deposited iridium oxide thin films. *Appl. Surf. Sci.*, **206**, 2003, 90-101.

[48] Uplane, M. M., Mujawar, S. H., Inamdar, A. I., Shinde, P. S., Sonavane, A. C. and Patil, P. S. Structural, optical and electrochromic properties of nickel oxide thin films grown from electrodeposited nickel sulphide. *Appl. Surf. Sci.*, **253**, 2007, 9365-71

[49] Bouessay, I., Rougier, A., Beaudoin, B. and Leriche, J. B. Pulsed Laser-Deposited nickel oxide thin films as electrochromic anodic materials. *Appl. Surf. Sci.*, **186**, 2002, 490-5.

[50] Bouessay, I., Rougier, A. and Tarascon, J.-M. Electrochemically inactive nickel oxide as electrochromic material. *J. Electrochem. Soc.*, **151**, 2004, H145-52.

[51] Bouessay, I., Rougier, A., Poizot, P., Moscovici, J., Michalowicz, A. and Tarascon, J.-M. Electrochromic degradation in nickel oxide thin film: A self-discharge and dissolution phenomenon. *Electrochim. Acta*, **50**, 2005, 3737-45.

[52] Huang, H., Tian, J., Zhang, W. K., Gan, Y. P., Tao, X. Y., Xia, X. and Tu, J. P. Electrochromic properties of porous NiO thin film as a counter electrode for NiO/WO_3 complementary electrochromic window. *Electrochim. Acta*, **56**, 2011, 4281-6.

[53] Lampert, C. M., Omstead, T. R. and Yu, P. C. Chemical and optical properties of electrochromic nickel oxide films. *Sol. Energy Mater.*, **14**, 1986, 161-174.

[54] Xia, X. H., Tu, J. P., Zhang, J., Wang, X. L., Zhang, W. K. and Huang, H. Electrochromic properties of porous NiO thin films prepared by a chemical bath deposition. *Sol. Energy Mater. Sol. Cells.*, **92**, 2008, 628-33.

5. Electrochromic properties and colorimetric measurements

5.1. Introduction

Over the past decade, electrochromic (EC) materials and devices have progressed significantly, with widespread applications particularly in emerging technologies. The increasing numbers of publications and patents filed in this area of research have often used formulated quantifiable parameters in order to compare different materials and devices (chapter 2). Furthermore, these formulated performance parameters can also be used to identify potential candidates towards commercialisation.

Quantitative measurements of colour on switching between the 'bleached' and coloured states is also considered to be an important factor, as choice of specific colours required will vary depending on the device application. In this regard, the development of a colorimetry (colour measurement) method, which allows a quantitative description of colour and relative transmissivity as sensed by the human eye has received much effort.[1] Quantifying or comparing two colours can be quite difficult as colour is a subjective phenomenon.[2,3]

In colorimetry, a numerical description of the colour stimulus is given by measuring the human eye's sensitivity to light across the visible region. Colour is described by three attributes. The first attribute is described as the location in the spectral sequence, i.e., what wavelength is associated with the colour. This is known as the hue, dominant wavelength, or chromatic colour, and is the wavelength where maximum contrast occurs. The second attribute, known as saturation, chroma, tone, intensity, or purity relates to the level of white and/or black. The third attribute, luminance of the colour is very important as it provides information about the perceived transparency of a sample over the entire visible range and is referred to as value, lightness, or brightness.

5. Electrochromic properties and colorimetric measurements

To generate chromaticity coordinates from the output of a visible region spectrophotometer, a computer spreadsheet was used which contains numerical data describing the colour-matching chromatic responses of the three types of cone in the human eye in the *CIE Standard Observer*. In the spreadsheet, the *CIE* tristimulus values *X*, *Y* and *Z* are calculated by discrete numerical summation, over the wavelength range, of the product of the colour-matching functions and the normalised spectral power distribution. In order to represent colour in 2-D space, the tristimulus values are converted to chromaticity coordinates (*x, y, z*) by the following equations:

$$x = \frac{X}{X+Y+Z} \tag{5.1}$$

$$y = \frac{Y}{X+Y+Z} \tag{5.2}$$

$$z = \frac{Z}{X+Y+Z} = 1 - x - z \tag{5.3}$$

Finally, the luminance factor Y_L is calculated as the ratio of the luminance of the transmitter (*Y*) to that of a perfect transmitter (Y_0) under the same conditions:

$$Y_L = \frac{Y}{Y_0} \tag{5.4}$$

A flow chart that describes the processing of data in the exact sequence of operations is given in reference.[4]

CIE introduced the CIE *L*a*b** (CIELAB) system in 1976, which is a uniform colour space defined to be a geometrical construct containing all possible colour sensations. This CIE *L*a*b** space is formulated in such a way that equal distances correspond to colours that are perceptually equidistant, and is a standard commonly used in the paint, plastic, and textile industries. The values of *L*, a** and *b** are defined as in equations:

$$L^* = 116 \times \left(\frac{Y}{Y_n}\right)^{1/3} - 16 \tag{5.5}$$

$$a^* = 500 \times \left[\left(\frac{X}{X_n}\right)^{1/3} - \left(\frac{Y}{Y_n}\right)^{1/3}\right] \tag{5.6}$$

5. Electrochromic properties and colorimetric measurements

$$b^* = 200 \times \left[\left(\frac{Y}{Y_n} \right)^{1/3} - \left(\frac{Z}{Z_n} \right)^{1/3} \right]$$ (5.7)

where X_n, Y_n, and Z_n are the tristimulus values of a perfect reflecting diffuser (as calculated from the background measurement). In the *L*a*b** chromaticity diagram, + *a** relates to the red direction, − *a** is the green direction, + *b** is the yellow direction, and − *b** is the blue direction. The centre of the chromaticity diagram (0, 0) is achromatic; as the values of *a** and *b** increase, the saturation of the colour increases.

In 2000, Reynolds and co-workers reported a simple portable colorimeter to introduce an *in-situ* colour measurement method for the precise control and measurements of the colour in electrochromic (EC) materials and devices.[5] This technique has since been used to characterise several EC systems, including: conjugated polymer films and devices,[6-27] thin films of WO_3[28] and an inorganic-organic electrochromic device (ECD) based on tungsten oxide and polyaniline.[29] However, studies concerning the chromaticity analysis of EC nickel oxide (NiO) films are limited and have focused on using a single deposition process. Avendaño *et al.*[30] (2004) investigated the optical properties of EC NiO films containing various metal additives, and more recently Dalavi *et al.*[31] measured the EC performance of sol-gel deposited NiO thin films.

This chapter will outline the EC properties of NiO and hydrated NiO films prepared on fluorine-doped tin oxide (SnO_2:F, FTO) on glass by electrochemical cathodic deposition and aerosol-assisted chemical vapor deposition (AACVD) techniques. To date, there is no apparent work on the colorimetric measurements of NiO films prepared by these two deposition techniques. Therefore, sections 5.4 and 5.5 will contain the chromaticity data generated using an earlier established Microsoft® Excel® spreadsheet[4] for the accurate calculation of CIE (Commission Internationale de l'Eclairage)[1] 1931 *xy* chromaticity coordinates and luminance data. Also, electrochemical measurements and chromaticity data produced for EC NiO and hydrated NiO thin films prepared by three different deposition techniques will be compared to highlight the differences in the redox process and any changes in the shade of colour on switching between the oxidised and reduced states.

5.2. Electrochromic properties of hydrated NiO thin films prepared by electrochemical cathodic deposition

In chapter 4, hydrated NiO films of different thicknesses and uniformity were produced for different deposition times and current densities in order to aim for film optimisation. Three of these films were examined further to evaluate their EC properties. Table 5.1 gives *in-situ* spectral data and calculated EC performance parameters for square-wave potential switching between the 'bleached' and coloured forms for as-deposited hydrated NiO films deposited at different times. For all three deposition times, similar colouration efficiency values were produced. Since the film deposited at 800 s showed the highest change in absorbance between the 'bleached' and coloured state, only the figures obtained for this film are shown.

Table 5.1. *In-situ* spectral data and EC performance parameters on square wave switching (0.00 V → +0.47 V → −0.10 V vs. Ag wire pseudo reference electrode) between the 'bleached' and coloured states in aqueous KOH (0.1 mol dm^{-3}).[a] Hydrated NiO films were deposited on FTO/glass from nickel nitrate (0.01 mol dm^{-3}) solution by applying a current of -0.2 mA for 100, 400 and 800 s.

Film deposition time (s)	%T_b	%T_c	Δ%T	ΔA	CE/ cm^2 C^{-1} film 1	CE/ cm^2 C^{-1} film 2	CE/ cm^2 C^{-1} film 3	Average CE/ cm^2 C^{-1}
100	96.7	56.4	40.3	0.23	30.2	27.8	27.1	28.4
400	97.0	15.7	81.3	0.82	34.3	31.8	32.2	32.9
800	97.1	13.9	83.2	0.87	30.1	28.2	30.4	29.6

[a]T_b = transmittance of 'bleached' form, T_c = transmittance of coloured form, Δ%T = change in transmittance between the 'bleached' and coloured forms, ΔA = change in absorbance, CE = colouration efficiency, t_c and t_b = switching times for colouration and bleaching. All measurements were taken at 432 nm, which had been found to be the wavelength for maximum absorbance change.

Figure 5.1 shows the transmittance spectra of the as-deposited hydrated NiO film (prepared via electrochemical cathodic deposition by applying a cathodic current of -0.2 mA for 800 seconds) in the 'bleached' and coloured states. On oxidation, the fully transparent hydrated NiO film was darkened to a brown-grey colour NiOOH phase, with the corresponding decrease in transmittance throughout the visible

region. The maximum change in optical transmittance ($\Delta\%T$) of 83.2% was achieved at λ_{max} (432 nm). Such a large $\Delta\%T$ value is seen as favourable for application towards architectural smart windows.
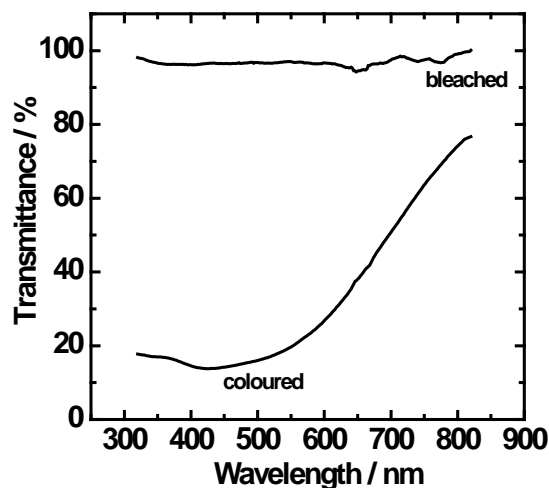
Figure 5.1. Visible region *in-situ* transmission spectra for the 'bleached' and coloured states for the as-deposited hydrated NiO film in aqueous KOH (0.1 mol dm^{-3}). Hydrated NiO film prepared on FTO/glass via electrochemical cathodic deposition from nickel nitrate (0.01 mol dm^{-3}) solution by applying a cathodic current of -0.2 mA for 800 seconds.

Spectral data were further used to calculate the electrical power consumption of the EC film, expressed as the colouration efficiency (CE = $(\Delta A)_{432\,nm}/Q_i$), where (ΔA) is the absorbance change between the 'bleached' and coloured states and Q_i is the charge density (mC cm^{-2}) for each switching process. An illustrative calculation is shown below for hydrated NiO film deposited on FTO/glass at -0.2 mA for 800 s (equation 5.8). Figure 5.2 shows the current-time, charge-time transients and visible region absorbance spectra on switching between the reduced ('bleached') and oxidised (coloured) states. Each charge density was calculated by integration of the current-time transient, recorded on switching colour states (figure 5.2 (b)). Between 12 and 21 s the slight increase in current and charge was due to the beginning of the oxygen evolution reaction (OER). The highest values of ΔA and CE (average of three films) were recorded as 0.87 and 32.9 cm^2 C^{-1} (table 5.1 and figure 5.3) at 432 nm, respectively. This CE value is greater than those obtained for other EC materials such as TiO$_2$ (7.6 cm^2 C^{-1}),[32] Nb$_2$O$_5$ (10 cm^2 C^{-1}),[33] but lower than WO$_3$ (118 cm^2 C^{-1}),[34] which is the most widely studied EC material.

5. Electrochromic properties and colorimetric measurements

Calculation of CE of a hydrated NiO film:

$$CE_{\lambda\,=\,432\,nm} = \frac{(\Delta A)_{432\,nm}}{Q_i} = \frac{0.87}{0.031} = 28.2\ cm^2 C^{-1} \tag{5.8}$$
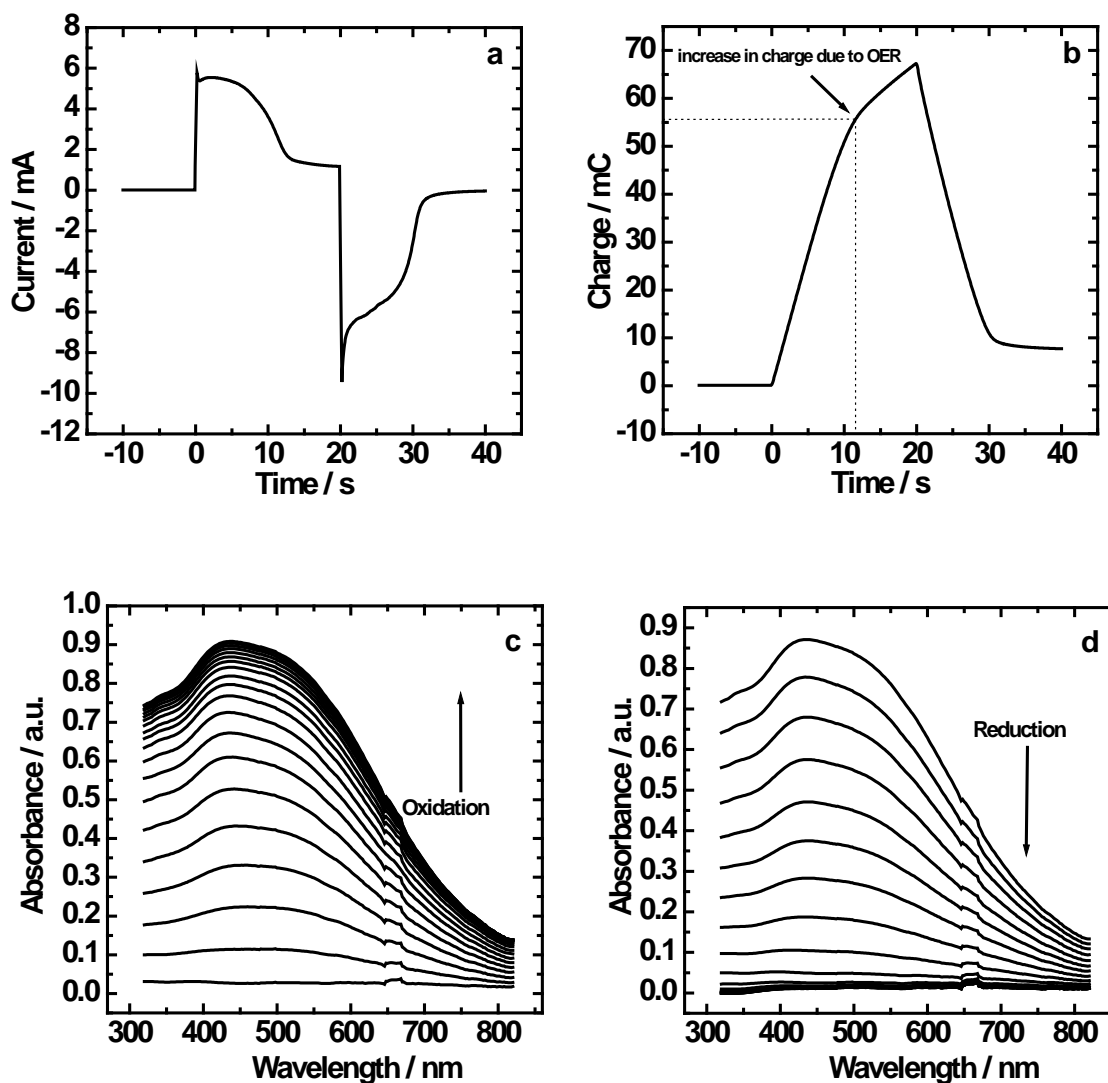
Figure 5.2. Current vs. time (a), charge vs time transients (b) and visible region absorbance spectra ((c) and (d), spectra recorded every 1 s from t = 0), for the reversible switching of hydrated NiO film in aqueous KOH (0.1 mol dm^{-3}) between the transmissive 'bleached' state and the coloured (brown-grey) state. EC switching was conducted by application of potential steps (0.00 V → +0.47 V → −0.10 V) vs. the Ag wire pseudo reference electrode. In (c) and (d) the arrows indicate the direction of change in absorbance.

5. Electrochromic properties and colorimetric measurements
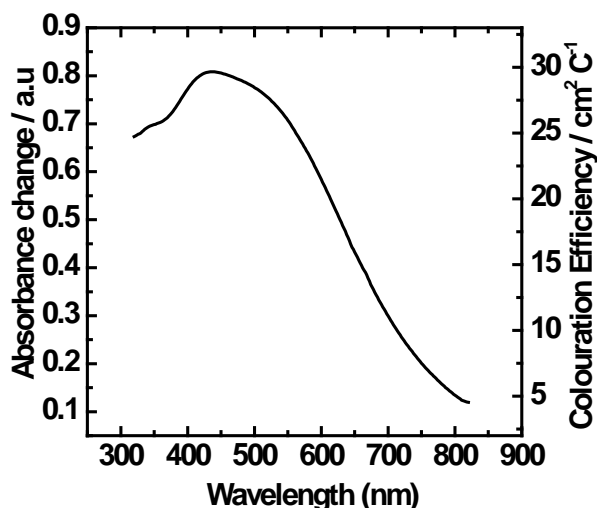
Figure 5.3. Change in absorbance and colouration efficiency of hydrated NiO film recorded in the wavelength range of 320-820 nm.

Response time is defined as the time required for obtaining partial or total change in absorbance between states and is another factor which is of great importance for EC devices.[35] Although, display devices often require response times of milliseconds or less, EC materials for smart window applications can tolerate slow colour change of seconds or even minutes. Here, response times are reported as the time taken for the absorbance to reach 95% of the total change for both colouration (t_c) and 'bleaching' (t_b) processes with values calculated to be 12.0 s for t_c and 9.5 s for t_b process (figure 5.4).

Cycle life is one of the key parameters for commercialisation as it is an experimental measure of the film durability. Figure 5.5 (a) shows cyclic voltammograms (CVs) recorded for the as-deposited hydrated NiO films after the 1st and 50th cycles in KOH (0.1 mol dm^{-3}). After 50 colouring and bleaching cycles, 17.2 % of the charge had faded. The visible *in-situ* transmittance spectra of the film were also recorded following the 1st and 50th cycles. The transmittance of the 'bleached' state was 98.5% and 72.7% respectively, after the 1st and 50th cycles. The transmittance of the 'coloured' state was 13.7% and 16.7% respectively, after the 1st and 50th cycles. The change in transmittance between the 1st ($\Delta\%T$ = 84.8%) and 50th ($\Delta\%T$ = 56.0%) cycle was 28.8%.

5. Electrochromic properties and colorimetric measurements
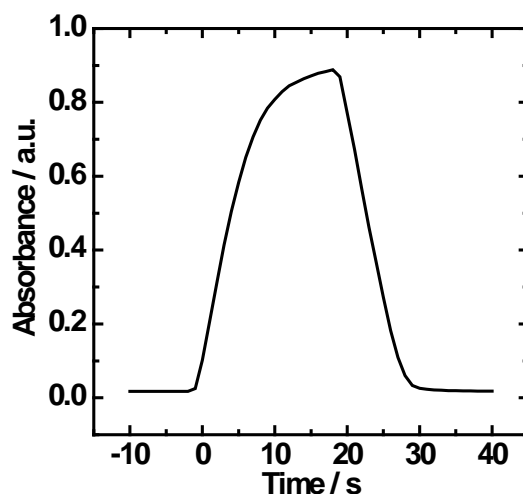
Figure 5.4. Absorbance vs. time transient for the as-deposited hydrated NiO film. Absorbance taken every 1 s at 432 nm, for the reversible switching of films in aqueous KOH (0.1 mol dm^{-3}) between the transmissive 'bleached' state and the coloured (brown-grey) state. EC switching was conducted by application of potential steps (0.00 V $\rightarrow$ +0.47 V $\rightarrow$ -0.10 V) vs. the Ag wire pseudo reference electrode.
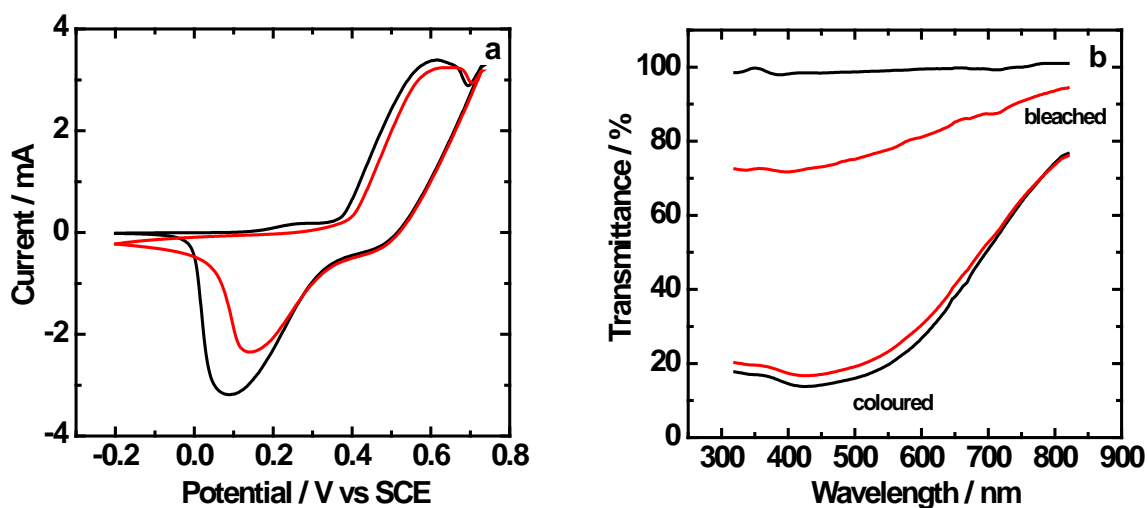
Figure 5.5. CVs (a) and visible region *in-situ* transmission spectra (b) for hydrated NiO film for the 1st (——) and 50th (——) CV. The film was cycled for 50 times ($-0.20 \rightarrow +0.75 \rightarrow -0.20$ V vs. SCE) at 10 mV s^{-1}. Visible region *in-situ* transmission spectra were recorded for the 'bleached' and coloured states in the wavelength range of 320–820 nm in aqueous KOH (0.1 mol dm^{-3}). EC switching for visible region spectra was conducted by application of potential steps (0.00 V $\rightarrow$ +0.47 V $\rightarrow$ −0.10 V) vs. the Ag wire pseudo reference electrode.

5.3. Electrochromic properties of NiO-based thin films prepared by AACVD technique

Table 5.2 gives *in-situ* spectral data and calculated EC performance parameters for square-wave potential switching between the 'bleached' and coloured forms after the as-deposited NiO films (prepared by AACVD for 10, 15 and 20 minutes) had been subject to 50, 100 and 500 continuous conditioning oxidative voltammetric cycles in aqueous KOH (0.1 mol dm^{-3}) electrolyte. Figure 5.6 shows example visible region *in-situ* transmittance spectra, in this case for the as-deposited NiO(15 min) film, and in the oxidised NiOOH coloured state, following increasing numbers of conditioning cycles. For such a film, it is noted from table 5.2, that after 500 cycles the change in optical transmittance between the 'bleached' and coloured forms increased from 21.4% to 54.8% when measured at 550 nm. This increase in transmittance change between the 'bleached' and coloured state on continuous cycling is due to the gradual change in film morphology from octahedral-like grains to a high surface area of porous interconnecting flakes (chapter 4). Such porous morphology shows greater EC performance due to increased contact between active material and electrolyte for facilitating hydroxide ion penetration.

5. Electrochromic properties and colorimetric measurements

Table 5.2. *In-situ* spectral data and EC performance parameters on square wave switching (0.00 V → +0.50 V → –0.20 V vs. Ag wire pseudo reference electrode) between the 'bleached' and coloured states after the as-deposited NiO films had been subject to 50, 100, and 500 continuous conditioning oxidative voltammetric cycles in aqueous KOH (0.1 mol dm^{-3})^a

original film source	cycle no.	%T_b	%T_c	Δ%T	ΔA	CE/ cm^2 C^{-1}	t_c/t_b (s)
NiO(10 min)	50	86.8	66.6	22.0	0.11	39.6	3.2/2.7
NiO(10 min)	100	85.6	55.4	30.2	0.19	40.3	3.4/2.9
NiO(10 min)	500	84.6	30.9	53.7	0.44	34.6	5.6/3.8
NiO(15 min)	50	75.3	53.9	21.4	0.18	55.3	2.8/2.7
NiO(15 min)	100	74.8	46.4	28.4	0.21	45.0	4.1/3.6
NiO(15 min)	500	74.4	19.6	54.8	0.58	39.8	5.7/5.6
NiO(20 min)	50	65.9	33.7	32.2	0.30	41.8	5.0/4.2
NiO(20 min)	100	65.5	24.0	41.5	0.44	41.8	5.0/4.2
NiO(20 min)	500	66.3	12.5	53.8	0.72	32.5	7.4/6.5

$^a T_b$ = transmittance of 'bleached' form, T_c = transmittance of coloured form, Δ%T = change in transmittance between the 'bleached' and coloured forms, ΔA = change in absorbance, CE = colouration efficiency, t_c and t_b = switching times for colouration and bleaching. All measurements were taken at 550 nm, which had been found to be the wavelength for maximum absorbance change.

5. Electrochromic properties and colorimetric measurements
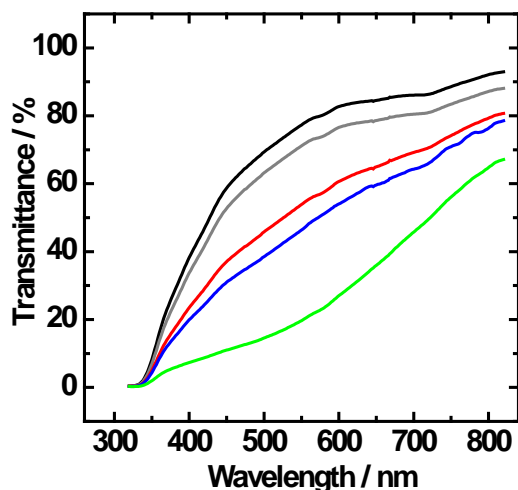
Figure 5.6. Visible region *in-situ* transmission spectra recorded in the wavelength range 320–820 nm in aqueous KOH (0.1 mol dm^{-3}), showing spectra of the coloured state as it forms with conditioning oxidative voltammetric cycle number. As-deposited NiO(15 min) film at 0.00 V vs. Ag wire pseudo reference electrode (——). As-deposited NiO(15 min) film at +0.40 V vs. Ag wire pseudo reference electrode (——). NiO(15 min) film at +0.40 V vs. Ag wire pseudo reference electrode, following 50 voltammetric cycles –0.50 V → +0.70 V → –0.50 V vs. SCE (——). NiO(15 min) film at +0.40 V vs. Ag wire pseudo reference electrode, following 100 voltammetric cycles –0.50 V → +0.70 V → –0.50 V vs. SCE (——). NiO(15) film at +0.60 V vs. Ag wire pseudo reference electrode, following 500 voltammetric cycles –0.50 V → +0.70 V → –0.50 V vs. SCE (——). All spectra were corrected for the transmittance of the uncoated FTO/glass substrate in aqueous KOH (0.1 mol dm^{-3}).

Figure 5.7 shows the transmittance spectra of all the as-deposited NiO films in the 'bleached' and coloured states. Transmittances for both the 'bleached' (T_b) and coloured (T_c) states decrease as the deposition time increases (table 5.2 and figure 5.7). On increase of deposition time the extent of colour change in the oxidised form increases but the films also appear less transparent in the reduced state (for photographs see figure 5.8). The films deposited for 10, 15, and 20 min, followed by 500 voltammetric cycles, each present the largest contrast (table 5.2), the transmittance change (~54% at 550 nm) between the 'bleached' and coloured states, being more than that of the films that were conditioned by only 50 and 100 cycles.
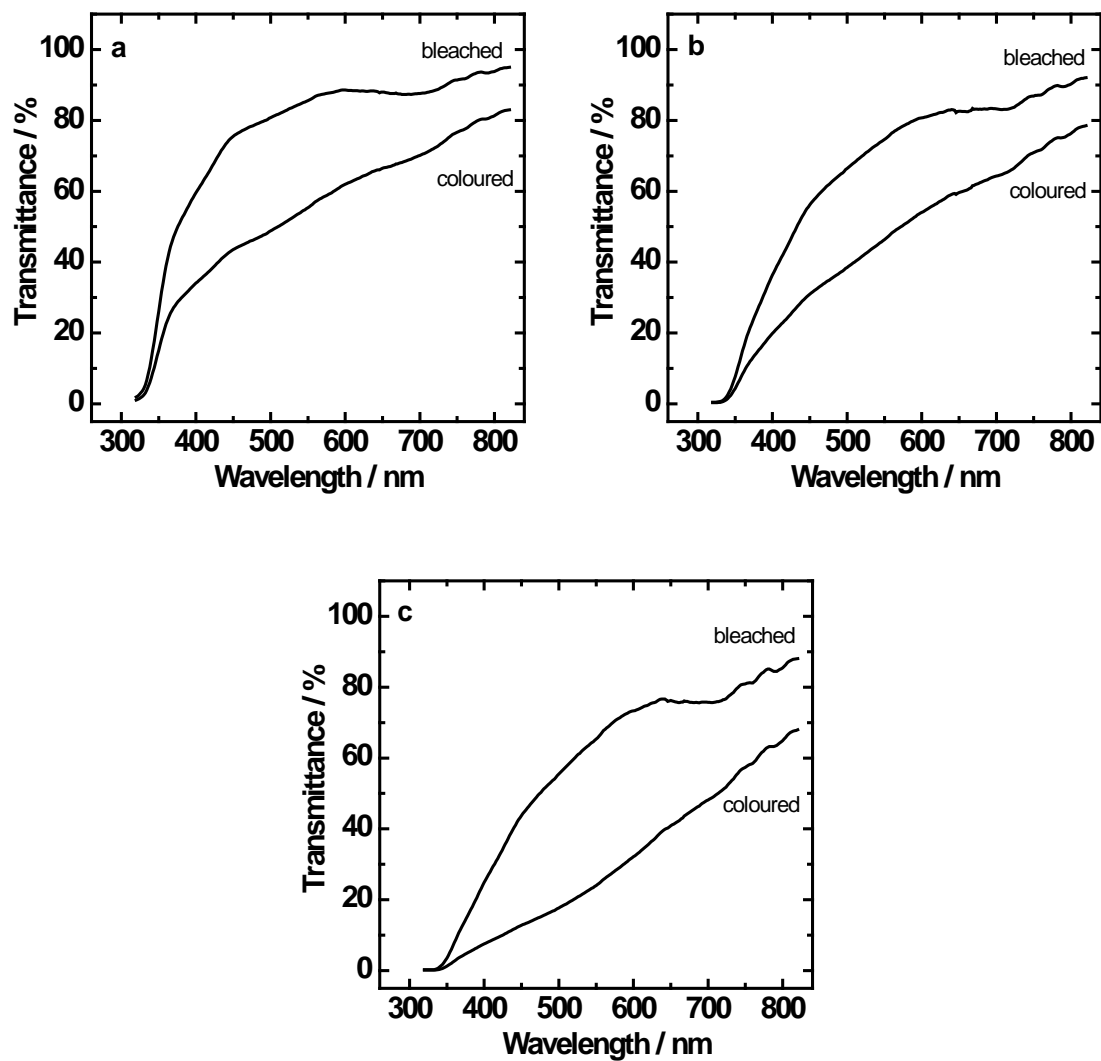
Figure 5.7. Visible region *in-situ* transmission spectra for the 'bleached' and coloured states following 100 voltammetric cycles in aqueous KOH (0.1 mol dm^{-3}): (a) NiO(10 min), (b) NiO(15 min) and (c) NiO(20 min).

5. Electrochromic properties and colorimetric measurements
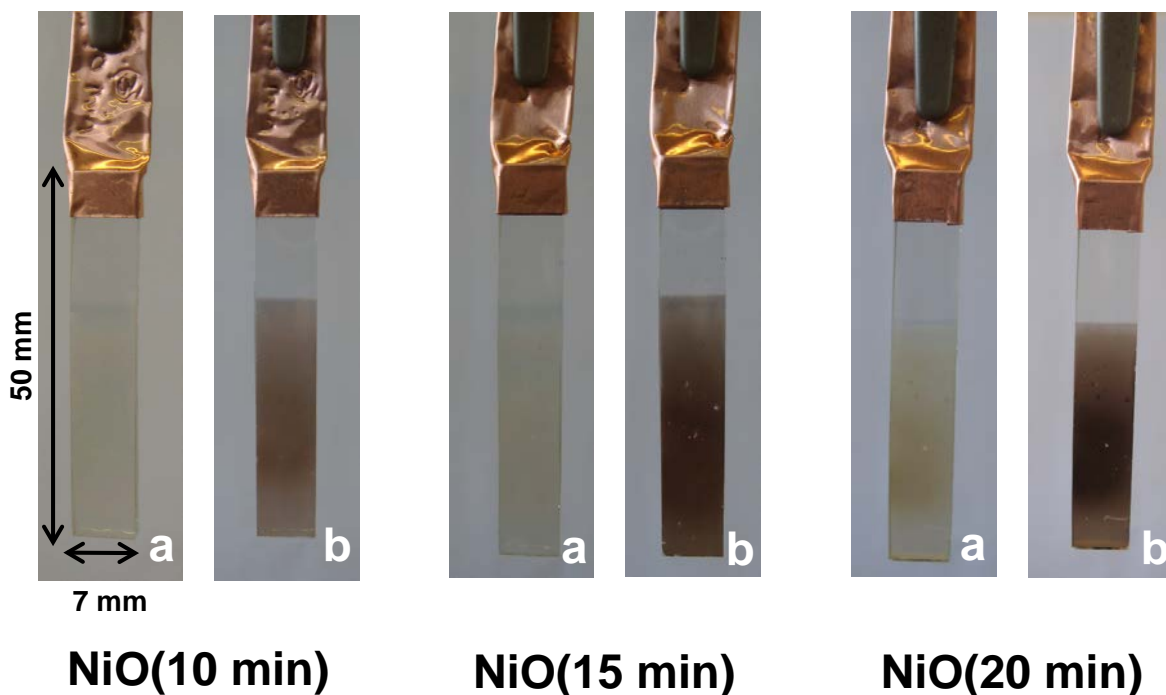
Figure 5.8. Photographs of (a) as deposited NiO films and (b) NiOOH films (following 3500 cycles –0.50 to +0.70 V vs. SCE at 50 mV s^{-1}, and then removal at +0.70 V). Each film was deposited on the lower 30 mm length of each 7 mm width FTO/glass). Although the as-deposited (photographs (a)) films appear grey in the above, by eye they appear light green.

Figure 5.9 shows examples of current-time transients and visible region absorbance spectra on reversibly switching between the 'bleached' and coloured states of one of the films. On oxidation of the transmissive green 'bleached' state, the visible region absorbance increases (figure 5.9 (b)) as the deep brown coloured state forms. On reduction, the deep brown coloured state reverts to the transmissive green 'bleached' state, with a decrease in the visible region absorbance (figure 5.9 (c)). The absorbance change, ΔA, increases with increasing deposition time and the number of 'bleached'/coloured cycles (table 5.2), the highest value (0.88) at 450 nm was obtained for NiO(20 min) recorded at 500 cycles (figure 5.10 (a)). The CE value (table 5.2 and figure 5.10 (b)) are comparable to those for films obtained by electrodeposition(~50 cm^2 C^{-1}),[36] CVD (44 cm^2 C^{-1}),[37] spray pyrolysis (30 cm^2 C^{-1}),[38] vacuum evaporation (32 cm^2 C^{-1}),[39] and electrochemical cathodic deposition (30 cm^2 C^{-1} in section 5.2).
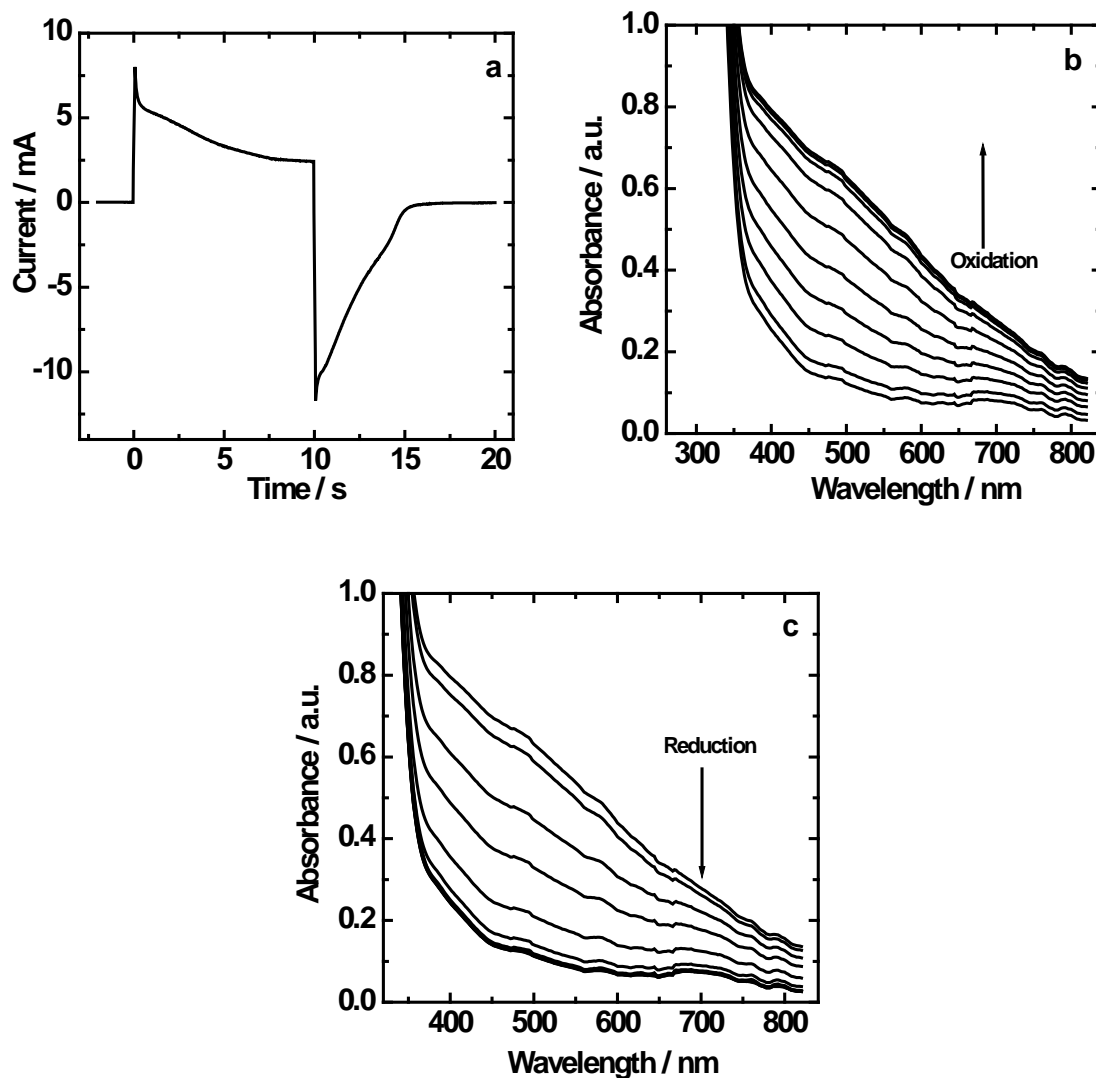
Figure 5.9. Current vs. time transients (a) and visible region absorbance spectra ((b) and (c), spectra recorded every 0.5 s), for the reversible switching of a NiO(10 min) film in aqueous KOH (0.1 mol dm^{-3}) between the transmissive green 'bleached' state and the coloured (deep brown) state. EC switching was conducted by application of potential steps (0.00 V → +0.50 V → −0.20 V) vs. the Ag wire pseudo reference electrode. In (b) and (c) the arrows indicate the direction of change in absorbance. The NiO(10 min) film had first been conditioned by 500 cycles (−0.50 → +0.70 → −0.50 V) vs. SCE, at 50 mV s^{-1}.

5. Electrochromic properties and colorimetric measurements
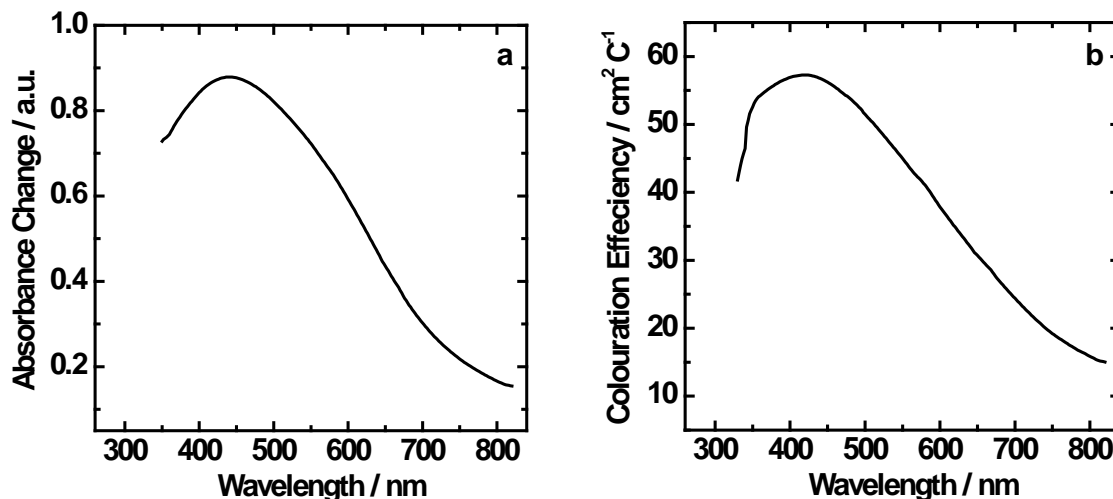
Figure 5.10. Change in absorbance of NiO(20 min) film recorded at cycle 500 (a) and colouration efficiency of NiO(15 min) film recorded at cycle 100 (b) in the wavelength range of 350–820 nm.

Absorbance vs. time plots (figure 5.11) were used to calculate the response times for all the NiO thin films. Table 5.2 also shows the response times, taken for the absorbance to reach a total change for both colouration (t_c) and 'bleaching' (t_b) processes. Response times for both colouration and 'bleaching' increased with both increasing number of cycles and film thickness. Generally, response times for the colouration process were longer than those for the 'bleaching' process.

Figure 5.12 shows the visible *in-situ* transmittance spectra of the as-deposited NiO(10 min) film following the 1000th and 10000th cycles. At 550 nm, the transmittance of the 'bleached' state was 93.5 and 88.7% respectively, after the 1000th and 10000th cycles. The transmittance of the 'coloured' state was 49.3 and 47.6%, respectively, after the 1000th and 10000th cycles. The change in transmittance between the 1000th ($\Delta\%T = 44.2\%$) and 10000th ($\Delta\%T = 41.1\%$) cycle was minimal, indicating good adherence of the film and consistent colour-switching properties. This shows that the NiO film deposited by AACVD is stable and suitable for EC window applications.

5. Electrochromic properties and colorimetric measurements
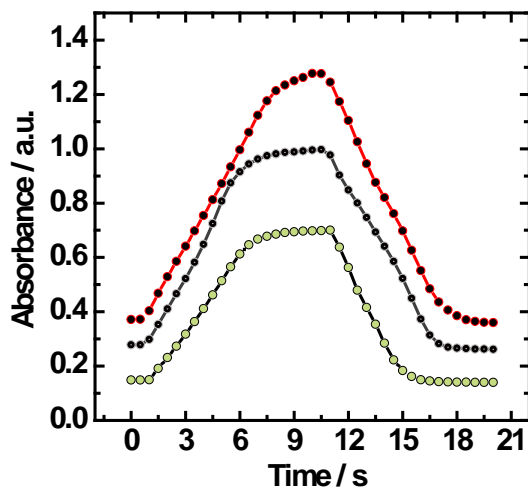
Figure 5.11. Absorbance vs. time transients recorded for NiO(10 min) (——), NiO(15 min) (——) and NiO(20 min) (——).Absorbance taken every 0.5 s at 550 nm for the reversible switching of films in aqueous KOH (0.1 mol dm^{-3}) between the transmissive green 'bleached' state and the coloured (deep brown) state. EC switching was conducted by application of potential steps (0.00 V → +0.50 V → −0.20 V) vs. the Ag wire pseudo reference electrode. The NiO films had first been conditioned for 500 cycles (−0.50 → +0.70 → −0.50 V) vs. SCE, at 50 mV s^{-1}.
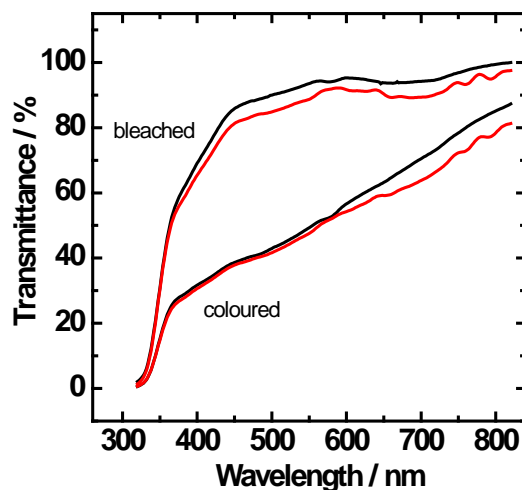
Figure 5.12. Visible region *in-situ* transmission spectra for a NiO(10 min) film following the 1000th (——) and 10000th (——) CV in the 'bleached' and coloured states recorded in the wavelength range of 320–820 nm in aqueous KOH (0.1 mol dm^{-3}). The film had been cycled for 1000 and 10000 cycles (−0.50 → +0.70 → −0.50 V) vs. SCE, at 50 mV s^{-1}.

5.4. Colour measurements of hydrated NiO thin films prepared by electrochemical cathodic deposition

Table 5.3 shows CIE 1931 %Y_L xy and CIELAB $L^*a^*b^*$ chromaticity coordinates for the hydrated NiO film as calculated from visible region absorbance spectra in figure 5.2 ((c) and (d)). At the initial applied potential (0.00 V), the reduced ('bleached') film appears by eye as fully transparent, at which point the coordinates coincided with those of the chosen illumination source (the 'white point', where x = 0.332, y = 0.347, and % Y_L = 100). On stepping the potential to +0.47 V, films switched to a brown-grey colour, with an increase in both the x and y coordinates. On switching back to the reduced state at an applied potential of -0.10 V, the colour changes back to the fully transparent form to highlight the complete reversibility of the redox system.

The xy data from table 5.3 are presented as a hue and saturation track in a chromaticity diagram (figure 5.13 (a)). Although the xy chromaticity diagram is not a uniform colour space, abrupt changes in the colour are found to correspond with significant changes in the xy coordinates. The changes in xy coordinates occur as the fully transparent hydrated NiO (figure 5.14 (a)) was oxidised to the coloured brown-grey NiOOH redox state (figure 5.14 (b)). Figure 5.13 (a) also shows the existence of hysteresis in the xy coordinates track on reversibly switching between the oxidised and reduced state. The presence of hysteresis may be due to the lack of stabilised chromaticity coordinates as a result of incomplete equilibrium at these switching time points. In figure 5.13 (b), the xy data for films prepared from as-deposited hydrated NiO are overlaid onto the CIE 1931 colour space template, showing the track of the xy coordinates between the 'bleached' and coloured states. In this representation, the line surrounding the horse-shoe shaped area is called the spectral locus, giving the visible light wavelength. The most saturated colours lie along the spectral locus. The line connecting the longest and shortest wavelength contains the non-spectral purples and is known as the purple line. Surrounded by the spectral locus and the purple line is the region known as the colour locus, which contains every colour that can exist. The hue may be determined by drawing a straight line from the white point, through the point of interest to the spectral locus,

thus obtaining the dominant wavelength (λ_d). The construction in figure 5.13 (b) gives an estimated value of 593 nm for coloured (brown-grey) state.

Table 5.3. Chromaticity coordinates (CIE 1931 %Y_L xy and CIELAB $L^*a^*b^*$) for a hydrated NiO/NiOOH film on FTO/glass[a]

time (s)	x	y	%Y_L	L^*	a^*	b^*
0	0.332	0.347	99.9	100	-0.2	-0.3
1	0.332	0.347	96.6	99	-0.1	-0.2
2	0.339	0.349	81.4	92	2.1	1.6
3	0.347	0.350	65.8	85	4.7	3.6
4	0.355	0.353	53.8	78	6.8	5.7
5	0.364	0.356	44.8	73	8.0	8.0
6	0.372	0.359	37.9	68	9.8	9.5
7	0.379	0.361	32.9	64	10.8	10.8
8	0.384	0.362	29.4	61	11.0	12.0
9	0.388	0.363	26.6	59	11.8	12.0
10	0.390	0.363	24.4	56	12.1	12.1
11	0.391	0.363	22.8	55	12.3	11.9
12	0.392	0.363	21.7	54	12.0	12.0
13	0.394	0.362	20.7	53	12.7	11.7
14	0.394	0.362	20.0	52	13.0	12.0
15	0.395	0.362	19.5	51	13.0	12.0
16	0.396	0.362	19.1	51	13.0	11.7
17	0.397	0.362	18.7	50	13.1	11.7
18	0.398	0.362	18.5	50	13.2	11.8
19	0.398	0.362	18.3	50	13.3	11.8
20	0.399	0.362	18.1	50	13.4	11.9
21	0.398	0.364	19.9	52	13.3	12.5
22	0.392	0.364	24.1	56	12.3	12.4
23	0.384	0.362	28.9	61	11.3	11.6

5. Electrochromic properties and colorimetric measurements

24	0.376	0.361	35.2	66	10.0	10.5
25	0.368	0.359	42.7	71	8.5	9.2
26	0.360	0.357	50.9	77	6.9	7.7
27	0.353	0.355	60.4	82	5.3	6.0
28	0.345	0.352	72.0	88	3.3	4.0
29	0.338	0.350	83.9	93	2.0	2.0
30	0.334	0.348	92.9	97	0.3	0.6
31	0.333	0.347	97.1	99	-0.1	-0.1
32	0.332	0.347	98.6	99	-0.1	-0.2
33	0.332	0.347	99.2	100	0.0	0.0
34	0.332	0.347	99.4	100	-0.2	-0.2
35	0.332	0.347	99.5	100	-0.2	-0.2
36	0.332	0.347	99.6	100	-0.1	-0.2
37	0.332	0.347	99.7	100	-0.2	-0.2
38	0.332	0.347	99.8	100	-0.1	-0.2
39	0.332	0.347	99.9	100	-0.2	-0.2
40	0.332	0.347	99.9	100	-0.2	-0.2

[a]Films were switched in aqueous KOH (0.1 mol dm^{-3}) between the 'bleached' and coloured states by application of potential steps (0.00 V $\rightarrow$ +0.47 V for 20 s and +0.47 V $\rightarrow$ –0.20 V for 20 s) vs. the Ag wire pseudo reference electrode.
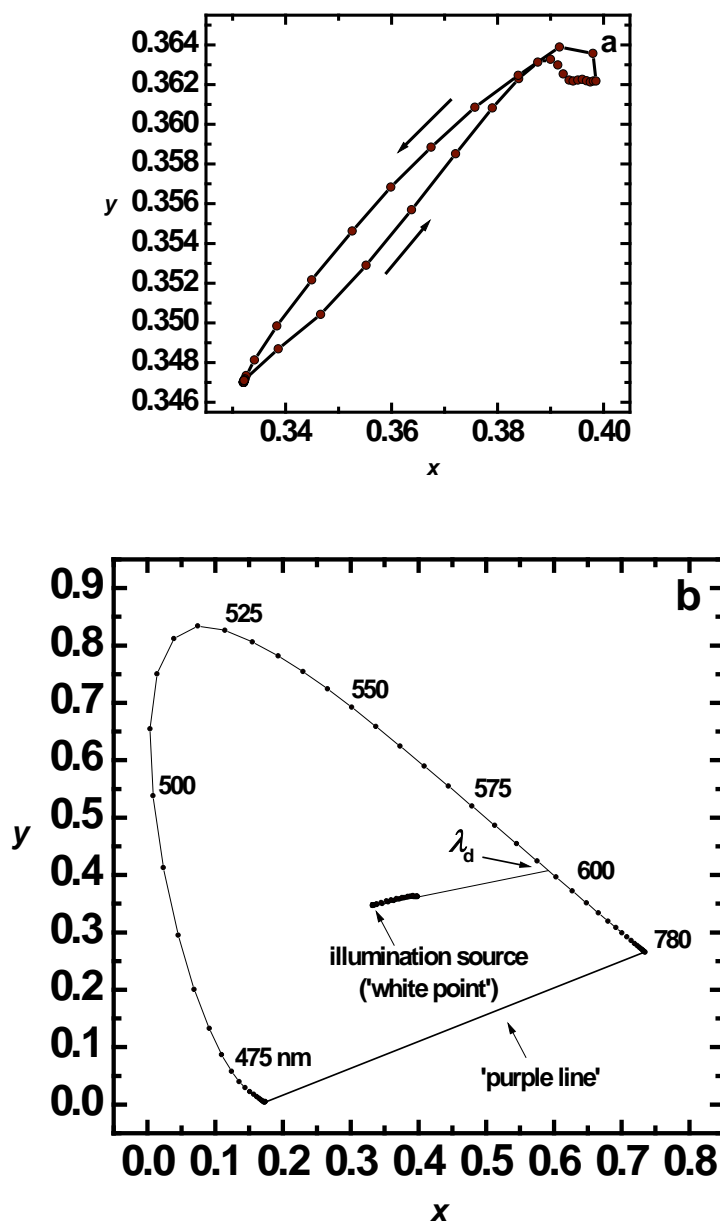
Figure 5.13. (a) CIE 1931 *xy* chromaticity plot for a hydrated NiO/NiOOH film on FTO/glass. The films were switched in aqueous KOH (0.1 mol dm^{-3}) between the 'bleached' and coloured states by application of potential steps (0.00 V → +0.47 V for 20 s and +0.47 V → −0.10 V for 20 s) vs. the Ag wire pseudo reference electrode. The arrows indicate the direction of the changes with the potential. (b) CIE 1931 *xy* coordinates for the hydrated NiO/NiOOH film on FTO/glass. This figure shows the locus coordinates, with labeled hue wavelengths, and the evaluation of the dominant wavelength (λ_d = 584 nm)) of the brown-grey state. Data were calculated from UV-visible absorbance spectra shown in figure 5.2.

5. Electrochromic properties and colorimetric measurements
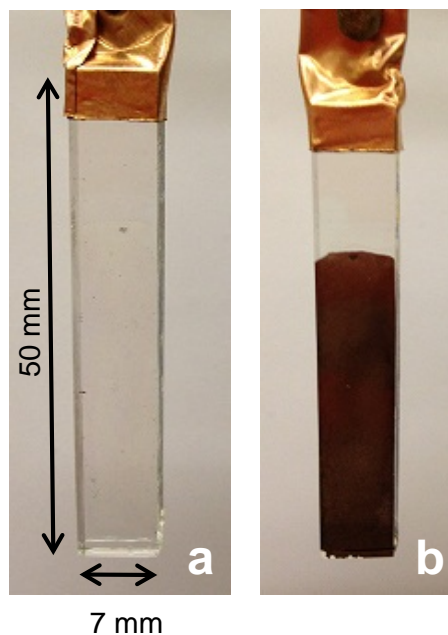
Figure 5.14. Photographs of (a) as deposited hydrated NiO films and (b) NiOOH film (film switched to the coloured state by cyclic voltammetry between –0.20 to +0.75 V vs. SCE at 10 mV s^{-1}, and then removed at +0.75 V). Film was deposited on the lower 30 mm length of each 7 mm width FTO/glass). Photographs correspond to the visible region *in-situ* transmission spectra for the 'bleached' and coloured state in figure 5.1

In CIE theory, colours cannot be specifically associated with a given pair of *xy* coordinates, because the third dimension of colour, lightness, is not included in the diagram. The relative lightness or darkness of a colour is very important in how it is perceived, and is presented as the relative or percentage luminance, Y_L, of the sample, to that of the background, Y_o. Relative luminance values can range from 100% for white/transparent samples (no light absorbed) to zero for samples that absorb all the light. Figure 5.15 shows the changes in the % Y_L on potential switching between the 'bleached' and coloured state. On redox switching of the deposited film by potential step, the relative luminance values decrease then increase dramatically for the oxidation and reduction process, respectively. The graphical form of the relative luminance is also in good correlation with electric charge (figure 5.2 (b)) as determined through integration of the current vs time transient in figure 5.2 (a).

5. Electrochromic properties and colorimetric measurements
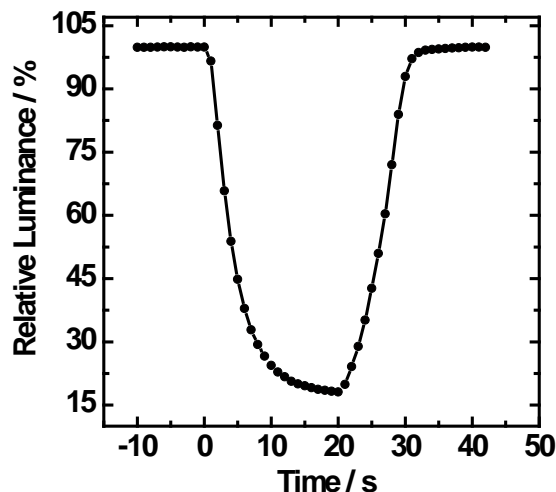
Figure 5.15. CIE 1931 relative luminance data vs. time for the hydrated NiO/NiOOH films on FTO/glass. Films were switched in aqueous KOH (0.1 mol dm^{-3}) between the 'bleached' and coloured states by application of potential steps (0.00 V → +0.47 V for 20 s and +0.47 V → −0.20 V for 10 s) vs. the Ag wire pseudo reference electrode.

The CIELAB *L*a*b** coordinates (table 5.3) are a uniform colour space defined by CIE in 1976 and offer a standard commonly used in the paint, plastic and textile industries (figure 5.16). *L** is the lightness variable of the sample, while *a** and *b** correspond to the two antagonistic chromatic processes (red–green and yellow–blue). In a *L*a*b** chromatic diagram, +*a** is the red direction, −*a** is the green direction, +*b** is the yellow direction, and −*b** is the blue direction. The centre (0, 0) of the chromaticity diagram is achromatic. As the *a** and *b** values increase, the saturation of the colour increases. At the initial 0.00 V applied potential, the 'bleached' state (*L** = 99.97, *a** = -0.2, *b** = -0.3) is close to the achromatic 'white point' (*L** = 100, *a** = 0, *b** = 0). As the potential is stepped to +0.47 V, *L** decreases and the saturation of the brown-grey colour increases, both *a** and *b** values becoming more positive. Although it might be expected that a combination of positive *a** and *b** values would produce orange, in combination with low *L** values, the films are perceived as deep brown.
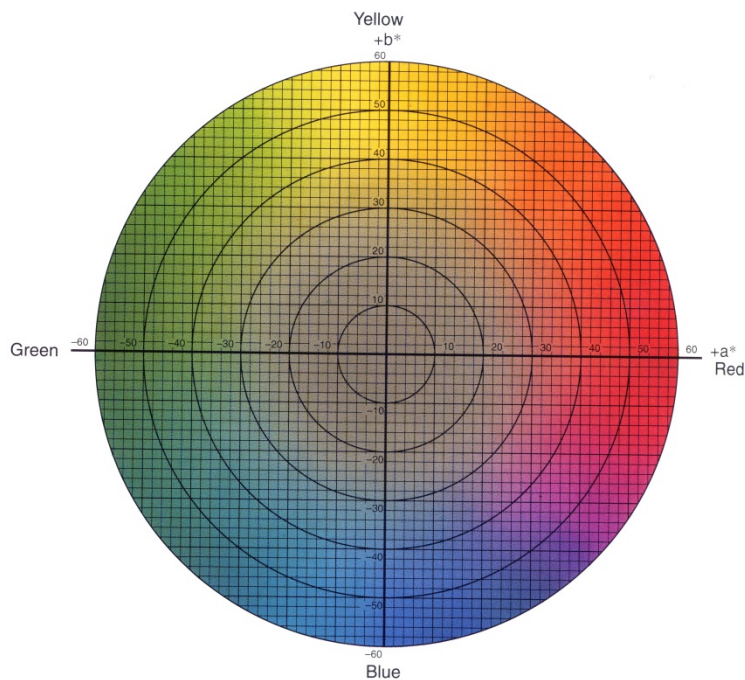
Figure 5.16. The CIE 1976 $L^*a^*b^*$ colorspace representing hue and saturation.

5.5. Colour measurements of NiO-based thin films prepared by AACVD

Table 5.4 gives CIE 1931 %$Y_L xy$ and CIELAB $L^*a^*b^*$ chromaticity coordinates for the various films in the 'bleached and coloured states as calculated from visible region absorbance spectra (such as figure 5.9 (b) and (c)).

Figure 5.17 (a) shows the dynamic changes of the CIE 1931 xy coordinates as a hue and saturation track, on potential stepping between the 'bleached' and coloured states, as a function of the deposition time of the original NiO films. At the initial applied potential (0.00 V), the 'bleached' films appear by eye as transmissive light green. With an increase in film thickness, the x, y and %Y_L coordinates (table 5.4) depart from those of the illumination source (the 'white point', where $x = 0.332$, $y = 0.347$, and %$Y_L = 100$), as the light green colour becomes slightly more intense. On stepping the applied potential to +0.50 V, films steadily turn to deep brown, with an increase in the x and y coordinates, and decrease in the luminance (%Y_L) (table 5.4 and figure 5.17 (a)). In figure 5.17 (b), the xy data for films prepared from as-deposited NiO(10 min) are overlaid onto the CIE 1931 colour space template,

showing the track of the *xy* coordinates between the 'bleached' and coloured states. The construction gives an estimated value of 584 nm for the coloured (deep brown) state of the film prepared from as-deposited NiO(10 min). There is a small increase in λ_d values with increase in deposition time, with values being 585 and 587 nm for films prepared from NiO(15 min) and NiO(20 min), respectively.

Table 5.4. Chromaticity coordinates (CIE 1931 %Y_L*xy* and CIELAB *L*a*b**) for each of the NiO/NiOOH films on FTO/glass[a]

original film source	*x*	*y*	%Y_L	*L**	*a**	*b**
NiO(10 min) 'bleached'	0.347	0.362	86.7	95	0	8
NiO(10 min) coloured	0.392	0.377	32.3	64	10	17
NiO(15 min) 'bleached'	0.361	0.376	77.1	90	1	16
NiO(15 min) coloured	0.420	0.391	21.3	53	12	23
NiO(20 min) 'bleached'	0.374	0.386	69.5	87	2	21
NiO(20 min) coloured	0.447	0.397	13.9	44	15	25

[a]Films were switched in aqueous KOH (0.1 mol dm^{-3}) between the 'bleached' and coloured states by application of potential steps (0.00 V → +0.50 V for 10 s and +0.50 V → −0.20 V for 10 s) vs. the Ag wire pseudo reference electrode.
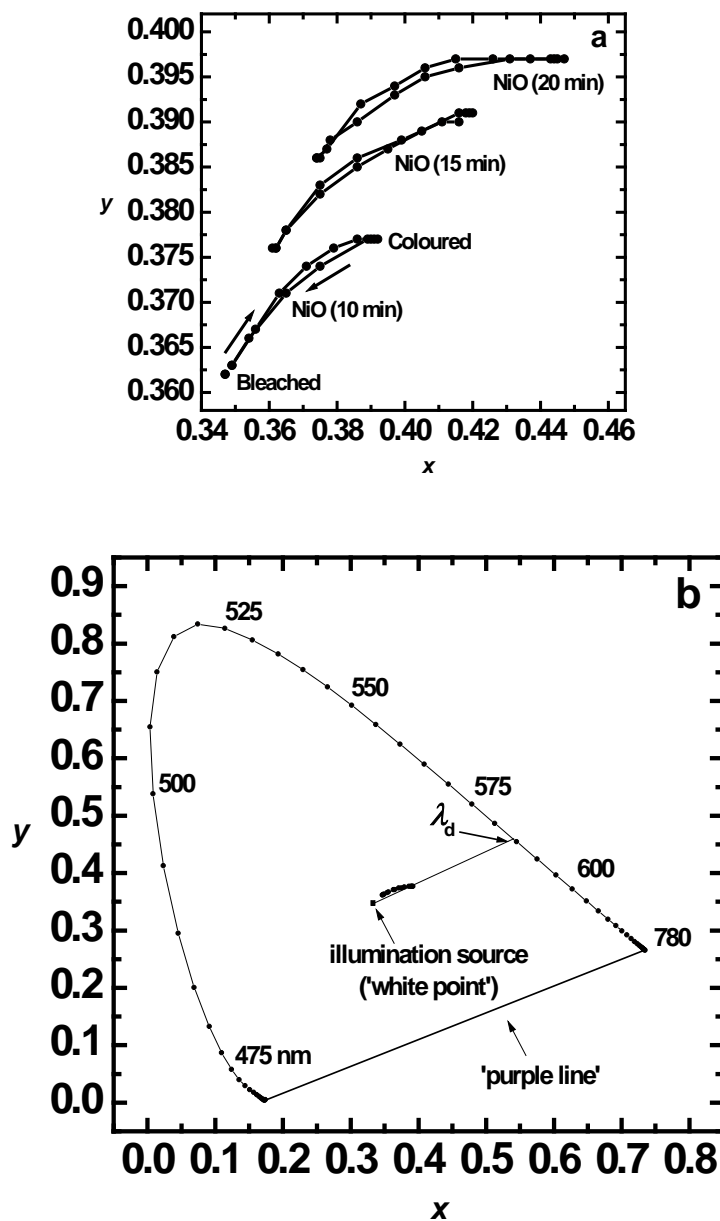
Figure 5.17. (a) CIE 1931 *xy* chromaticity plots for each of the NiO/NiOOH films on FTO/glass. Films were switched in aqueous KOH (0.1 mol dm^{-3}) between the 'bleached' and coloured states by application of potential steps (0.00 V → +0.50 V for 10 s and +0.50 V → −0.20 V for 10 s) vs. the Ag wire pseudo reference electrode. The arrows indicate the direction of the changes with the potential. (b) CIE 1931 *xy* coordinates for the NiO/NiOOH film on FTO/glass prepared from the as-deposited NiO(10 min). This figure shows the locus coordinates, with labeled hue wavelengths, and the evaluation of the dominant wavelength (λ_d = 584 nm)) of the deep brown state.

5. Electrochromic properties and colorimetric measurements

Figure 5.18 shows the graphical form of the changes in the %Y_L on potential switching between the 'bleached' and coloured state for all the NiO-based films. When the films are oxidised, the luminance dramatically decreases, as the deep brown colour forms and steadily becomes more saturated.
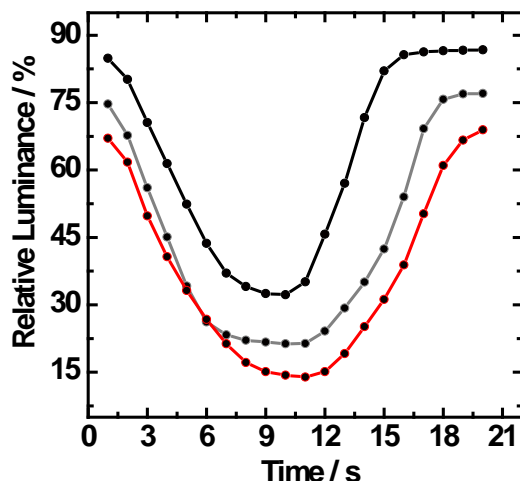
Figure 5.18. CIE 1931 relative luminance data vs. time for each of the NiO/NiOOH films on FTO/glass. The films were prepared from the original as-deposited NiO films as indicated: NiO(10 min) (——), NiO(15 min) (——) and NiO(20 min) (——). Films were switched in aqueous KOH (0.1 mol dm^{-3}) between the 'bleached' and coloured states by application of potential steps (0.00 V → +0.50 V for 10 s and +0.50 V → –0.20 V for 10 s) vs. the Ag wire pseudo reference electrode.

Table 5.4 also shows the CIELAB $L^*a^*b^*$ coordinates for all the films at the 'bleached and coloured state. At the initial 0.00 V applied potential, the 'bleached' state (L^* = 95, a^* = 0, b^* = 8) prepared from as-deposited NiO(10 min) is close to the achromatic 'white point' (L^* = 100, a^* = 0, b^* = 0). For thicker films, there is a small decrease in the initial L^* value, and an increase in a^* and b^* (table 5.4). As the potential is stepped to +0.50 V, L^* decreases and the saturation of the brown colour increases, both a^* and b^* values becoming more positive (table 5.4). With increase in film thickness, the brown colouration becomes more saturated as quantified by a decrease in L^* when in its coloured state and an increase in a^* and b^* (table 5.4). Similarly to the electrochemically deposited hydrated NiO film, the combination of positive a^*, b^* and low L^* values produced a deep brown coloured films.

134

5.6. Comparison of the colour measurements of electrochromic nickel (II) oxide/hydroxide thin films prepared by electrochemical cathodic deposition, aerosol-assisted chemical vapour deposition and layer-by-layer deposition techniques

This section outlines the chromaticity data produced for EC NiO-based thin films again prepared by cathodic electrodeposition, aerosol-assisted chemical vapor deposition (AACVD). However, thinner films than those prepared in section 5.2 and 5.3 were deposited in order to compare the chromaticity results with hydrated NiO thin films prepared by a layer-by-layer (LbL) deposition technique.

5.6.1. Thin film preparation

For accurate chromaticity comparison, film thicknesses for each deposition method were controlled so that the amount of active material deposited produced a similar change of absorbance between the bleached and the coloured state by application of potential steps in aqueous KOH (0.1 mol dm^{-3}).

Electrochemically hydrated NiO films were formed on to FTO/glass from aqueous nickel nitrate (0.01 mol dm^{-3}) solution by applying a cathodic current of -0.2 mA (-0.1 mA cm^{-2}) for 50 s.[40] For NiO thin films prepared by the AACVD technique, nickel acetylacetonate and 1 cm^3 of N,N-dimethylaminoethanol in toluene was used as a the precursor. Films were deposited for 4 min on a FTO/glass substrate, which was heated to 450°C by placing it on a temperature controlled hot plate. Hydrated NiO LbL assembly was conducted through electrostatic interactions, where multiple layers of cationic poly(allylamine hydrochloride) (PAH) and anionic hydrated NiO nanoparticles were prepared onto tin-doped indium oxide (In$_2$O$_3$(Sn), ITO) on glass transparent conducting substrate.[41] Two electrostatic bilayers were performed by dipping the ITO/glass in a solution of PAH for 5 min. The substrate was then rinsed with deionised water and dried in N$_2$ gas. It was then placed in a hydrated NiO nanoparticles solution for 5 mins, washed and dried again. Multiple bilayers were created by repeating these steps (see chapter 3 for more details).

5.6.2. Potential step and *in-situ* absorbance measurements

Figures 5.19, 5.20 and 5.21 show the current-time transients on switching between the 'bleached' and coloured states for films deposited using all three deposition techniques. For the first 10 s (on the plot indicated as -10 to 0 s), the potential was held at -0.10 V to ensure complete equilibrium. The potential was then stepped to a positive value of +0.35 V from 1 to 20 s for the oxidation and negative value of -0.10 V from 21 to 40 s for the reduction process. The longer time scale current-time transients (figures 5.19(a), 5.20 (a) and 5.21 (a)) for all three films showed similar symmetrical amperometric responses for the Ni^{2+} to Ni^{3+} redox system. However, closer observations indicated that for the hydrated NiO films prepared by electrochemical cathodic deposition and LbL technique, the current responses were not symmetrical and the traces appeared to be biphasic, an effect which is said to involve two mechanisms with different time courses.[42]

Figures 5.19 (b) and 5.21(b) shows the expanded views for the oxidation of the hydrated NiO films prepared by the electrochemical cathodic deposition and LbL techniques, respectively. For the electrochemically deposited film (figure 5.19 (b)), after an initial increase in current at 0 s, a second peak was observed between 0 and 3 s, with a similar response during the reverse reduction process between 20 and 22 s (figure 5.19 (c)). In the case of the LbL deposited film (figure 5.21(b)), after a sharp increase in current, a broad peak between 0 and 6 s was seen. However, for the reduction process, a symmetrical current transient was produced.

5. Electrochromic properties and colorimetric measurements

Figure 5.19. Current vs. time transients for hydrated NiO deposited by electrochemical cathodic deposition technique (a), expanded view of anodic process (b) and expanded view of cathodic process (c). EC switching was conducted by application of potential steps (-0.10 V → +0.35 V → -0.10 V) vs. the Ag wire pseudo reference electrode.

This biphasic behaviour observed for hydrated NiO films prepared by electrochemical cathodic and LbL deposition techniques can be explained by examining the redox mechanism (figure 5.22 and equation. 5.9). On oxidation, the first mechanism involved the deintercalation of protons which combined with hydroxide ions at the interface to form water. Simultaneously, the second step was the insertion of hydroxide ions, a process responsible for the oxidation of hydrated NiO to the NiOOH phase. Similarly, the reduction process also involved a two-step process; firstly, water is dissociated at the interface to generate H^+, which is re-intercalated into the film structure. Concurrently, the second step involves the expulsion of hydroxide ions back into the solution.[43]

5. Electrochromic properties and colorimetric measurements
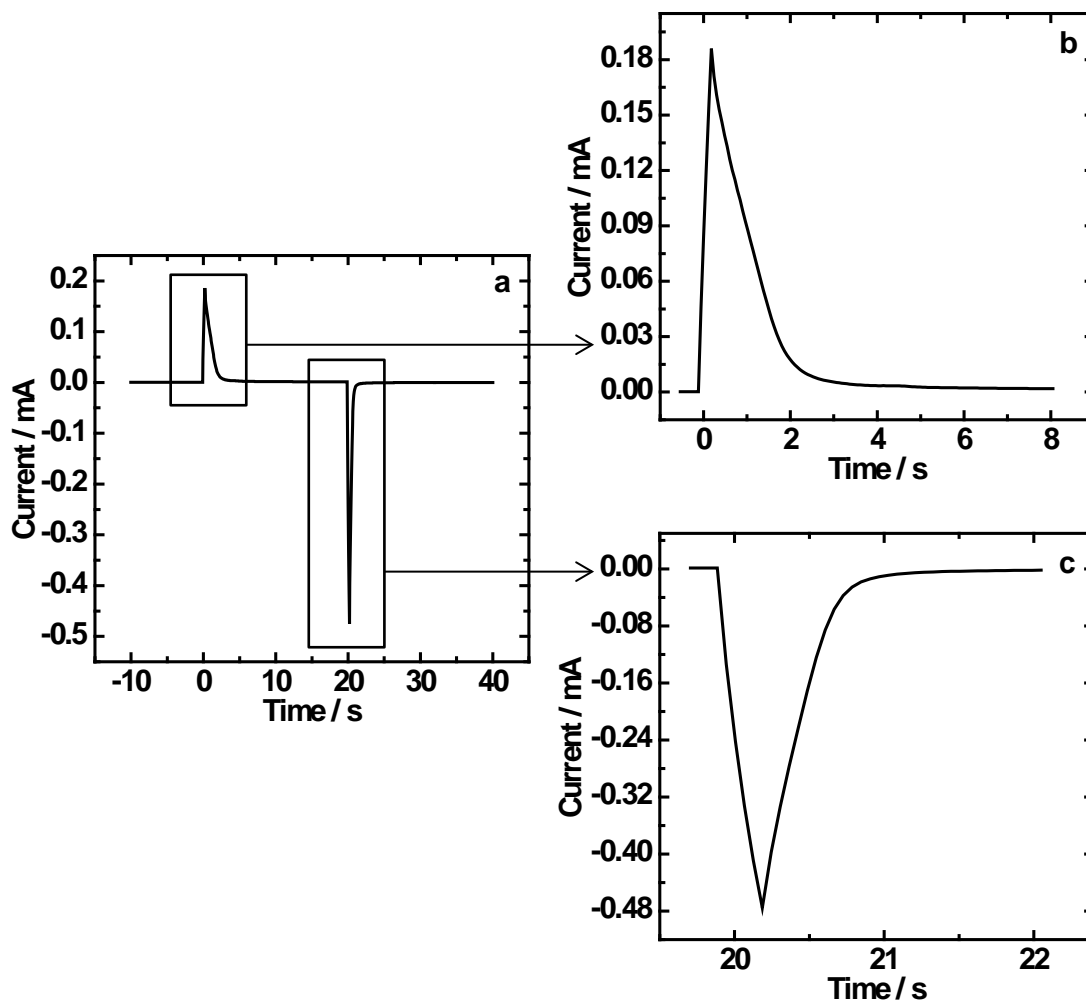
Figure 5.20. Current vs. time transient for NiO deposited by AACVD Technique (a), expanded view of anodic process (b) and expanded view of cathodic process (c). EC switching was conducted by application of potential steps (-0.10 V → +0.35 V → -0.10 V) vs. the Ag wire pseudo reference electrode.

In the case of the NiO film deposited by AACVD technique, both the oxidation and reduction process showed a symmetrical current-time response (figures 5.20 (b) and (c)). This observation might suggest that the process for the oxidation of NiO into NiOOH may only involve the one step of hydroxide ion insertion into the film structure. Equation 5.10 can be used to describe this process.

$$Ni(OH)_2 + OH^- \rightleftharpoons NiOOH + H_2O + e^- \tag{5.9}$$
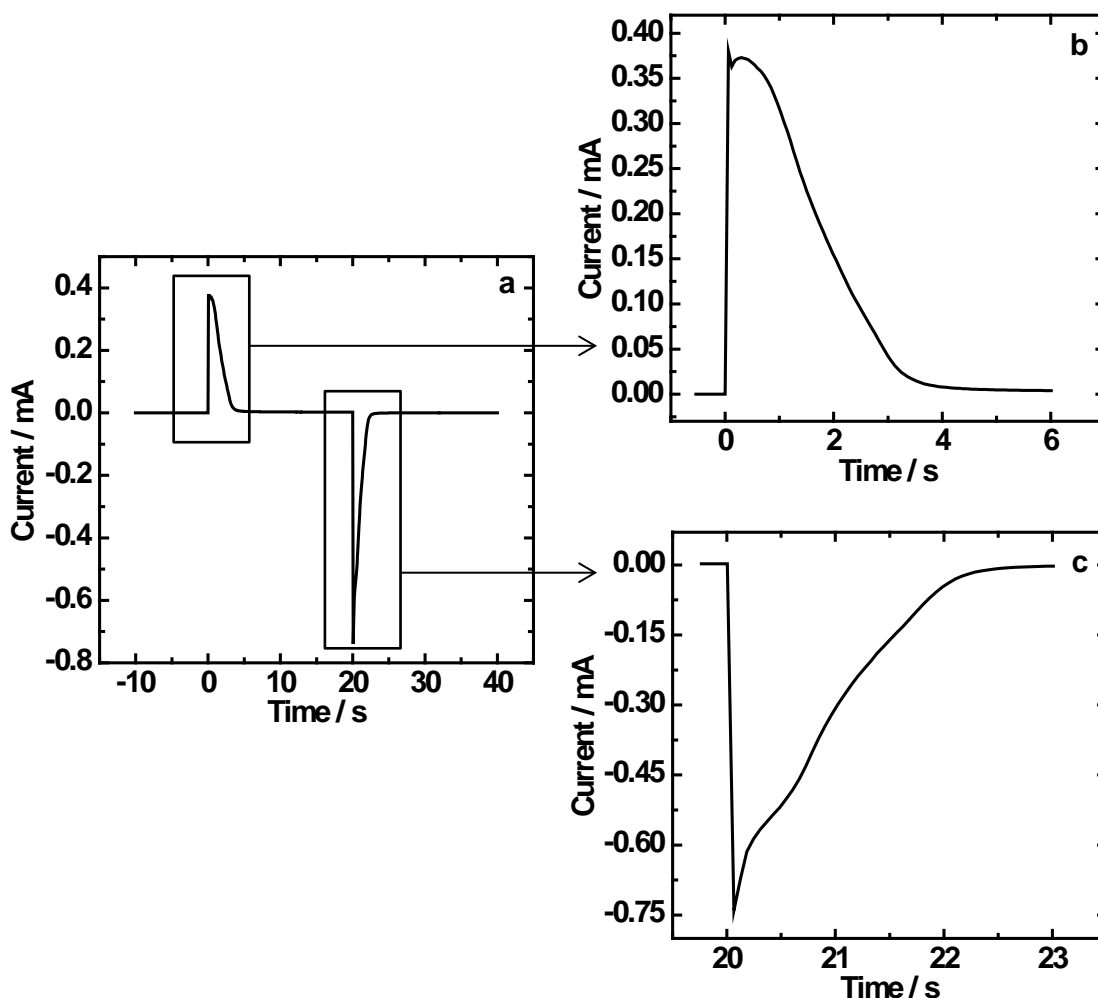
$$NiO + OH^- \rightleftharpoons NiOOH + e^- \tag{5.10}$$
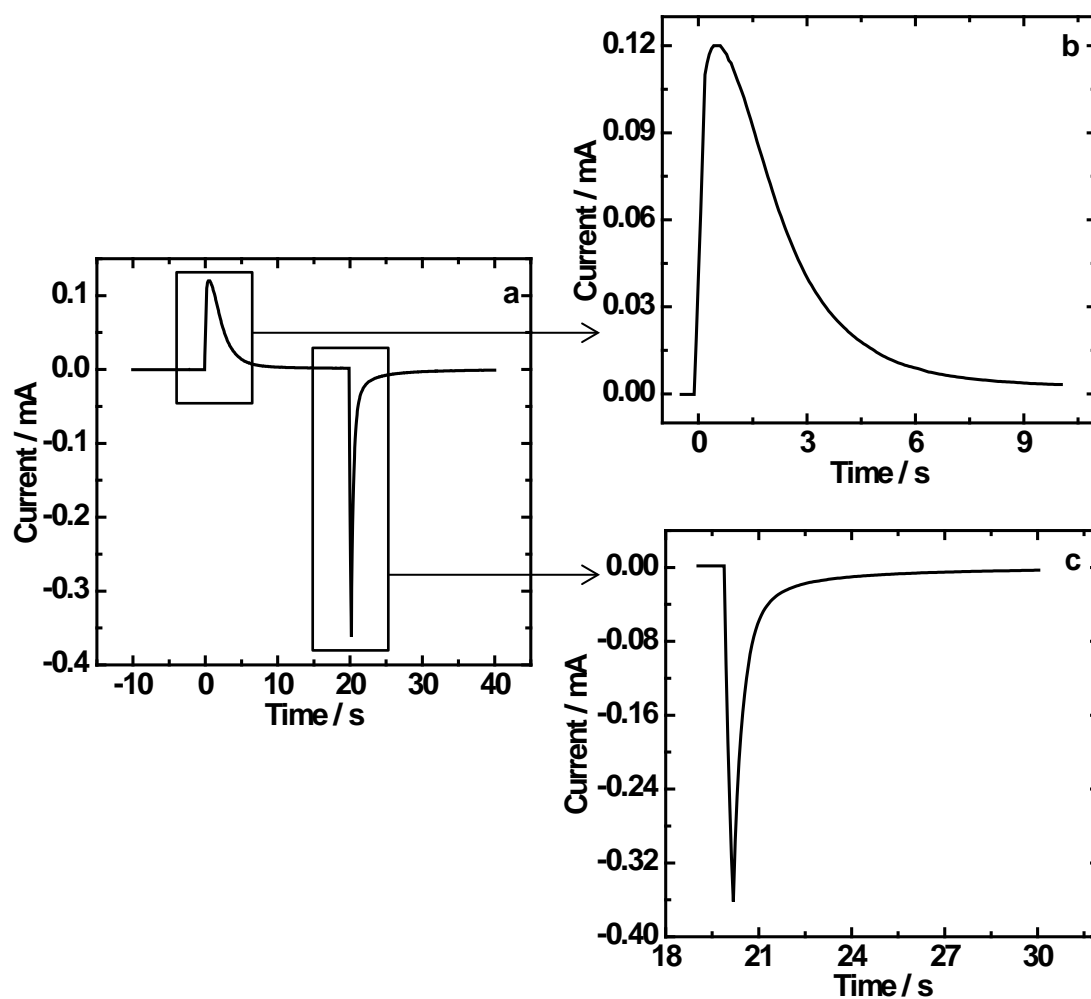
Figure 5.21. Current vs. time transient for hydrated NiO film prepared by LbL deposition technique (a), expanded view of anodic process (b) and expanded view of cathodic process (c). EC switching was conducted by application of potential steps (-0.10 V → +0.35 V → -0.10 V) vs. the Ag wire pseudo reference electrode.

5. Electrochromic properties and colorimetric measurements

Oxidation

Reduction
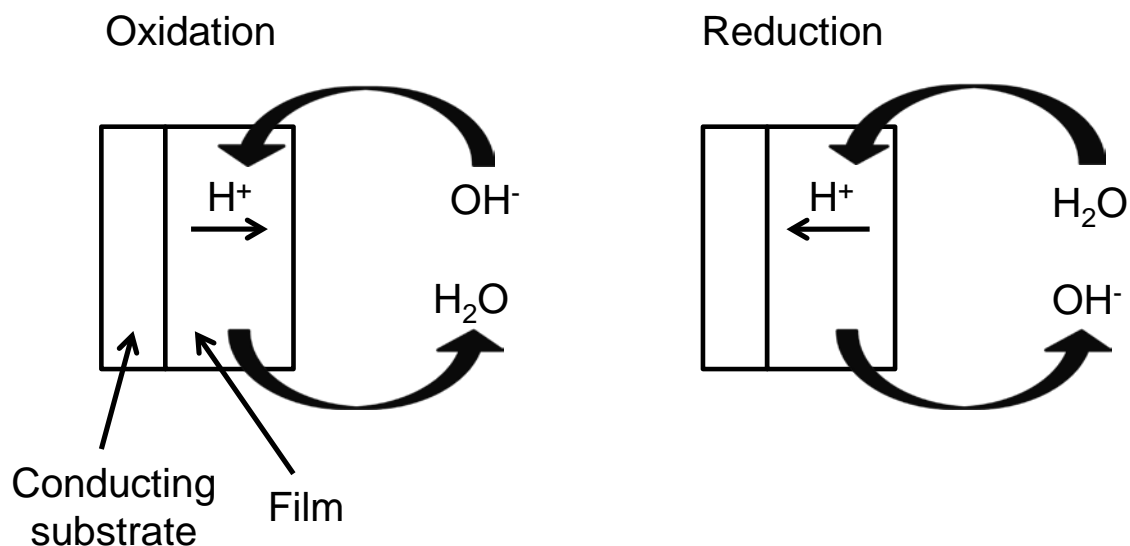
Figure 5.22. Schematic representation of redox mechanism for hydrated NiO film cycled in KOH (0.1 mol dm^{-3}). Diagram redrawn from.[43]

Figures 5.23 and 5.24 show the *in-situ* visible region absorbance spectra for films deposited using all three deposition techniques for the oxidation and reduction process, respectively. During the oxidation process (figure 5.23), the EC NiO-based films switched from a 'bleached' (transmissive) state to a coloured NiOOH (brown) state, with the subsequent increase in the visible region absorbance spectra. On reduction (figure 5.24), the coloured NiOOH switched back to the 'bleached' NiO state. By comparing the three sets of absorbance spectra, during the reduced ('bleached') state, it was observed that the absorbance spectrum did not exhibit any significant absorption band. However, on oxidation (coloured), a broad absorption band through the visible region was seen, which suggests the involvement of a delocalised electronic state with a semiconductor like behaviour.[44] Furthermore, there were clear differences in the spectral positions of maxima (λ_{max}), with values of 490, 450, and 530 nm for films deposited using electrochemical cathodic deposition, AACVD and LbL deposition techniques, respectively. The difference in λ_{max} suggested that for different film preparation methods, the optical properties for the oxidised state presented a slight difference in the tone of the colour change, although the difference was impossible to see by naked eye as the deposited films were relatively thin.
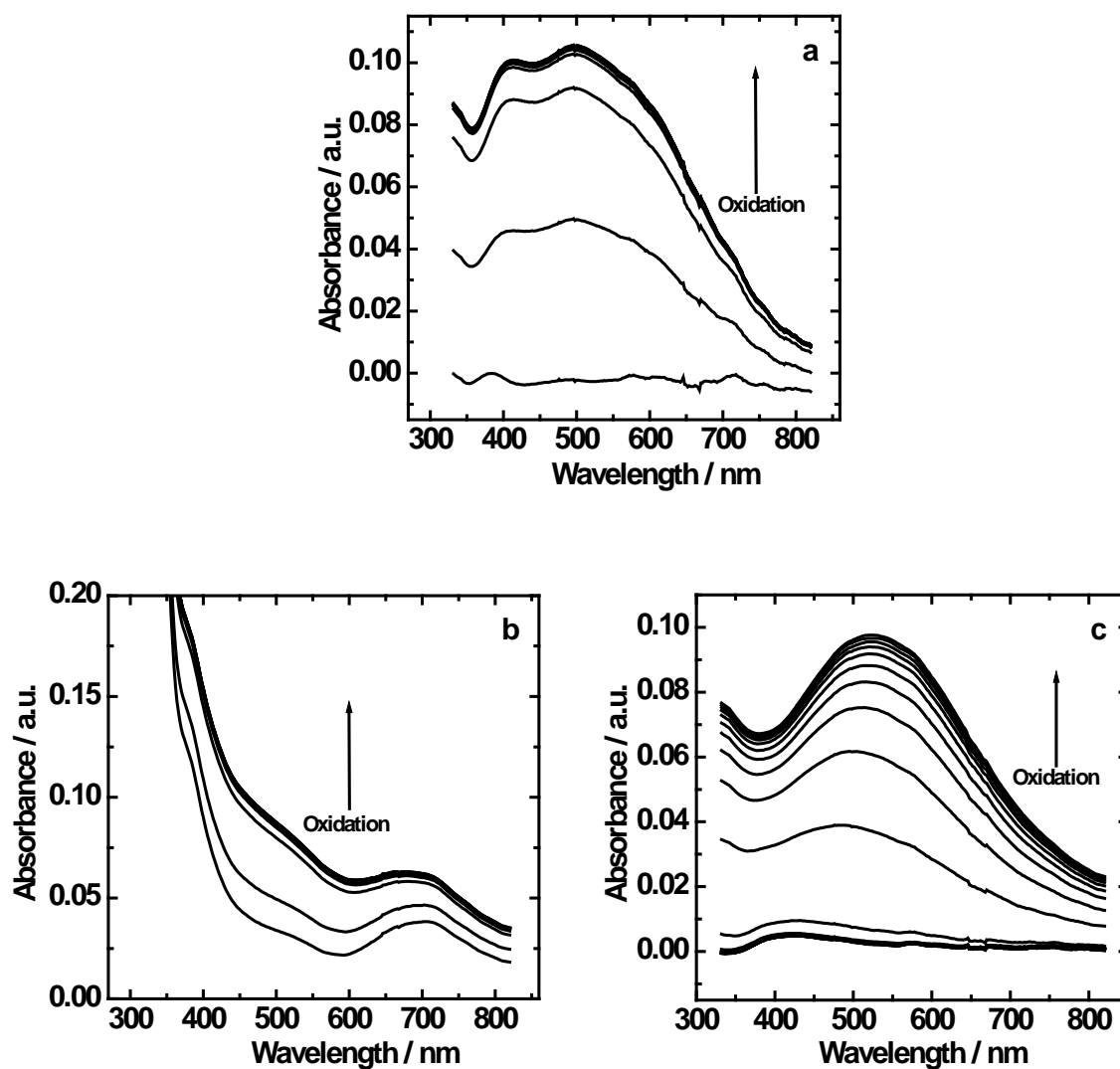
Figure 5.23. Visible region absorbance spectra recorded during the oxidation process for films prepared by electrochemical cathodic (a), AACVD (b) and LbL (c) deposition techniques. Spectra recorded every 1 s for the reversible switching in aqueous KOH (0.1 mol dm^{-3}) between the transmissive 'bleached' state and the coloured (brown) state. EC switching was conducted by application of potential steps (-0.10 V $\rightarrow$ +0.35 V $\rightarrow$ -0.10 V) vs. the Ag wire pseudo reference electrode. The figure shows the oxidation process (-0.10 V $\rightarrow$ +0.35 V).

5. Electrochromic properties and colorimetric measurements
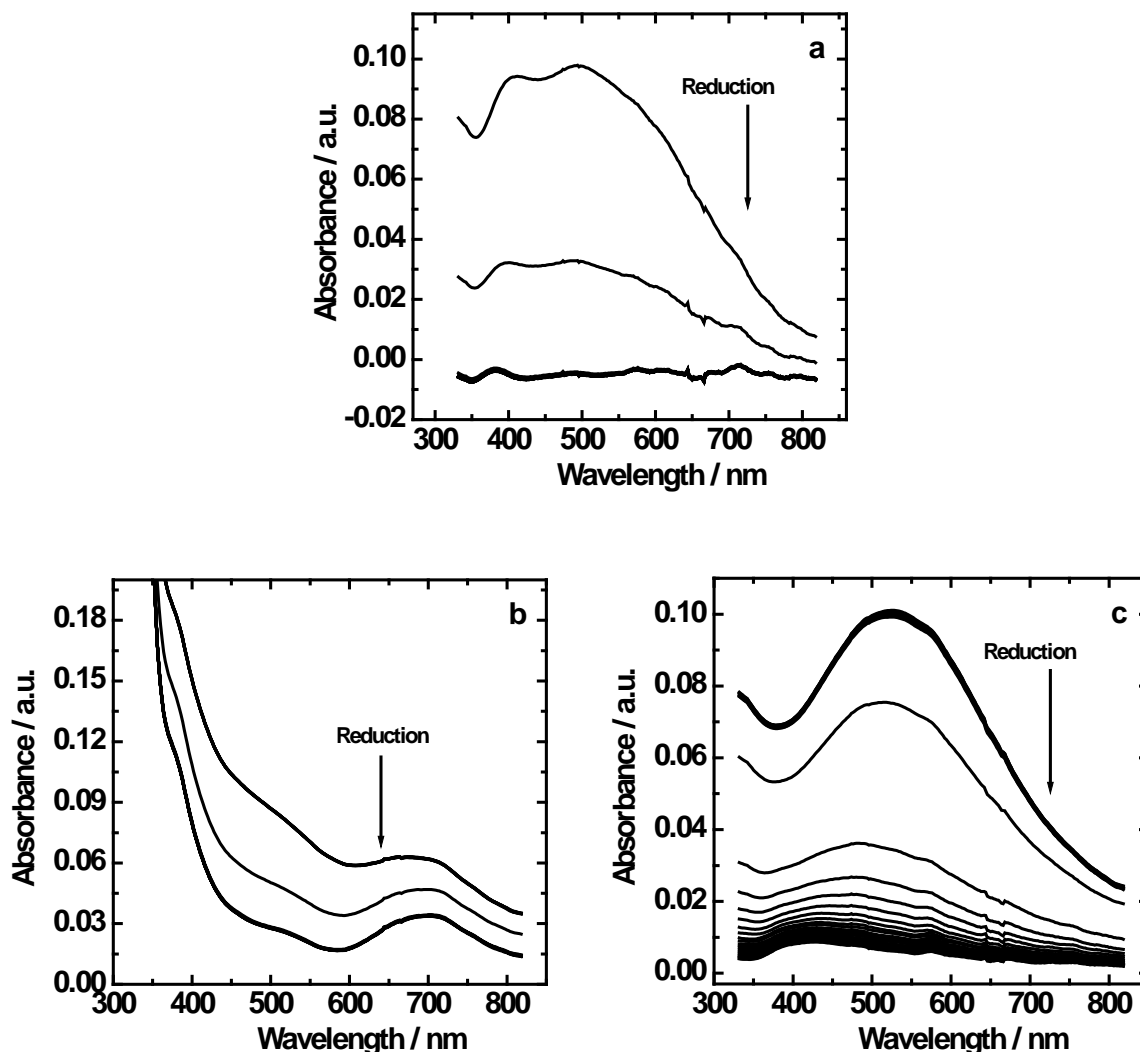
Figure 5.24. Visible region absorbance spectra recorded during the reduction process for films prepared by electrochemical cathodic (a), AACVD (b) and LbL (c) deposition techniques. Spectra recorded every 1 s for the reversible switching in aqueous KOH (0.1 mol dm^{-3}) between the transmissive 'bleached' state and the coloured (brown) state. EC switching was conducted by application of potential steps (-0.10 V $\rightarrow$ +0.35 V $\rightarrow$ -0.10 V) vs. the Ag wire pseudo reference electrode. The figure shows the reduction process (+0.35 V $\rightarrow$ -0.10 V).

5.6.3. Colorimetric measurements

Table 5.5 shows the CIE (Commission Internationale de l'Eclairage) 1931 colorimetric luminance (*%Y$_L$*), *x-y* coordinates, and the resulting calculated CIELAB *L*a*b** coordinates for all the films along with the deposition technique and switching state. The *x-y* chromaticity coordinates are also presented in the shape of colour tracks (figure 5.25), which can be used to highlight several apparent features. At the

initial applied potential (-0.10 V), for all three films, the 'bleached' states appeared by naked eye as fully transparent and the *x*, *y* and %*Y*$_L$ coordinates (table 5.5) were close to those of the illumination source (the 'white point', where *x* = 0.332, *y* = 0.347, and %*Y*$_L$ = 100). On stepping the applied potential to +0.35 V, the films steadily turned to a light brown colour, with generally an increase in the *x* and *y* coordinates values for the electrochemically deposited and the AACVD deposited films (figures 5.25 (a) and (b)). In the case of the LbL film, the *x* coordinate decreased after an initial increase and the *y* coordinates generally decreased.

Comparing the *x-y* coordinates for each deposition technique highlighted a few differences in the shape of the colour tracks. It can be seen in figure 5.25 (a) for the hydrated NiO film deposited by electrochemical cathodic deposition technique that the *x-y* coordinates for the reduction process did not coincide with those of the oxidation process, a trend which is said to show significant hysteresis. Similar results have also been reported in a previous study for the oxidation and reduction of PProDOT-(Hx)$_2$ polymer films.[20] Furthermore, a tailing or kink was also observed towards the latter stages of the oxidation process (between 15 and 20 s). In the case of the NiO film deposited by AACVD technique (figure 5.25 (b)), the chromaticity coordinates lacked the hysteresis described above, instead a linear oxidation and reduction response was produced. The LbL film showed a similar *x-y* colour track response when compared to the film deposited by electrochemical cathodic deposition, again there was significant hysteresis when switching between the oxidised and reduced states.

The presence of hysteresis for the films prepared by electrochemical cathodic and LbL deposition techniques may be attributed to the slightly longer switching times for the oxidation and reduction process (figures 5.19 and 5.21). Consequently, at each of these switching time points the resulting film may not have achieved complete equilibrium and as a result colour formation was not fully stabilised. The redox reaction mechanism for the hydrated NiO film may also have played a part in the hysteresis effect (figure 5.22). As previously mentioned, during the oxidation process for the hydrated NiO film a two-step process of proton deintercalation and hydroxide ion insertion takes place with different time courses. Therefore, the delay in reaching

complete equilibrium is due to the different time courses for these two steps thereby affecting colour stabilisation.

The relative lightness or darkness of a colour is very important in how it is perceived, and is presented as the relative or percentage luminance, $\%Y_L$, of the sample. EC materials also benefit from such values, a low value of luminance corresponds to an opaque material and a high value represents a transparent one. Figure 5.26 (a) shows the variation of $\%Y_L$ for all three films on switching between the 'bleached' and coloured state. The as-deposited films prepared by electrochemical cathodic and LbL deposition techniques appeared fully transparent with values very close to 100%. In the case of NiO film prepared by AACVD, the transparency is slightly lower due to the deposited film showing a transmissive light green appearance. On oxidation, the luminance decreases for all three films, as the brown colour was formed. The graphical representation of relative luminance in figure 5.26 (a) can also be used to compare with electrical charge data (figure 5.26 (b)), with a parallel response being observed.

Table 5.5. Chromaticity coordinates (CIE 1931 $\%Y_L xy$ and CIELAB $L^*a^*b^*$) for each of the NiO/NiOOH films[a].

original film source	x	Y	$\%Y_L$	L^*	a^*	b^*
Electro-Ni(OH)$_2$ 'bleached'	0.332	0.347	100.0	99.9	-0.3	-0.2
Electro-NiOOH) coloured	0.337	0.347	79.6	92.9	2.1	0.9
AACVD-Ni(OH)$_2$ 'bleached'	0.336	0.352	96.7	99.0	-0.7	2.6
AACVD-NiOOH coloured	0.341	0.355	87.6	95.0	0.3	4.8
LbL-Ni(OH)$_2$ 'bleached'	0.333	0.348	99.7	100.0	-0.1	0.3
LbL-NiOOH coloured	0.335	0.344	81.2	92.0	3.0	-1.0

[a]Films were switched in aqueous KOH (0.1 mol dm^{-3}) between the 'bleached' and coloured states by application of potential steps (-0.10 V $\rightarrow$ +0.35 V for 20 s and +0.35 V $\rightarrow$ −0.10 V for 20 s) vs. the Ag wire pseudo reference electrode.
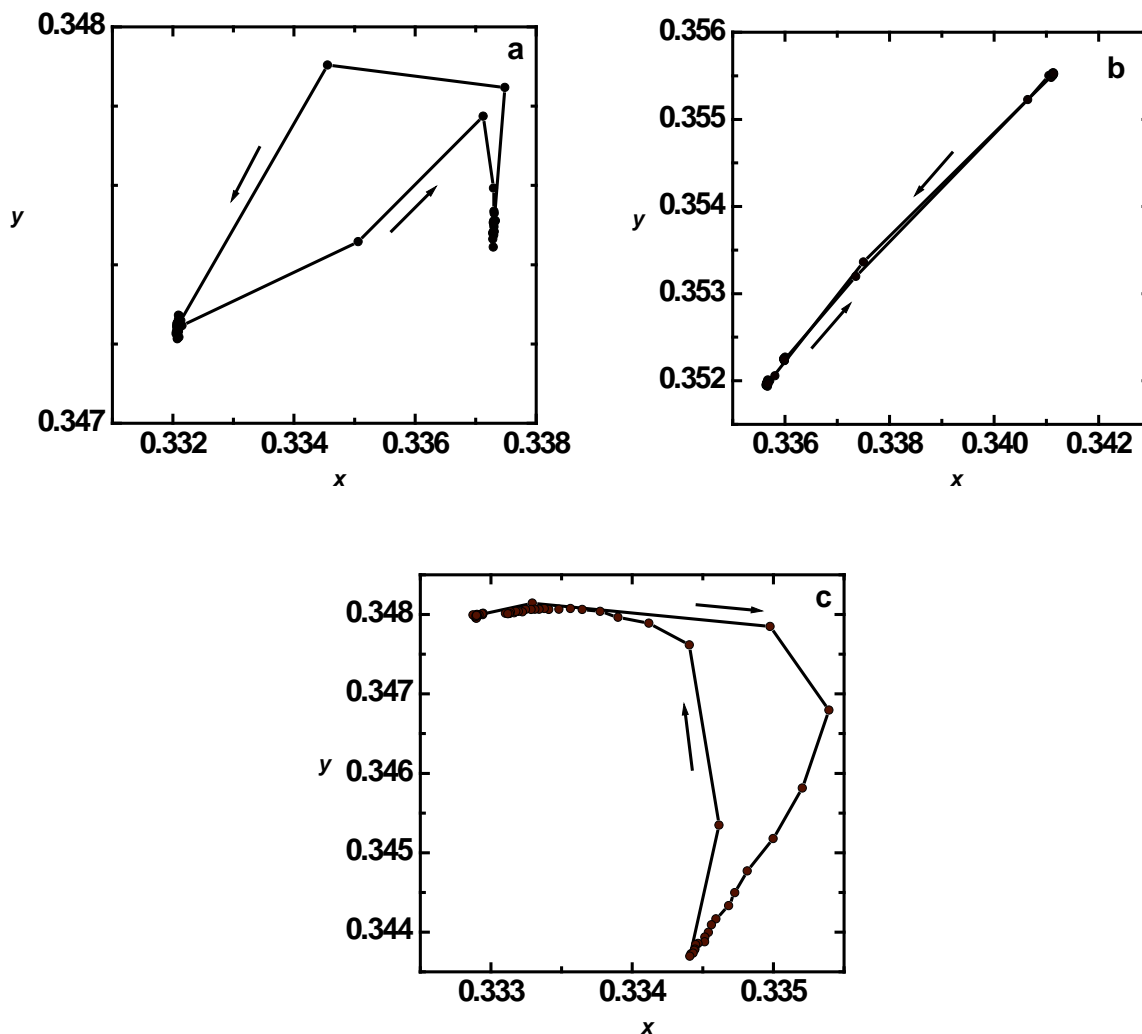
Figure 5.25. CIE 1931 *xy* chromaticity plots for films prepared by electrochemical cathodic deposition (a), AACVD (b) and LbL (c) deposition technique. Films were switched in aqueous KOH (0.1 mol dm^{-3}) between the 'bleached' and coloured states by application of potential steps (-0.10 V → +0.35 V for 20 s and +0.35 V → −0.10 V for 20 s) vs. the Ag wire pseudo reference electrode. The arrows indicate the direction of the changes with the potential.

Table 5.5, also shows the calculated $L^* a^* b^*$ coordinates for all three films during the coloured and 'bleached' phase. At the initial -0.10 V, the 'bleached' state for all three as-deposited films are close to the achromatic 'white point' ($L^* = 100$, $a^* = 0$, $b^* = 0$). On potential stepping to +0.35 V, the L^* values for films deposited by electrochemical cathodic deposition and AACVD techniques decreased with the a^* and b^* values becoming more positive. As a result, with the combination of red and yellow and low L^* values, the films were perceived to be light brown. For the LbL hydrated NiO film, the L^* values decreased and the a^* values moved towards positive direction during

colour saturation. However, with negative *b** values, the perceived colour produced a different shade of brown when comparing to the films deposited by electrochemical cathodic and AACVD deposition techniques.
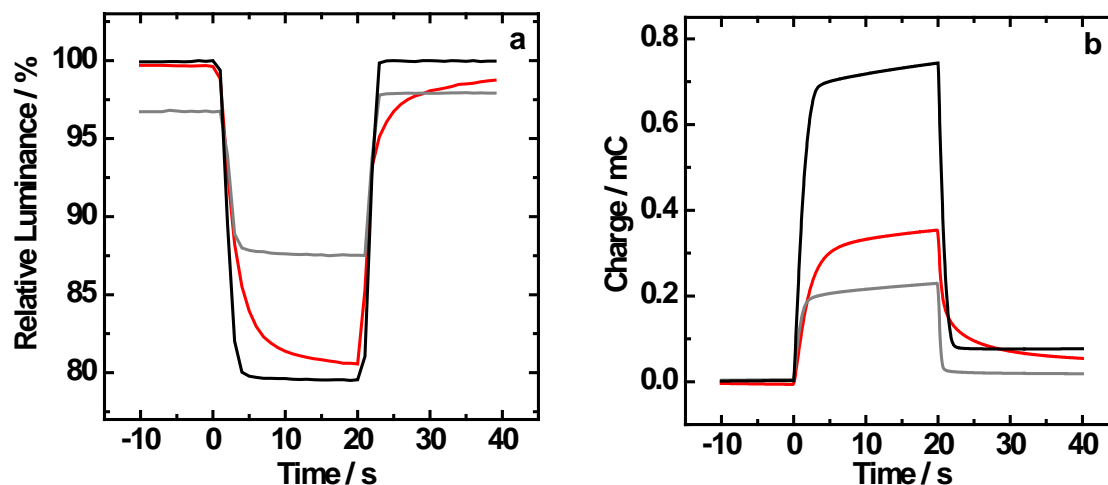
Figure 5.26. CIE 1931 relative luminance data vs. time (a) and charge vs time transient (b) for films prepared by electrochemical cathodic (——), AACVD (——) and LbL (——) deposition technique. Films were switched in aqueous KOH (0.1 mol dm^{-3}) between the 'bleached' and coloured states by application of potential steps (-0.10 V → +0.35 V for 20 s and +0.35 V → −0.10 V for 20 s) vs. the Ag wire pseudo reference electrode.

5.7. Conclusion

Electrochromic (EC) properties of NiO-based thin films prepared by electrochemical cathodic deposition and aerosol-assisted chemical vapour deposition (AACVD) techniques were investigated. The as-deposited hydrated NiO film prepared by electrochemical cathodic deposition showed excellent transmittance modulation ($\Delta\%T = 83.2$ at 434 nm), with CE of 30.1 cm^2 C^{-1} and low response times. However, after 50 voltammetric cycles, the cycle life was found to fade by 17.2% from charge measurements, and 28.8 % from *in-situ* transmittance spectra measurements.

NiO films prepared at different deposition times by the AACVD technique also showed good EC properties with low response times and excellent durability of up to 10000 voltammetric cycles. The film prepared at 10 min (NiO(10 min)) at 500 cycles

presented the optimal EC response with large contrast and the highest transmittance change of 53.7% at 550 nm.

Using a calculation method based on the integration of experimental spectral power distributions derived from *in-situ* visible region spectra over the CIE 1931 colour-matching functions, the colour stimuli of the NiO-based films, and the changes that take place on reversibly switching between the 'bleached' and coloured forms have been calculated. Films prepared by both deposition techniques gave positive *a** and *b** values to produce orange. However, in combination with low *L** values, the films were perceived as brown.

Finally, the effect of different deposition techniques on NiO-based thin films was investigated with switching times and the different reaction mechanism having an effect on the colour coordinate measurements. The underlying reasons for the different properties of the films prepared on FTO/ITO/glass substrates by the three methods relate to the chemical identity and spectroelectrochemical properties of the different materials. In the case of the AACVD films, their EC and colorimetric properties are due to the presence of NiO. Whereas, for the electrochemical cathodic and LbL deposition techniques the active material is hydrated NiO ($Ni(OH)_2$).

5.8. References

[1]   Wyszecki, G. and Stiles, W. S. *Color Science: Concepts and Methods, Quantitative Data and Formulae, 2nd ed.*, John Wiley and Sons, New York, 1982.

[2]   Christie, R. M. *Colour Chemistry*, Royal Society of Chemistry, Cambridge, 2001.

[3]   Kuehni, R. G. *Color: An Introduction to Practice and Principles*, 2nd ed., John Wiley and Sons, Hoboken, New Jersey, 2005.

[4]   Mortimer, R. J., Varley, T. S. Quantification of colour stimuli through the calculation of CIE chromaticity coordinates and luminance data for application to *in situ* colorimetry studies of electrochromic materials, *Displays*, **32**, 2011, 35-44.

5. Electrochromic properties and colorimetric measurements

[5]   Thompson, B. C., Schottland, P., Zong, K. and Reynolds, J. R. *In situ* colorimetric analysis of electrochromic polymers and devices. *Chem. Mater.*, **12**, 2000, 1563-71.

[6]   Schwendeman, I., Hickman, R., Sönmez, G., Schottland, P., Zong, K., Welsh, D. M. and Reynolds, J. R. Enhanced contrast dual electrochromic devices. *Chem. Mater.*, **14**, 2002, 3118-22.

[7]   Sönmez, G., Schwendeman, I., Schottland, P., Zong, K. and Reynolds, J. R. N-substituted poly(3,4-propylenedioxypyrrole)s: high gap and low redox potential switching electroactive and electrochromic polymers. *Macromolecules*, **36**, 2003, 639-47.

[8]   Cirpan, A., Argun, A. A., Grenier, C. R. G., Reeves, B. D. and Reynolds, J. R. Electrochromic devices based on soluble and processable dioxythiophene polymers. *J. Mater. Chem.*, **13**, 2003, 2422-28.

[9]   Sönmez, G., Meng, H. and Wudl, F. Organic polymeric electrochromic devices: polychromism with very high coloration efficiency. *Chem. Mater.*, **16**, 2004, 574-80.

[10]   Thomas, C. A., Zong, K., Abboud, K. A., Steel, P. J. and Reynolds, J. R. Donor-mediated band gap reduction in a homologous series of conjugated polymers. *J. Am. Chem. Soc.*, **126**, 2004, 16440-50.

[11]   Unur, E., Jung, J.-H., Mortimer, R. J. and Reynolds, J. R. Dual-polymer electrochromic film characterization using bipotentiostatic control. *Chem. Mater.*, **20**, 2008, 2328-34.

[12]   Beaujuge, P. M., Ellinger, S. and Reynolds, J. R. Spray processable green to highly transmissive electrochromics via chemically polymerizable donor–acceptor heterocyclic pentamers. *Adv. Mater.*, **20**, 2008, 2772-76.

[13]   Beaujuge, P. M., Ellinger, S. and Reynolds, J. R. The donor–acceptor approach allows a black-to-transmissive switching polymeric electrochrome. *Nat. Mater.*, **7**, 2008, 795-99.

[14]   Reeves, B. D., Grenier, C. R. G., Argun, A. A., Cirpan, A., McCarley, T. D. and Reynolds, J.R. Spray coatable electrochromic dioxythiophene polymers with high coloration efficiencies. *Macromolecules*, **37**, 2004, 7559-69.

[15]   Sönmez, G., Shen, C. K. F., Rubin, Y. and Wudl, F. A red, green, and blue (RGB) polymeric electrochromic device (PECD): the dawning of the PECD era. *Angew. Chem. Int. Ed.,* **43**, 2004, 1498-502.

[16]   Sacan, L., Cirpan, A., Camurlu, P. and Toppare, L. Conducting polymers of succinic acid bis-(2-thiophen-3-yl-ethyl)ester and their electrochromic properties. *Synth. Met.*,**156**, 2006, 190-5.

[17]   Nunes, S. C., de Zea Bermudez, V., Silva, M. M., Smith, M. J., Ostrovskii, D., Sá Ferreira, R. A., Carlos, L. D., Rocha, J., Gonçalves, A. and Fortunato, E. Sol–gel-derived potassium-based di-ureasils for 'smart windows'. *J. Mater. Chem.*, **17**, 2007, 4239-48.

[18]   Tarkuc, S., Arslan Udum, Y. and Toppare, L. Tuning of the neutral state color of the π-conjugated donor–acceptor–donor type polymer from blue to green via changing the donor state of the polymer. *Polymer*, **50**, 2009, 3458-64.

[19]   Seol, H., Jeong, H. and Jeon, S. Optoelectrochemical properties of copolymer of terthiophene with 3,4-ethlenedioxypyrrole. *J. Electroanal. Chem.*, **636**, 2009, 107-12.

[20]   Mortimer, R. J., Graham, K. R., Grenier, C. R. G. and Reynolds, J. R. Influence of the film thickness and morphology on the colorimetric properties of spray-coated electrochromic disubstituted 3,4-propylenedioxythiophene polymers. *ACS Appl. Mater. Interfaces*, **1**, 2009, 2269-76.

[21]   Vasilyeva, S. V., Unur, E., Walczak, R. M., Donoghue, E. P., Rinzler, A. G. and Reynolds, J.R. Color purity in polymer electrochromic window devices on indium-tin oxide and single-walled carbon nanotube electrodes. *ACS Appl. Mater. Interfaces*, **1**, 2009, 2288-97.

[22]   Unur, E., Beaujuge, P. M., Ellinger, S., Jung, J. H. and Reynolds, J. R. Black to transmissive switching in a pseudo three-electrode electrochromic device. *Chem. Mater.*, **21**, 2009, 5145-53.

[23]   Amb, C. M., Beaujuge, P. M. and Reynolds, J. R. Spray-processable blue-to-highly transmissive switching polymer electrochromes via the donor–acceptor approach. *Adv. Mater.*, **22**, 2010, 724-8.

[24]   Dyer, A. L., Craig, M. R., Babiarz, J. E., Kiyak, K. and Reynolds, J. R. Orange and red to transmissive electrochromic polymers based on electron-rich dioxythiophenes. *Macromolecules*, **43**, 2010, 4460-7.

[25]   Vasilyeva, S. V., Beaujuge, P. M., Wang, S., Babiarz, J. E., Ballarotto, V. W. and Reynolds, J. R. Material strategies for black-to-transmissive window-type polymer electrochromic devices. *ACS Appl. Mater. Interfaces*, **3**, 2011, 1022-32.

[26] Amb, C. M., Kerszulis, J. A., Thompson, E. J., Dyer, A. L. and Reynolds, J. R. Propylenedioxythiophene (ProDOT)-phenylene copolymers allow a yellow-to-transmissive electrochrome. *Polym. Chem.*, **2**, 2011, 812-4.

[27] Dyer, A. L., Thompson, E. J. and Reynolds, J. R. Completing the color palette with spray-processable polymer electrochromics. *ACS Appl. Mater. Interfaces*, **3**, 201, 1787-95.

[28] Kalagi, S. S., Mali, S. S., Dalavi, D. S., Inamdar, A. I., Im, H. and Patil, P. S. Transmission attenuation and chromic contrast characterization of R.F. sputtered WO_3 thin films for electrochromic device applications, *Electrochim. Acta*, **85**, 2012, 501-8.

[29] Kalagi, S. S., Mali, S. S., Dalavi, D. S., Inamdar, A.I ., Im, H. and Patil, P. S. Limitations of dual and complementary inorganic–organic electrochromic device for smart window application and its colorimetric analysis. *Synth. Met.* **161**, 2011, 1105-12.

[30] Avendaño, E., Azens, A., Niklasson, G. A. and Granqvist, C. G. Electrochromism in nickel oxide films containing Mg, Al, Si, V, Zr, Nb, Ag, or Ta. *Sol. Energy Mater. Sol. Cells*, **84**, 2004, 337-50.

[31] Dalavi, D. S., Devan, R. S., Patil, R. S., Ma, Y. R. and Patil, P. S. Electrochromic performance of sol–gel deposited NiO thin film. *Mater. Lett.*, **90**, 2013, 60-3.

[32] Yonghong, Y., Jiayu, Z., Peifu, G., Xu, L and Jinfa, T. Electrochromism of titanium oxide thin film. *Thin Solid Films*, **298**, 1997, 197-9.

[33] Maruyama, T. and Arai, K. Electrochromic properties of niobium oxide thin films prepared by radio-frequency magnetron sputtering method. *Appl. Phys. Lett.*, **63**, 1993, 869-70.

[34] Deepa, M., Srivastava, A. K., Singh, S. and Agnihotry, S. A. Structure-property correlation of nanostructured WO_3 thin films produced by electrodeposition. *J. Mater Res.*, **19**, 2004, 2576-85.

[35] Monk, P. M. S., Mortimer, R. J. and Rosseinsky, D. R. *Electrochromism and electrochromic devices*, Cambridge Univ Press, Cambridge, 2007.

[36] Liquan, C., Ming, D., Yunfa, C., Chunxiang, S. and Rungjian, X. Study on EC Ni-O thin film and new EC device. Seventh International Conference on Solid State Ionics, Japan, 1989, abs. 6pB-38. As cited in reference [35].

[37] Maruyama, T. and Arai, S. The electrochromic properties of nickel oxide thin films prepared by chemical vapour deposition. *Sol. Energy Mater. Sol. Cells.*, **30**, 1993, 257-62.

[38] Arakaki, J., Reyes, R., Horn, M. and Estrada, W. Electrochromism in NiO_x and WO_x obtained by spray pyrolysis. *Sol. Energy Mater. Sol. Cells.*, **37**, 1995, 33-41.

[39] Velevska, J. and Ristova, M. Electrochromic properties of NiOx prepared by low vacuum evaporation. *Sol. Energy Mater. Sol. Cells.*, **73**, 2002,131-39.

[40] Carpenter, M. K., Conell, R. S. and Corrigan, D. A. The electrochromic properties of hydrous nickel oxide. *Sol. Energy Mater.*, **16**, 1987, 333-46.

[41] Vidotti, M. and Córdoba de Torresi, S. I. Electrostatic layer-by-layer and electrophoretic deposition as methods for electrochromic nanoparticle immobilization. *Electrochim. Acta.*, **54**, 2009, 2800-4.

[42] French, H, M., Henderson, M. J., Hillman, A. R. and Vieil, E. Temporal resolution of ion and solvent transfers at nickel hydroxide films exposed to LiOH. *Solid State Ionics*, **150**, 2002, 27-37.

[43] French, H, M., Henderson, M. J., Hillman, A. R. and Vieil, E. Ion and solvent transfer discrimination at a nickel hydroxide film exposed to LiOH by combined electrochemical quartz crystal microbalance (EQCM) and probe beam deflection (PBD) techniques. *J. Electroanal. Chem.*, **500**, 2001, 192–207.

[44] Madou, M. J. and McKubre, M. C. H. Impedance Measurements and Photoeffects on Ni electrodes. *J. Electrochem. Soc.*, **130**, 1983, 1056-61.

6. Effect of metal ion additives on the electrochemical and electrochromic performance of hydrated NiO

6.1. Introduction

In the field of hydrated NiO ($Ni(OH)_2$) research, it is necessary to overcome two well-known limitations. Firstly, hydrated NiO shows catalytic properties towards the oxygen evolution reaction (OER), which is a process very close to the Ni(II)/Ni(III) redox process. For electrochromic (EC) applications, this reaction needs to be avoided as it could create gassing problems. The co-deposition of cobalt is a recognised technique to increase the conductivity of the active material,[1] thereby, shifting the Ni(II)/Ni(III) redox process to less positive potentials. Secondly, hydrated NiO shows poor cycling durability in alkaline solution, which has been the topic of research for many studies.[2,3] Oliva *et al.*[3] highlighted that during cycling, slight changes occur in the electrochemical mechanism and in the structure of the involved species. Their study used the well-known Bode reaction scheme[4,5] (figure 6.1) to explain the structural characterisation of the phases involved in hydrated NiO redox behaviour.

Hydrated NiO can exist in diverse structures; β-$Ni(OH)_2$ (figure 6.2 (a)) forms a brucite structure (based on $Mg(OH)_2$) and is most commonly used for battery applications as it presents a closed and thermodynamically favourable structure.[6] The α-phase (figure (6.2 (b)) consists of nickel and hydroxide layers similar to the brucite structure but in an opened and disarranged form, with water molecules occupying the interstitial sites between the layers. Due to the presence of water molecules the α-phase presents a greater interlamellar distance (~8 Å) than the β-phase (~4.6 Å) and as a result a higher electrochemical performance with a larger charge capacity than the β-phase. It is well known that during continuous cycling in alkaline solution the α-$Ni(OH)_2$ transforms to β-$Ni(OH)_2$. Consequently,

oxidation/reduction cycles take place between β-Ni(OH)$_2$ and β-NiOOH. Furthermore, during overcharging β-Ni(OH)$_2$ converts to γ-NiOOH causing a high mechanical stress due to the abrupt change in the interlamellar distance between the β-Ni(OH)$_2$ (~4.6 Å) and γ-NiOOH (~7 Å). This leads to the EC material swelling[7] and the so called γ-effect.

A widely employed strategy to avoid the γ-effect is the use of additives so the α-phase is stabilised and the oxidation/reduction cycling take place is between the favoured α-Ni(OH)$_2$ and γ-NiOOH. Additives such as Co and Cd were incorporated into hydrated NiO films by Vidotti *et al.*[8] to diminish the electrostatic repulsion between layers, avoiding the material swelling and as a result improving the long term stability of the electrode. Other additives, such as Al,[9] and Mn,[10] have also been used to achieve the same effect.

The role of water molecules trapped preferentially at defect and grain boundaries is also said to play a crucial role in the EC reaction.[11] Due to hydrated NiO degradation the amount of water in the solid film increases with cycle life and therefore promotes chemical degradation.

This chapter will describe a systematic study to investigate the effects of incorporating different metal ions (Ce, Cd, Co, Cu and La) into the hydrated NiO active material. Films have been prepared with single and double (bimetallic) additives on fluorine-doped tin oxide (SnO$_2$:F, FTO) on glass by electrochemical cathodic deposition. The role of metal ion additives on the OER, film durability and the EC properties of hydrated NiO films will be discussed. Also in this chapter the effect of metal ion additives on tuning the EC colour formed will be highlighted by generating chromaticity data.

6. Effect of metal ion additives on the electrochemical and electrochromic performance of hydrated NiO
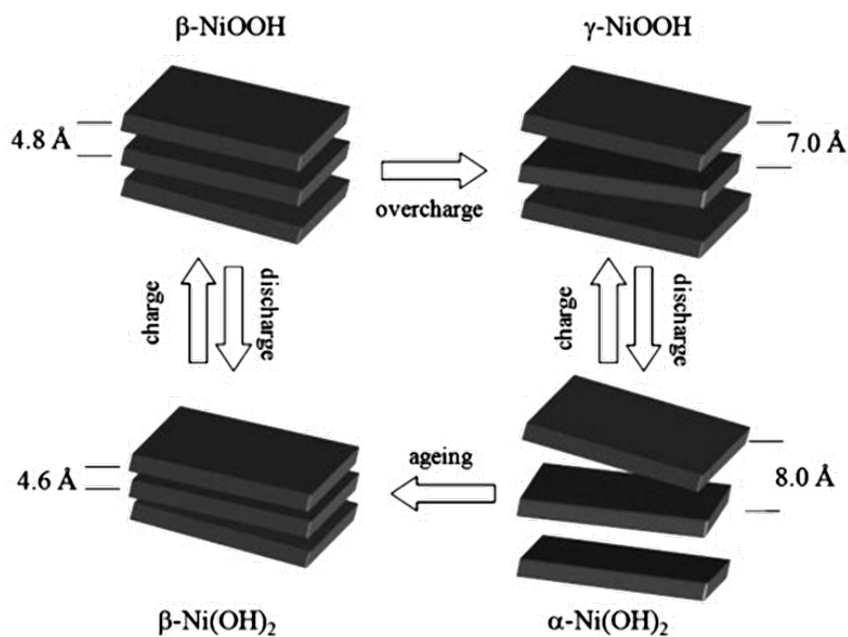
Figure 6.1. Bode diagram which represents the transformation between phases for hydrated NiO. Figure taken from.[8]
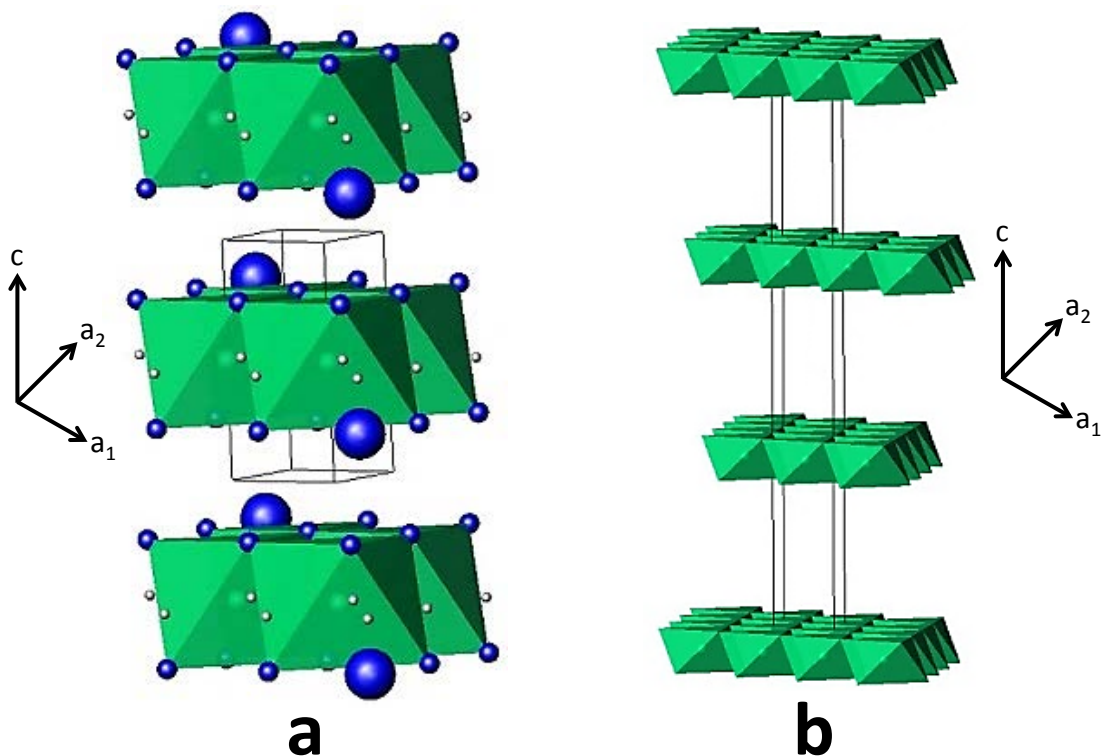
Figure 6.2. Structure of β-Ni(OH)$_2$ (a) and α-Ni(OH)$_2$ (b). In (a) the small blue circles represent oxygen and the large blue circles hydrogen atoms. Diagrams drawn by C. A. Kirk using ATOMS software (version 6.4) and crystallographic data from the following references: β-Ni(OH)$_2$[12] and α-Ni(OH)$_2$.[13]

6.2. The effect of metal ion additives on the oxygen evolution reaction (OER)

Figure 6.3 compares the catalytic effects on the OER for the pure hydrated NiO with the films deposited with different metal ion additives. Composite films were prepared using the optimised deposition condition (chapter 4.4) of -0.2 mA for 50s in 0.01 mol dm^{-3} nickel nitrate and on FTO/glass substrate. Different metal ion additives of M(NO$_3$)$_2$ or M(NO$_3$)$_3$ (where M = Ce, Cd, Co, Cu and La) were used with a solution containing 90% of Ni(NO$_3$)$_2$ and 10% of the additive in moles. From the figure it can be seen that in most cases, the catalytic effect on the OER was enhanced as shown by shift in potential, with either the Ni(II)/(III) redox process moving to more positive potentials (Cu, La or Ce) or the OER moving to more negative potentials (Ce). For the film co-deposited with cadmium, similar behaviour to that of the pure hydrated NiO was observed. However, a slight reduction in both the oxidation and reduction peak currents was observed. Similarly to other studies,[1,8] when compared with the pure hydrated NiO film, co-deposition with cobalt produced a favourable response with both the anodic and cathodic peak potentials shifting to less positive values of 40 and 61 mV, respectively.

These results on the FTO/glass substrate are consistent with Corrigan and Bendert's[14] results for the co-precipitated hydrated NiO films prepared on nickel foil substrate from 0.1 mol dm^{-3} mixed nitrate solution (0.090 mol dm^{-3} nickel and 0.010 mol dm^{-3} of some other metal) and then cycled in 1.0 mol dm^{-3} KOH electrolyte. In 1978, Pickett and Maloy[15] also used electrochemical cathodic deposition to prepare co-precipitated hydrated NiO films onto a nickel microelectrode. They used a boiling ethanol solution containing Ni(NO$_3$)$_2$ in the presence and absence of cobalt and found that its addition appeared to render the charge-discharge reaction more reversible thereby allowing charging to occur at less positive potentials. More recently, Vidotti *et al.*[1] immobilised cobalt co-deposited nanoparticles by an electrostatic layer-by-layer deposition method. They also reported the Ni(II)/Ni(III) redox process to shift to less positive potentials when the amount of cobalt is increased.

6. Effect of metal ion additives on the electrochemical and electrochromic performance of hydrated NiO
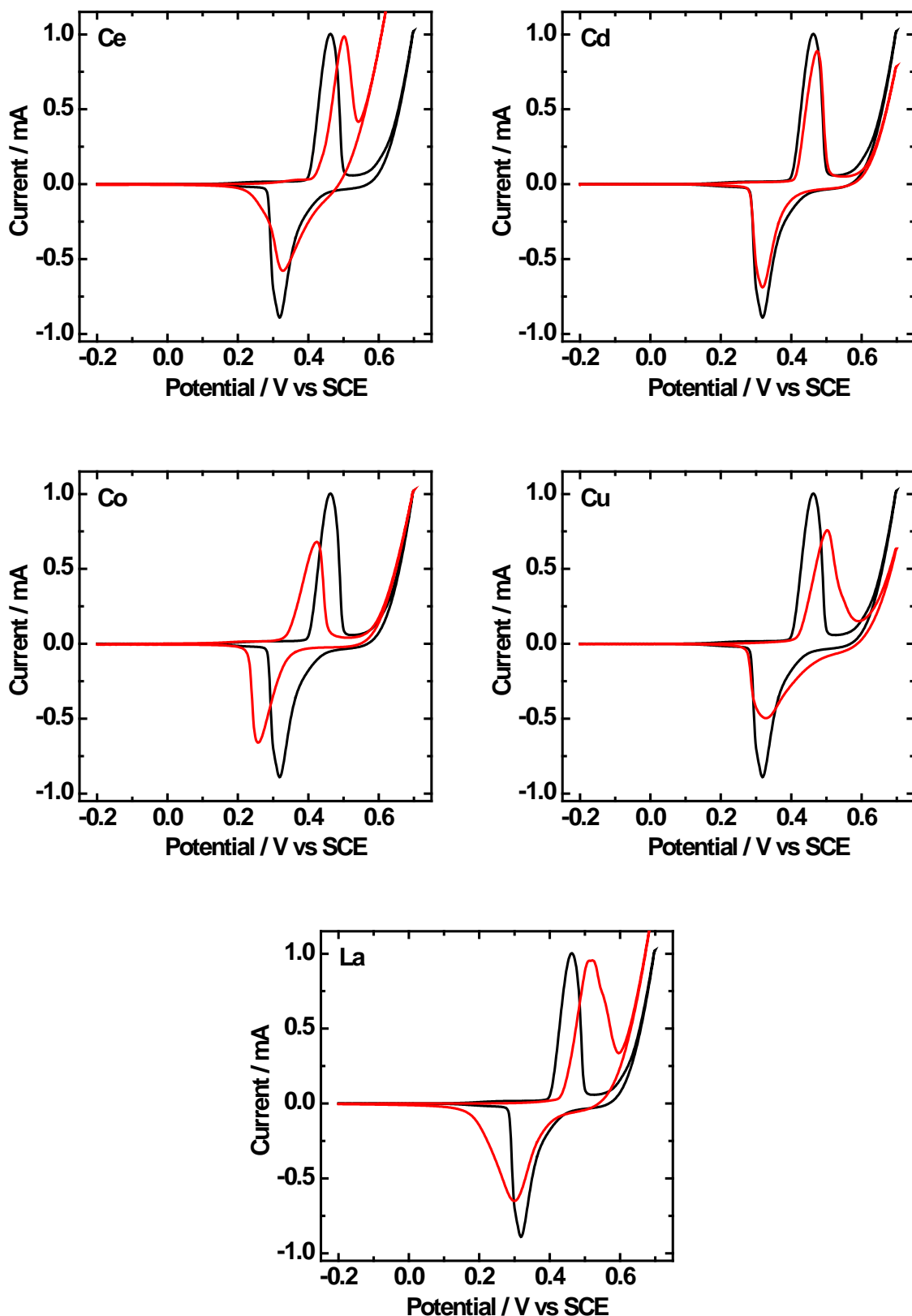
Figure 6.3. CVs for hydrated NiO film (——) compared with co-deposited film (——). Films deposited on FTO/glass (electrode surface area = 30 x 7 mm) then cycled in aqueous KOH (0.1 mol dm^{-3}) electrolyte at 10 mV s^{-1}. The potential range was -0.20 V $\rightarrow$ +0.70 V $\rightarrow$ -0.20 V vs. SCE.

6.3. The effect of metal ion additives on the durability of the hydrated NiO films

High durability or cycle life is one of the key factors for a commercially viable EC material. As previously mentioned, hydrated NiO films show poor cycling durability in alkaline solution. Figure 6.4 shows CVs recorded for the as-deposited hydrated NiO film after the 1st and 50th charge/discharge cycles in KOH (0.1 mol dm^{-3}) electrolyte. After 50 cycles, 22.8 % of the charge had been lost. This unstable behaviour in alkaline solution is due to the transformation of the α-Ni(OH)$_2$ into the β- Ni(OH)$_2$ and on overcharging leads to the deterioration of the electrode with the so called γ-effect taking place. In an attempt to investigate this phase transformation further, the process of α-phase conversion into the β-phase was examined by preparing hydrated NiO films with different metal ion additives then performing ageing tests in KOH (5.0 mol dm^{-3}) electrolyte at room temperature. Continuous redox cycling in KOH (0.1 mol dm^{-3}) solution was also performed with the aim of understanding the electrochemical nature of the process.
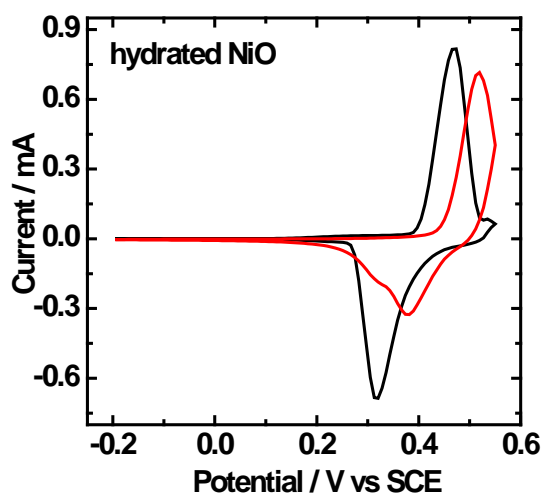
Figure 6.4. CVs showing the durability of the as-deposited hydrated NiO film for the 1st (━━) and 50th (━━) cycle. Film prepared at an applied current of -0.2 mA for 50 s on FTO/glass then cycled in aqueous KOH (0.1 mol dm^{-3}). The potential range was -0.20 V $\rightarrow$ $+0.55$ V $\rightarrow$ -0.20 V vs. SCE for 50 cycles at the scan rate of 10 mV s^{-1}.

6. Effect of metal ion additives on the electrochemical and electrochromic performance of hydrated NiO

Figure 6.5 (a) shows the CVs for the comparison of the as-deposited hydrated NiO film with the same film then being immersed in strong alkaline solution for 1, 2 and 3 hours. The process of α to β-phase conversion can be seen from the electrochemical behaviour, the main difference being the β-phase showing a lower charge capacity with the shifting of the Ni(II)/Ni(III) redox process to more positive potentials. Furthermore, on increasing the ageing process, the film became more irreversible. This observation was in agreement with the results of Córdoba de Torresi *et al.*[16] who also looked at the effect of metal ion additives in the stabilisation of α-Ni(OH)$_2$ but on the surface of gold evaporated quartz crystals. X-ray diffraction (XRD) patterns were also obtained to determine the different phases (figure 6.5 (b)), with the patterns also supporting the electrochemical switching behaviour. The XRD pattern of the as-deposited powder was confirmed to be of the α-phase with the β-phase conversion taking place after 1h as apparent from the disappearance of the 003 reflections at 11.5° and the appearance of the 001 reflection at 19.3°. Additionally, on increasing the ageing process the amorphous β-phase progressively became more crystalline with the intensity of the β-phase reflections becoming more pronounced.
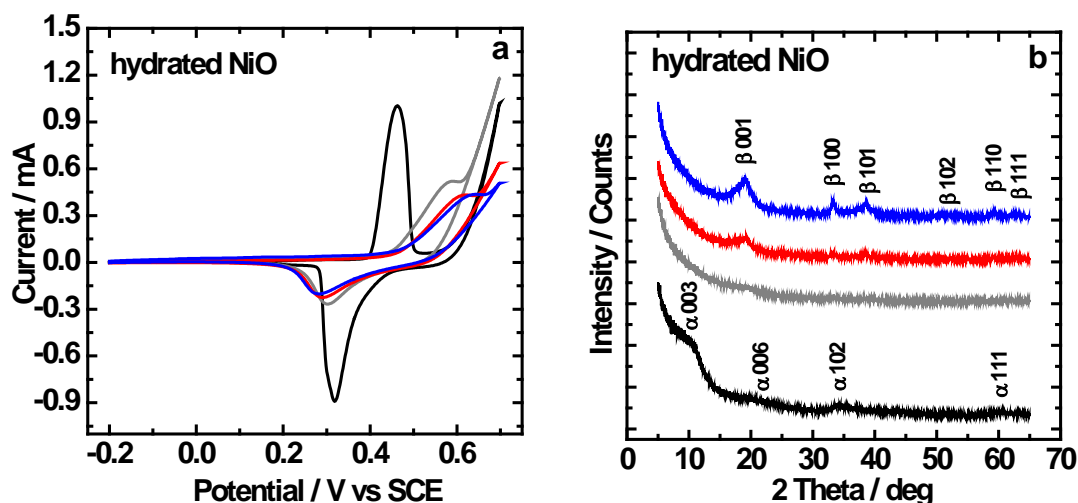
Figure 6.5. CVs (a) and XRD patterns (b) showing the transformation of α- Ni(OH)$_2$ into β- Ni(OH)$_2$ by aging. Data recorded using the as-deposited film (——), and film immersed in KOH (5.0 mol dm^{-3}) solution for 1 h (——), 2 h (——) and 3 h (——) then cycled in KOH (0.1 mol dm^{-3}) at 10 mV s^{-1}. XRD analysis carried out on hydrated NiO powder accumulated by scraping the film away from a palladium foil electrode (50 x 50 mm). Film deposited from nickel nitrate (0.01 mol dm^{-3}) solution at an applied current of -0.2 mA for 10 hours.

6. Effect of metal ion additives on the electrochemical and electrochromic performance of hydrated NiO

Table 6.1 and figure 6.6 show the effect of metal ion additives on the durability of the hydrated NiO films. Divalent additives, such as cadmium, cobalt and copper and trivalent additives, such as cerium and lanthanum were incorporated into the hydrated NiO active material. Results showed that the percentage drop in charge after 50 charge/discharge voltammetric cycles decreased from 22.8% for hydrated NiO to 6.1, 8.3 and 6.3% for films co-deposited with cobalt, copper and lanthanum, respectively. In the case of films prepared with cerium as additives, the percentage drop in charge was found to be greater than pure hydrated NiO film. In section 6.2, cobalt was identified as the best additive for improving the charge efficiency of hydrated NiO by separating the Ni(II)/Ni(III) redox and the OER. Therefore, in an attempt to further enhance the film's durability, the effect of incorporating a second additive into the cobalt co-deposited hydrated NiO films was investigated. Figure 6.7 shows the 1st and the 50th cycles for the cobalt (10%) co-deposited hydrated NiO films with 5% in moles of cadmium, copper and lanthanum. The durability was found to decrease with the addition of cadmium, however, an improvement in response was evident for films prepared with copper or lanthanum as a bimetallic additive with values for the drop in charge of 5.6 and 3.4%, respectively. The improved durability with incorporation of cobalt[8,16,17] and lanthanum[18] as additives has been reported previously. However, to date there are no apparent studies which have looked at the effects of bimetallic additives (cobalt (10%) and lanthanum (5%)) on the properties of hydrated NiO films prepared by electrochemical cathodic deposition.

Hydrated NiO films prepared with different single (figure 6.8) and bimetallic (figure 6.9) additives were further tested to examine the rate of transformation from the α to the β-phase by ageing in KOH (5.0 mol dm^{-3}) solution. From the CVs it can be seen that with all the single additives, except for the addition of cobalt, the electrode showed strong catalysis of the OER. In the case of cobalt, the phase transformation process was slowed down with the voltammetric behaviour after 12 h of aging still being of a response similar to the α-phase. In the absence of overcharge, the redox reaction takes place between the α-Ni(OH)$_2$/γ-NiOOH system (figure 6.5 (a), as-deposited film), after aging or continuous redox cycling the transformation to the β-Ni(OH)$_2$/β-NiOOH (figure 6.5 (a), aging for 1 h) system takes place. Furthermore, with several of the co-deposited films, the third λ-effect due to overcharging was also evident with an additional cathodic peak between 0.3 and 0.5 V being shown for the

β-Ni(OH)$_2$ and λ-NiOOH phases. This observation was similar to those reported by Olivia *et al.*[3] Films prepared with a bimetallic additive showed the slowest rate of α to β-phase transformation and therefore agreeing with the optimal durability results as shown in figure 6.7.

The XRD patterns of the as-deposited and the aged films in KOH (5.0 mol dm^{-3}) solution for 3 h are compared in figures 6.10 and 6.11. For most of the films prepared with single or double additives, the XRD patterns of the metal compound are not found which suggests that metals ions are doped into the hydrated NiO crystal lattices by replacing the nickel ions. In the case of co-deposition with cerium, the XRD patterns confirmed the presence of isolated cerium hydroxide (Ce(OH)$_3$) and hydrated NiO, mixture in the active material. The as-deposited films for all the additives were confirmed to be the α-phase. However, after ageing for 3 hours, the existence of the β-phase hydrated NiO was confirmed for films prepared with cadmium as additive. With the addition of cobalt, the crystallinity of the as-deposited films was enhanced with the increase and narrowing of the 003 reflection. Furthermore, the α-phase was still shown to present after the aging process. Films prepared with cadmium, copper and lanthanum as bimetallic additives showed the presence of the α-phase for both the as-deposited and the aged film, again confirming the reduced rate of α to β-phase transformation, thereby the redox process taking place between the preferred α-Ni(OH)$_2$ /λ-NiOOH redox system with an improved film durability.

In order to examine the surface morphology and to quantify the composition of the co-deposited powders, high resolution field emission gun scanning electron microscope (FEGSEM) and energy dispersive X-ray spectroscopy (EDS) elemental analysis was carried out (table 6.1 and figures 6.12 and 6.13). The morphology of the co-deposited powders was found to be very similar to the pure hydrated NiO powder, indicating that the metal ions can be deposited homogeneously in a hydroxide form. Large differences in the calculated (solution composition) and EDS determined atomic percentage (at.%) values was observed for powders obtained with different additives. These observations can be explained by comparing the different solubility (K_{sp}) values of the hydroxides and the size of the co-deposited cations (picometre).[19] For hydrated NiO films prepared with cobalt, a slightly lower

EDS determined value (6.8**%)** than the calculated value was observed. This is due to Co(OH)$_2$ having a slightly bigger K_{sp} (5.92 x 10^{-15}) value than Ni(OH)$_2$ (5.47 x 10^{-16}). Furthermore, the atomic radii value of cobalt (74.5 picometre) is also bigger than nickel (69 picometre), therefore, the deposition of Ni(OH)$_2$ is favoured. Although, cobalt is a more suitable additive, a higher EDS determined at.% values was observed for the co-deposition of cerium (7.1%) and copper (11.6%). This fact is related to the presence of cerium hydroxide as confirmed by XRD (figure 6.10), while a high at.% for copper is due to the formation of a thermodynamically-preferred reaction of reductive metal, as was seen by an orange coloured deposit on the FTO/glass substrate, although XRD analysis did not confirm this. Finally, the reduced EDS determined at.% value for lanthanum (1.4%) can be explained with reference to the size of the trivalent cation. Lanthanum (103.2 picometre) is a much larger cation than the divalent Ni (69 picometre), therefore a lower ratio of precipitation is expected.

The increased durability of hydrated NiO with the addition of cobalt is related to the shifting of the Ni(II)/Ni(III) redox process to less positive potentials. This effect not only increases the reversibility of the system but optimises the lattice imperfections in the active material so that the conductivity is substantially increased.[16,20] However, the maintenance of film electroneutrality during continuous redox cycling may involve the intercalation/deintercalation of H$^+$, OH$^-$ and hydrated cations which may lead to the expulsion of the cobalt ions from the lattice structure. As a result, the Ni(II)/Ni(III) redox process is displaced to more positive potentials which leads to the material swelling and the so called λ-effect taking place. To negate this process, the addition of a second additive is necessary which acts to further improve the conductivity thereby reducing the expansion or contraction of the nickel and hydroxide layers. By this way, the displacement of the redox peaks is avoided and the formation of the λ-phase is reduced. As a result the durability of the electrode is increased. Vidotti *et al.*[8] co-deposited cobalt and cadmium into the structure of hydrated NiO nanoparticles to achieve this effect. They stabilised the α-phase and improved the durability of the electrode during long electrochemical cycling. The same results were achieved in the present work but with the addition of cobalt and lanthanum.

6. Effect of metal ion additives on the electrochemical and electrochromic performance of hydrated NiO

Table 6.1. Durability, calculated and determined additive (%) of co-deposited hydrated NiO film prepared on FTO glass (electrode surface area = 30 x 7 mm). Drop in charge data for pure hydrated NiO from chapter 5.2.

additive	durability, drop in charge (%)	additive calculated (mole %)	additive determined by EDS (at.%), average of three measurements
(pure hydrated NiO)	22.8	-	-
cerium	29.7	10	7.1
cadmium	22.5	10	2.7
cobalt	6.1	10	6.8
copper	8.3	10	11.6
lanthanum	6.3	10	1.4
cobalt and cadmium	12.8	10 and 5	6.8 and 1.1
cobalt and copper	5.6	10 and 5	4.4 and 2.1
cobalt and lanthanum	3.4	10 and 5	5.0 and 0.8

6. Effect of metal ion additives on the electrochemical and electrochromic performance of hydrated NiO
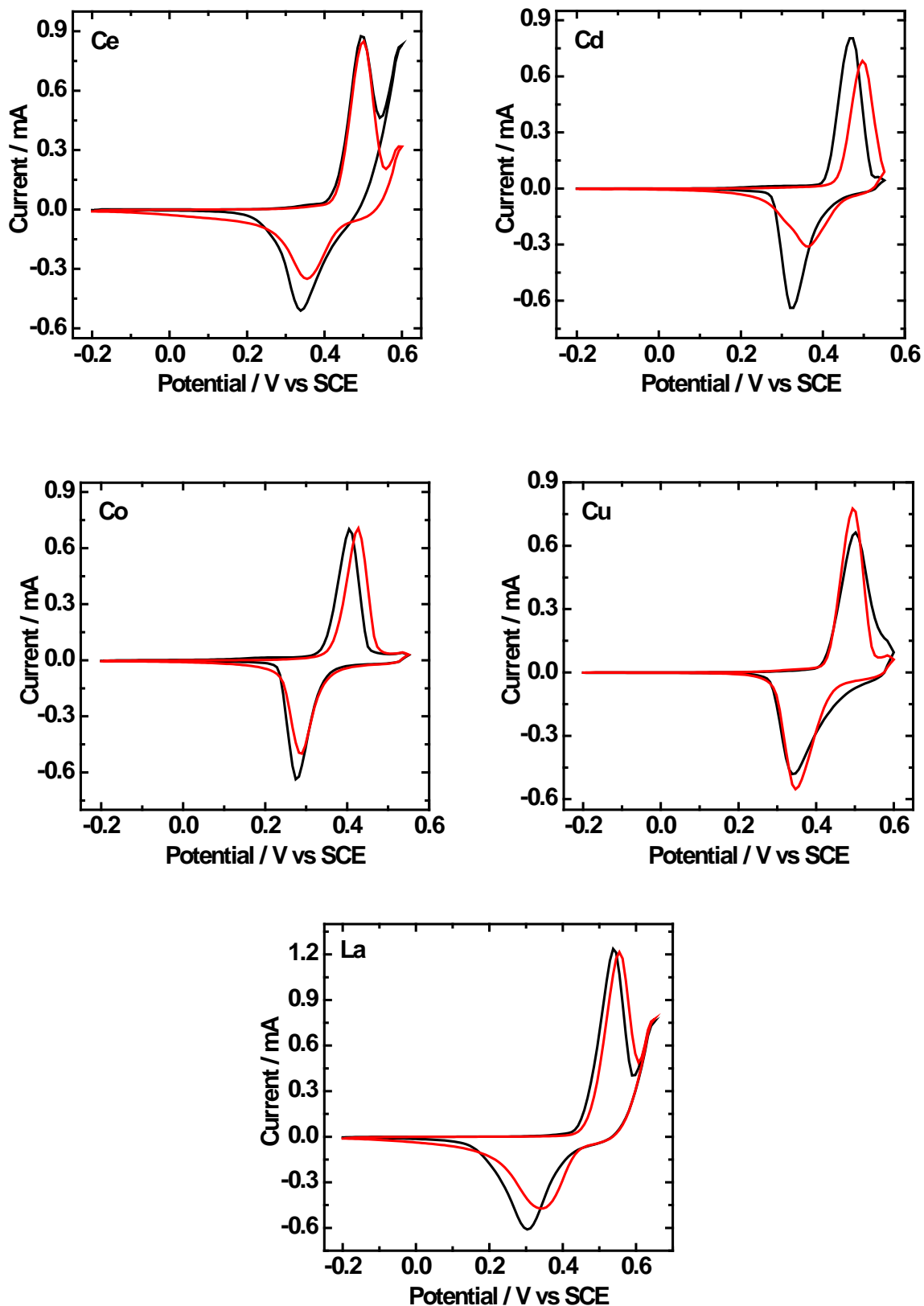
Figure 6.6. CVs showing the 1st (——) and 50th (——) cycle of the as-deposited hydrated NiO films co-deposited with different additives (single). Films cycled in aqueous KOH (0.1 mol dm^{-3}) at a scan rate of 10 mV s^{-1}.

6. Effect of metal ion additives on the electrochemical and electrochromic performance of hydrated NiO
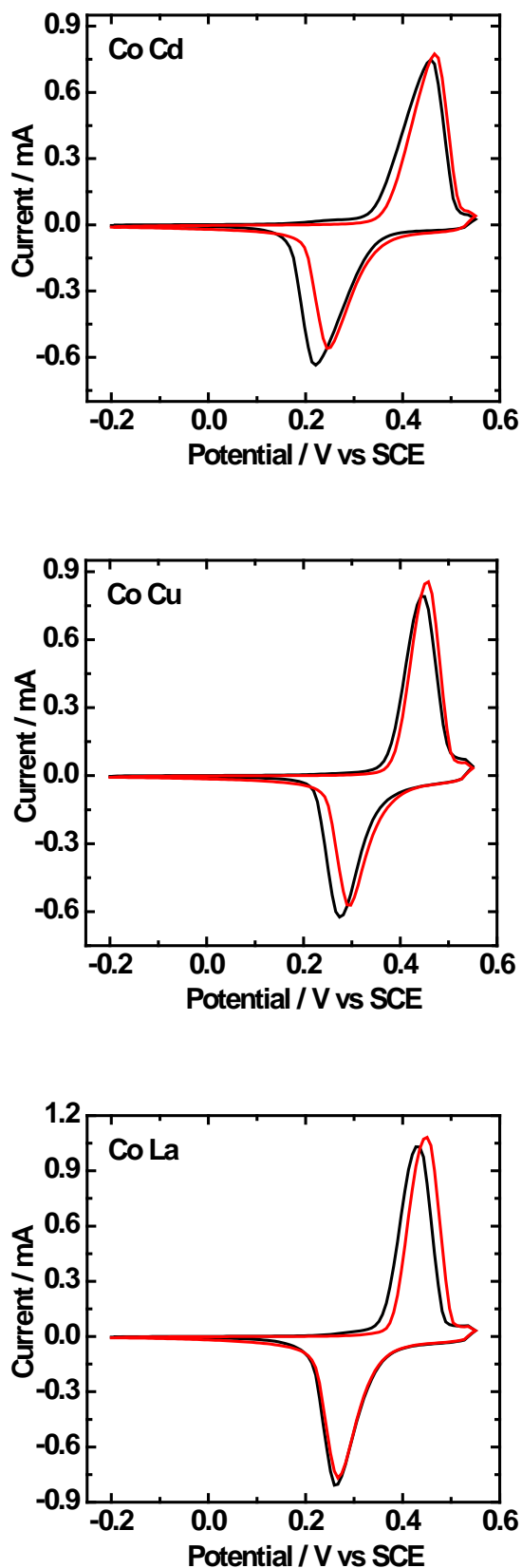
Figure 6.7. CVs showing the 1st (——) and 50th (——) cycle of the as-deposited hydrated NiO films co-deposited with different bimetallic additives. Films cycled in aqueous KOH (0.1 mol dm^{-3}) at a scan rate of 10 mV s^{-1}.
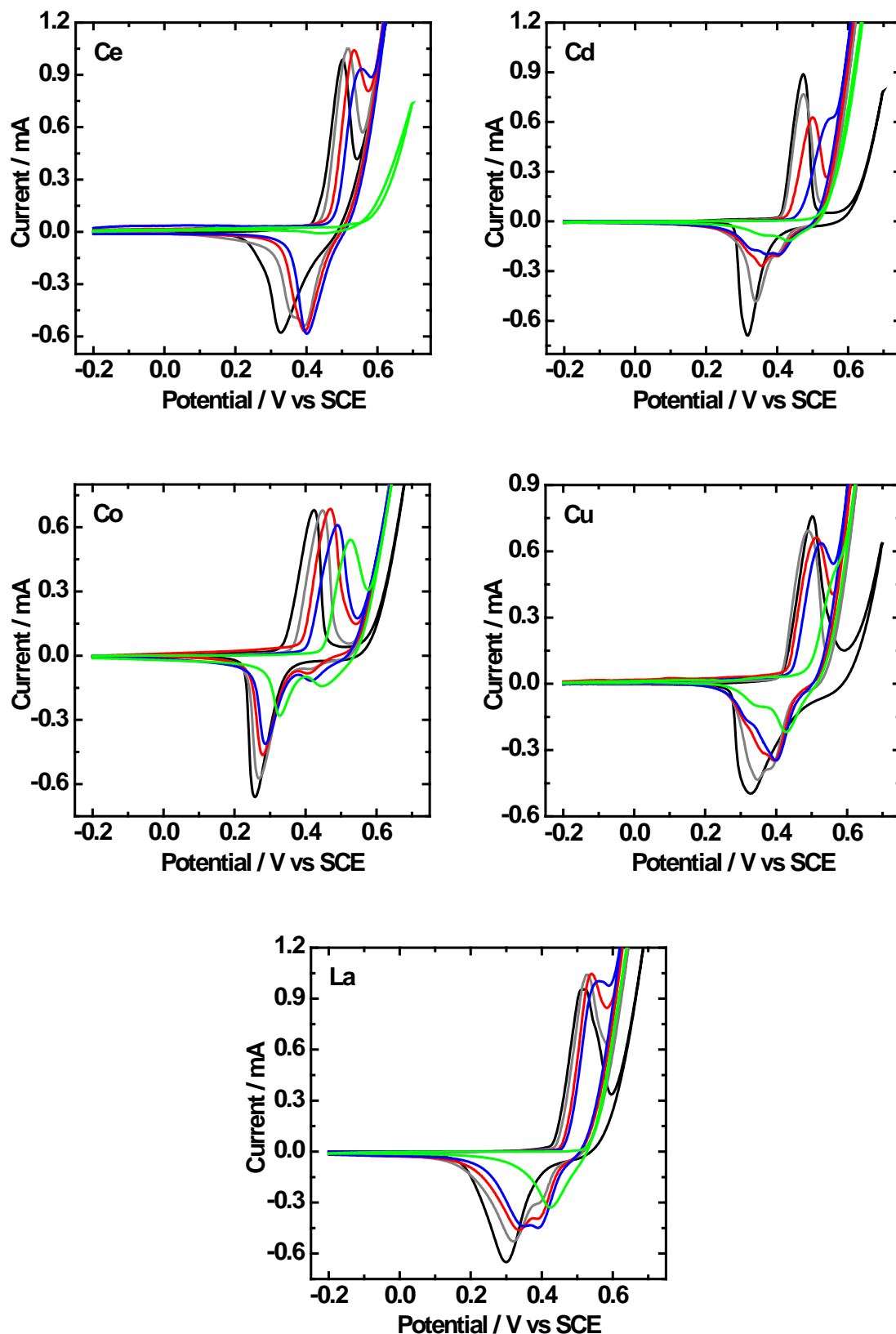
Figure 6.8. Aging effect on films prepared with different additives (single). CVs recorded using the as-deposited film (——), and film immersed in KOH (5.0 mol dm^{-3}) solution for 1 h (——), 2 h (——), 3 h (——) and 12 h (——). Films cycled in aqueous KOH (0.1 mol dm^{-3}) at a scan rate of 10 mV s^{-1}.
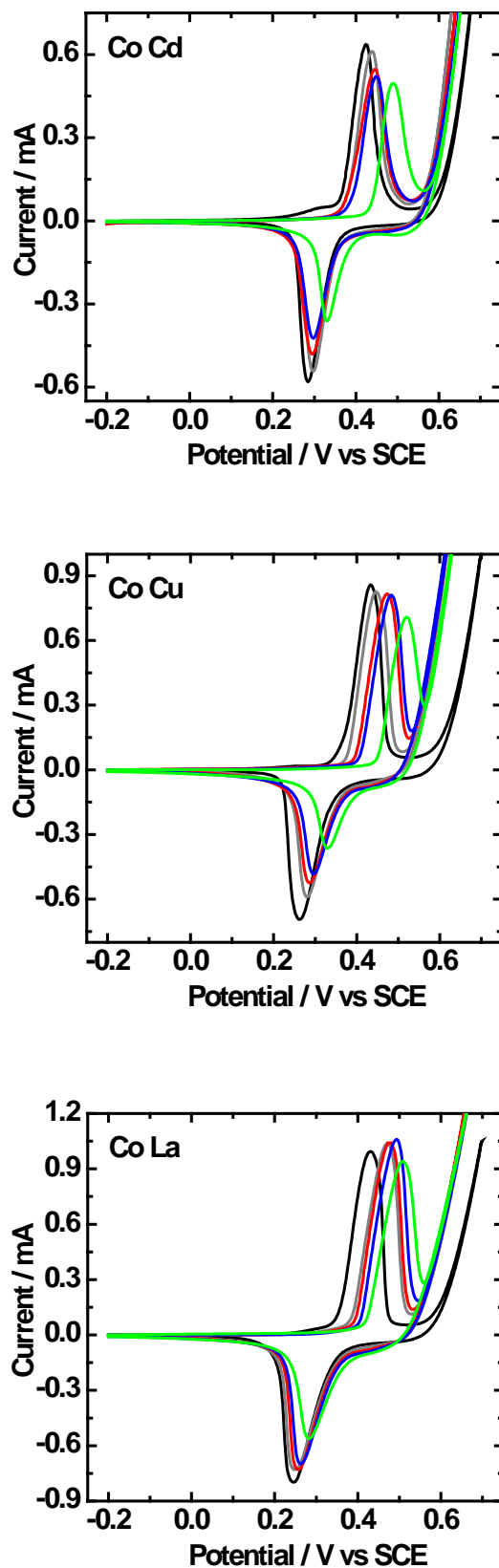
Figure 6.9. Aging effect on films prepared with different bimetallic additives. CVs recorded using the as-deposited film (——), and film immersed in KOH (5.0 mol dm^{-3}) solution for 1 h (——), 2 h (——), 3 h (——) and 12 h (——). Films cycled in aqueous KOH (0.1 mol dm^{-3}) at a scan rate of 10 mV s^{-1}.

6. Effect of metal ion additives on the electrochemical and electrochromic performance of hydrated NiO
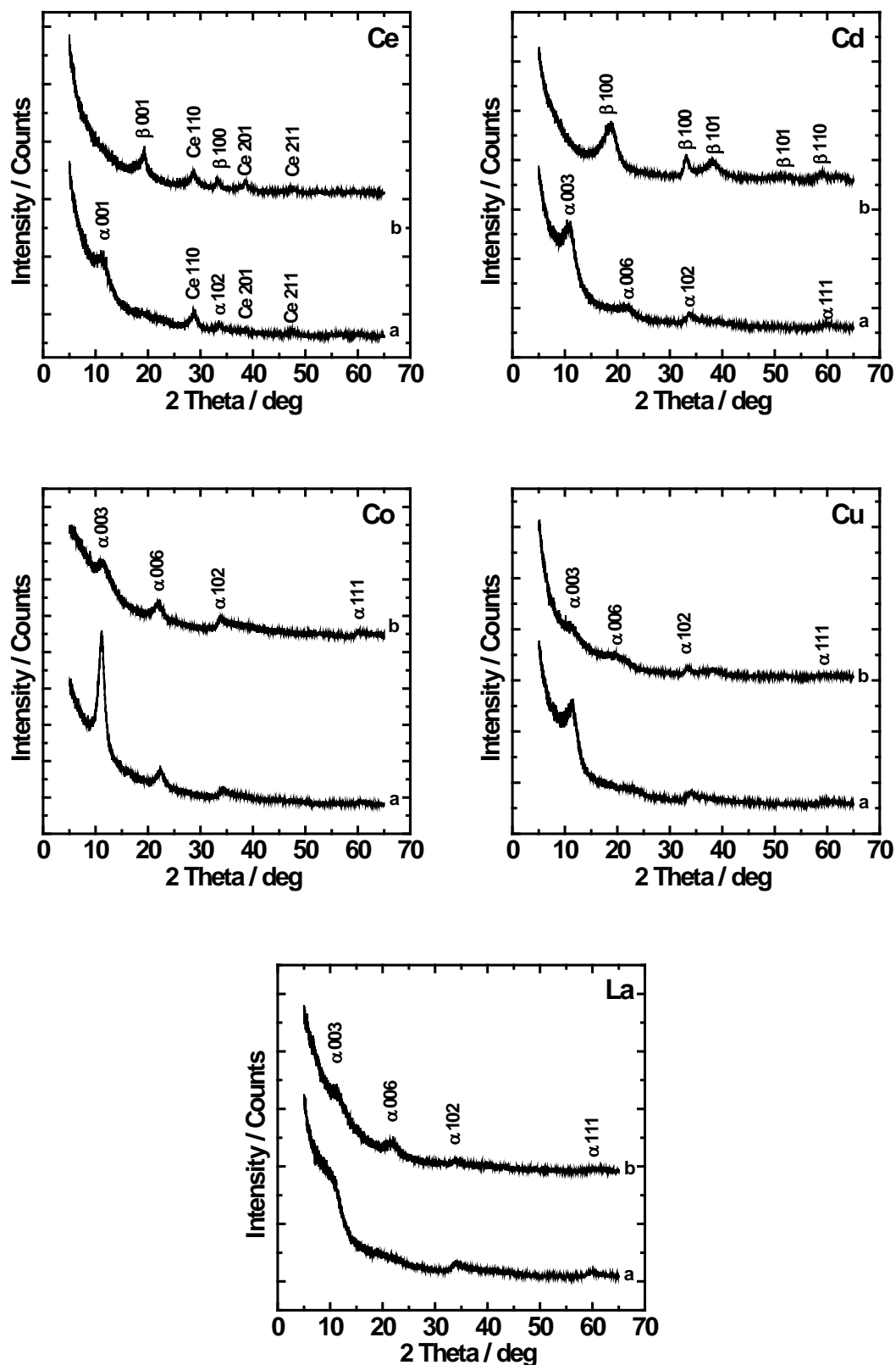
Figure 6.10. XRD patterns of hydrated NiO powders obtained with different additives (single). Patterns recorded for the as-deposited powders (a), and powders immersed in KOH (5.0 mol dm^{-3}) solution for 3 h (b).

167
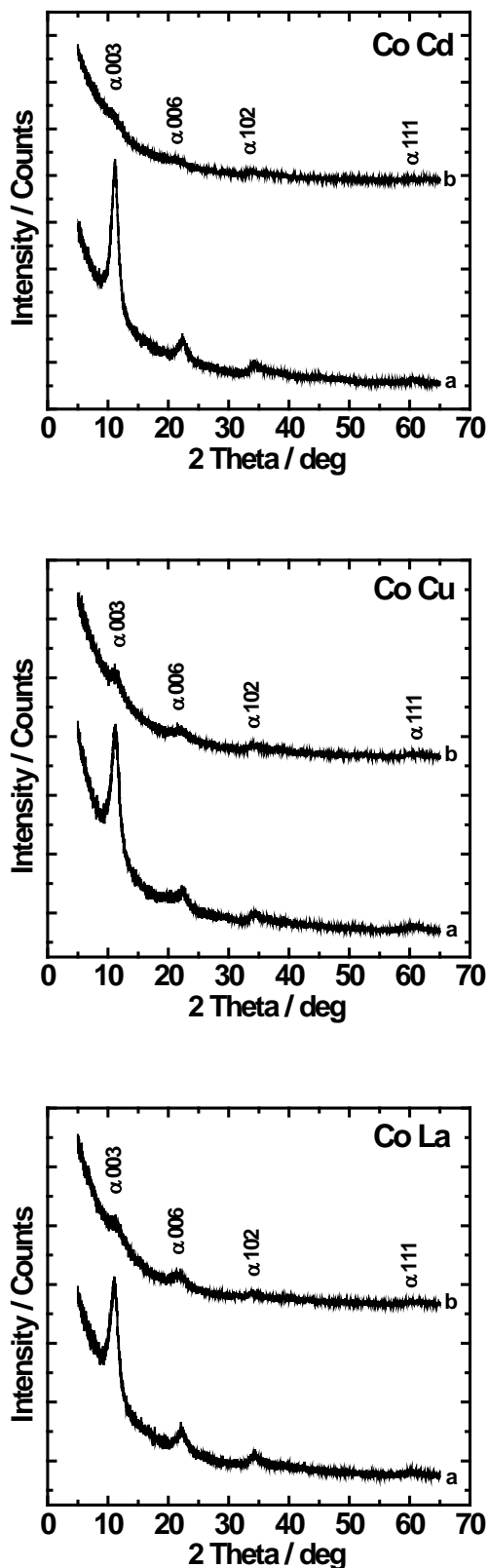
Figure 6.11. XRD patterns of hydrated NiO powders obtained with different bimetallic additives. Patterns recorded for the as-deposited powders (a), and powders immersed in KOH (5.0 mol dm^{-3}) solution for 3 h (b).
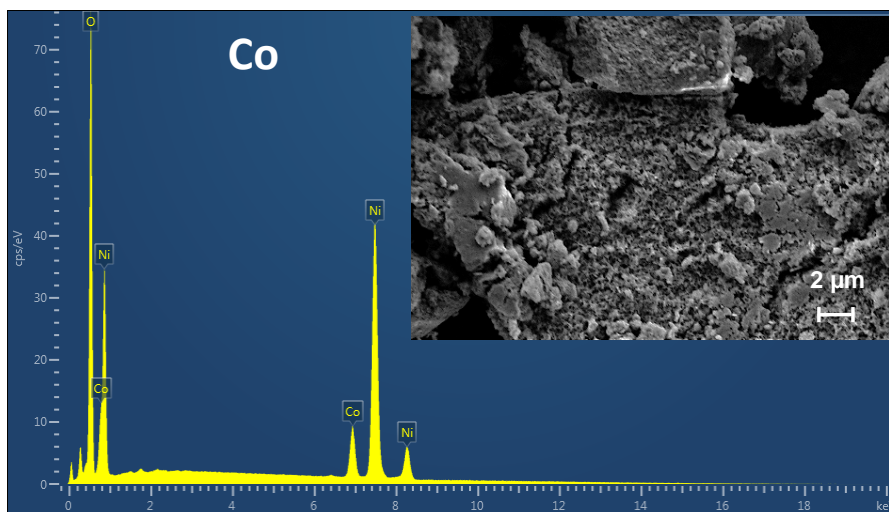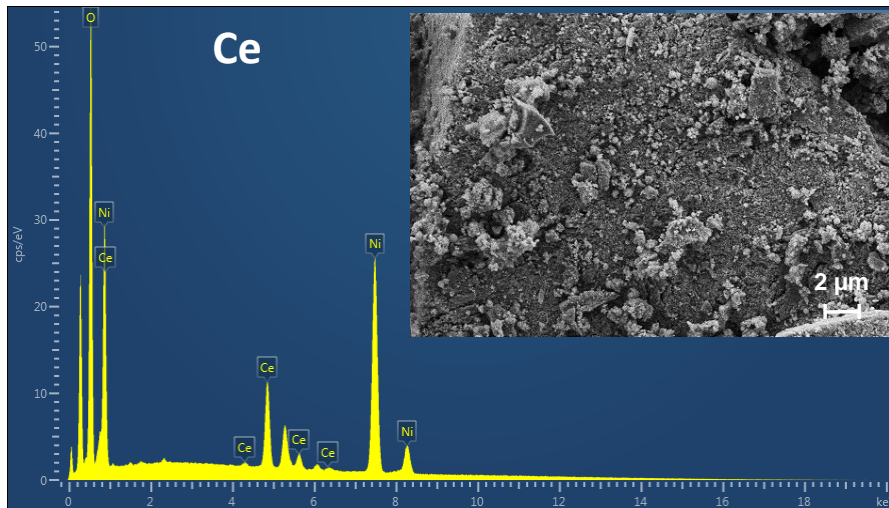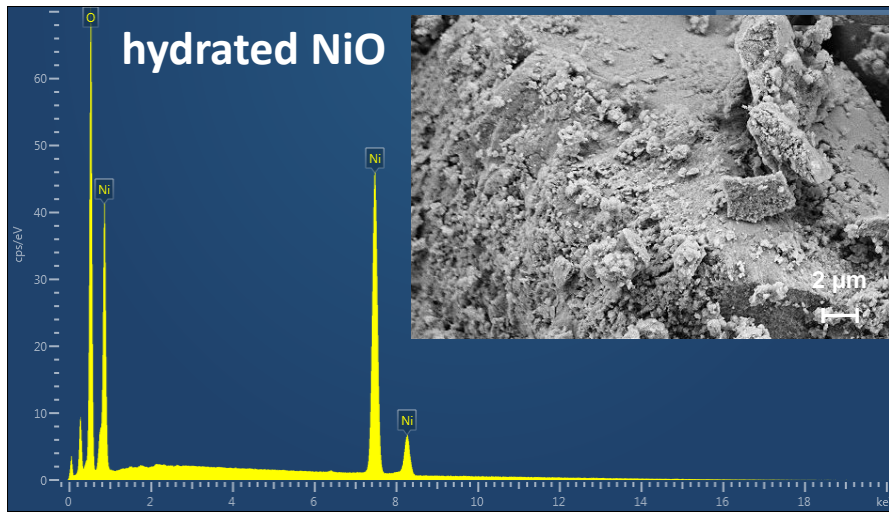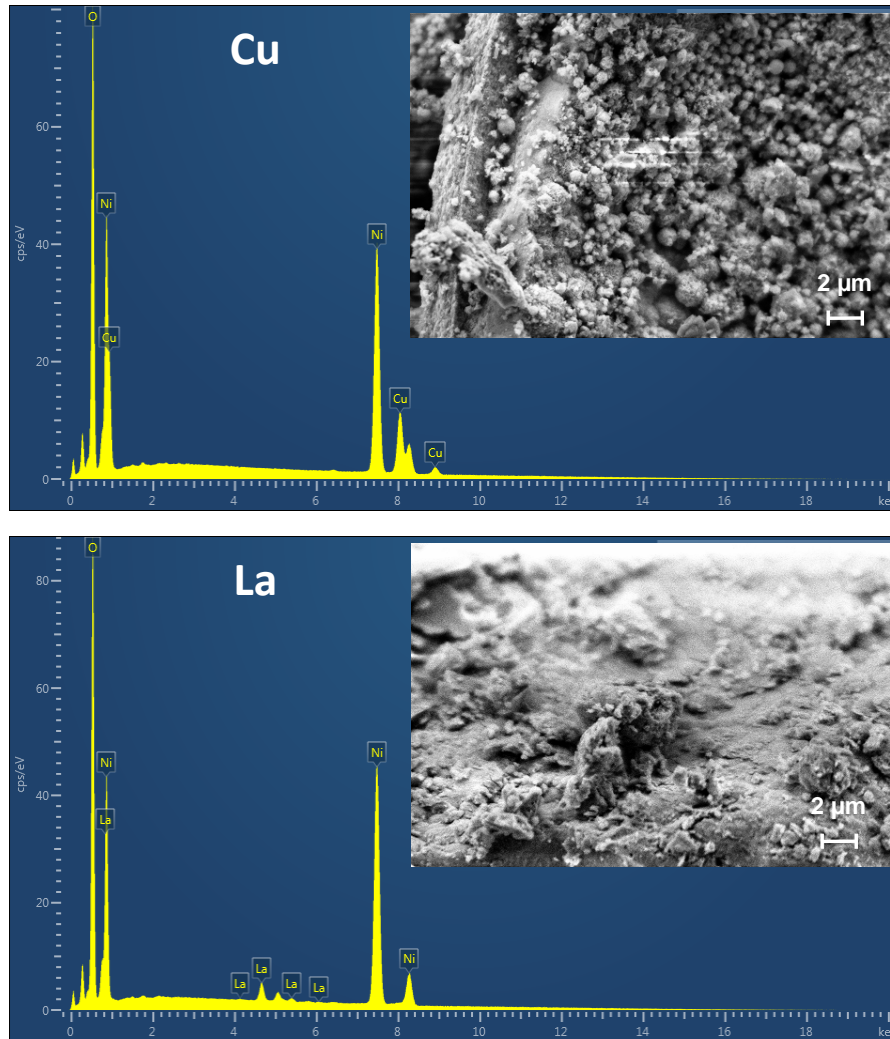
Figure 6.12. An energy dispersive X-ray spectroscopy (EDS) analysis showing the chemical composition of the hydrated NiO films with different additives (single). Insert shows high resolution field emission gun scanning electron microscope (FEGSEM) images of the surface of hydrated NiO powders with different additives (single).

6. Effect of metal ion additives on the electrochemical and electrochromic performance of hydrated NiO
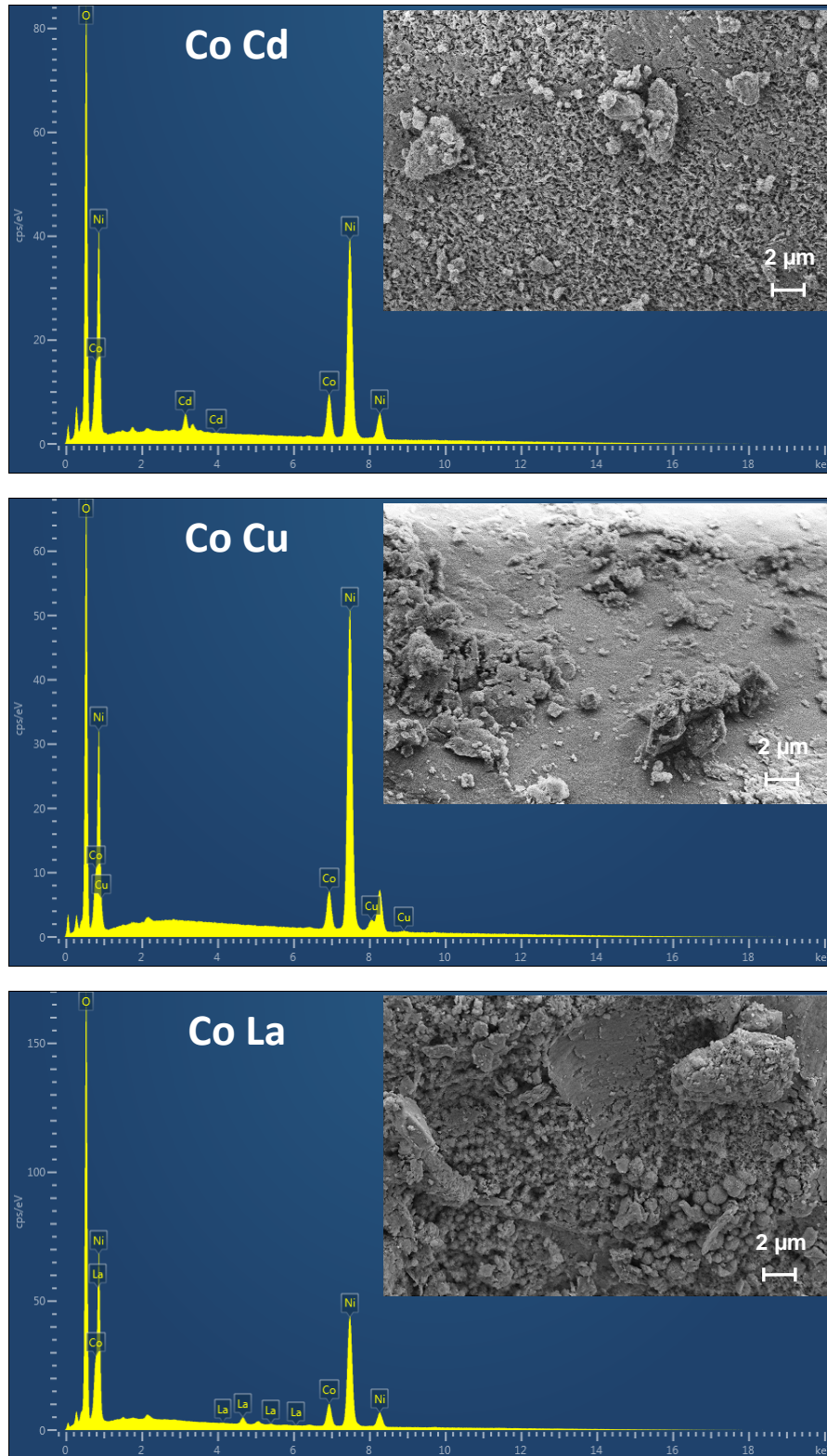
Figure 6.13. An energy dispersive X-ray spectroscopy (EDS) analysis showing the chemical composition of the hydrated NiO films with different bimetallic additives. Insert shows high resolution field emission gun scanning electron microscope (FEGSEM) images of the surface of hydrated NiO powders with different bimetallic additives.

6.4. The effect of metal ion additives on the electrochromic properties of the hydrated NiO films

Table 6.2 gives *in-situ* spectral data and calculated EC performance parameters for square-wave potential switching between the 'bleached' and coloured forms for the as-deposited hydrated NiO films co-deposited with different additives. Figures 6.14 to 6.21 (a) show visible region *in-situ* transmittances spectra, for the as-deposited hydrated NiO films with different additives in the bleached and coloured state. For all the films, it is noted from table 6.2 that the optical transmittance for the 'bleached' states were generally very similar to those obtained for a pure hydrated NiO film. The transmittance for the coloured states increased slightly from 13.9% for pure hydrated NiO to between 18.1 and 18.4% for films with additives. Furthermore, the absorbance change (ΔA) (figures 6.14 to 6.21 (b)) also varied slightly, with decrease in values when compared with a pure hydrated NiO film. In the case of colouration efficiency (CE) (figures 6.14 to 6.21 (b)), the values decreased with the addition of cobalt, copper, lanthanum and cobalt/copper. However, when co-deposited with cerium, cadmium, cobalt/cadmium and cobalt/lanthanum CE increased with a maximum of 41.9 cm^2 C^{-1} recorded for hydrated NiO film co-deposited with cadmium, when measured at 432 nm.

Absorbance vs. time (figures 6.14 to 6.21 (c)) and charge vs. time (figures 6.14 to 6.21 (d)) plots were also used to calculate the response times for all the co-deposited hydrated NiO films. The values are also listed in table 6.2 and are the response times taken for the absorbance to reach 95% of the total change for both colouration (t_c) and 'bleaching' (t_b) processes. Generally, the response times for the colouration process were longer than those for the 'bleaching' process, with the exception of cerium where the 'bleaching' process time was found to be greater.

6. Effect of metal ion additives on the electrochemical and electrochromic performance of hydrated NiO

Table 6.2. *In-situ* spectral data and EC performance parameters on square wave switching between the 'bleached' and coloured states of the as-deposited NiO films with different additives in aqueous KOH (0.1 mol dm^{-3})^a

Additive	%T_b	%T_c	Δ%T	ΔA	CE/ cm^2 C^{-1}	t_c/t_b (s)
(Pure hydrated NiO)^b	97.1	13.9	83.2	0.87	29.6	12.0/9.5
Cerium	99.0	18.1	80.9	0.77	40.6	9.9/15.3
Cadmium	99.2	18.4	80.8	0.73	41.9	11.4/9.2
Cobalt	94.0	18.3	75.7	0.71	21.6	11.4/10.1
Copper	97.9	18.3	79.6	0.73	26.9	13.6/9.9
Lanthanum	99.8	18.3	81.5	0.79	24.7	13.5/12.5
Cobalt and cadmium	91.6	18.3	73.3	0.70	38.8	8.1/7.3
Cobalt and copper	97.2	18.3	78.9	0.73	27.4	11.8/8.3
Cobalt and lanthanum	98.1	18.3	79.8	0.73	31.0	10.0/8.9

$^a T_b$ = transmittance of 'bleached' form, T_c = transmittance of coloured form, Δ%T = change in transmittance between the 'bleached' and coloured forms, ΔA = change in absorbance, CE = colouration efficiency, t_c and t_b = switching times for colouration and bleaching. All measurements were taken at 432 nm, which had been found to be the wavelength for maximum absorbance change. ^{b}Data for pure hydrated NiO film obtained from chapter 5.2.
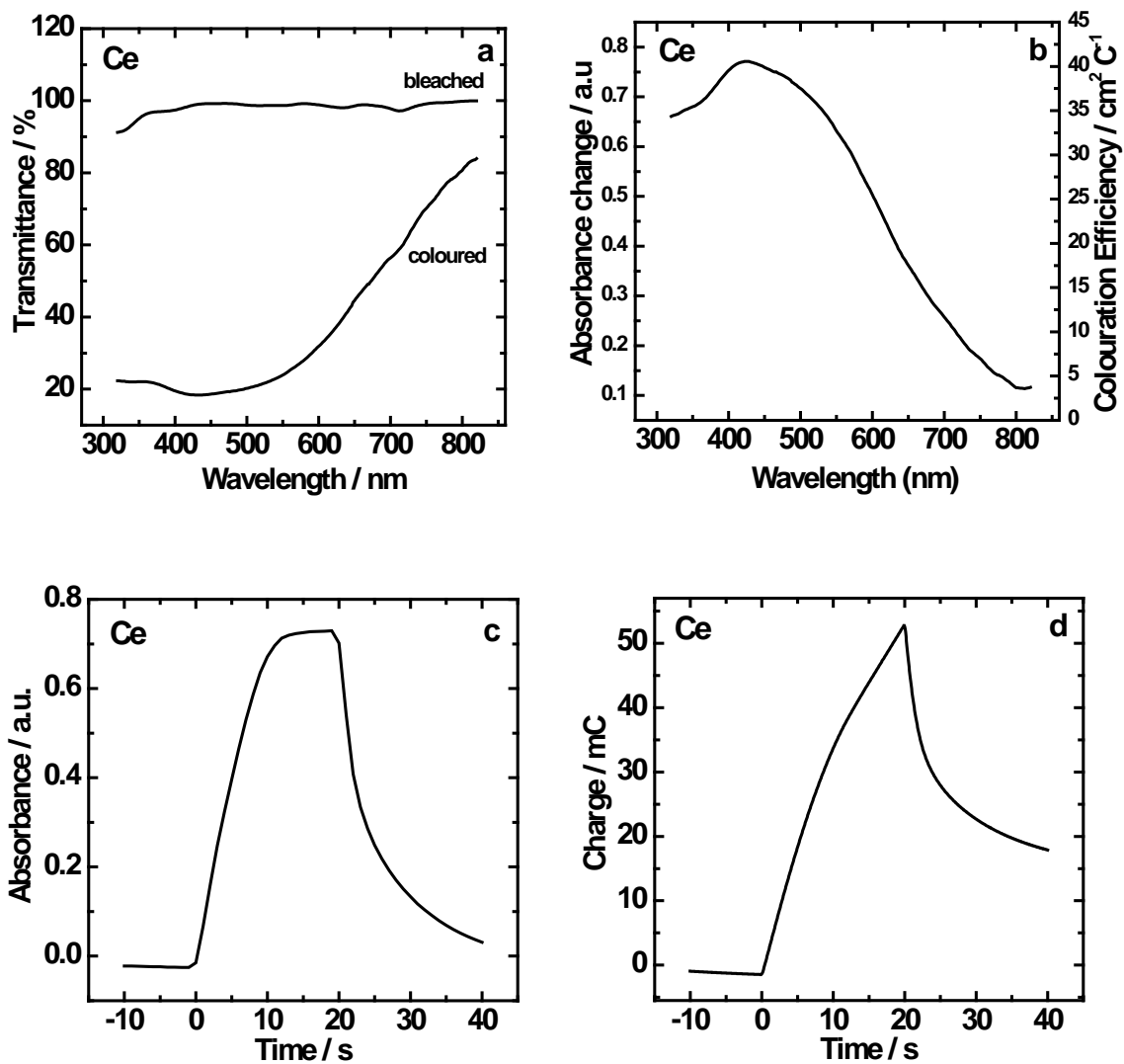
Figure 6.14. Visible region *in-situ* transmission spectra for the 'bleached' and coloured states (a), change in absorbance and colouration efficiency (b), absorbance vs. time transient (c) and charge vs time transients (d) of hydrated NiO film co-deposited with cerium.
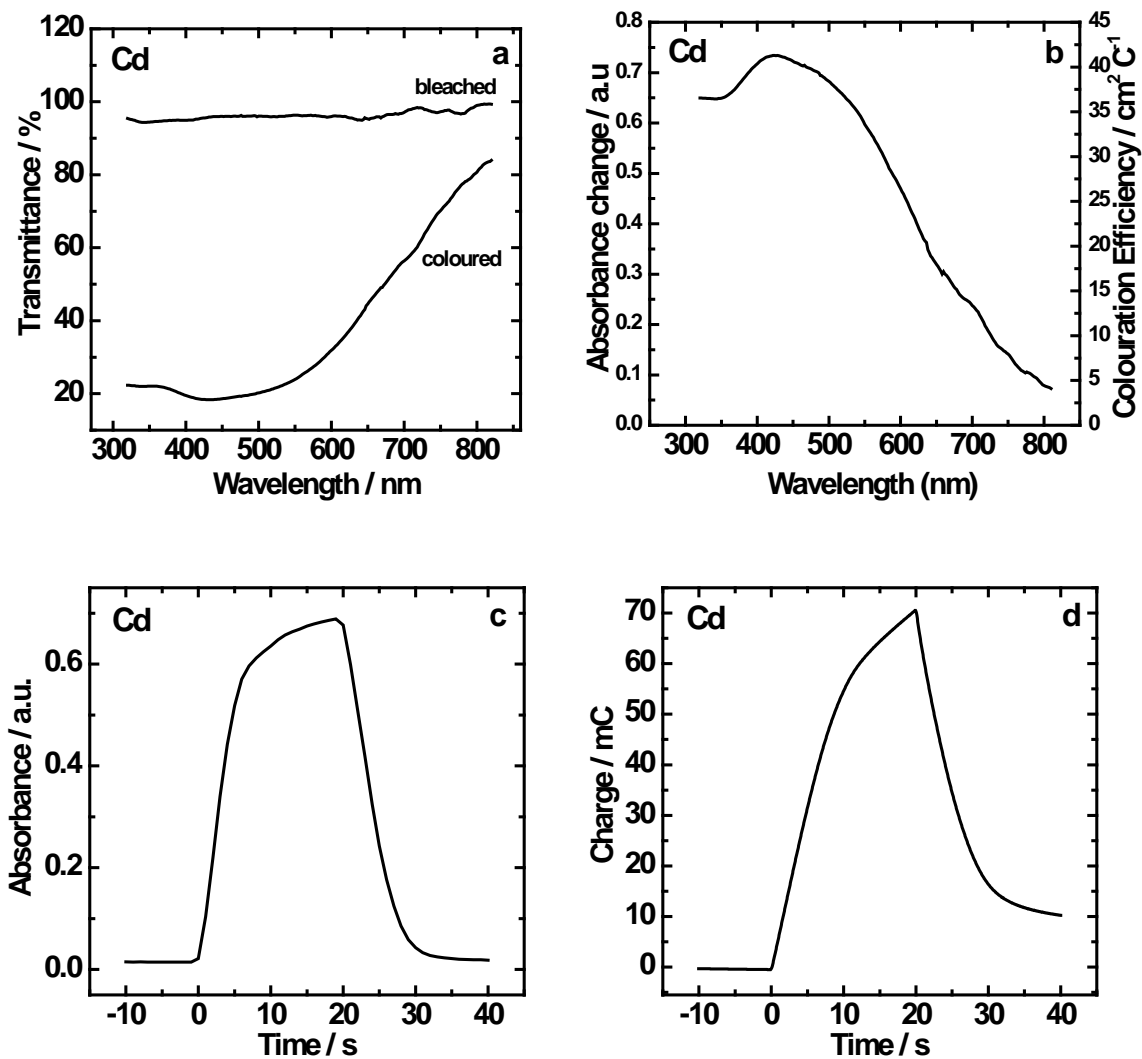
Figure 6.15. Visible region *in-situ* transmission spectra for the 'bleached' and coloured states (a), change in absorbance and colouration efficiency (b), absorbance vs. time transient (c) and charge vs time transients (d) of hydrated NiO film co-deposited with cadmium.
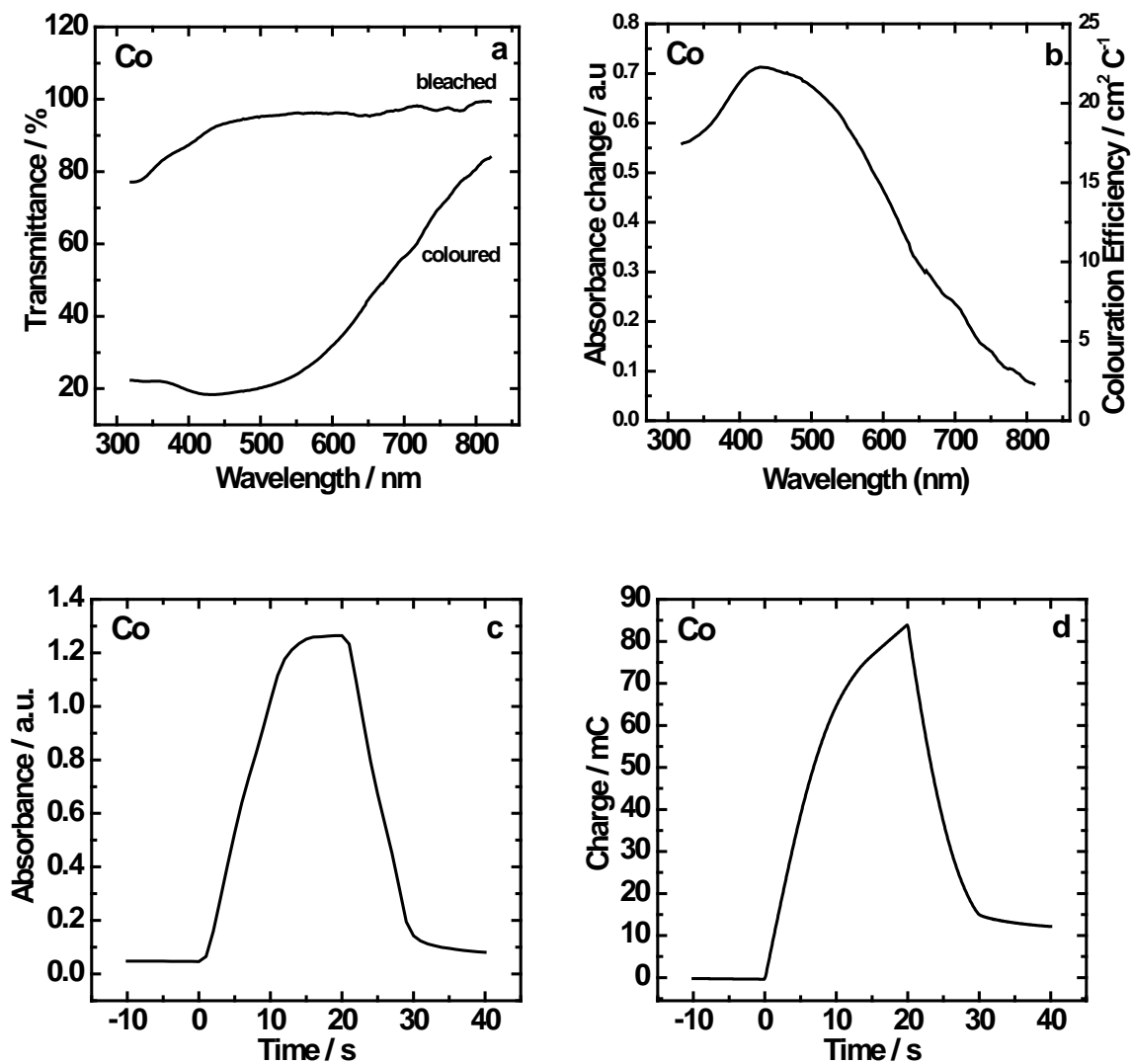
Figure 6.16. Visible region *in-situ* transmission spectra for the 'bleached' and coloured states (a), change in absorbance and colouration efficiency (b), absorbance vs. time transient (c) and charge vs time transients (d) of hydrated NiO film co-deposited with cobalt.

Figure 6.17. Visible region *in-situ* transmission spectra for the 'bleached' and coloured states (a), change in absorbance and colouration efficiency (b), absorbance vs. time transient (c) and charge vs time transients (d) of hydrated NiO film co-deposited with copper.

Figure 6.18. Visible region *in-situ* transmission spectra for the 'bleached' and coloured states (a), change in absorbance and colouration efficiency (b), absorbance vs. time transient (c) and charge vs time transients (d) of hydrated NiO film co-deposited with lanthanum.

Figure 6.19. Visible region *in-situ* transmission spectra for the 'bleached' and coloured states (a), change in absorbance and colouration efficiency (b), absorbance vs. time transient (c) and charge vs time transients (d) of hydrated NiO film co-deposited with cobalt and cadmium.

Figure 6.20. Visible region *in-situ* transmission spectra for the 'bleached' and coloured states (a), change in absorbance and colouration efficiency (b), absorbance vs. time transient (c) and charge vs time transients (d) of hydrated NiO film co-deposited with cobalt and copper.
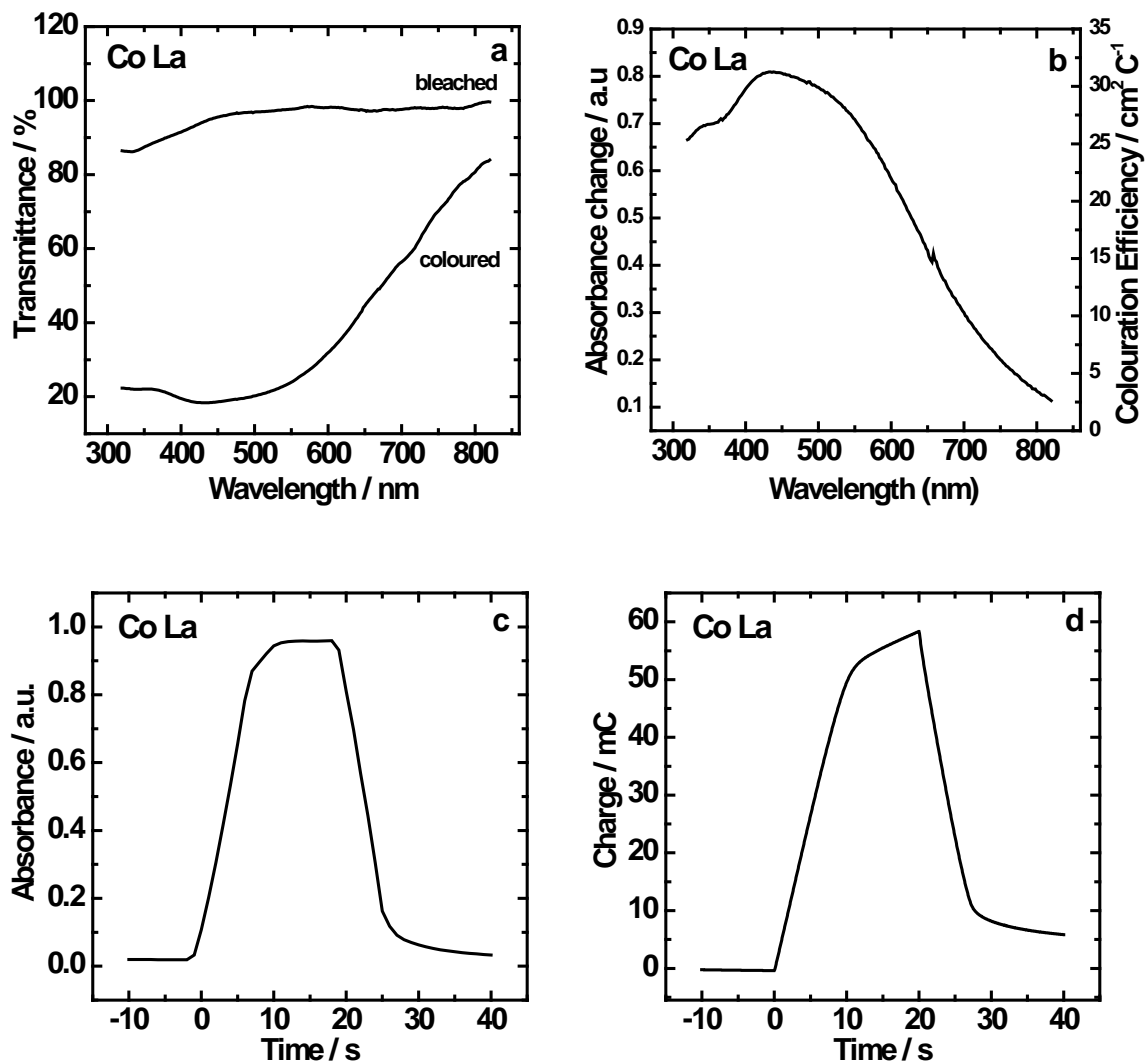
Figure 6.21. Visible region *in-situ* transmission spectra for the 'bleached' and coloured states (a), change in absorbance and colouration efficiency (b), absorbance vs. time transient (c) and charge vs time transients (d) of hydrated NiO film co-deposited with cobalt and lanthanum.

6.5. The effect of metal ion additives on the colour measurements of the hydrated NiO films

Table 6.3 shows CIE 1931 $\%Y_L$ xy and CIELAB $L^*a^*b^*$ chromaticity coordinates for the hydrated NiO film co-deposited with different additives as calculated from visible region absorbance spectra in figures 6.22 to 6.29 ((b) and (c)), recorded in the same experimental conditions as in section 6.4 but in this case showing the complete spectral change. In table 6.3 one value for the 'bleached' and one value for the coloured states are given for each film. The complete calculation of the CIE chromaticity coordinates and luminance data during dynamic colour switching between the 'bleached' (transmissive) and coloured (brown-grey) redox states can be found in appendix A.

The generated xy data are also presented as a hue and saturation track in chromaticity diagrams (figures 6.30 and 6.31). Comparing the xy chromaticity diagrams and the values in table 6.3 show several trends. The shape of the colour tracks for each film is consistent with those obtained in chapter 5, section 4 and 6.3 with the existence of hysteresis and a tailing or kink towards the latter stages of the oxidation process (between 15 and 20 s). It can be seen from the xy chromaticity figures that for all the films as the potential is stepped to a positive value both the x and y values increased as the fully transparent hydrated NiO was oxidised to the coloured brown-grey NiOOH redox state. In many of the co-deposited films (cerium, copper, lanthanum, cobalt/copper and cobalt/lanthanum) the xy trajectories follow a very similar track to those generated for pure hydrated NiO. However, with the addition of cobalt, cadmium and cobalt/cadmium a different xy trajectory was observed, with a decrease in y and an increase in x values for the colouration process.

Figures 6.32 and 6.33 show the changes in the relative luminance ($\%Y_L$) on potential switching between the 'bleached' and coloured state. Generally, for all the co-deposited films the values of $\%Y_L$ coincide with pure hydrated NiO with the graphical form of the relative luminance being in good correlation with electric charge (figures 6.14 to 6.21(d)).

In table 6.3, the CIELAB $L^*a^*b^*$ coordinates are also given which, when combined with the xy chromaticity and $\%Y_L$ data, provide valuable information in quantifying the perceived colour of the EC film. As outlined above, the preparation of hydrated NiO with additives is an effective way to enhance the electrochemical and EC properties of the film. Furthermore, with the addition of additives, the ability to 'fine-tune' the colour states is another asset when considering the EC materials' properties towards smart window applications. From table 6.3 it can be noted that at the initial 0.00 V applied potential, the 'bleached' state of all the films is close to the achromatic 'white point' ($L^* = 100$, $a^* = 0$, $b^* = 0$). As the potential is stepped to positive values, the L^* values decrease with the increasing saturation of the brown-grey colour, with both a^* and b^* values becoming more positive. On potential switching, the colour perceived for films co-deposited with cobalt was reddish-brown as indicated by a high a^* and b^* values. Similar colours were also produced for films co-deposited with cobalt/lanthanum. In the case of films prepared with cadmium as an additive, the colour perceived was a more brown/black tone, as indicated by low a^* and b^* values.

Table 6.3. Chromaticity coordinates (CIE 1931 %$Y_L xy$ and CIELAB $L^*a^*b^*$) for the 'bleached' and the coloured states of the hydrated NiO films co-deposited with different additives on FTO/glass.

Additive	x	y	%Y_L	L^*	a^*	b^*
(hydrated NiO 'bleached')	0.332	0.347	99.9	100	-0.2	-0.3
(hydrated NiO coloured)	0.390	0.363	24.4	56	12.1	12.1
cerium 'bleached'	0.332	0.347	99.6	100	-0.1	-0.4
cerium coloured	0.391	0.365	29.8	61	12.5	13.5
cadmium 'bleached'	0.333	0.348	100.0	100	-0.1	0.1
cadmium coloured	0.371	0.351	26.2	58	10.7	6.2
cobalt 'bleached'	0.335	0.351	98.4	99	-0.5	1.7
cobalt coloured	0.446	0.362	13.8	43	22.6	17.3
copper 'bleached'	0.334	0.347	97.5	99	0.9	-0.0
copper coloured	0.396	0.361	18.3	50	13.0	11.2
lanthanum 'bleached'	0.331	0.346	100	100	-0.1	-1.2
lanthanum coloured	0.394	0.360	16.2	47	12.6	10.6
cobalt and cadmium 'bleached'	0.336	0.350	96.5	98	0.3	1.9
cobalt and cadmium coloured	0.405	0.354	23.5	56	28.8	11.7
cobalt and copper 'bleached'	0.334	0.349	100.0	199	-0.3	0.9
cobalt and copper coloured	0.392	0.359	26.8	59	14.4	11.7
cobalt and lanthanum 'bleached'	0.335	0.350	99.8	100	-0.2	1.3
cobalt and lanthanum coloured	0.432	0.368	21.8	54	21.4	19.4
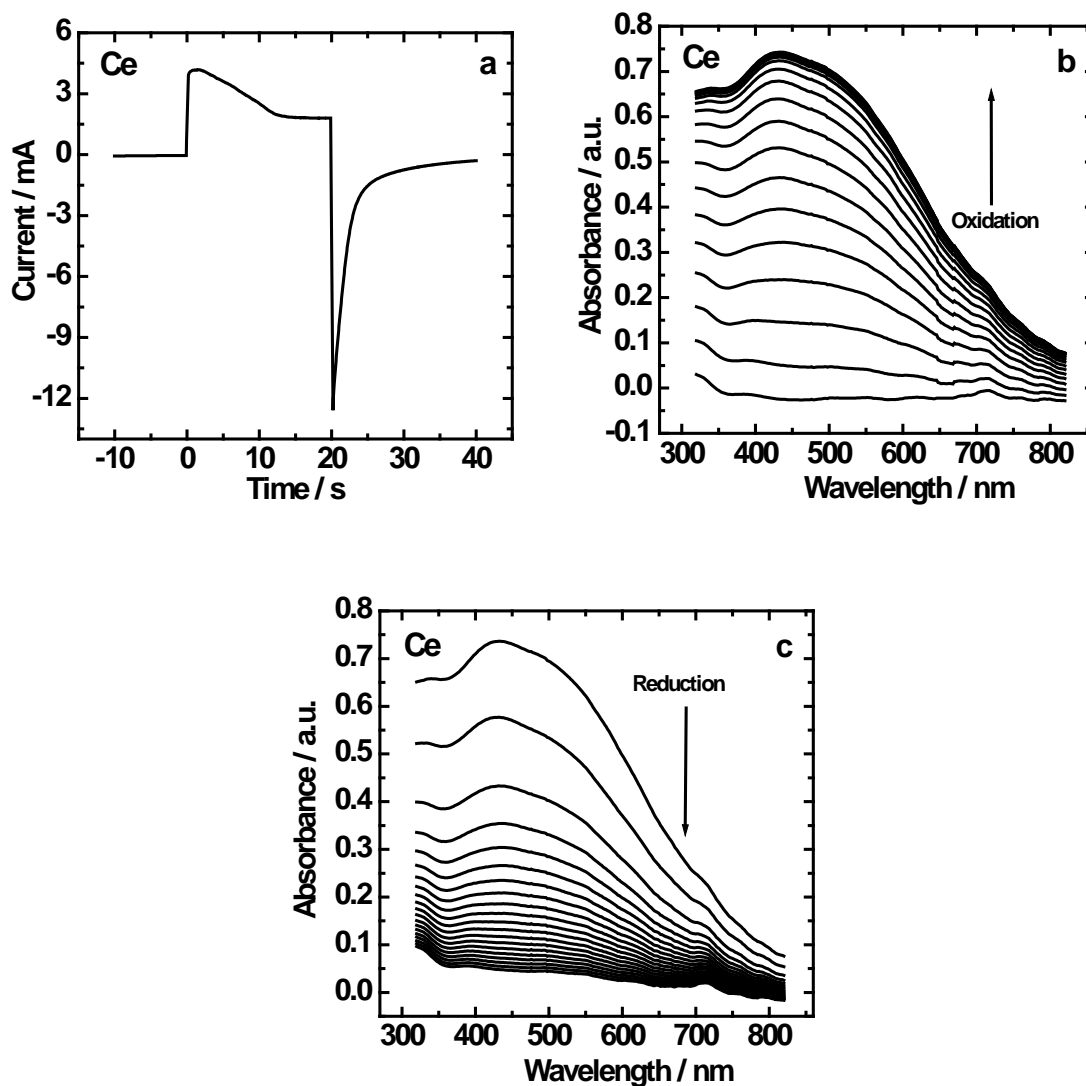
Figure 6.22. Current vs. time transients (a) and visible region absorbance spectra ((b) and (c), spectra recorded every 1 s), for the reversible switching of a hydrated NiO film co-deposited with cerium in aqueous KOH (0.1 mol dm^{-3}) between the transmissive green 'bleached' state and the coloured (brown-grey) state. EC switching was conducted by application of potential steps (-0.30 V $\rightarrow$ +0.45 V $\rightarrow$ -0.30 V) vs. the Ag wire pseudo reference electrode. In (b) and (c) the arrows indicate the direction of change in absorbance.
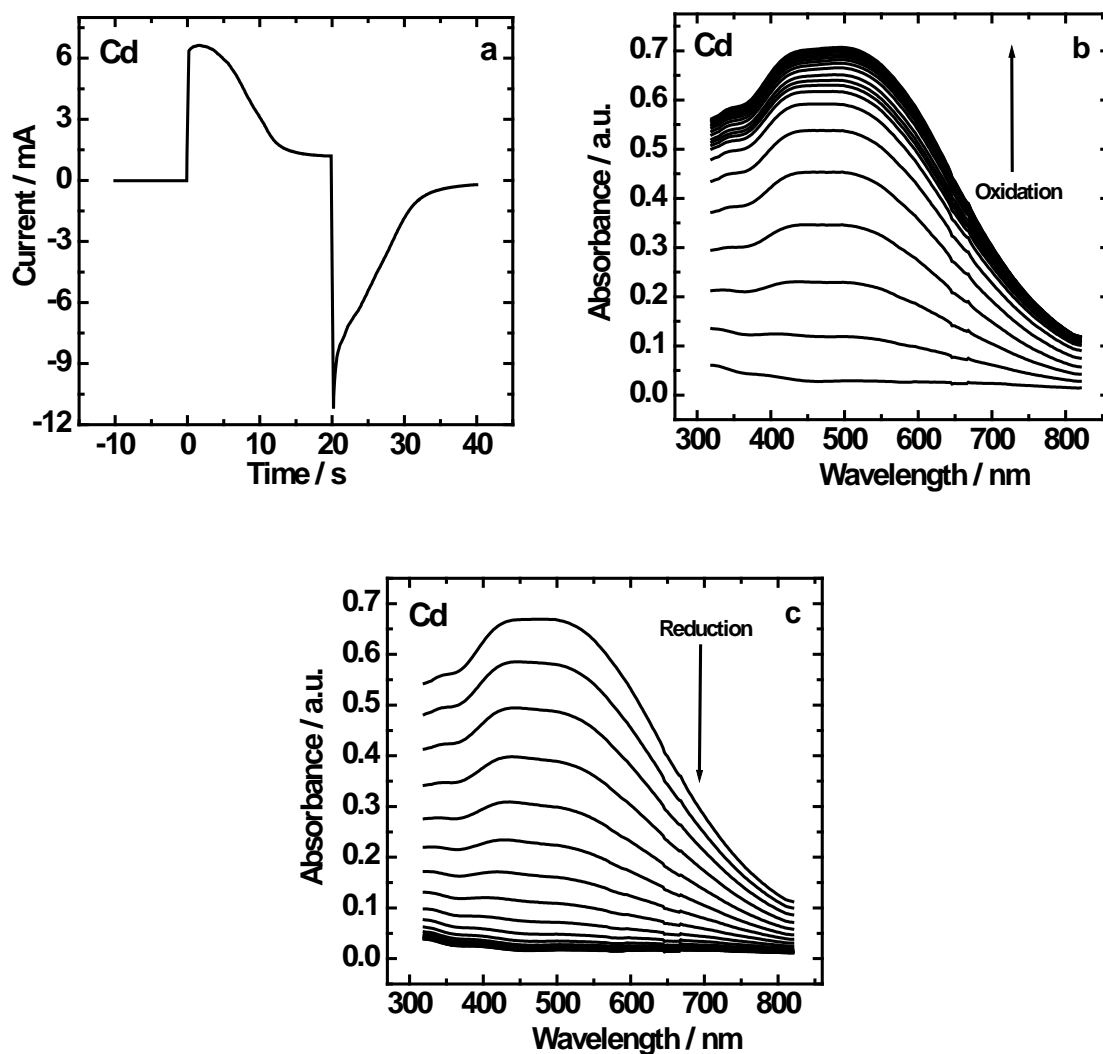
Figure 6.23. Current vs. time transients (a) and visible region absorbance spectra ((b) and (c), spectra recorded every 1 s), for the reversible switching of a hydrated NiO film co-deposited with cadmium in aqueous KOH (0.1 mol dm^{-3}) between the transmissive green 'bleached' state and the coloured (brown-grey) state. EC switching was conducted by application of potential steps (-0.20 V $\rightarrow$ $+0.48$ V $\rightarrow$ -0.20 V) vs. the Ag wire pseudo reference electrode. In (b) and (c) the arrows indicate the direction of change in absorbance.
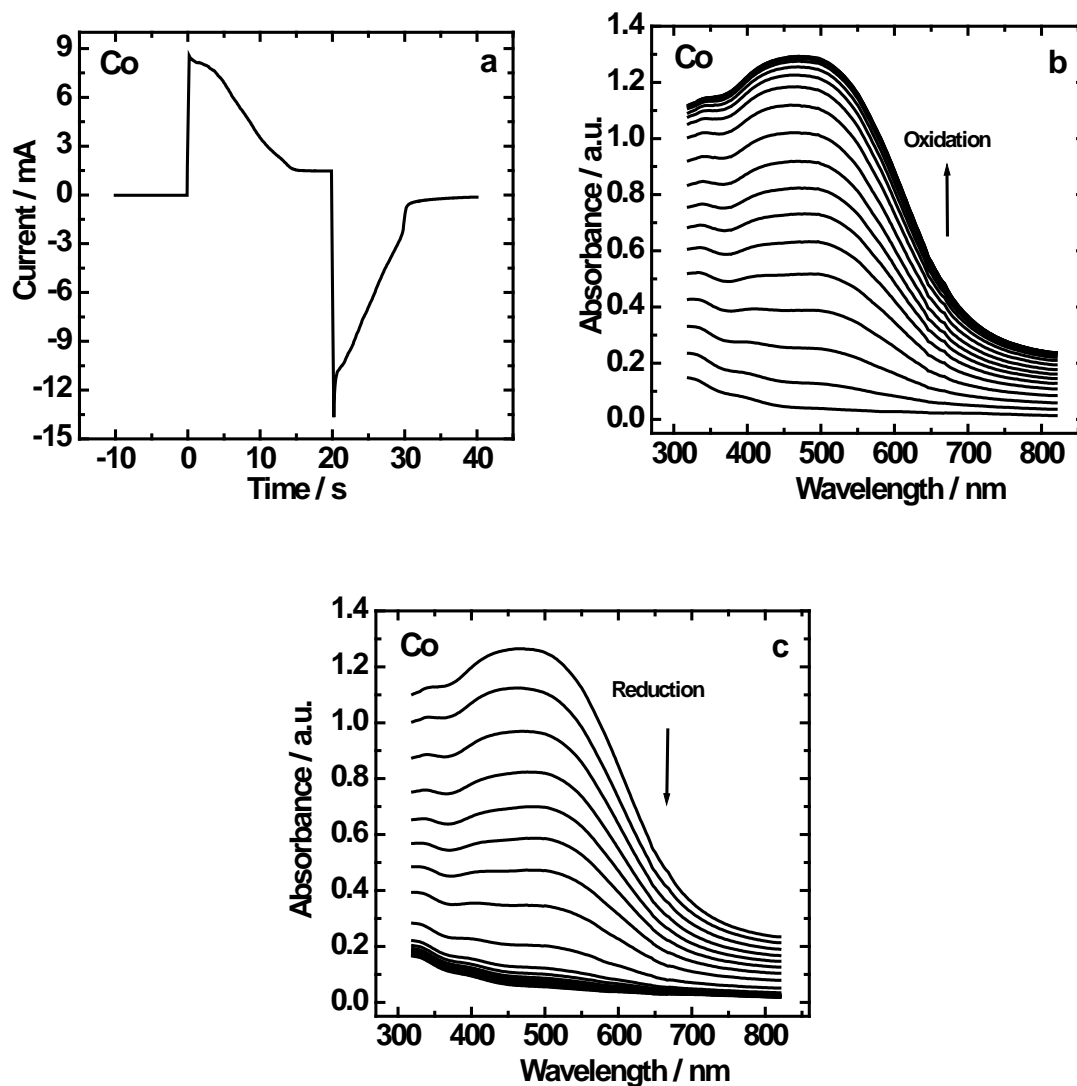
Figure 6.24. Current vs. time transients (a) and visible region absorbance spectra ((b) and (c), spectra recorded every 1 s), for the reversible switching of a hydrated NiO film co-deposited with cobalt in aqueous KOH (0.1 mol dm^{-3}) between the transmissive green 'bleached' state and the coloured (brown-grey) state. EC switching was conducted by application of potential steps (–0.20 V → +0.46 V → –0.20 V) vs. the Ag wire pseudo reference electrode. In (b) and (c) the arrows indicate the direction of change in absorbance.
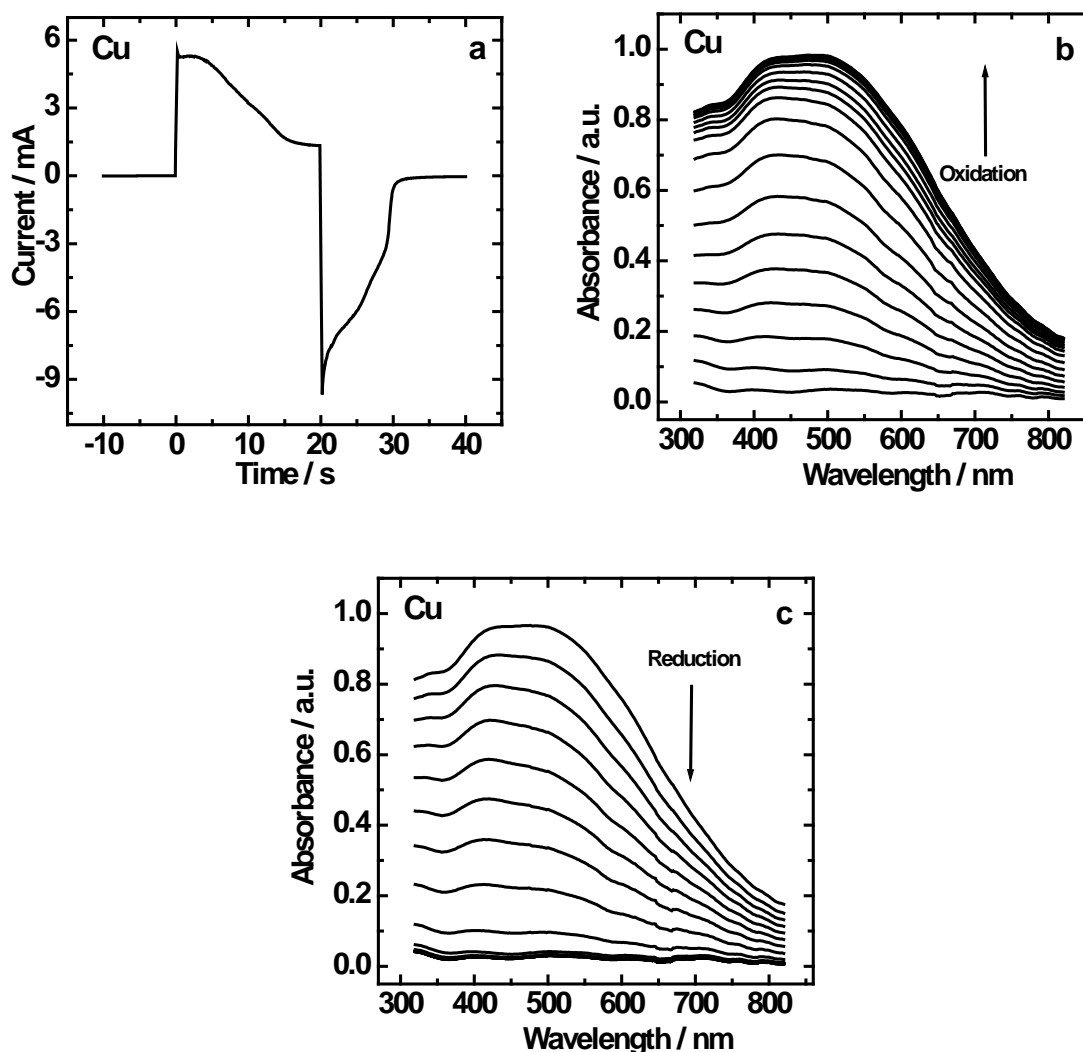
Figure 6.25. Current vs. time transients (a) and visible region absorbance spectra ((b) and (c), spectra recorded every 1 s), for the reversible switching of a hydrated NiO film co-deposited with copper in aqueous KOH (0.1 mol dm^{-3}) between the transmissive green 'bleached' state and the coloured (brown-grey) state. EC switching was conducted by application of potential steps (−0.20 V → +0.49 V → −0.20 V) vs. the Ag wire pseudo reference electrode. In (b) and (c) the arrows indicate the direction of change in absorbance.
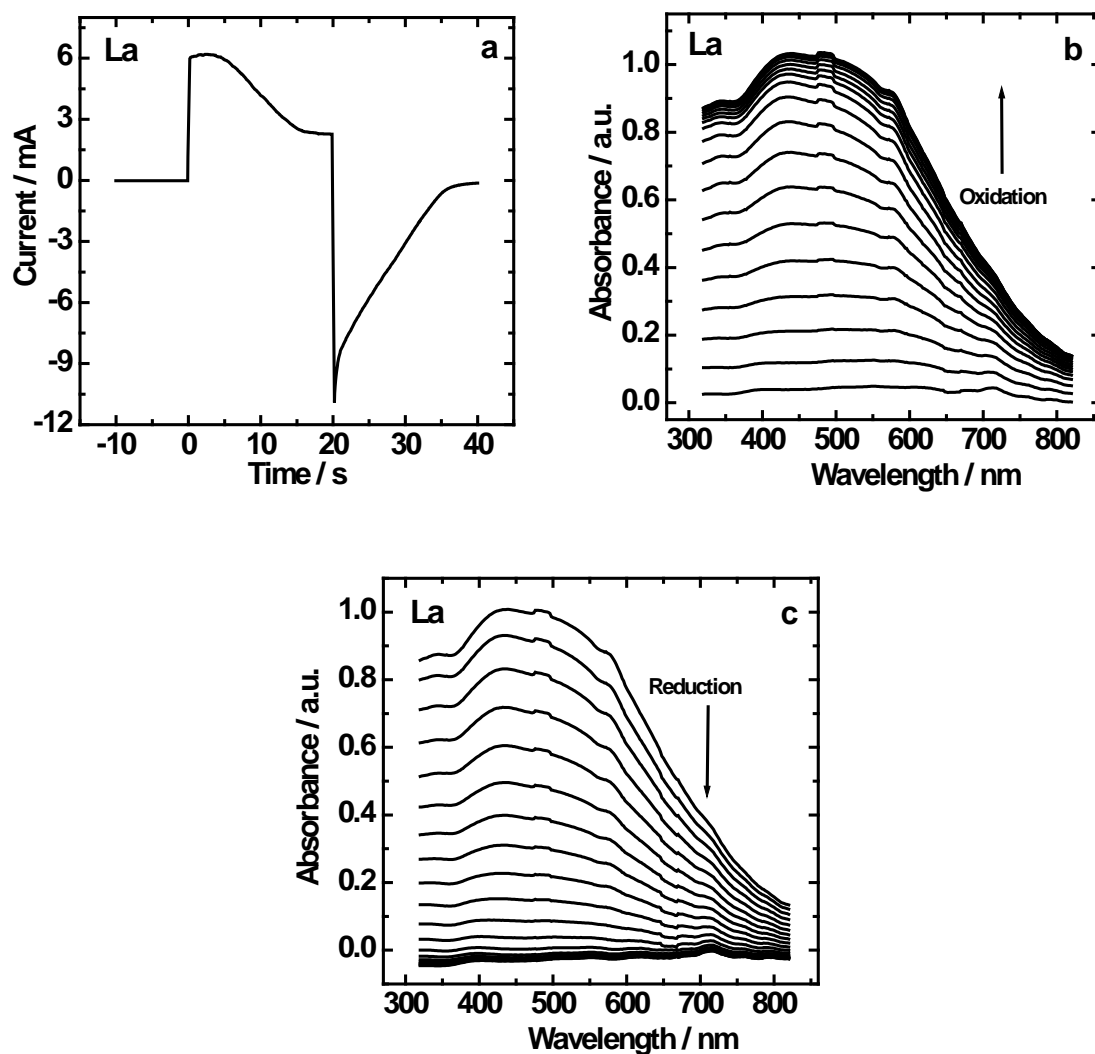
Figure 6.26. Current vs. time transients (a) and visible region absorbance spectra ((b) and (c), spectra recorded every 1 s), for the reversible switching of a hydrated NiO film co-deposited with lanthanum in aqueous KOH (0.1 mol dm⁻³) between the transmissive green 'bleached' state and the coloured (brown-grey) state. EC switching was conducted by application of potential steps (−0.30 V → +0.55 V → −0.30 V) vs. the Ag wire pseudo reference electrode. In (b) and (c) the arrows indicate the direction of change in absorbance.
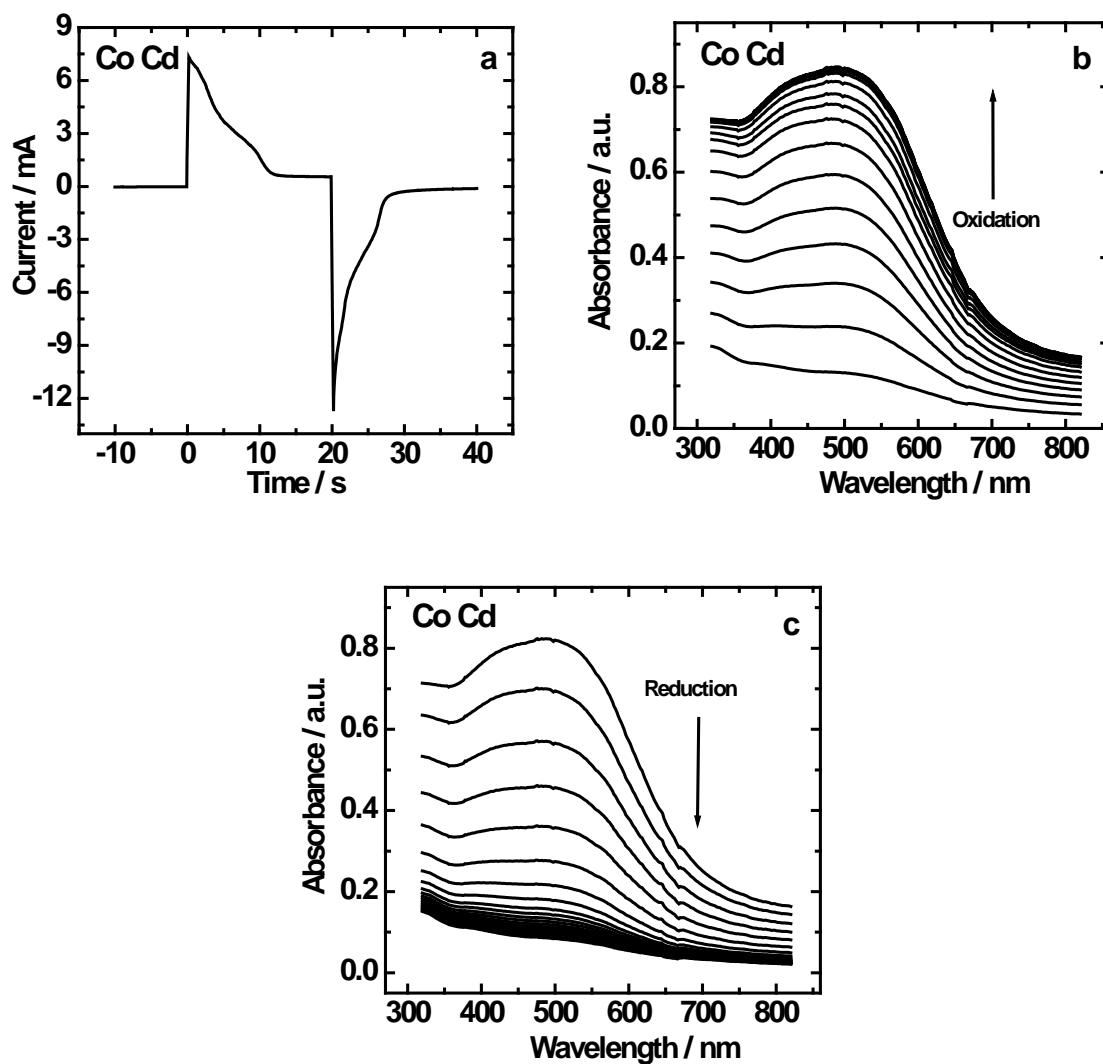
Figure 6.27. Current vs. time transients (a) and visible region absorbance spectra ((b) and (c), spectra recorded every 1 s), for the reversible switching of a hydrated NiO film co-deposited with cobalt and cadmium in aqueous KOH (0.1 mol dm^{-3}) between the transmissive green 'bleached' state and the coloured (brown-grey) state. EC switching was conducted by application of potential steps (−0.20 V → +0.43 V → −0.20 V) vs. the Ag wire pseudo reference electrode. In (b) and (c) the arrows indicate the direction of change in absorbance.
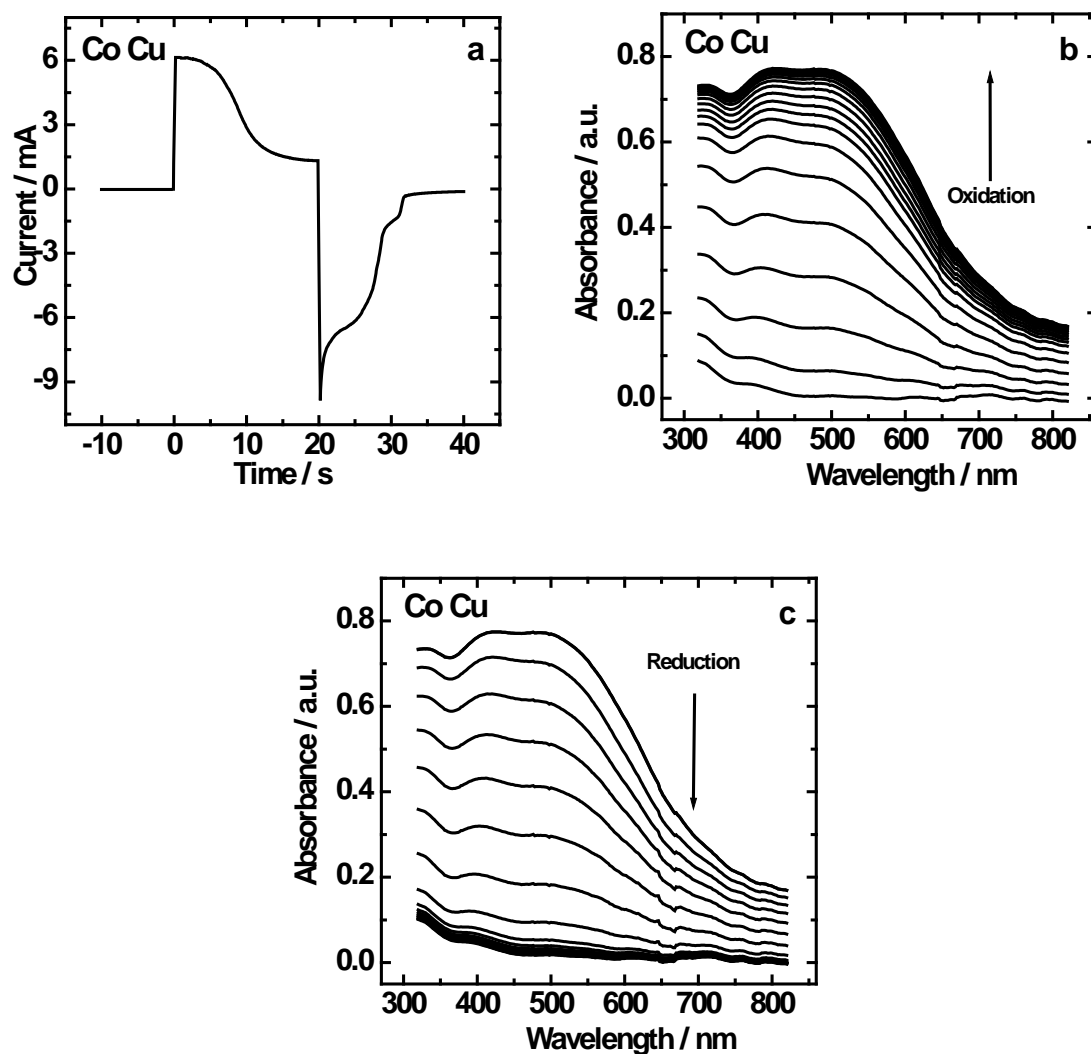
Figure 6.28. Current vs. time transients (a) and visible region absorbance spectra ((b) and (c), spectra recorded every 1 s), for the reversible switching of a hydrated NiO film co-deposited with cobalt and copper in aqueous KOH (0.1 mol dm^{-3}) between the transmissive green 'bleached' state and the coloured (brown-grey) state. EC switching was conducted by application of potential steps (-0.20 V $\rightarrow$ $+0.48$ V $\rightarrow$ -0.20 V) vs. the Ag wire pseudo reference electrode. In (b) and (c) the arrows indicate the direction of change in absorbance.
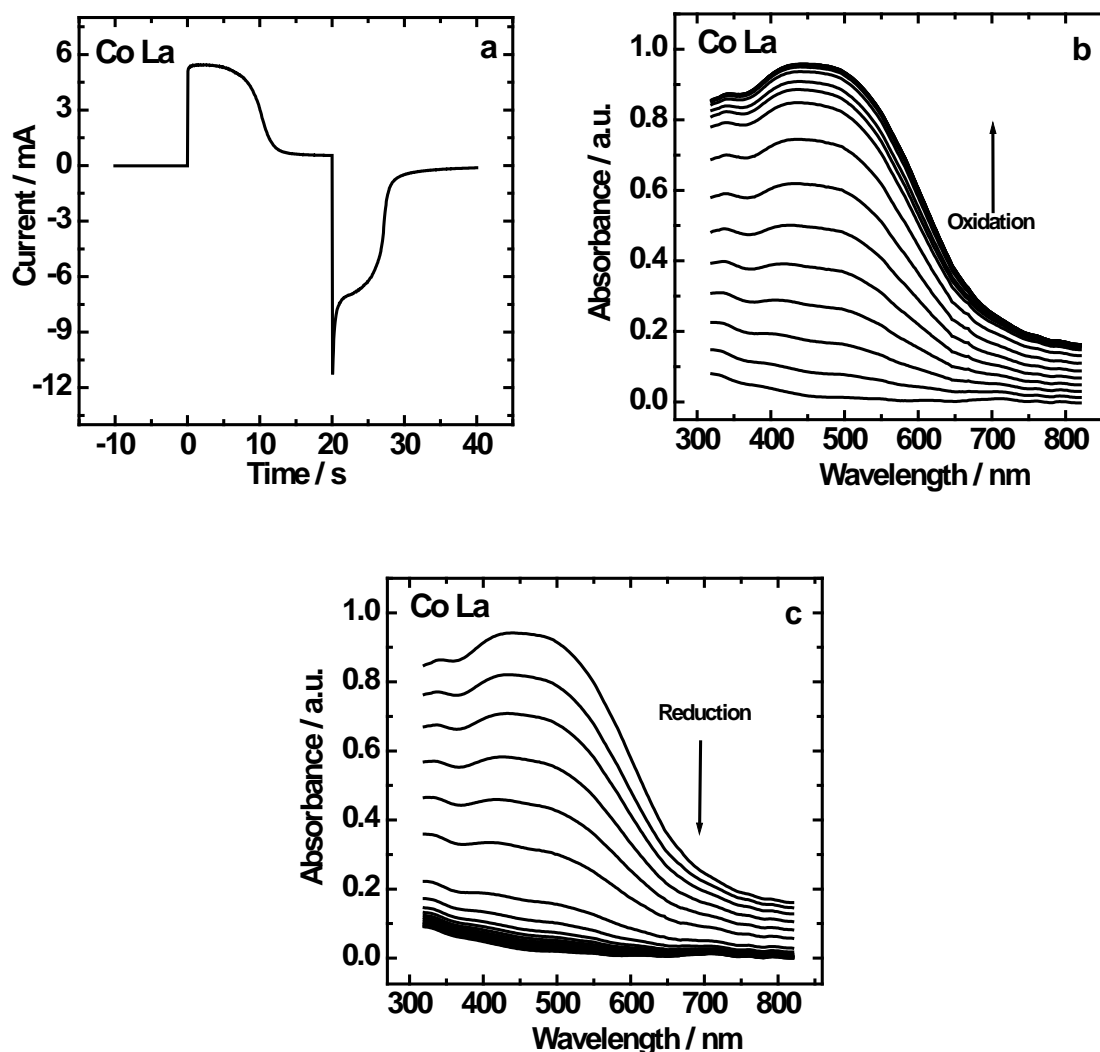
Figure 6.29. Current vs. time transients (a) and visible region absorbance spectra ((b) and (c), spectra recorded every 1 s), for the reversible switching of a hydrated NiO film co-deposited with cobalt and lanthanum in aqueous KOH (0.1 mol dm^{-3}) between the transmissive green 'bleached' state and the coloured (brown-grey) state. EC switching was conducted by application of potential steps (–0.20 V → +0.43 V → –0.20 V) vs. the Ag wire pseudo reference electrode. In (b) and (c) the arrows indicate the direction of change in absorbance.
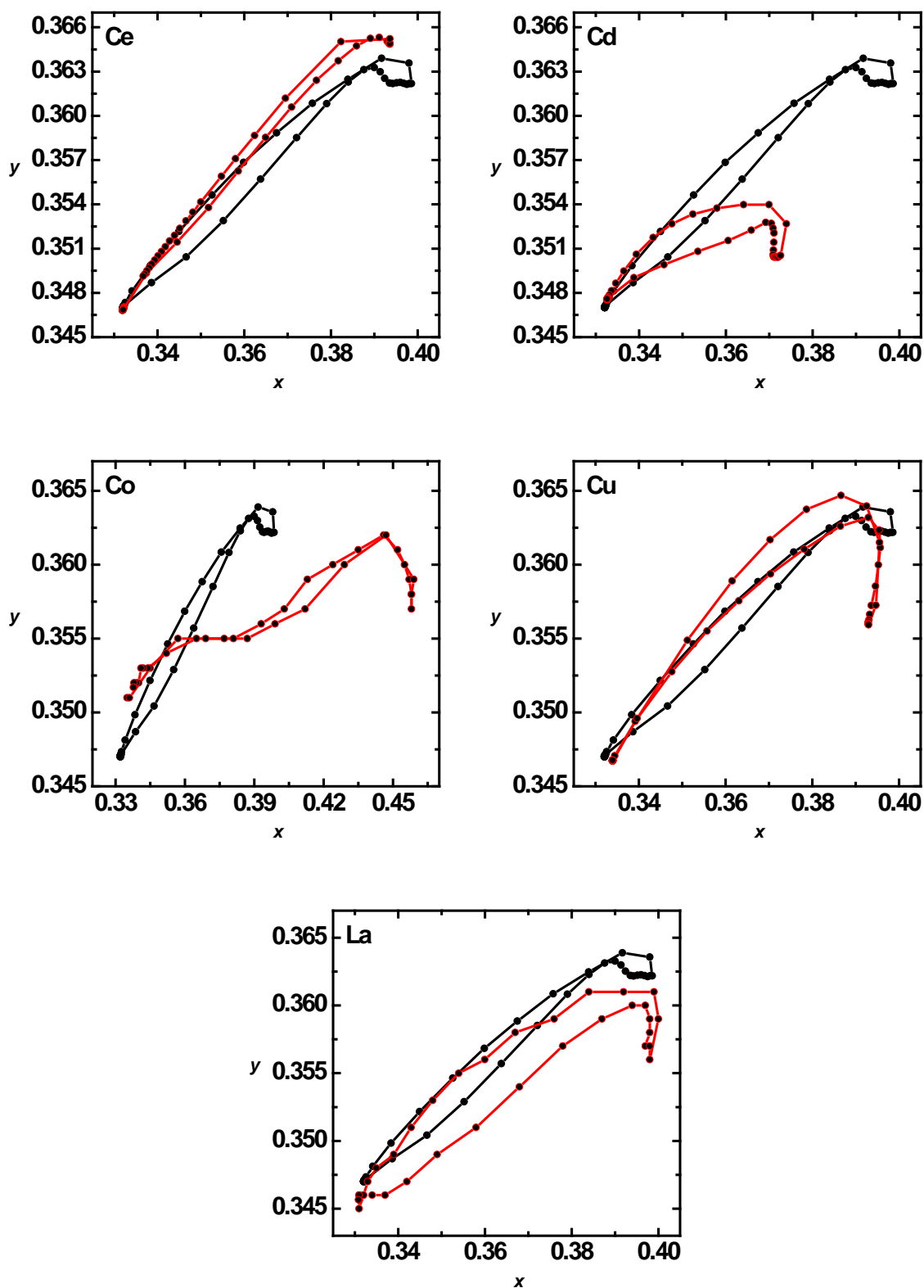
Figure 6.30. CIE 1931 *xy* chromaticity plots for pure hydrated NiO film (———) and films co-deposited with different additives (single) (———) on FTO/glass. The films were switched in aqueous KOH (0.1 mol dm⁻³) between the 'bleached' and coloured states by application of potential steps.

Figure 6.31. CIE 1931 *xy* chromaticity plots for pure hydrated NiO film (——) and films co-deposited with different bimetallic additives (——) on FTO/glass. The films were switched in aqueous KOH (0.1 mol dm^{-3}) between the 'bleached' and coloured states by application of potential steps.

6. Effect of metal ion additives on the electrochemical and electrochromic performance of hydrated NiO
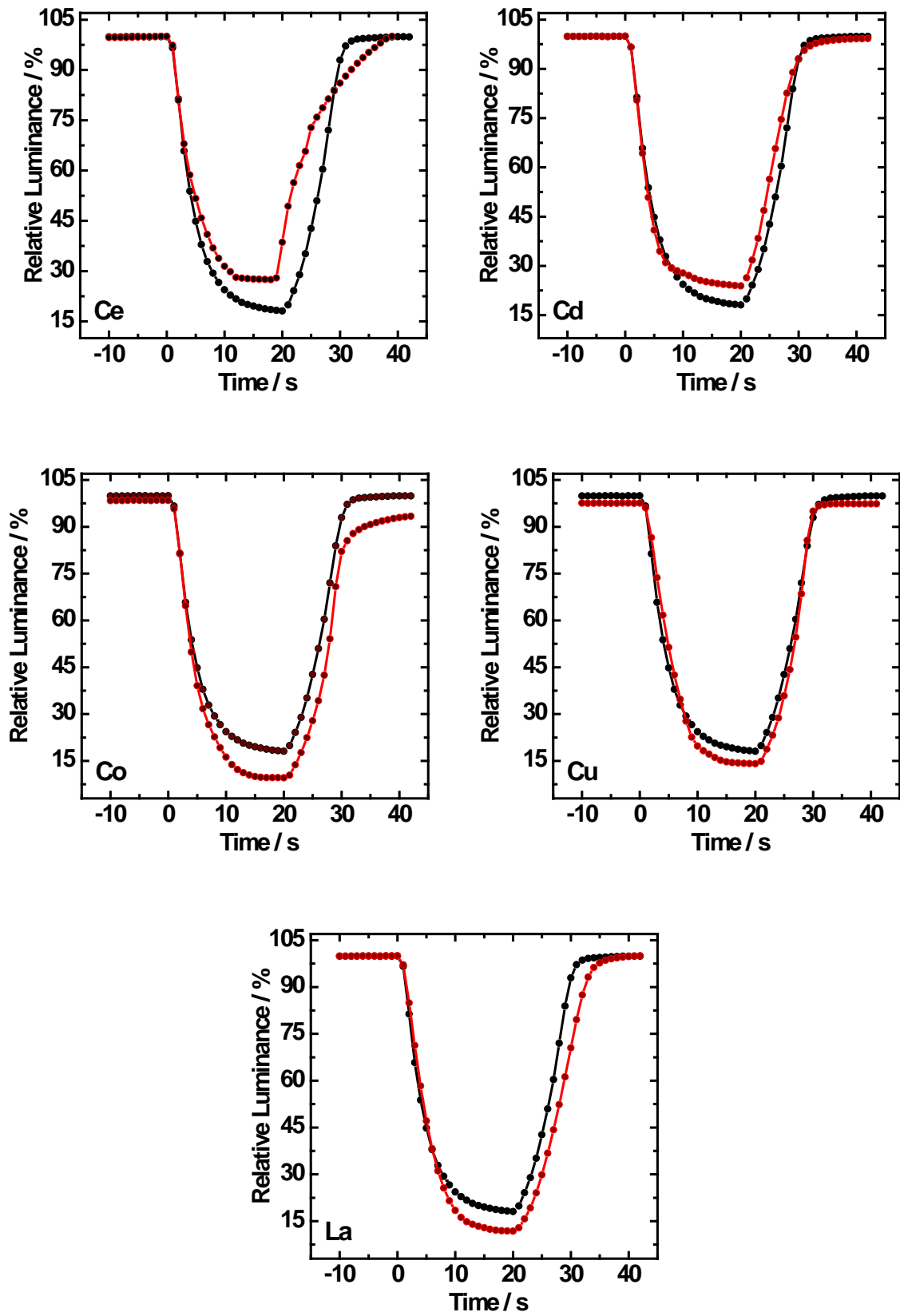
Figure 6.32. CIE 1931 relative luminance data vs. time for pure hydrated NiO film (━━) and films co-deposited with different additives (single) (━━) on FTO/glass.

6. Effect of metal ion additives on the electrochemical and electrochromic performance of hydrated NiO
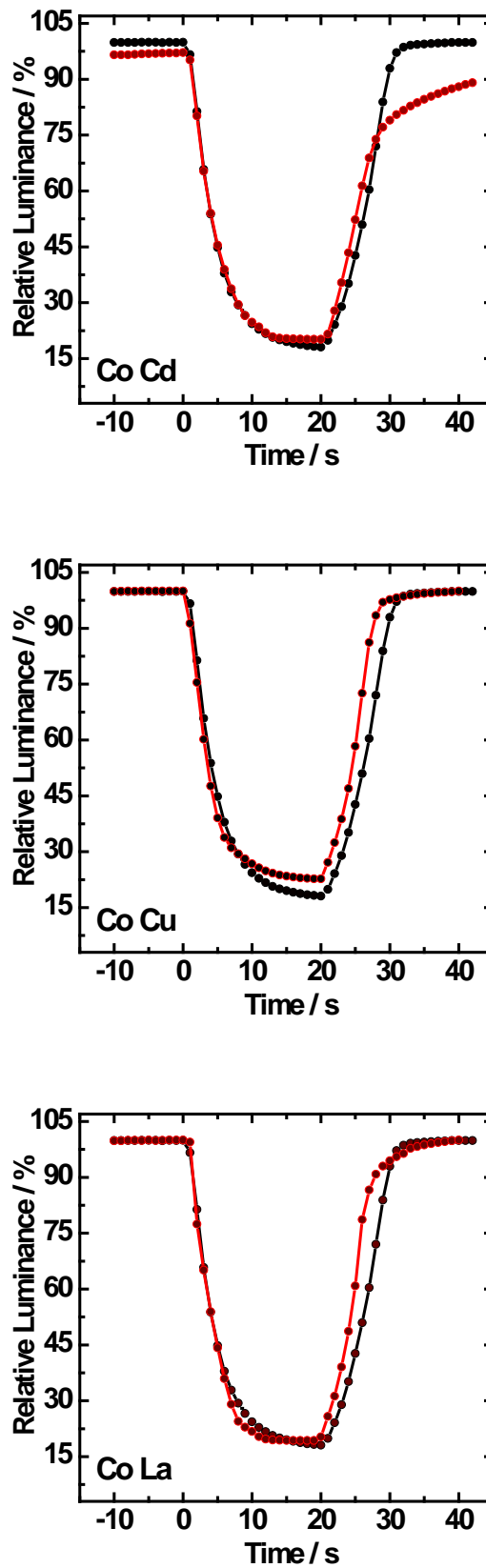
Figure 6.33. CIE 1931 relative luminance data vs. time for pure hydrated NiO film (━━━) and films co-deposited with different bimetallic additives (━━━) on FTO/glass.

6.6. Conclusion

This chapter has detailed the formation of hydrated NiO films prepared with various metal ion additives. The effect of single and bimetallic additives on the electrochemical, electrochromic (EC) and colour-tuning properties was considered. Electrochemical studies revealed that films prepared with cobalt (10%) as an additive increased the conductivity of the film thereby shifting the Ni(II)/Ni(III) redox process to less positive potentials and avoiding the OER. Additionally, the incorporation of a second additive further increased the durability by reducing the expansion or contraction of the nickel and hydroxide layers during redox cycling. In this way, the displacement of the redox peaks is avoided and the formation of the γ-phase is reduced. In particular the combination of cobalt (10%) with lanthanum (5%) was found to be the optimal composition for preparing hydrated NiO films with improved film durability. Finally, the effect of additives on fine-tuning the colour states was investigated using the CIE 1931 %Y_L xy and CIELAB $L^*a^*b^*$ chromaticity coordinates, with the addition of cobalt producing a reddish-brown tone and the addition of cadmium producing a brown-black coloured film upon oxidation.

From the results, it is evident that with the addition of certain elements, the EC properties of hydrated NiO films can be enhanced or tailored towards specific commercial applications. Variation of the metal additives allows the colouration of the EC material to be fine-tuned.

6.7. References

[1]   Vidotti, M., Salvador, R. P., Ponzio, E. A. and Córdoba de Torresi, S. I. Mixed Ni/Co hydroxide nanoparticles synthesized by sonochemical method. *J. Nanosci. Nanotechnol.*, **7**, 2007, 3221-26.

[2]   Wehrens-Dijksma, M. and Notten P. H. L. Electrochemical quartz microbalance characterization of Ni(OH)$_2$-based thin film electrodes. *Electrochim. Acta*, **51**, 2006, 3609-2.

[3]   Oliva, P., Leonardi, J., Laurent, J. F., Delmas, C., Braconnier, J. J., Figlarz, M., Fievet, F. and de Guibert, A. Review of the structure and the electrochemistry of nickel hydroxides and oxy-hydroxides. *J. Power Sources*, **8**, 1992, 229-55.

[4]   Bode, H., Dehmelt, K. and Witte, J. Zur kenntnis der nickelhydroxidelektrode—I. Über das nickel (II)-hydroxidhydrat. *Electrochim. Acta*, **11**, 1966, 1079-87.

[5]   Bode, H., Dehmelt, K. and Witte, J. Zur Kenntnis der Nickelhydroxidelektrode. II. Über die Oxydationsprodukte von Nickel(II)-hydroxiden. *Z. Anorg. Allg. Chem.*, **366**, 1969, 1-21.

[6]   Portemer, F., Delahaye-Vidal, A. and Figlarz. M. Characterization of active material deposited at the nickel hydroxide electrode by electrochemical impregnation. *J. Electrochem. Soc.*, **139**, 1992, 671-8.

[7]   Oshitani, M., Takayama, T., Takashima, K. and Tsuji, S. A study on the swelling of a sintered nickel hydroxide electrode. *J. Appl. Electrochem.*, **16**, 1986, 403-12.

[8]   Vidotti, M., Salvador, R. P. and Córdoba de Torresi, S. I. Synthesis and characterization of stable Co and Cd doped nickel hydroxide nanoparticles for electrochemical applications. *Ultrason. Sonochem.*, **16**, 2009, 35-40.

[9]   Bing, L., Huatang, Y., Yunshi, Z., Zuoxiang, Z. and Deying, S. Cyclic voltammetric studies of stabilized α-nickel hydroxide electrode. *J. Power Sources*, **79**, 1999, 277-80.

[10]   Córdoba de Torresi, S. I. The effect of manganese addition on nickel hydroxide electrode with emphasis on its electrochromic properties. *Electrochim. Acta.*, **40**, 1995, 1101-07.

[11]   Chen, X., Hu, X. and Feng, J. Nanostructured nickel oxide films and their electrochromic properties. *Nanostruct. Mater.*, **6**, 1995, 309-12.

[12]   Szytula, A., Murasik, A. and Balanda, M. Neutron Diffraction Study of $Ni(OH)_2$. *Phys. Status Solidi B*, **43**, 1971, 125-8.

[13]   Glemser, O. and Einerhand, J. Die Struktur der hoeheren Nickelhydroxide. *Anorg. Allg. Chem.*, **261**, 1950, 43-51.

[14]   Corrigan, D. A. and Bendert, R. M. Effect of coprecipitated metal ions on the electrochemistry of nickel hydroxide thin films: cyclic voltammetry in 1M KOH. *J. Electrochem. Soc.*, **136**, 1989, 723-8.

[15]   Pickett, D. F., Maloy, J. T. Microelectrode studies of electrochemically coprecipitated cobalt hydroxide in nickel hydroxide electrodes. *J. Electrochem. Soc.*, **125**, 1978, 1026-32.

[16]   Córdoba de Torresi, S. I., Provazi, K., Malta, M and Torresi, R. M. Effect of additives in the stabilization of the α Phase of Ni(OH)$_2$ Electrodes. *J. Electrochem. Soc.*, **148**, 2001, A1179-84.

[17]   Zhang, Y., Cao, X., Yuan, H., Zhang, W. and Zhou, Z. Oxygen evolution reaction on Ni hydroxide film electrode containing various content of Co. *Int. J. Hydrogen Energy*, **24**, 1999, 529-36.

[18]   Bendert, R. M. and Corrigan, D. A. Effect of coprecipitated metal Ions on the electrochromic properties of nickel hydroxide. *J. Electrochem. Soc.*, **136**, 1989, 1369-74.

[19]   Lide, D. R. *CRC handbook of chemistry and physics*, CRC Press, 2000-2001.

[20]   Provazi, K., Giz, M. J., Dall'Antonia, L. H. and Córdoba de Torresi, S. I. The effect of Cd, Co, and Zn as additives on nickel hydroxide opto-electrochemical behaviour. *J. Power Sources*, **102**, 2001, 224-32.

7. Large-area electrochromic hydrated nickel oxide film deposition

7.1. Introduction

The first experimental investigation into the use of electrochromic (EC) films towards smart window applications appeared in 1984 by Svensson and Granqvist.[1] Although the technology was first considered nearly 30 years ago, its implementation towards commercialisation has been relatively slow. One of the main reasons for this lack of progress might be due to its complex nature and the need to optimise the different components of a working device (figure 1.1 (chapter 1)) and failure in one aspect of the device will affect the integrity of the entire working prototype.[2,3] Furthermore, for an EC device to be judged suitable for a smart windows application, it must meet or exceed many of the key performance parameters as outlined (table 7.1) by Mathew *et al.*[4] With this in mind, over the past 15 years, numerous research investigations have been carried out in an attempt to identify the optimal primary and secondary EC materials towards smart window applications (chapter 2).

More recently, with the widespread concerns of global warming, rise in energy demands and the realisation of large energy saving associated with the use of smart windows has resulted in an increased interest in this area of research.[5] As a result, a number of companies have gained momentum by producing commercially available smart windows up to a maximum size of 120 x 220 cm^2. An excellent review of these companies is given by Baetens *et al.*[6]

As already mentioned, due to the complex nature of a large-area EC device it is important to understand the various operating factors associated at the different stages of development. From the initial small-scale lab investigations to the final large-area practical product, careful attention is given to every experimental problem and at every development stage in order to optimise the device design with precise

EC performance ability. An important step along this lab to market phenomena is scale-up of deposition.

In this chapter, optimised deposition conditions from small-scale (chapter 4.4) were used to prepare hydrated NiO films onto two different sized large-area fluorine-doped tin oxide (SnO_2:F, FTO) on glass (10 x 7.5 and 30 x 30 cm) substrates via an electrochemical cathodic deposition. For films deposited onto 30 x 30 cm FTO/glass substrate, a special designed electrochemical tank (figure 3.8 (chapter 3)) was used to deposit the films. The deposited films were experimentally tested and compared with the minimum acceptable performance parameters outlined in table 7.1.

Table 7.1. Performance criteria for EC window. Table redrawn from.[4]

Performance parameter	EC glazing requirement
Clear state transmittance	60 to 80%, photopic
Coloured state transmittance	5 to 20%, photopic
Contrast ratio	4:1 to 10:1
Switching speed (>0.1 m^2)	1 to 5 min
Cycling lifetime	>50,000 (full cycles)
Static lifetime	10 to 40 years
Darkened state memory	Minutes to hours
Colour	Neutral grey
Operating temperature	-20 to 85 °C

7.2. Hydrated NiO film preparation on 10 x 7.5 cm active area FTO/glass substrate

Figure 7.1 (a) shows the potential-time transient for the deposition of hydrated NiO thin film using the optimised (small-scale) deposition conditions of -0.2 mA for 800 s in 0.01 mol dm^{-3} nickel nitrate and on FTO/glass substrate. From the plot it can be seen that the optimised small-scale current of -0.2 mA was negligible in sustaining the required potentials (between -0.80 and -1.0 V) to deposit a thick film. This was

further evident from the corresponding CV which produced low oxidation and reduction peak currents (figure 7.1 (b)) and a lack of film colouration on switching to the NiOOH state. Therefore, a wide range of applied currents (-0.2 to -5 mA) were tested and -3 mA for 800 seconds was found to be sufficient for producing uniform coloured films with proportional properties to the optimised small-scale films. Figure 7.2 shows photographs of the hydrated NiO films deposited at different times in the 'bleached' and coloured states. Upon potential switching by CV, the films were oxidised to the oxy-hydroxide form with a uniform brown-grey colouration being formed.
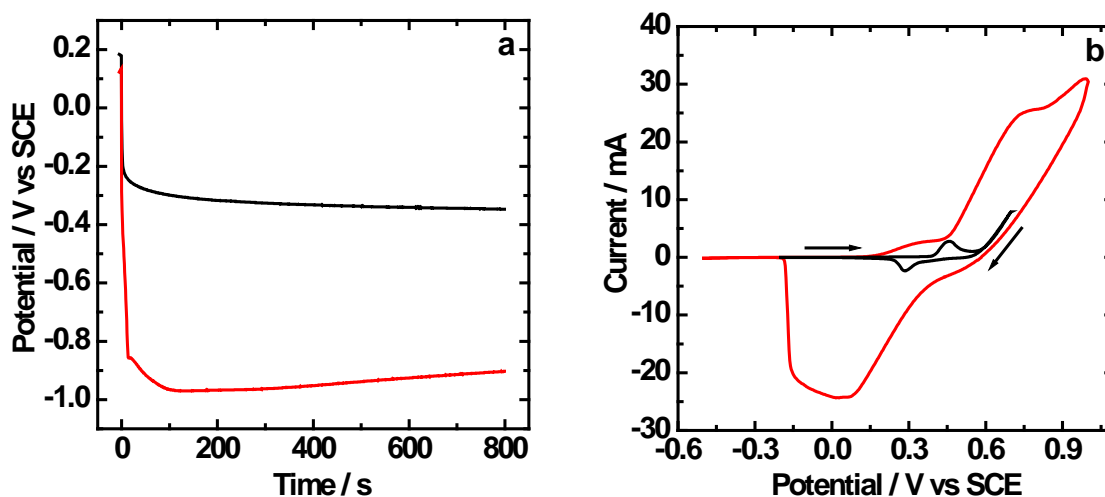
Figure 7.1. Potential-time transients (a) and CVs (b) for hydrated NiO films prepared by electrochemical cathodic deposition on FTO/glass (electrode surface area = 10 x 7.5 cm) from 0.01 mol dm^{-3} nickel nitrate solutions, with an applied current of -0.2 mA for 800 s (——) and -3 mA for 800 s (——). The potential range was -0.20 V → +0.70 V → -0.20 V vs. SCE (-0.2 mA for 800 s) and -0.50 V → +1.00 V → -0.50 V vs. SCE (-3 mA for 800 s) at a scan rate of 10 mV s^{-1}. The arrows in (b) indicate the direction of potential scan.
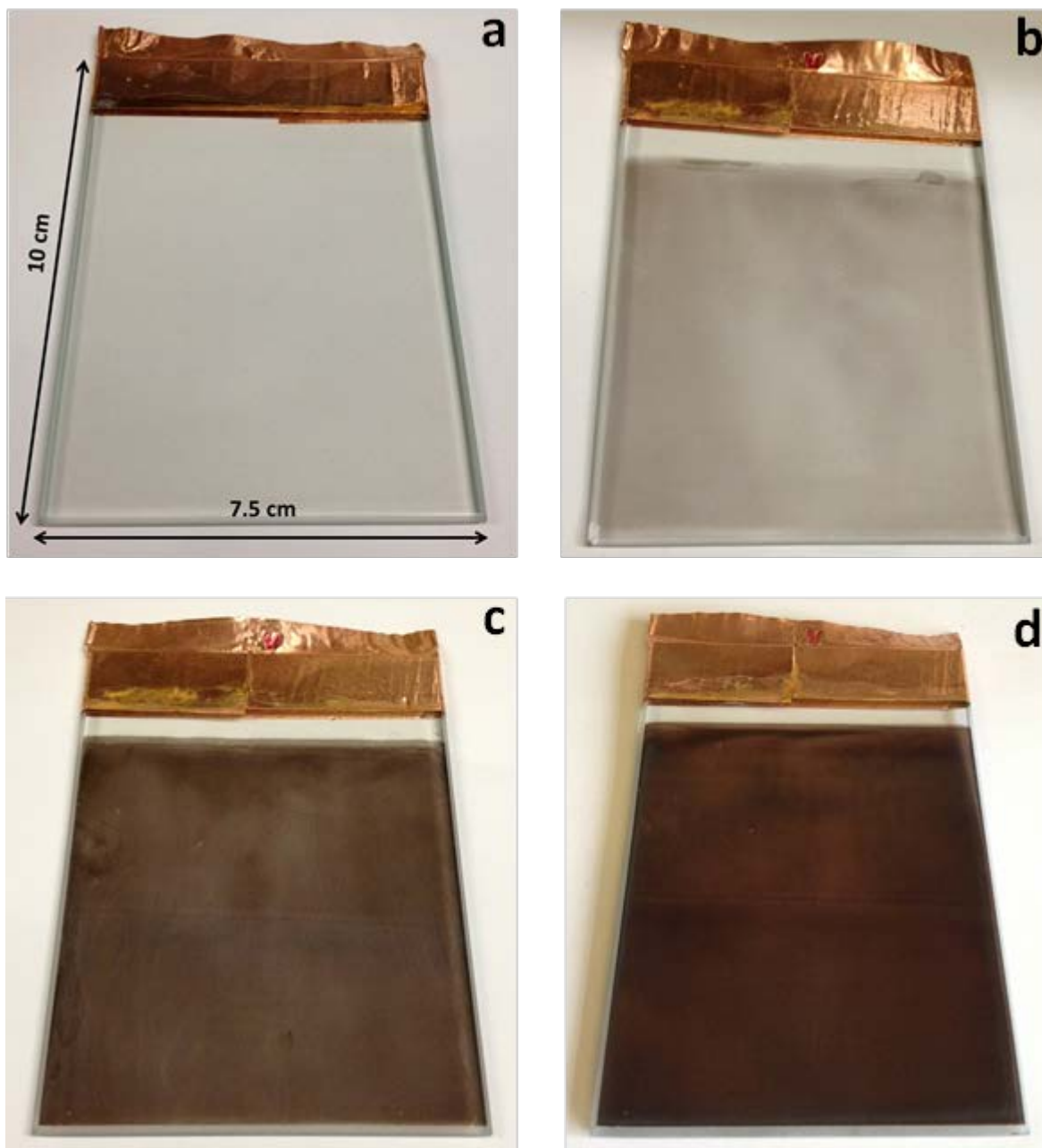
Figure 7.2. Photographs of hydrated NiO film prepared by electrochemical cathodic deposition, (a) as deposited 'bleached' hydrated NiO films (b) NiOOH coloured films prepared at -3 mA for 100 s, (c) NiOOH coloured films prepared at -3 mA for 400 s and (d) NiOOH coloured films prepared at -3 mA for 800 s Coloured films were obtained by cycling in KOH (0.1 mol dm^{-3}) electrolyte (–0.50 to +0.85 V vs. SCE at 10 mV s^{-1}, and then removal at +0.85 V). Each film was deposited on the lower 8 cm length of each 10 cm width FTO/glass).

For large-scale deposition, hydrated NiO films were also co-deposited with metals that were found to enhance the EC properties of the films (chapter 6). The effects of

cobalt and lanthanum as single and combined double additives on the electrodes' properties such as reversibility, switching times, durability and film uniformity were studied. Table 7.2 outlines the experimental results for the different composite films obtained from the respective CVs (figure 7.3), current vs. time (figure 7.4 (a)) and charge vs. time (figure 7.4 (b)) transients. Figures for pure hydrated NiO are included as a reference.

The reversibility of the electrode reaction can be measured by the difference $(E_O - E_R)$ between the oxidation potential (E_O) and the reduction potential (E_R). From the table it can be concluded that the reversibility improves with all three composite films, with cobalt (10%) as an additive showing the best performance. Response time for the colouration (t_c) and bleaching (t_b) process were estimated from the current vs. time and charge vs. time transients and were taken as the time required to achieve a fully coloured film. It can be inferred from the results that for the pure hydrated NiO film the colouration and bleaching processes were about 24.6 and 14.6 s, respectively. With the addition of cobalt (10%), both t_c and t_b were found to increase. However, the addition of single additive (lanthanum (10%)) and bimetallic additives (cobalt (10%) and lanthanum (5%)) yielded a faster response both for the oxidation and reduction processes. Finally, the cycle life or the durability of the deposited films were examined by calculating the percentage drop in charge (C) between the 1st and 50th charge and discharge cycles (figure 7.3). Similar results to those obtained in chapter 6 for the small-scale deposited films were observed. For all three composite films, the drop in charge was found to be less than pure hydrated NiO. A double additive film prepared with cobalt (10%) and lanthanum (5%) still retained 95% of its initial capacity after 50 cycles in KOH (0.1 mol dm^{-3}) electrolyte.

More subjective specifications such as film uniformity and the tone of colour change are also very important attributes for EC films prepared for smart window applications. As during the active coloured state, the window must show a uniform appearance but also with a neutral coloured transmission. Although, it has been observed that co-deposition of hydrated NiO films with other metals show an improved reversibility and EC performance, the films do lack the uniformity of the pure hydrated NiO (figure 7.5).

Table 7.2. Electrochemical properties, switching times and durability data of hydrated NiO film prepared on FTO glass (electrode surface area = 10 x 7.5 cm) with different additives.[a]

additive	E_O / V	E_R / V	E_O / V − E_R / V	t_c/t_b (s)	durability, drop in charge (%)
(Pure hydrated NiO)	0.94	0.02	0.92	24.6 / 14.6	16.4
Co	0.68	-0.09	0.77	33.4 / 16.9	13.1
La	0.77	-0.01	0.78	23.4 / 14.0	5.0
Co and La	0.79	-0.01	0.80	23.4 / 12.0	4.6

[a]E_O = anodic peak potential, E_R = cathodic peak potential, t_c and t_b = switching times for colouration and bleaching.
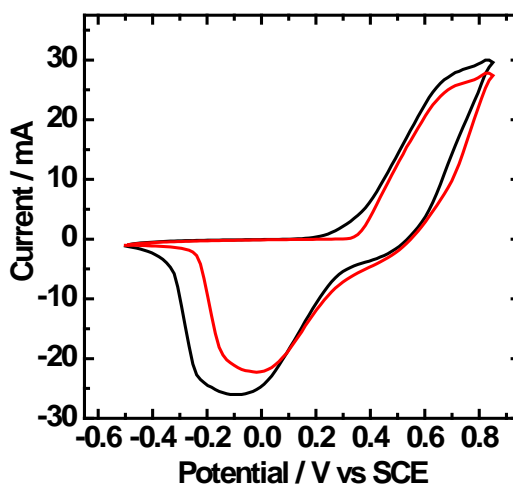
Figure 7.3. CVs for hydrated NiO film for the 1st (——) and 50th (——) cycle. The film was cycled 50 times (−0.50 → +0.85 → −0.50 V vs. SCE) at 10 mV s^{-1}. Hydrated NiO films prepared by electrochemical cathodic deposition on FTO/glass (electrode surface area = 10 x 7.5 cm) at an applied current of -0.2 mA for 800 s.
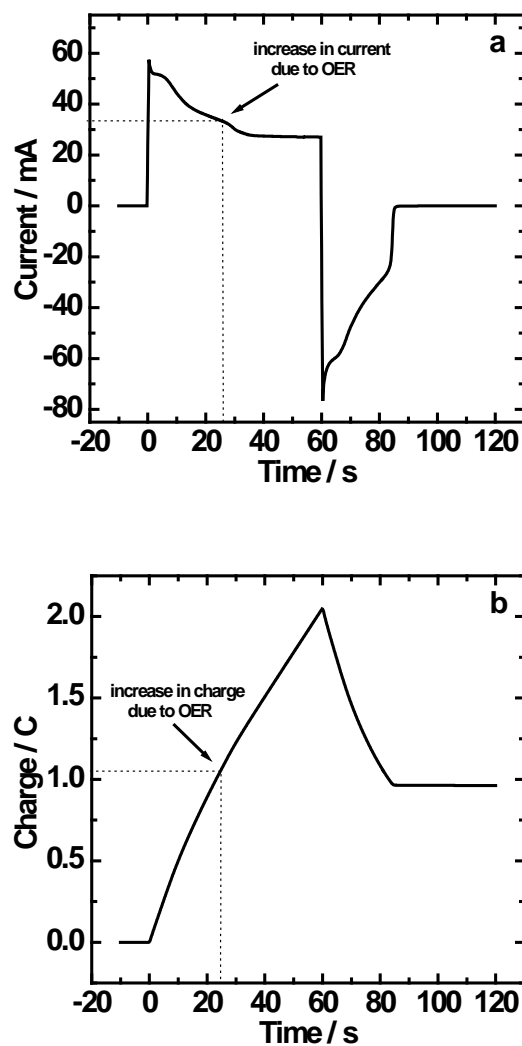
Figure 7.4. Current vs. time (a), charge vs time transients (b) for the reversible switching of hydrated NiO film in aqueous KOH (0.1 mol dm^{-3}) between the transmissive 'bleached' state and the coloured (brown-grey) state. EC switching was conducted by application of potential steps (0.00 V → +0.47 V → −0.10 V) vs. SCE reference electrode.
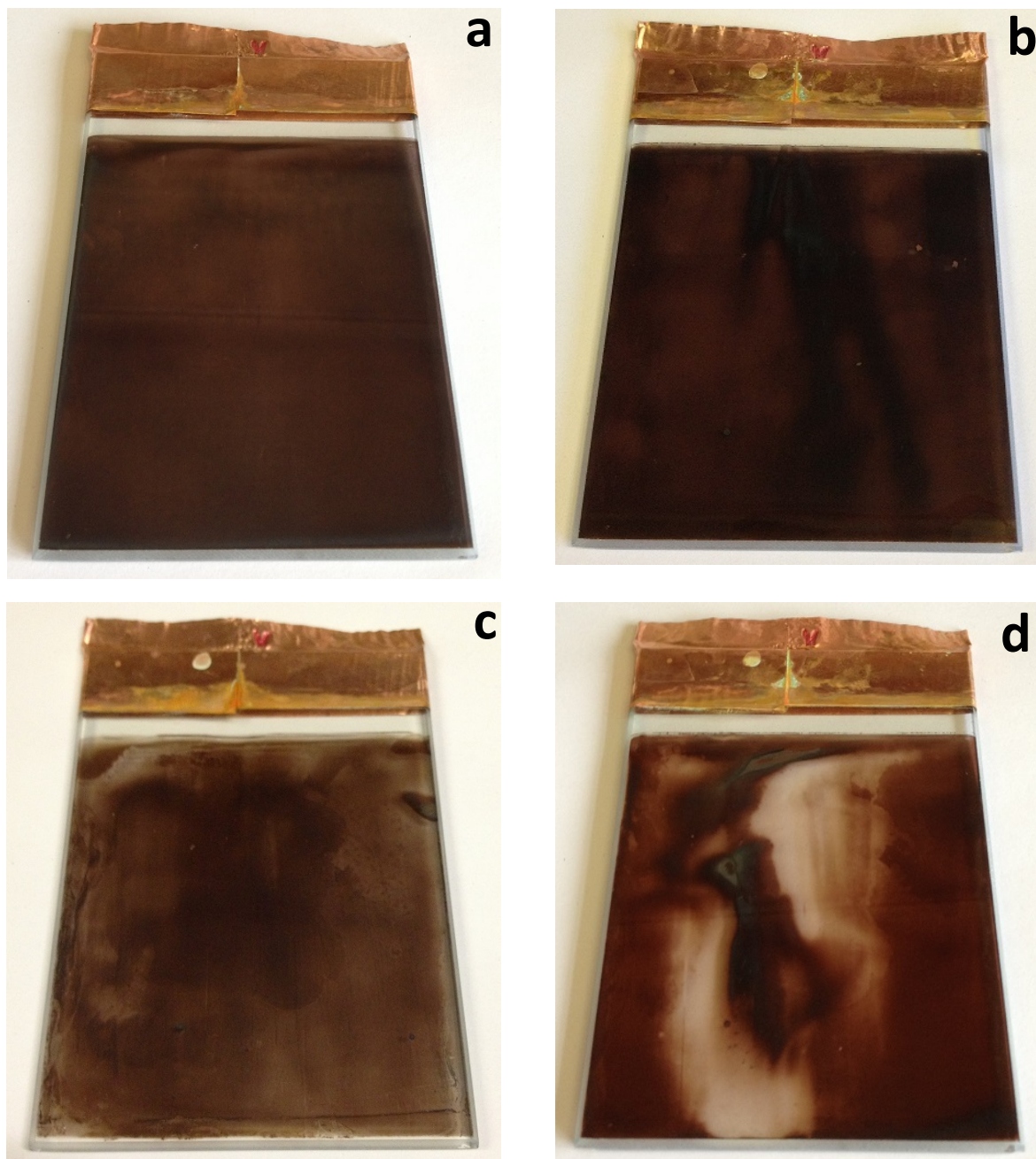
Figure 7.5. Photographs of hydrated NiO film prepared by electrochemical cathodic deposition with different additives, (a) pure NiOOH films prepared at -3 mA for 800 s, (b) Cobalt (10%) co-deposited NiOOH films prepared at -3 mA for 800 s, (c) Lanthanum (10%) co-deposited NiOOH coloured films prepared at -3 mA for 1600 s and (d) cobalt (10%) and lanthanum (5%) co-deposited NiOOH coloured films prepared at -3 mA for 800 s. Coloured films were obtained by cycling in KOH (0.1 mol dm^{-3}) electrolyte (–0.50 to +0.85 V vs. SCE at 10 mV s^{-1}, and then removal at +0.85 V).

7.3. Hydrated NiO film preparation on 30 x 30 cm active area FTO/glass substrate

The emphasis of this work was on scale-up of deposition. Therefore, optimised deposition conditions from small-scale (chapter 4.4 and 6) and relativity large-scale (chapter 7.2) were used to prepare hydrated NiO films on a 30 x 30 cm conducting FTO/glass substrate. The cell arrangement for large-scale deposition was two glass tanks custom made to hold two sheets of 30 x 30 cm FTO/glass, with one acting as a working and the other as a counter electrode (figure 3.8 (chapter 3)). It was crucial during experiment design that in the cell both electrodes were held parallel to one another. This maintained an even current distribution needed to deposit a uniform film across the whole substrate. Generally, due to the size of the substrate, a potential drop down the surface is inevitable and upon switching to the coloured state, the top part of the film was initially coloured, but over time the colouration of the film gradually moved down the substrate to show a complete colour change. In a device formation this problem would not persist as electrical connection will cover the perimeter of the EC device. However, potential drop going to the centre of the substrate would still be possible, as seen in a recent demonstration video of the Gentex smart window for an aircraft.[7]

Figure 7.6 shows photographs of the hydrated NiO films deposited on FTO/glass at different times. From the photographs, it can be noted that the films' uniformity and the neutral colouration over a large-area substrate is stable and its formation is independent of the film thickness. Similarly to the co-deposited hydrated NiO films on the 10 x 7.5 cm FTO/glass substrate, non-uniformity of films were also evident for deposition on 30 x 30 cm FTO/glass substrate, in particular the addition of cadmium (10%) showing the least uniform colour change (figure 7.7).
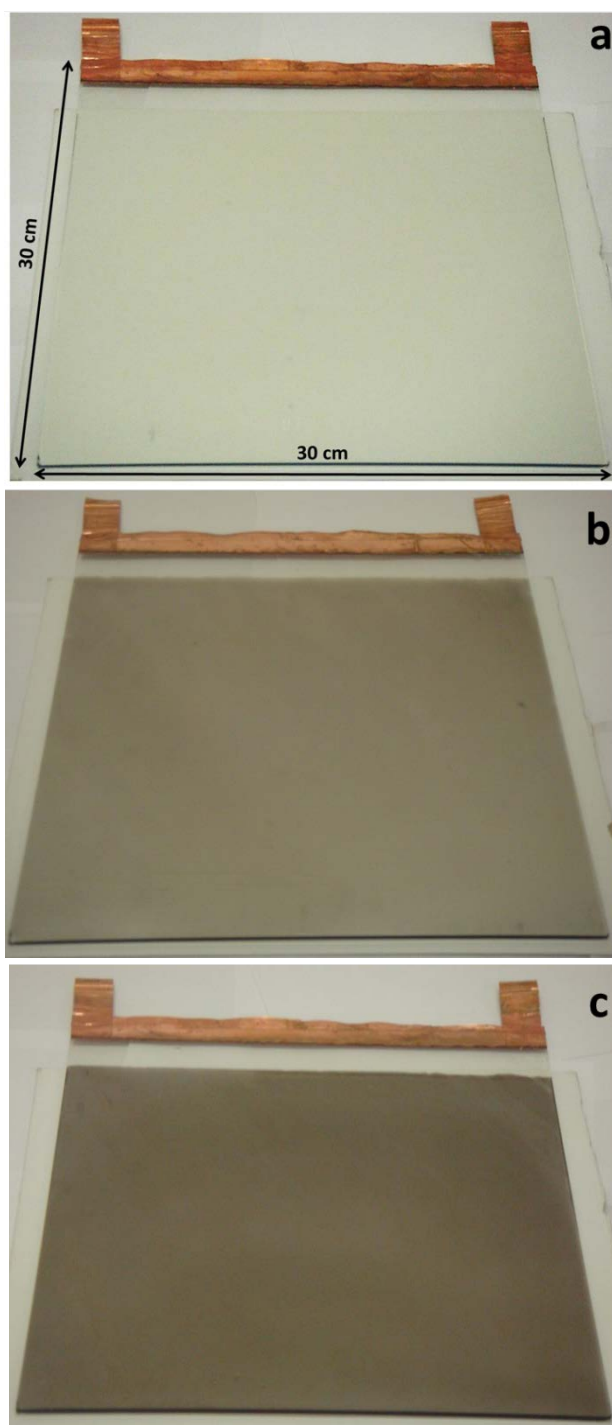
Figure 7.6. Photographs of hydrated NiO films prepared on FTO/glass (electrode surface area = 30 x 30 cm) by electrochemical cathodic deposition at -5 mA for different deposition times, (a) as deposited 'bleached' hydrated NiO films deposited for 1800 s (b) NiOOH coloured films prepared for 1800 s and (c) NiOOH coloured films prepared for 3600 s. Coloured films were obtained by cycling in KOH (0.1 mol dm^{-3}) electrolyte (–0.50 to +0.85 V vs. SCE at 10 mV s^{-1}, and then removal at +0.85 V). Each film was deposited on the lower 25 cm length of each 30 cm width FTO/glass).
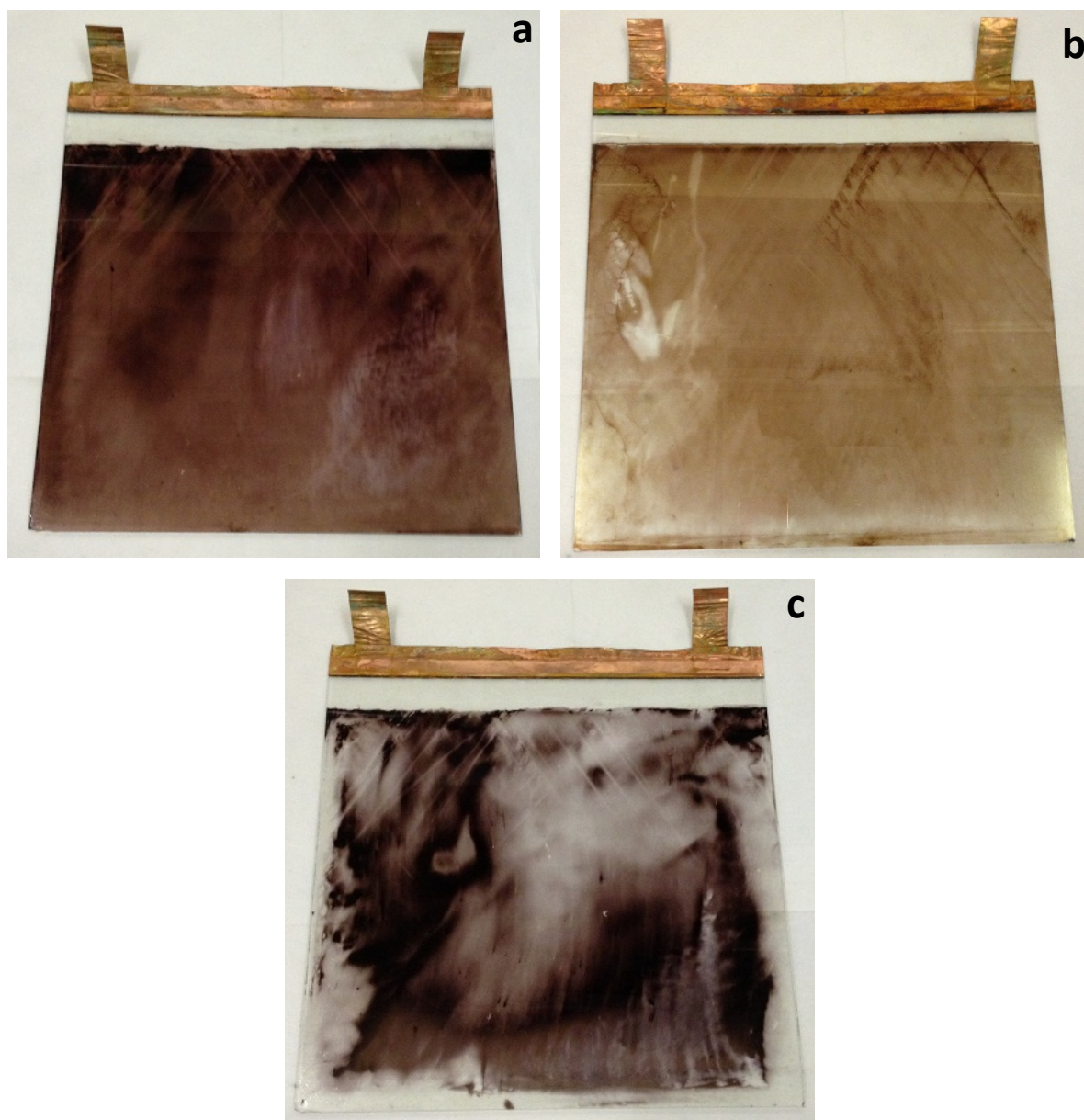
Figure 7.7. Photographs of hydrated NiO film prepared on FTO/glass (electrode surface area = 30 x 30 cm) by an electrochemical cathodic deposition with different additives, (a) cobalt (10%) co-deposited NiOOH films prepared at -5 mA for 3600 s, (b) lanthanum (10%) co-deposited NiOOH coloured films prepared at -5 mA for 3600 s and (c) cadmium (10%) co-deposited NiOOH coloured films prepared at -3 mA for 3600 s. Coloured films were obtained by cycling in KOH (0.1 mol dm^{-3}) electrolyte (–0.50 to +0.85 V vs. SCE at 10 mV s^{-1}, and then removal at +0.85 V).

7. Large-area electrochromic hydrated nickel oxide film deposition

Table 7.3 lists the performance criteria for a pure hydrated NiO film deposited onto 30 x 30 cm FTO/glass substrate. For smart window applications, the expected transmittance specifications for the coloured and the 'bleached' state are between 5 and 10% and 70 and 80%, respectively. In the case of hydrated NiO films, it was observed that with increasing deposition time not only does the transmittance of the coloured film reach as low as 13.9%, the transmittance of the bleached state was still almost 100% (97.1% - chapter 4.4). The films' response times were also calculated and are reported here as the time taken for the absorbance to reach 100% of the total change for both colouration (t_c) and 'bleaching' (t_b) processes with values of 95 s for t_c and 51 s for t_b process. The durability of the film was examined following 1000 charge and discharge cycles, with the hydrated NiO film co-deposited with cobalt (10%) and lanthanum (5%) showing the longest cycle life, with the electrode still retaining 10% of its initial capacity. Finally, the colour of the oxidised films was shown to be neutral brown-grey, which would be ideal in a device formation to complement the blue colouring WO_3.

Please see the accompanying CD which contains video clips of the large-area hydrated NiO film and its reversible switching in aqueous KOH (0.1 mol dm^{-3}) between the transmissive 'bleached' state and the coloured (brown-grey) state.

Table 7.3. Minimum performance criteria for an EC window and for the hydrated NiO film prepared by electrochemical cathodic deposition technique on 30 x 30 cm FTO/glass substrate.

Performance parameter	EC glazing requirement	Hydrated NiO film on FTO/glass
Clear state transmittance	60 to 80%, photopic	97.1%
Coloured state transmittance	5 to 20%, photopic	13.9%
Switching speed	1 to 5 min (>0.1 m^2)	t_c = 95 s and t_b = 51 s (30 x 30 cm)
Cycling lifetime	>50,000 (full cycles)	1000 (full cycles)
Colour	Neutral grey	Neutral brown-grey with the ability to tune colour with additives

7.4. Conclusion

This chapter has demonstrated that optimised deposition conditions from small-scale can be used to successfully deposit uniform EC hydrated NiO films onto large-area FTO/glass substrates. The deposited films exhibit good EC properties that meet or exceed most of the minimum required performance criteria towards smart window applications.

7.5. References

[1] Svensson, J. S. E. M. and Granqvist, C. G. Electrochromic tungsten oxide films for energy efficient windows. *Sol. Energy Mater.*, **11**, 1984, 29-34.

[2] Granqvist, C. G. Oxide electrochromics: Why, how, and whither. *Sol. Energy Mater. Sol. Cells*, **92**, 2008, 203-8.

[3] Granqvist, C. G., Green, S., Jonson, E. K., Marsal, R., Niklasson, G. A., Roos, A., Topalian, Z., Azens, A., Georén, P., Gustavsson, G., Karmhag, R.,

Smulko, J. and Kish L. B. Electrochromic foil-based devices: Optical transmittance and modulation range, effect of ultraviolet irradiation, and quality assessment by 1/f noise. *Thin Solid Films*, **516**, 2008, 5921-26.

[4]   Mathew, J. G. H., Sapers, S. P. Cumbo, M. J., O'Brien, N. A., Sargent, R. B., Raksha, V. P., Lahaderne, R. B. and Hichwa, B. P. Large area electrochromics for architectural applications. *J. Non-Cryst. Solids*, **218**, 1997, 342-6.

[5]   Granqvist, C. G. Oxide electrochromics: An introduction to devices and materials. *Sol. Energy Mater. Sol. Cells*, **99**, 2012, 1-13.

[6]   Baetens, R., Jelle, B. P. and Gustavsen, A. Properties, requirements and possibilities of smart windows for dynamic daylight and solar energy control in buildings: A state-of-the-art review. *Sol. Energy Mater. Sol. Cells*,. **94**, 2010, 87-105.

[7]   http://aviation.bernama.com/news.php?id=502856&lang=en   (accessed   05 April 2013).

8. Conclusion

This thesis contains experimental investigations into the formation of nickel oxide-based ceramic precursor films and the evaluation of their electrochromic (EC) properties towards smart window applications. The motivation for this work was to use optimise deposition condition from small-scale (5 x 0.7 cm) to produce uniform large-area (30 x 30 cm) deposits. Two different deposition techniques were used to immobilise the films onto transparent conducting substrates.

Firstly, a simple, quick and inexpensive electrochemical cathodic deposition technique was used to prepare hydrated NiO films. In chapter 4, various deposition factors were investigated in order to optimise the preparation of EC hydrated NiO films. It was shown that deposition using nickel chloride and sulphate solutions produced non-uniform deposits due to the coexistence of hydrated NiO and metallic nickel. In contrast, deposition using nickel nitrate (0.01 mol dm^{-3}) solution produced films with a uniform porous interconnecting flake-like structure. Furthermore, deposition on FTO/glass at an applied current of -0.2 mA (-0.1 mA cm^{-2}) for 800 s was found to be the optimal film preparation conditions.

Secondly, a variant of the conventional chemical vapour deposition (CVD) process, the aerosol-assisted chemical vapor deposition (AACVD) was used for the preparation of nickel(II) oxide (NiO) thin films. Unlike the electrochemically prepared films, the as-deposited AACVD films exhibited a non-porous octahedral-like grain structure. However, on continuous oxidative voltammetric cycling in aqueous KOH (0.1 mol dm^{-3}) electrolyte, an increase in capacity under the oxidation and reduction process takes place. This so-called activation period gradually changed the morphology to an open porous interconnected flake-like structure, which showed greater EC performance due to increased contact between active material and electrolyte for facilitating hydroxide ion penetration. Furthermore, during this activation period the optical transmittance between the 'bleached' and coloured forms increased from 21.4% to 54.8% when measured at 550 nm for film deposited for 15 min.

8. Conclusion

Having optimised the deposition conditions, the EC properties of NiO-based thin films were investigated in chapter 5. The as-deposited hydrated NiO film prepared by electrochemical cathodic deposition showed excellent transmittance modulation ($\Delta\%T$ = 83.2 at 434 nm), with average colouration efficiency (CE) of 29.6 cm^2 C^{-1} and low response times. However, the cycle life of the film was found to fade drastically only after 50 cycles. NiO films prepared by the AACVD technique on the other hand showed excellent durability of up to 10000 voltammetric cycles. However, the films presented lower transmittance change (53.7% at 550 nm for film deposited at 10 min) between the 'bleached' and coloured state when compared with hydrated NiO films prepared by electrochemical cathodic deposition.

Also in chapter 5, a calculation method based on the integration of experimental spectral power distributions derived from *in-situ* visible region spectra over the CIE 1931 colour-matching functions was used to calculate the colour stimuli of the NiO-based films, and the changes that take place on reversibly switching between the 'bleached' and coloured forms. Films prepared by both deposition techniques gave positive *a** and *b** values to produce orange. However, in combination with low *L** values, the films were perceived as brown. Moreover, NiO-based thin films prepared by three different deposition techniques were tested in order to compare their electrochemical, *in-situ* absorbance and chromaticity data. Results showed that for hydrated NiO films prepared by electrochemical cathodic deposition and by layer-by-layer (LbL) technique, the current responses appeared to be biphasic, an effect which is said to involve two mechanisms with different time courses. The optical properties for the oxidised states also presented a slight difference in the tone of the colour change with the *x-y* coordinates producing a different shape for the colour tracks. The underlying reasons for the different properties of the films prepared on FTO/ITO/glass substrates by the three methods relate to the chemical identity and spectroelectrochemical properties of the different materials. In the case of the AACVD films, their EC and colorimetric properties are due to the presence of NiO. Whereas, for the electrochemical cathodic and LbL deposition techniques the active material is hydrated NiO (Ni(OH)$_2$).

The effect of single and bimetallic additives on the electrochemical, EC and colour-tuning properties of hydrated NiO film was described in chapter 6. Electrochemical

8. Conclusion

studies revealed that films prepared with cobalt (10%) as an additive increased the conductivity of the film thereby shifting the Ni(II)/Ni(III) redox process to less positive potentials and avoiding the OER. Additionally, the incorporation of a second additive further increased the durability by reducing the expansion or contraction of the nickel and hydroxide layers during redox cycling. In this way, the displacement of the redox peaks is avoided and the formation of the γ-phase is reduced. In particular the combination of cobalt (10%) with lanthanum (5%) was found to be the optimal composition for preparing hydrated NiO films with improved film durability. Finally, the effect of additives on fine-tuning the colour states was investigated using the CIE 1931 %Y_L *xy* and CIELAB *L*a*b** chromaticity coordinates, with the addition of cobalt producing a reddish-brown tone and the addition of cadmium producing a brown-black coloured film upon oxidation.

Finally, chapter 7 demonstrated that optimised deposition conditions from small-scale can be used to successfully deposit uniform EC hydrated NiO films onto large-area FTO/glass substrates. The EC response of the large-area films was found to meet or exceed most of the minimum required performance criteria towards smart window applications.

The basis for some interesting further research may involve preparing a two layered NiO-based film. First layer, using the electrochemical cathodic deposition and the second layer, using the AACVD technique. This could result in utilising the advantages of both deposition methods, thereby, producing films with high transmittance modulation and increased durability. Also the addition of metal ions as additives for films prepared via AACVD technique may further enhance the films already promising EC properties.

A. Chromaticity coordinates (CIE 1931 %Y_L xy and CIELAB $L*a*b*$)

This appendix contains the complete results for the calculation of the CIE chromaticity coordinates and luminance data during dynamic colour switching between the 'bleached' (transmissive) and coloured (brown-grey) redox states of hydrated NiO films co-deposited with different additives. The films were prepared via an electrochemical cathodic deposition method on fluorine-doped tin oxide (SnO$_2$:F, FTO) on glass.

Table A.1. Chromaticity coordinates (CIE 1931 %Y_L xy and CIELAB $L*a*b*$) for a hydrated NiO film co-deposited with cerium on FTO/glass[a]

time (s)	x	y	%Y_L	$L*$	$a*$	$b*$
1	0.332	0.347	100.0	100	-0.1	-0.4
2	0.337	0.349	97.3	99	1.4	1.7
3	0.345	0.351	80.9	92	3.6	3.8
4	0.352	0.354	68.0	86	5.5	5.8
5	0.359	0.356	58.7	81	6.9	7.6
6	0.365	0.359	51.6	77	8.1	9.1
7	0.371	0.361	45.8	73	9.2	10.4
8	0.377	0.362	40.9	70	10.1	11.6
9	0.382	0.364	36.9	67	11.0	12.4
10	0.386	0.365	33.8	65	11.6	13.0
11	0.389	0.365	31.4	63	12.1	13.4
12	0.391	0.365	29.8	61	12.5	13.5
13	0.393	0.365	28.1	60	12.9	13.5
14	0.393	0.365	27.9	60	12.9	13.4
15	0.393	0.365	27.7	60	12.9	13.4
16	0.393	0.365	27.6	59	13.0	13.4

A. Chromaticity coordinates (CIE 1931 %Y_L xy and CIELAB $L^*a^*b^*$)

17	0.394	0.365	27.5	59	13.0	13.4
18	0.394	0.365	27.5	59	13.0	13.4
19	0.394	0.365	27.4	59	13.0	13.4
20	0.394	0.365	28.0	60	13.0	13.6
21	0.382	0.365	38.6	68	10.9	13.1
22	0.370	0.361	49.4	76	8.7	10.6
23	0.362	0.359	56.4	80	7.3	9.0
24	0.358	0.357	61.5	83	6.4	7.9
25	0.355	0.356	65.7	85	5.7	7.0
26	0.350	0.354	72.8	88	4.7	5.7
27	0.348	0.353	75.9	90	4.2	5.2
28	0.347	0.353	78.7	91	3.8	4.7
29	0.345	0.352	81.3	92	3.4	4.3
30	0.344	0.352	83.8	93	3.1	3.9
31	0.343	0.352	86.1	94	2.8	3.6
32	0.342	0.351	88.2	95	2.6	3.2
33	0.341	0.351	90.1	96	2.3	2.9
34	0.340	0.351	92.0	97	2.1	2.7
35	0.339	0.350	93.7	97	1.9	2.4
36	0.339	0.350	95.2	98	1.7	2.2
37	0.338	0.350	96.7	99	1.5	2.0
38	0.338	0.349	98.0	99	1.4	1.8
39	0.337	0.349	99.2	100	1.2	1.6
40	0.337	0.349	100.0	100	1.1	1.5

[a]Films were switched in aqueous KOH (0.1 mol dm^{-3}) between the 'bleached' and coloured states by application of potential steps (−0.30 V → +0.45 V for 20 s and +0.45 V → −0.30 V for 20 s) vs. the Ag wire pseudo reference electrode.

A. Chromaticity coordinates (CIE 1931 %Y_L xy and CIELAB $L^*a^*b^*$)

Table A.2. Chromaticity coordinates (CIE 1931 %Y_L xy and CIELAB $L^*a^*b^*$) for a hydrated NiO film co-deposited with cadmium on FTO/glass[a]

time (s)	x	y	%Y_L	L^*	a^*	b^*
1	0.339	0.349	80.4	92	2.0	1.8
2	0.346	0.350	64.3	84	4.5	3.2
3	0.354	0.351	50.8	77	6.8	4.6
4	0.361	0.352	40.9	70	8.5	5.7
5	0.366	0.352	34.5	65	9.6	6.4
6	0.369	0.353	31.0	62	10.1	6.8
7	0.371	0.353	29.3	61	10.4	6.9
8	0.371	0.352	28.5	60	10.5	6.8
9	0.371	0.352	27.8	60	10.6	6.7
10	0.371	0.351	27.1	59	10.7	6.5
11	0.371	0.351	26.2	58	10.7	6.2
12	0.371	0.351	25.6	58	10.7	6.1
13	0.371	0.350	25.2	57	10.7	6.0
14	0.371	0.350	24.9	57	10.7	6.0
15	0.371	0.350	24.6	57	10.8	6.1
16	0.372	0.350	24.4	56	10.8	6.1
17	0.372	0.350	24.2	56	10.9	6.1
18	0.372	0.351	24.0	56	10.9	6.2
19	0.373	0.351	23.9	56	11.0	6.2
20	0.374	0.353	26.4	58	11.0	7.1
21	0.370	0.354	31.8	63	10.1	7.3
22	0.364	0.354	38.4	68	8.7	6.9
23	0.358	0.354	46.9	74	7.2	6.2
24	0.352	0.353	56.4	80	5.6	5.4
25	0.348	0.353	65.7	85	4.1	4.6
26	0.343	0.352	74.6	89	2.8	3.6

A. Chromaticity coordinates (CIE 1931 %Y_L xy and CIELAB $L^*a^*b^*$)

27	0.339	0.351	82.6	93	1.6	2.5
28	0.336	0.349	88.9	96	0.8	1.5
29	0.335	0.349	93.1	97	0.3	0.9
30	0.334	0.348	95.6	98	0.1	0.5
31	0.333	0.348	97.0	99	0.0	0.3
32	0.333	0.348	97.7	99	-0.1	0.2
33	0.333	0.348	98.2	99	-0.1	0.1
34	0.333	0.348	98.5	99	-0.1	0.1
35	0.333	0.348	98.7	100	-0.1	0.1
36	0.333	0.348	98.9	100	-0.1	0.1
37	0.333	0.348	99.0	100	-0.1	0.1
38	0.333	0.348	99.1	100	-0.1	0.1
39	0.333	0.348	99.2	100	-0.2	0.1
40	0.333	0.348	99.2	100	-0.1	0.0

[a]Films were switched in aqueous KOH (0.1 mol dm^{-3}) between the 'bleached' and coloured states by application of potential steps (–0.20 V $\rightarrow$ +0.48 V for 20 s and +0.48 V $\rightarrow$ –0.20 V for 20 s) vs. the Ag wire pseudo reference electrode.

A. Chromaticity coordinates (CIE 1931 %Y_L xy and CIELAB $L^*a^*b^*$)

Table A.3. Chromaticity coordinates (CIE 1931 %Y_L xy and CIELAB $L^*a^*b^*$) for a hydrated NiO film co-deposited with cobalt on FTO/glass[a]

time (s)	x	y	%Y_L	L^*	a^*	b^*
1	0.345	0.353	81.5	92	2.9	4.6
2	0.357	0.355	64.7	84	7.0	7.1
3	0.369	0.355	49.9	76	10.9	8.6
4	0.381	0.355	39.1	69	13.9	10.1
5	0.393	0.356	31.7	63	16.0	12.0
6	0.403	0.357	26.6	59	18.0	12.9
7	0.413	0.359	22.6	55	19.3	14.1
8	0.424	0.360	19.2	51	21.0	15.0
9	0.435	0.361	16.2	47	21.7	16.4
10	0.446	0.362	13.8	44	22.6	17.3
11	0.452	0.361	12.2	42	23.1	17.4
12	0.455	0.360	11.2	40	23.0	17.0
13	0.457	0.359	10.5	39	23.5	16.7
14	0.458	0.358	10.0	38	23.0	16.0
15	0.458	0.358	9.7	37	23.0	16.0
16	0.458	0.357	9.7	37	23.4	16.1
17	0.458	0.358	9.6	37	23.4	16.1
18	0.458	0.358	9.6	37	23.3	16.1
19	0.458	0.358	9.6	37	23.4	16.1
20	0.459	0.359	10.4	39	23.7	17.1
21	0.447	0.362	13.8	44	22.8	17.5
22	0.429	0.360	17.6	49	21.3	15.7
23	0.412	0.357	22.5	55	19.5	13.6
24	0.399	0.356	27.9	60	17.6	11.9
25	0.387	0.355	34.3	65	15.6	10.6
26	0.377	0.355	42.5	71	13.1	9.5

A. Chromaticity coordinates (CIE 1931 %Y_L xy and CIELAB $L^*a^*b^*$)

27	0.365	0.355	54.1	79	10.0	8.2
28	0.352	0.354	70.8	87	5.7	6.0
29	0.344	0.353	82.1	93	3.0	4.0
30	0.342	0.353	85.6	94	2.1	4.0
31	0.341	0.353	87.8	95	1.6	3.7
32	0.340	0.352	89.1	96	1.3	3.5
33	0.340	0.352	90.0	96	1.0	3.0
34	0.339	0.352	90.7	96	1.0	3.2
35	0.339	0.352	91.3	97	0.8	3.1
36	0.339	0.352	91.8	97	0.7	3.0
37	0.339	0.352	92.2	97	0.7	2.9
38	0.338	0.352	92.6	97	0.6	2.9
39	0.338	0.352	92.9	97	0.5	2.8
40	0.338	0.352	93.2	97	0.4	2.7

[a]Films were switched in aqueous KOH (0.1 mol dm^{-3}) between the 'bleached' and coloured states by application of potential steps (–0.20 V $\rightarrow$ +0.46 V for 20 s and +0.46 V $\rightarrow$ –0.20 V for 20 s) vs. the Ag wire pseudo reference electrode.

A. Chromaticity coordinates (CIE 1931 %Y_L xy and CIELAB $L^*a^*b^*$)

Table A.4. Chromaticity coordinates (CIE 1931 %Y_L xy and CIELAB $L^*a^*b^*$) for a hydrated NiO film co-deposited with copper on FTO/glass[a]

time (s)	x	y	%Y_L	L^*	a^*	b^*
1	0.339	0.349	86.5	95	2.1	2.0
2	0.348	0.353	73.7	89	4.3	4.8
3	0.356	0.356	61.7	83	6.2	7.0
4	0.363	0.358	51.4	77	7.9	8.5
5	0.370	0.359	42.5	71	9.3	9.8
6	0.378	0.361	34.7	66	10.6	10.9
7	0.387	0.363	27.7	60	11.8	11.8
8	0.393	0.363	22.6	55	12.6	12.2
9	0.395	0.362	19.7	52	12.9	11.8
10	0.396	0.361	18.3	50	13.0	11.2
11	0.395	0.360	17.2	49	12.9	10.7
12	0.395	0.359	16.1	47	12.9	10.0
13	0.394	0.357	15.2	46	12.7	9.4
14	0.393	0.357	14.7	45	12.7	9.2
15	0.393	0.356	14.5	45	12.7	9.0
16	0.393	0.356	14.3	45	12.6	8.9
17	0.393	0.356	14.2	45	12.6	8.9
18	0.393	0.356	14.2	44	12.6	8.9
19	0.393	0.356	14.1	44	12.6	8.8
20	0.395	0.357	14.9	45	12.9	9.5
21	0.396	0.362	18.7	50	13.0	11.4
22	0.393	0.364	23.2	55	12.4	12.4
23	0.387	0.365	28.8	61	11.3	12.6
24	0.379	0.364	35.9	66	10.0	11.9
25	0.370	0.362	44.3	72	8.5	10.6
26	0.362	0.359	54.6	79	6.9	8.9

A. Chromaticity coordinates (CIE 1931 %Y_L xy and CIELAB $L^*a^*b^*$)

27	0.351	0.355	68.5	86	4.8	6.1
28	0.340	0.350	85.6	94	2.2	2.2
29	0.334	0.347	95.0	98	1.0	0.2
30	0.334	0.347	96.7	99	0.9	0.0
31	0.334	0.347	97.0	99	0.9	0.0
32	0.334	0.347	97.3	99	0.9	0.0
33	0.334	0.347	97.4	99	0.9	0.0
34	0.334	0.347	97.4	99	0.9	0.0
35	0.334	0.347	97.4	99	0.9	0.0
36	0.334	0.347	97.4	99	0.9	0.0
37	0.334	0.347	97.4	99	0.9	0.0
38	0.334	0.347	97.4	99	0.9	0.0
39	0.334	0.347	97.4	99	0.9	0.0
40	0.334	0.347	97.4	99	0.9	0.0

[a]Films were switched in aqueous KOH (0.1 mol dm^{-3}) between the 'bleached' and coloured states by application of potential steps (–0.20 V → +0.49 V for 20 s and +0.49 V → –0.20 V for 20 s) vs. the Ag wire pseudo reference electrode.

A. Chromaticity coordinates (CIE 1931 %Y_L xy and CIELAB $L^*a^*b^*$)

Table A.5. Chromaticity coordinates (CIE 1931 %Y_L xy and CIELAB $L^*a^*b^*$) for a hydrated NiO film co-deposited with lanthanum on FTO/glass[a]

time (s)	x	y	%Y_L	L^*	a^*	b^*
1	0.334	0.346	71.3	88	1.2	-0.4
2	0.337	0.346	58.3	81	2.4	0.4
3	0.342	0.347	47.1	74	3.8	1.5
4	0.349	0.349	38.2	68	5.5	3.0
5	0.358	0.351	31.1	63	7.3	4.8
6	0.368	0.354	25.6	58	9.0	6.7
7	0.378	0.357	21.5	54	10.6	8.4
8	0.387	0.359	18.4	50	11.8	9.8
9	0.394	0.360	16.2	47	12.6	10.6
10	0.397	0.360	14.8	46	13.0	10.7
11	0.398	0.359	14.0	44	13.2	10.5
12	0.398	0.359	13.4	44	13.2	10.1
13	0.398	0.358	12.9	43	13.2	9.8
14	0.397	0.357	12.4	42	13.2	9.5
15	0.398	0.357	12.1	42	13.2	9.4
16	0.398	0.356	12.0	41	13.3	9.3
17	0.398	0.356	11.9	41	13.3	9.3
18	0.398	0.356	11.8	41	13.3	9.3
19	0.400	0.359	12.9	43	13.6	10.4
20	0.399	0.361	15.7	47	13.4	11.5
21	0.392	0.361	19.2	51	12.6	11.3
22	0.384	0.361	24.0	56	11.4	10.8
23	0.376	0.359	29.9	62	10.1	9.8
24	0.367	0.358	36.8	67	8.6	8.7
25	0.360	0.356	44.2	73	7.2	7.5
26	0.354	0.355	52.3	78	5.8	6.2

A. Chromaticity coordinates (CIE 1931 %Y_L xy and CIELAB $L^*a^*b^*$)

27	0.348	0.353	61.2	83	4.4	4.7
28	0.343	0.351	70.5	87	3.1	3.2
29	0.339	0.349	79.5	92	2.0	1.8
30	0.335	0.348	87.5	95	1.0	0.6
31	0.333	0.347	93.2	97	0.4	-0.3
32	0.332	0.346	96.3	99	0.1	-0.7
33	0.331	0.346	97.7	99	-0.1	-0.9
34	0.331	0.346	98.5	99	-0.1	-1.0
35	0.331	0.346	99.0	100	-0.1	-1.0
36	0.331	0.346	99.4	100	-0.1	-1.1
37	0.331	0.346	99.6	100	-0.1	-1.1
38	0.331	0.346	99.8	100	-0.1	-1.1
39	0.331	0.346	99.9	100	-0.1	-1.1
40	0.331	0.346	100.0	100	-0.1	-1.1

[a]Films were switched in aqueous KOH (0.1 mol dm^{-3}) between the 'bleached' and coloured states by application of potential steps (–0.30 V → +0.55 V for 20 s and +0.55 V → –0.30 V for 20 s) vs. the Ag wire pseudo reference electrode.

A. Chromaticity coordinates (CIE 1931 %Y_L xy and CIELAB $L*a*b*$)

Table A.6. Chromaticity coordinates (CIE 1931 %Y_L xy and CIELAB $L*a*b*$) for a hydrated NiO film co-deposited with cobalt and cadmium on FTO/glass[a]

time (s)	x	y	%Y_L	$L*$	$a*$	$b*$
1	0.336	0.350	97.1	99	0.1	1.7
2	0.336	0.350	95.2	98	0.4	1.9
3	0.344	0.351	80.2	92	3.4	3.6
4	0.353	0.352	65.3	85	7.0	5.3
5	0.363	0.352	54.0	78	10.1	6.8
6	0.372	0.353	45.5	73	12.6	8.2
7	0.380	0.353	39.0	69	14.5	9.4
8	0.388	0.354	33.7	65	16.1	10.5
9	0.396	0.355	29.5	61	17.3	11.4
10	0.401	0.355	26.6	59	18.1	11.9
11	0.404	0.355	24.8	57	18.5	12.0
12	0.405	0.354	23.5	56	18.8	11.7
13	0.405	0.352	21.9	54	18.9	11.2
14	0.405	0.351	20.9	53	18.9	10.7
15	0.405	0.351	20.5	52	18.9	10.6
16	0.405	0.351	20.4	52	18.9	10.5
17	0.405	0.351	20.3	52	18.9	10.5
18	0.405	0.351	20.2	52	18.9	10.5
19	0.405	0.351	20.2	52	18.9	10.5
20	0.405	0.351	20.2	52	18.9	10.4
21	0.405	0.351	20.2	52	18.9	10.4
22	0.407	0.353	21.6	54	19.2	11.4
23	0.399	0.355	27.9	60	17.6	11.9
24	0.386	0.355	35.4	66	15.2	10.5
25	0.375	0.354	43.4	72	12.9	9.0
26	0.366	0.353	52.3	77	10.6	7.6

A. Chromaticity coordinates (CIE 1931 %Y_L xy and CIELAB $L*a*b*$)

27	0.358	0.353	61.4	83	8.3	6.5
28	0.353	0.353	68.9	86	6.6	5.8
29	0.350	0.353	73.9	89	5.4	5.3
30	0.348	0.353	77.2	90	4.6	4.9
31	0.347	0.352	79.0	91	4.1	4.6
32	0.346	0.352	80.5	92	3.8	4.4
33	0.345	0.352	81.7	92	3.5	4.2
34	0.344	0.352	82.8	93	3.3	4.0
35	0.344	0.352	83.7	93	3.1	3.9
36	0.343	0.352	84.6	94	2.9	3.7
37	0.343	0.352	85.4	94	2.7	3.6
38	0.342	0.352	86.1	94	2.5	3.5
39	0.342	0.352	86.8	95	2.3	3.4
40	0.341	0.351	87.4	95	2.2	3.3

[a]Films were switched in aqueous KOH (0.1 mol dm^{-3}) between the 'bleached' and coloured states by application of potential steps (–0.30 V → +0.43 V for 20 s and +0.43 V → –0.30 V for 20 s) vs. the Ag wire pseudo reference electrode.

A. Chromaticity coordinates (CIE 1931 $\%Y_L$ xy and CIELAB $L^*a^*b^*$)

Table A.7. Chromaticity coordinates (CIE 1931 $\%Y_L$ xy and CIELAB $L^*a^*b^*$) for a hydrated NiO film co-deposited with cobalt and copper on FTO/glass[a]

time (s)	x	y	$\%Y_L$	L^*	a^*	b^*
1	0.334	0.349	100.0	100	-0.3	1.0
2	0.339	0.351	91.3	97	1.2	2.5
3	0.347	0.353	75.5	90	4.0	4.7
4	0.357	0.355	60.2	82	7.0	7.1
5	0.369	0.358	47.6	75	9.7	9.5
6	0.379	0.360	39.1	69	11.8	11.3
7	0.386	0.361	33.8	65	13.1	12.2
8	0.389	0.361	31.0	63	13.7	12.2
9	0.390	0.360	29.4	61	14.0	12.1
10	0.391	0.360	28.1	60	14.2	11.9
11	0.392	0.359	26.8	59	14.4	11.7
12	0.393	0.359	25.7	58	14.5	11.5
13	0.393	0.358	24.8	57	14.5	11.3
14	0.393	0.358	24.2	56	14.5	11.1
15	0.393	0.357	23.8	56	14.5	10.9
16	0.393	0.357	23.5	56	14.5	10.8
17	0.392	0.357	23.2	55	14.4	10.7
18	0.392	0.357	23.0	55	14.4	10.6
19	0.392	0.357	22.8	55	14.4	10.5
20	0.392	0.357	22.7	55	14.4	10.5
21	0.393	0.357	22.7	55	14.4	10.5
22	0.394	0.360	27.2	59	14.7	12.3
23	0.387	0.360	32.5	64	13.4	11.9
24	0.378	0.359	38.8	69	11.6	10.6
25	0.368	0.357	47.0	74	9.7	8.9
26	0.358	0.355	58.3	81	7.3	7.1

A. Chromaticity coordinates (CIE 1931 %Y_L xy and CIELAB $L*a*b*$)

27	0.348	0.353	72.5	88	4.6	4.9
28	0.341	0.351	86.2	94	2.3	3.2
29	0.338	0.351	93.4	97	1.0	2.5
30	0.336	0.350	97.0	99	0.4	1.9
31	0.336	0.350	97.7	99	0.3	1.8
32	0.336	0.350	98.2	99	0.2	1.7
33	0.336	0.350	98.6	99	0.2	1.6
34	0.335	0.350	98.9	100	0.1	1.5
35	0.335	0.350	99.1	100	0.1	1.5
36	0.335	0.350	99.3	100	0.0	1.4
37	0.335	0.350	99.5	100	0.0	1.4
38	0.335	0.350	99.6	100	0.0	1.4
39	0.335	0.350	99.7	100	0.0	1.4
40	0.335	0.350	99.8	100	0.0	1.3

[a]Films were switched in aqueous KOH (0.1 mol dm^{-3}) between the 'bleached' and coloured states by application of potential steps (–0.30 V → +0.48 V for 20 s and +0.48 V → –0.30 V for 20 s) vs. the Ag wire pseudo reference electrode.

A. Chromaticity coordinates (CIE 1931 %Y_L xy and CIELAB $L^*a^*b^*$)

Table A.8. Chromaticity coordinates (CIE 1931 %Y_L xy and CIELAB $L^*a^*b^*$) for a hydrated NiO film co-deposited with cobalt and lanthanum on FTO/glass[a]

time (s)	x	y	%Y_L	L^*	a^*	b^*
1	0.333	0.347	99.5	100	0.0	0.0
2	0.352	0.356	77.5	91	4.6	7.1
3	0.363	0.359	65.1	85	7.7	9.9
4	0.375	0.362	53.9	78	10.8	12.2
5	0.387	0.363	44.2	72	13.8	14.3
6	0.401	0.365	35.9	66	16.4	16.2
7	0.415	0.367	29.1	61	18.8	18.0
8	0.426	0.368	24.5	57	20.4	19.3
9	0.430	0.368	22.9	55	21.0	19.5
10	0.432	0.368	21.8	54	21.4	19.4
11	0.434	0.366	20.4	52	21.6	19.0
12	0.435	0.366	19.7	52	21.7	18.6
13	0.435	0.366	19.5	51	21.7	18.6
14	0.435	0.366	19.4	51	21.7	18.5
15	0.435	0.365	19.4	51	21.7	18.5
16	0.435	0.366	19.3	51	21.7	18.5
17	0.435	0.366	19.3	51	21.7	18.6
18	0.435	0.366	19.3	51	21.7	18.5
19	0.435	0.366	19.3	51	21.7	18.5
20	0.436	0.367	20.3	52	21.9	19.2
21	0.424	0.369	25.8	58	20.0	19.2
22	0.411	0.367	31.2	63	17.9	17.8
23	0.396	0.366	39.0	69	15.2	16.2
24	0.383	0.364	48.6	75	12.3	14.1
25	0.369	0.362	60.8	82	8.9	11.5
26	0.352	0.357	78.6	91	4.5	7.3

A. Chromaticity coordinates (CIE 1931 %Y_L xy and CIELAB $L^*a^*b^*$)

27	0.346	0.355	86.6	95	2.7	5.6
28	0.343	0.354	90.8	96	1.8	4.5
29	0.341	0.353	93.0	97	1.4	3.9
30	0.340	0.353	94.4	98	1.1	3.5
31	0.339	0.352	95.5	98	0.8	3.2
32	0.338	0.352	96.4	99	0.6	3.0
33	0.337	0.351	97.8	99	0.4	2.6
34	0.337	0.351	98.3	99	0.3	2.4
35	0.337	0.351	98.7	99	0.3	2.3
36	0.337	0.351	99.1	100	0.2	2.2
37	0.336	0.351	99.3	100	0.1	2.1
38	0.336	0.351	99.6	100	0.1	2.0
39	0.336	0.351	99.8	100	0.0	1.9
40	0.336	0.350	100.0	100	0.0	1.9

[a]Films were switched in aqueous KOH (0.1 mol dm^{-3}) between the 'bleached' and coloured states by application of potential steps (-0.30 V $\rightarrow$ $+0.43$ V for 20 s and $+0.43$ V $\rightarrow$ -0.30 V for 20 s) vs. the Ag wire pseudo reference electrode.

B. Conferences, lectures and professional development

Conferences

Smart materials for smart buildings, Materials KTN, BRE Watford, November 2008.

The Institute of Materials Finishing AGM, Birmingham, November 2008.

MEG (Midlands Electrochemistry Group), Nottingham University, Nottingham, April 2009.

Research day, Department of Materials, Loughborough University, Loughborough, June 2009.

Electrochem 2009, The University of Manchester, Manchester, September 2009.

MEG (Midlands Electrochemistry Group), Leicester University, Leicester, April 2010.

Future technologies, applications and opportunities for surface engineering, Derby, June 2010.

Research day, Department of Materials, Loughborough University, Loughborough, June 2010

Electrochem 2010, University of Wolverhampton, Wolverhampton, September 2010.

MEG (Midlands Electrochemistry Group), University of Warwick, Warwick, May 2011.

Research day, Department of Materials, Loughborough University, Loughborough, June 2011.

Lectures

Health and safety lecture, Dave Wilson, Loughborough University, October 2008.

Introduction to surface analysis techniques–SEM, John Bates, Loughborough University, November 2008.

Introduction to surface analysis techniques–XRD, Dave Hall, Loughborough University, November 2008.

Guest lecture, Professor Peter Bruce, University of St Andrews, "The materials chemistry and electrochemistry of energy storage", November 2010.

Safety talk–Flammable materials, Anish Patel, Loughborough University, Loughborough, March 2012.

Safety talk–Fire, Professor Paul Thomas, Loughborough University, Loughborough, April 2012.

Safety talk–Cryogenics, Claire Camp, Loughborough University, Loughborough, April 2012.

Safety talk–Electrical hazards, Dr Iain Kirkpatrick, Loughborough University, Loughborough, July 2012.

Safety talk–High pressure/high temperature operations, Tom Smith, Loughborough University, Loughborough, September 2012.

Safety talk–Waste disposal, Nolwenn Derrien, Loughborough University, Loughborough, January 2013.

Guest lecture, Professor Robert Hillman, The University of Leicester, "Characterizing electroactive films on surfaces: from fundamentals to fingerprints", January 2013.

Guest lecture, Professor Mat Mahmut, Nigde University, Turkey, "Recent advances on solid oxide fuel cells and PEM electrolyser", January 2013.

Guest lecture, Dr Siva Bohm, TATA Steel R&D, "Functional coatings development on metals for energy applications", February 2013.

Professional development

Postgraduate research induction, Loughborough University, October 2008.

Teaching skills–Preparing to teach and promote learning part 1, Loughborough University, March 2009.

Networking skills–Attending conferences, Loughborough University, March 2009.

Teaching skills–Preparing to teach and promote learning part 2, Loughborough University, March 2009.

Teaching skills–Supervising practical activities, Loughborough University, March 2009.

SEM training, John Bates, Loughborough University, October 2009.

Introduction to refWorks, Loughborough University, February 2010.

B. Conference, lectures and professional development

Research workshop for undergraduates part 1, Martin White, Loughborough University, November 2010.

Research workshop for undergraduates part 2, Martin White, Loughborough University, February 2011.

XRD training, Dr Caroline Kirk, Loughborough University, November 2011.

SEM training, Dr Keith Yendall, Loughborough University, April 2012.

First aid course, Loughborough University, March 2012.

C. Conference presentations

MEG, Nottingham University, Nottingham, April 2009

'Electrochemical Deposition and Optimization of Nickel Hydroxide Films'

M. Z. Sialvi, R. J. Mortimer and G. D. Wilcox

Presented in the poster session.

Research Day, Department of Materials, Loughborough University, Loughborough, June 2009.

'Electrochemical and Electrostatic Deposition of Nickel Hydroxide and Cobalt Hydroxide Films'

M. Z. Sialvi, R. J. Mortimer and G. D. Wilcox

Oral presentation. **(1st prize)**

MEG, Leicester University, Leicester, April 2010.

'Electrochemical Deposition and Stabilisation of the α-phase of Nickel Hydroxide'

M. Z. Sialvi, R. J. Mortimer and G. D. Wilcox

Oral Presentation.

Research Day, Department of Materials, Loughborough University, Loughborough, June 2010.

'Electrochemical Deposition and Stabilisation of the α-phase of Nickel Hydroxide'

M. Z. Sialvi, R. J. Mortimer and G. D. Wilcox

Presented in the poster session.

Materials Research School Poster Competition, Department of Materials, Loughborough University, Loughborough, August 2010

'Enhanced Nickel Hydroxide Electrochromic Performance for Low Energy Consumption'

M. Z. Sialvi, R. J. Mortimer and G. D. Wilcox

Presented in the poster session. **(1st prize)**

C. Conference presentations

Electrochem 2010, University of Wolverhampton, Wolverhampton, September 2010.

'Enhanced Nickel Hydroxide Electrochromic Performance for Low Energy Consumption'

M. Z. Sialvi, R. J. Mortimer and G. D. Wilcox

Oral Presentation.

MEG, University of Warwick, Warwick, May 2011.

'Enhanced Electrochromic Performance of Nickel Oxide/Hydroxide'

M. Z. Sialvi, R. J. Mortimer and G. D. Wilcox

Presented in the poster session.

Research Day, Department of Materials, Loughborough University, Loughborough, June 2011.

'Enhanced Nickel Hydroxide Electrochromic Performance for Low Energy Consumption'

M. Z. Sialvi, R. J. Mortimer and G. D. Wilcox

Oral presentation.

Research Network Meeting, Department of Chemistry, Loughborough University, Loughborough, April 2012.

'Enhanced Electrochromic Performance of Nickel Oxide/Hydroxide for Energy Efficient Smart Windows'

M. Z. Sialvi, R. J. Mortimer, G. D. Wilcox, K. G. U. Wijayantha and C. A. Kirk

Oral presentation.

D. Publications

- Mortimer, R. M. and Sialvi, M. Z. Electrochem 2010: Electrochemistry and sustainability conference report, *Trans. Inst. Met. Fin.*, **89**, 2011, 10-12.

In this report we make reference to the oral presentation as listed in appendix C (Electrochem 2010, University of Wolverhampton).

- Sialvi, M. Z., Mortimer, R. J., Wilcox, G. D., Teridi, AM., Varley, T. S., Wijayantha, K. G. U. and Kirk, C. A. Electrochromic and colorimetric properties of nickel(II) oxide thin films prepared by aerosol-assisted chemical vapor deposition. *ACS Appl. Mater. Interfaces*, **5**, 2013, 5675−82.

Electrochem 2010: electrochemistry and sustainability

An exciting scientific programme with over 60 lectures and 40 posters on the conference themes of Electrochemical Energy Storage and Conversion, Electrochemical Surface Technology, Bio/electroanalysis and Sensors, Nano/advanced Materials, Environmental Treatment and Recycling, Lab to Market, and a symposium for Postgraduate Students was presented at the 15th Annual International Electrochemistry Conference, Electrochem 2010, held at the University of Wolverhampton ,Telford campus, on Tuesday 14th and Wednesday 15th September 2010. Electrochem 2010 was organised by the Society of Chemical Industry's (SCI) Electrochemical Technology Group and the Electrochemistry and Electroanalytical Groups of the Royal Society of Chemistry (RSC). Although a significant part of the conference was not directly involved in electrochemical processes for coatings, the lessons given on sustainability are relevant to this industry.

On the morning of 14 September, the conference was warmly opened by the Chair of the Scientific Organising Committee, Professor Chike Oduoza from the School of Engineering and the Built Environment of the University of Wolverhampton and Professor Caroline Gipps, Vice Chancellor. The opening plenary talk, 'From volcanoes to urban air quality; extending the range of amperometric gas sensors', by **John Saffell**, Alphasense, covered experimental assessment of amperometric four-electrode electrochemical gas sensors used to detect CO, NO and NO_2 gases from volcanoes, for US navy submarines, and for urban and rural roadside pollution levels. Such sensors are used to detect plumes around Heathrow airport, and are placed on lamposts to detect levels of pollution around Newcastle, Cambridge and Valencia. This plenary talk was followed by three parallel symposia, with selected talks being briefly described below.

Electrochemical energy storage and conversion

The symposium keynote lecture, 'Advances in fuel cell metrology diagnostics, imaging and sensors' was given by **Dan Brett**, University College London. This presentation introduced the role of metrology in the development of fuel cells and reviewed the diagnostics, imaging and sensor technologies being applied to map the inner workings of fuel cells. The lecture further outlined techniques developed by the author and colleagues and work needed to be done to advance fuel cell metrology. The symposium then comprised 11 talks covering aspects of redox flow cells, batteries, nanoscale simulation, tomography of electrochemical devices, water electrolysers, fuel cells, supercapacitors, and photoelectrochemistry. An example of the latter was the talk from **Asif Ali Tahir** (from Upul Wijayantha's group, at Loughborough University), who discussed the use of sunlight to produce hydrogen by splitting water molecules into its constituents. The key emphasis was on the use of nanocrystalline $ZnFe_2O_4$ electrodes as a suitable material for the photoelectrochemical water splitting process. Results indicated that $ZnFe_2O_4$ can be considered as potential candidate material as it fulfils most of the optical, energetic, chemical, economic and environmental requirements.

Bio/electroanalysis and sensors

The symposium keynote lecture, 'Robust individual gold nanowire-based electrode for electrochemistry' was given by **Alan O'Riorden**, University College Cork. The lecture discussed the recent emergence of nanoelectrodes, to include their development using a robust, low-cost approach for fabrication of individual gold nanowires assembled on a silicon chip substrate electrically contacted by interconnection tracks and passivated by an insulating layer. To explore the applicability of these nanowire devices for future electrochemical based sensing applications, pristine nanowire devices were employed for the detection of H_2O_2. A 220±90 pM limit of detection was determined, with a linear calibration range extending over nine orders of magnitude of H_2O_2 (10^{-10}–10^{-2}M). The symposium then comprised seven talks covering aspects of biocompatible microfabricated electrodes, electroanalysis at a junction, liquid chromatographic electrode detectors, catalytic oxygen reduction, localised surface plasmon sensors, biosensors, and membrane studies. The microfabricated electrode systems talk was presented by **Andrew Mount**, University of Edinburgh. He explained that microfabrication technology ensures that each electrode in an array system has accurate and reproducible dimensions with micron scale resolution, which provides a significant enhancement of device performance. **Frank Marken**, University of Bath, described the use of two adjacent platinum disc electrodes in a generator-collector electrode system. Gold electrodeposition is employed to decrease the gap size between the two electrodes down to submicron dimensions. The resulting junction is employed to generate high feedback currents due to fast diffusion within the gap, to measure ion diffusion when a microdroplet of water immiscible liquid is placed into the gap, and to create conditions where a wide range of analytes can be detected with novel pulse voltammetric methods. **Kevin Honeychurch**, University of the West England, described a novel liquid chromatographic dual electrode detection system for the determination of flunitrazepam (rohypnol), lorazepam (ativan) and diazepam (valium) in serum samples.

Lab to market

This new symposium topic gave real insight to attendees who may be interested in developing commercial opportunities from their research.

Graham Cooley, representing ITM Powers PLC, gave the keynote lecture where he described his experiences of commercialising electrochemistry, with focus on three case studies. Regenesys had been a huge and secret energy storage project based on regenerative bromide/polysulphide flow cell technology. The project culminated in a 12 MW 10 h energy storage plant completed in Little Barford in July 2003. Following acquisition from RWE, the plant closed 1 year later! ITM Power is a company that engineers zero carbon hydrogen energy systems, based around water electrolysis, that provide security and independence

from fossil fuels. Metalysis is a University of Cambridge spin-out company where titanium, tantalum and other high value metals are extracted from metal oxides. The theme of spin-out companies was further illustrated by **Nigel Brandon**, Imperial College London, who described the formation of Ceres Power, a company that develops fuel cell technology for use in small scale combined heat and power products for the residential sector and in energy security applications. **Edward Roberts**, University of Manchester, described innovation in water treatment through the spin-out of Arvia Technology, a company formed from a concept initiated by **Nigel Brown**, which led to a collaborative EPSRC project. **Andrew Abbott**, University of Leicester, next gave a detailed description of the development of Scionix, a spin-out company based on metal finishing using eutectic based ionic liquids that are formed by mixing substituted quaternary ammonium salts such as choline chloride with various metal salts or hydrogen bond donors. Advantages of ionic liquids include ease of preparation, insensitivity to liquid and air moisture, good conductivity, negligible vapour pressure and that they are inexpensive. The presentation outlined the possible applications of ionic liquids as the first economically viable alternative to aqueous metal finishing processes, including metal deposition, electropolishing, immersion coatings, and deposition of novel alloys and composites. Other talks in the Lab to Market symposium focused on patenting, exploiting university intellectual property and the role of the technology transfer office, and strategies for recruiting key personnel for a spin-out company. The symposium ended with a question and answer session, with a panel of three Venture Capitalists.

Following a poster presentation session and exhibition from electrochemical instrumentation suppliers, the first day ended with a Gala dinner in Ironbridge.

The second day began with a plenary talk from the Geoffrey Barker medallist, **Patrick Unwin**, University of Warwick. The Geoffrey Barker Medal is awarded by the Electrochemistry Group of the RSC to outstanding UK electrochemists who contribute to the field with important experimental or theoretical

achievements. The research work should be recognised internationally, and seen as strengthening the standing of UK Electrochemistry. The award is named after the inventor of square wave, pulse and radiofrequency polarography. Following the presentation of the medal by Andrew Mount, Chair of the Electrochemistry Group, Patrick Unwin described 'New directions in electrochemical imaging: probes, modes and combinations'. He noted that electrochemical imaging methods have thrived and expanded over the past two decades as a consequence of continued developments in instrumentation, theory and a diversity of applications. These developments have taken electrochemical imaging methods beyond electrochemistry into chemistry in general and its borders with materials science, engineering and the life sciences. He outlined the importance of multifunctional imaging with the use of new types of probes and modes for scanning micropipette contact methods (SMCM), to allow high resolution investigation of electrode and mineral surfaces and resolving surface topography. The importance of combining techniques from earlier work on scanning electrochemical microscopy–atomic force microscopy (SEM-AFM) and SEM with fluorescence confocal laser scanning microscopy (CLSM) was presented. This plenary talk was followed by three parallel symposia, with selected talks being briefly described below.

Electrochemical surface technology

The symposium keynote lecture, 'Colloidal templates for the electrodeposition of structured surfaces', was given by **Philip Bartlett**, University of Southampton. The preparation of structured thin films is accessible by template electrochemical deposition through close packed monolayers of uniform polystyrene colloidal particles assembled on electrode surfaces. Templates can be combined with patterning by conventional photolithography or by double templating approaches to make metal films structured on the submicron scale which demonstrate novel optical, magnetic and semiconducting properties. The symposium then comprised 10 talks covering aspects of electrodeposition from ionic liquids and

conventional baths, surface alloying, and magnetic field effects on copper growth modes. Metal electrodeposition from ionic liquids was a strong theme of several talks. **Karl Ryder**, University of Leicester, and **Swatilekha Ghosh**, Newcastle University, described mechanistic aspects of the electrodeposition of copper composites and alloys from deep eutectic solvents based on chlorine chloride and hydrogen bond donors. With applications towards zinc-polymer batteries, **Emma Smith**, University of Leicester, described the electrolytic deposition and stripping of zinc, likewise, from ionic liquids based on eutectic mixtures.

Nano/advanced materials

Nano/advanced materials is a topic which is heavily researched and has a high number of publications each year due to its vast number of potential applications towards electronics, materials, pharmaceuticals, aerospace and chemical manufacturing. The symposium keynote lecture was given by **James Rusling**, University of Connecticut, who explained the importance of nanomaterials based on microfluidic arrays for multiplexed detection of cancer biomarker proteins. He outlined the advantages of nanomaterials towards the development of ultrasensitive immunosensors for cancer biomarker proteins for prostate and oral cancer detection. The symposium then comprised six talks covering aspects of electrochemistry within lyotropic liquid crystal nanostructures, titanium oxide nanotubes, functionalised metal nanoparticles for oxygen reduction, electrodeposition of nanostructured platinum films, and the electrodeposition of nickel, cobalt and their alloys. **Dmitry Bavykin**, University of Southampton, described the synthesis of titanium oxide nanotubes by hydrothermal and anodising methods. Using these methods, random fibres and tubes of various diameters were produced with applications towards dye sensitised solar cells, catalysis, biomedical implants and lithium batteries. Electrodeposited nanomaterials for surface coatings was another key theme, with **Samina Akbar**, University of Reading, describing the formation of high surface area three-dimensional nanostructured platinum films through self-assembled cubic templates, and

Mosaad Negem and **Tri Widayatno**, Newcastle University, respectively discussing the deposition of nickel, cobalt and their alloys from gluconate baths, and nickel electrodeposition using a newly developed micropatterned transfer process (without photolithography), named EnFACE.

Environment treatment and recycling

The concern for water quality throughout the world has led to a significant research effort towards new water treatment methods that are capable of decontaminating effluents that contain pollutants and the removal of heavy metals from ground water. The symposium keynote lecture was given by **Edward Roberts**, University of Manchester, who described an innovative process for water treatment using adsorption and electrochemical regeneration. As noted above in 'Lab to Market', a university spin-out company, Arvia Technology, has been formed to exploit a process where a graphite based adsorbent is used to electrochemically oxidise and adsorb contaminants and 100% regenerate initial adsorptive capacity. The symposium then comprised five talks covering electrochemical oxidation at boron doped diamond anodes, microbial fuel cell catalysts, electrochemical recovery of nickel and platinum, and the application of bioelectrochemical systems in water treatment.

Postgraduate

The symposium keynote lecture was given by an experienced practitioner from the electroplating industry,

Paul Lansdell, of Kohler Mira, and new President of the Institute of Metal Finishing, who was able to demonstrate to the postgraduate students the importance of surface analysis techniques. His lecture surveyed the instrumental techniques, SEM, TEM, AFM, XRF, RBS, XPS, EMA, AES, SIMS and PRA. He also emphasised that basic techniques such as the use of a magnifying glass and the light microscope still have their use! Next, five postgraduate students, at different stages of their research, had the opportunity to showcase their research to date. **Zeeshan Sialvi**, Loughborough University, described enhanced nickel hydroxide electrochromic performance for low energy consumption. The nickel oxyhydroxide redox system is well known from its application in NiCd batteries. As thin films, it is known to demonstrate electrochromic properties for application in 'smart windows', that have the potential to reduce energy consumption of highly glazed buildings by reducing cooling loads, heating loads, the demand for electric lighting, as well as improving indoor comfort due to less glare and thermal discomfort. **Ann Beresford**, University of Leicester, next described the electrochromic enhancement of latent fingerprints on metal. Spatially selective electrochemical polymerisation of aniline allows the visualisation of the negative image of fingerprints on metallic surfaces. On transfer to a monomer free solution, electrochemical variation of the electrochromic polymer's optical properties allows the optimisation of visual contrast. **Stacey Handy**, University of Wolverhampton,

described an investigation into the use of white bronze (Cu/Sn, with a few percentage of Zn) as a replacement for the nickel layer in the decorative chromium electroplating process. Studies involved linear polarisation and salt spray corrosion testing, surface analysis using SEM and AFM, and the measurement of chromaticity coordinates for colour stimuli quantification. **Edmund Dickinson**, University of Oxford, presented a comprehensive dynamic theory of the free liquid junction potential, with consideration of the evidence of the simulated concentration profiles and electric field in the system. The final talk in the postgraduate symposium, and indeed the conference, was from **Lauren Wallis**, University of Southampton, who described research into new electrode materials for lightweight lead acid batteries. Possible lightweight replacements for lead include electrically conductive, chemically inert materials, such as carbon, conductive ceramics and their composites.

Following this year's successful conference at Telford, Electrochem 2011 will be held at the University of Bath, 5–6 September 2011. **Frank Marken**, University of Bath, is Chair of the Scientific Organising Committee, and planned symposia comprise Nano-Electrocrystallisation, Corrosion, Nano-Carbon in Electrochemistry, Microbial Electrochemistry, CO_2 Conversion, Nano-Electroanalysis, Photovoltaics, Electro-Organic Synthesis, Sustainability, Fundamental Electrochemistry, and Electrochemical Processes in Exotic Media.

R. J. Mortimer and Z. M. Sialvi
Loughborough University

Electrochromic and Colorimetric Properties of Nickel(II) Oxide Thin Films Prepared by Aerosol-Assisted Chemical Vapor Deposition

Muhammad Z. Sialvi,[†,‡] Roger J. Mortimer,*[,†] Geoffrey D. Wilcox,[‡] Asri Mat Teridi,[†] Thomas S. Varley,[§] K. G. Upul Wijayantha,[†] and Caroline A. Kirk[†]

[†]Department of Chemistry and [‡]Department of Materials, Loughborough University, Loughborough, Leicestershire LE11 3TU, United Kingdom

[§]Department of Chemistry, University College London, 20 Gordon Street, London WC1H 0AJ, United Kingdom

S Supporting Information

ABSTRACT: Aerosol-assisted chemical vapor deposition (AACVD) was used for the first time in the preparation of thin-film electrochromic nickel(II) oxide (NiO). The as-deposited films were cubic NiO, with an octahedral-like grain structure, and an optical band gap that decreased from 3.61 to 3.48 eV on increase in film thickness (in the range 500−1000 nm). On oxidative voltammetric cycling in aqueous KOH (0.1 mol dm^{-3}) electrolyte, the morphology gradually changed to

an open porous NiO structure. The electrochromic properties of the films were investigated as a function of film thickness, following 50, 100, and 500 conditioning oxidative voltammetric cycles in aqueous KOH (0.1 mol dm^{-3}). Light modulation of the films increased with the number of conditioning cycles. The maximum coloration efficiency (CE) for the NiO (transmissive light green, the "bleached" state) to NiOOH (deep brown, the colored state) electrochromic process was found to be 56.3 cm^2 C^{-1} (at 450 nm) for films prepared by AACVD for 15 min followed by 100 "bleached"-to-colored conditioning oxidative voltammetric cycles. Electrochromic response times were <10 s and generally longer for the coloration than the bleaching process. The films showed good stability when tested for up to 10 000 color/bleach cycles. Using the CIE (Commission Internationale de l'Eclairage) system of colorimetry the color stimuli of the electrochromic NiO films and the changes that take place on reversibly oxidatively switching to the NiOOH form were calculated from in situ visible spectra recorded under electrochemical control. Reversible changes in the hue and saturation occur on oxidation of the NiO (transmissive light green) form to the NiOOH (deep brown) form, as shown by the track of the CIE 1931 xy chromaticity coordinates. As the NiO film is oxidized, a sharp decrease in luminance was observed. CIELAB $L*a*b*$ coordinates were also used to quantify the electrochromic color states. A combination of a low $L*$ and positive $a*$ and $b*$ values quantified the perceived deep brown colored state.

KEYWORDS: AACVD, nickel(II) oxide, electrochromic, electrochromism, CIE chromaticity coordinates, colorimetry
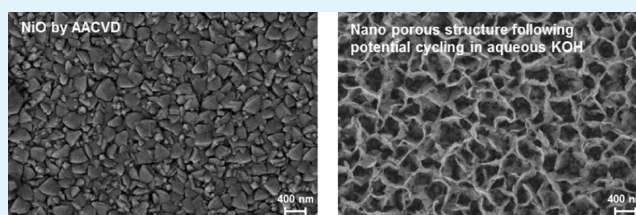
INTRODUCTION

Electrochromic materials have the property of a change, evocation, or bleaching of color, as effected by an applied electrical potential, sufficient to induce an electrochemical redox process.[1,2] Applications of electrochromic materials include "smart" windows for architectural applications,[3] and antiglare car mirrors,[4] based on the modulation of transmitted and reflected visible radiation, respectively. The development of smart windows is the subject of intensive research, as implementation of such technology would lead to a significant reduction in energy consumption in highly glazed buildings by reducing cooling loads, heating loads, and the demand for electric lighting,[3] as well as improving indoor comfort because of less glare and thermal discomfort.[5]

Anodically coloring thin-film nickel(II) oxide (NiO) is often used as a secondary electrochromic material to complement cathodically coloring tungsten(VI) trioxide (WO$_3$) in prototype smart windows.[6,7] Color switching properties of NiO (transmissive light green to deep brown) also make it potentially

useful as a primary electrochromic material, where a "neutral" colored state is desired. Electrochromic NiO thin films have been prepared by sputtering,[8−10] electron-beam deposition,[11] thermal evaporation,[12] electrodeposition,[13] template-assisted electrodeposition,[14] sol−gel,[15,16] chemical bath,[17] hydrothermal deposition,[18] chemical precipitation,[19] hot-filament metal-oxide vapor deposition,[20] and chemical vapor deposition (CVD)[21] techniques. We here report the first study of aerosol-assisted chemical vapor deposition (AACVD) of electrochromic NiO thin films and their characterization using powder X-ray diffraction (XRD), scanning electron microscopy (SEM), and optical absorption. As a variant of conventional CVD, AACVD involves the atomization of precursor solution into submicrometer-sized aerosol droplets. The droplets are then transported into a heating zone, where the solvent is rapidly

evaporated, and the chemical precursors undergo decomposition and/or chemical reaction near or on a heated substrate to form the desired films.[22] When compared to CVD, the AACVD method has several advantages.[23−27] These include a wide choice and availability of precursor for depositing high-quality coatings, the generation of aerosol to simplify the delivery and vaporization of precursor, and the ability to synthesize multicomponent products with precise stoichiometric control. Furthermore, low cost, high deposition rates, and the ability to operate under varied environments at low pressure, or even in open atmosphere, make AACVD an ideal process for scale up toward smart window applications.

The electrochromic properties of the NiO-based films prepared by AACVD are reported following transfer to aqueous KOH (0.1 mol dm^{-3}) electrolyte, with colorimetric properties being quantified using CIE (Commission Internationale de l'Eclairage) principles.[28] In colorimetry, the human eye's sensitivity to visible light is measured and a numerical description of the color stimulus is given, thus providing a more precise way to define color than qualitatively interpreting spectral absorption bands.

EXPERIMENTAL SECTION

Formation of NiO Films by AACVD. Fluorine-doped tin oxide (SnO$_2$:F, FTO) on glass (Pilkington group limited, NSG TEC C15, R_s 14 Ω □$^{-1}$, light transmittance of 84%) was used as the substrate for preparation of NiO films. To obtain uniform adherent films the FTO/glass substrates (each cut to 50 × 7 mm dimensions) were cleaned by rinsing in deionized water, followed by sonication for 10 min each in deionized water, propan-2-ol, acetone and ethanol. Prior to AACVD, the top 20 mm of each FTO/glass substrate was masked with glass, such that the NiO would deposit on the lower 30 × 7 mm area.

Figure 1 shows a schematic diagram of the two chamber configuration AACVD apparatus. Each FTO/glass substrate was
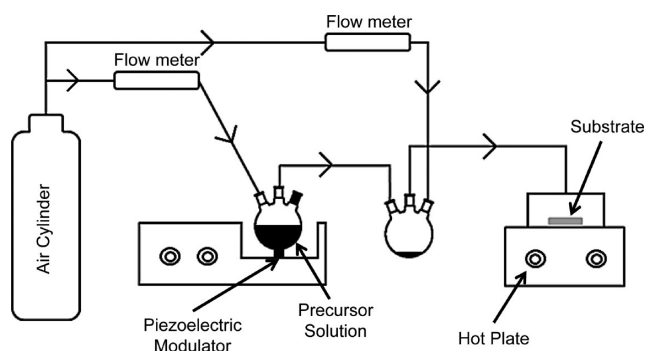

Figure 1. Schematic diagram of the experimental AACVD apparatus.

heated to 450 °C on a temperature controlled hot plate. For preparation of the NiO films, nickel(II) acetylacetonate (0.05 mol dm^{-3}) was used as the source material. Precursor solution was prepared by heating and stirring nickel(II) acetylacetonate and 1 cm^3 of N,N-dimethylaminoethanol (used to improve the solubility of the nickel(II) complex and to enhance volatility) in toluene for 30 min then allowing the solution to cool to room temperature. The precursor solution was then placed above the piezoelectric modulator of an ultrasonic humidifier to atomize the solution into fine aerosol droplets. Using air as a carrier gas, the aerosol droplets were first transferred at a flow rate of 0.21 dm^3 min^{-1} into the first chamber where any large particles were separated and held. A second carrier gas (air) at a flow rate of 2.34 dm^3 min^{-1} was then used to direct the small particles toward the heated substrate, where they underwent evaporation, decomposition and chemical reaction to synthesize the desired films. The flow rate was controlled by a L1X linear flow meter. Films were

deposited for 10, 15, and 20 min and are here abbreviated as NiO(10 min), NiO(15 min), and NiO(20 min), respectively.

XRD and SEM Characterization. Powder XRD data were collected on a Bruker Advance D8 powder X-ray diffractometer in reflection geometry using Cu Kα$_1$ radiation with a Ge monochromator and linear position sensitive detector (PSD) over the two theta range 5−65° 2θ with a step size of 0.014° 2θ and a total collection time of 4 h. Films deposited onto FTO/glass substrates were mounted on perspex sample holders. Shifts in the reflection positions were observed as no internal standard could be added to the sample for calibration of the reflection positions.

A Leo 1530 field-emission gun scanning electron microscopy (SEM) system was used to examine the film morphologies. The deposited films were washed with distilled water, dried in air and then mounted on SEM stubs using conducting silver paint. Samples were coated with a thin layer of gold to improve the conductivity of the films. A Polaron Emitech SC7604 sputter coater was used.

Electrochemical, Spectroelectrochemical, and Color Measurement. A Princeton Applied Research 263A potentiostat was used for electrode potential control. NiO/FTO/glass substrates (with adhesive copper tape at the top for uniform electrical contact), platinized titanium and a saturated calomel (Hg/Hg$_2$Cl$_2$) electrode (SCE) were used as working, counter, and reference electrodes, respectively. A single compartment electrochemical cell was used for all measurements.

In situ visible-region spectra were recorded in transmission mode using a Hewlett-Packard 8452A diode array spectrophotometer. A standard 1 cm path length polystyrene cuvette was used as the spectroelectrochemical cell, with a machined polytetrafluoroethylene lid that allowed each NiO/FTO/glass substrate to be placed parallel to the optical faces. In this case, a silver wire acted as a pseudo reference electrode, with a platinized titanium counter electrode. CIE 1931 xy chromaticity coordinates and luminance data were calculated from the spectral absorbance-wavelength data as described earlier.[29] For simulation of midmorning to midafternoon natural light, the relative power distribution of a D55 constant temperature (5500 K blackbody radiation) standard illuminant was used in the calculations. Chromaticity coordinates were also transformed to L*a*b* coordinates, a uniform color space (CIELAB) defined by the CIE in 1976.[30]

RESULTS AND DISCUSSION

Crystalline Phases Identified, Film Morphology, and Optical Absorption of the As-Deposited NiO Films. Figure 2 shows the powder XRD patterns for NiO films on FTO/glass at different deposition times. The reflections at 37.3, 43.3, and 62.9° 2Θ can be assigned to cubic NiO (International Centre for Diffraction Data (ICDD) Powder Diffraction File (PDF) 47−1049). The NiO phase is stable and its formation is independent of the film thickness. The intensity of the NiO
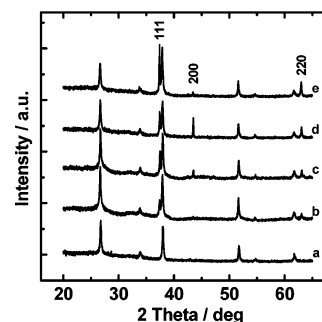

Figure 2. Powder XRD patterns for: (a) FTO/glass, (b) NiO(10 min), (c) NiO(15 min), (d) NiO(20 min), and (e) NiO(20 min) after 3500 oxidative conditioning voltammetric cycles in aqueous KOH (0.1 mol dm^{-3}).

reflections suggests preferred orientation of the films, as the (111) reflection is more intense than the (200). In a randomly oriented sample of NiO, the (200) reflection should be the most intense.

Figure 3 includes photographs for the as-deposited NiO films at the three deposition times, with SEM images shown in
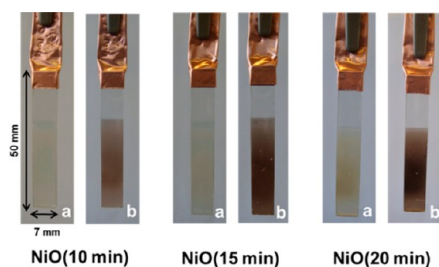

Figure 3. Photographs of (a) as-deposited NiO films and (b) NiOOH films (following 3500 cycles −0.50 to +0.70 V vs SCE at 50 mV s^{-1}, and then removal at +0.70 V). Each film was deposited on the lower 30 mm length of each 7 mm width FTO/glass).

Figure 4. Uniform NiO film covers the FTO/glass substrate surface and exhibits a nanoscale morphology of octahedral-like grains. EDS analysis (see Figures S1 and S2 in the Supporting Information) shows no evidence of the presence of nitrogen from the decomposition of the dimethylaminoethanol. The cross-sectional images (insets in Figure 4) show that film thickness increases with deposition time.
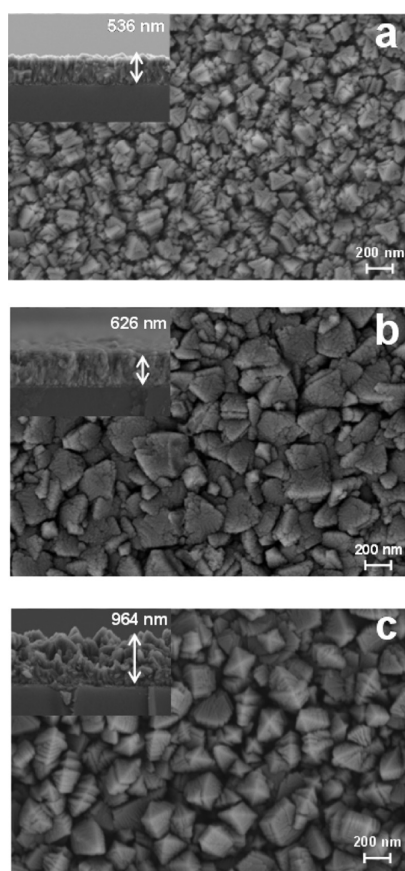

Figure 4. SEM images of NiO films deposited on FTO/glass for three deposition times: (a) NiO(10 min), (b) NiO(15 min), and (c) NiO(20 min). Insets illustrate the cross-sectional images.

Figure S3 in the Supporting Information shows the optical absorption spectra for the as-deposited films recorded in the wavelength range 330−820 nm (3.75−1.51 eV). The data were analyzed using a classical relation for near edge optical absorption in semiconductor materials.[31] Analyzing the variation of $(\alpha h\nu)^2$ vs photon energy ($h\nu$) in eV for NiO films suggests a direct interband transition. The band gaps were 3.61, 3.53, and 3.48 eV for the NiO(10 min), NiO(15 min), and NiO(20 min) films, respectively. These direct band energy values are in good agreement with literature values for NiO thin films prepared by spray pyrolysis using aqueous nickel chloride solutions, with the slight decrease in band gap with increasing film thickness being attributed to increased grain size.[32]

Transformation of NiO Morphology on Voltammetric Cycling in Aqueous KOH (0.1 mol dm^{-3}) Electrolyte. Figure 5 shows an example of cyclic voltammograms (CVs) in
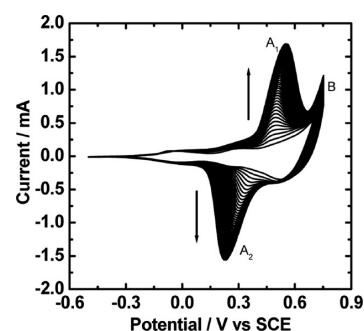

Figure 5. CVs starting from the as-deposited NiO(15 min) film in aqueous KOH (0.1 mol dm^{-3}). The potential range was −0.50 V → +0.70 V → −0.50 V vs SCE for 50 cycles at the scan rate of 50 mV s^{-1}.

aqueous KOH (0.1 mol dm^{-3}) electrolyte commencing with, in this case, an as-deposited NiO(15 min) film. From the plot it can be seen that during the first 50 cycles, a continuous increase in capacity under the oxidation and reduction process takes place. This process is known as the so-called activation period and has been reported for NiO films prepared by sol−gel,[33] and pulsed laser-deposition.[34−36] Furthermore, because of this activation process, on continuous oxidative voltammetric cycling, the octahedral-like grains of as-deposited NiO (Figure 6a), gradually transform to an open porous structure of interconnected flakes (see Figure 6b, following 3500 voltammetric cycles and Figure S4 (Supporting Information), for a NiO(20 min) film following 500 voltammetric cycles). Such a porous interconnecting structure will enhance the intercalation/deintercalation of hydroxide ions (eq 1, a simplified form of the redox process) during voltammetric cycling, thus leading to enhanced electrochromic performance. Similar porous morphologies have been previously reported for NiO-based films prepared by chemical bath deposition methods.[17,37]

$$NiO + OH^- \rightleftharpoons NiOOH + e^- \qquad (1)$$
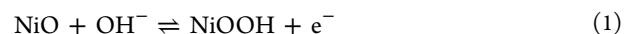
The electrochemically generated porous NiO is electrochromic and oxidatively switches (eq 1) from a "bleached" (transmissive light green) state to the colored nickel oxyhydroxide (NiOOH) (deep brown; for photographs see Figure 3) state. On continuous cycling, this process of morphology transformation is enhanced as the peak currents gradually increase with cycle number (Figure 5).

The two broad redox peaks in the CVs (Figure 5) are associated with the coloration and bleaching process for NiO,[38] one anodic peak (A$_1$), responsible for the oxidation, and one
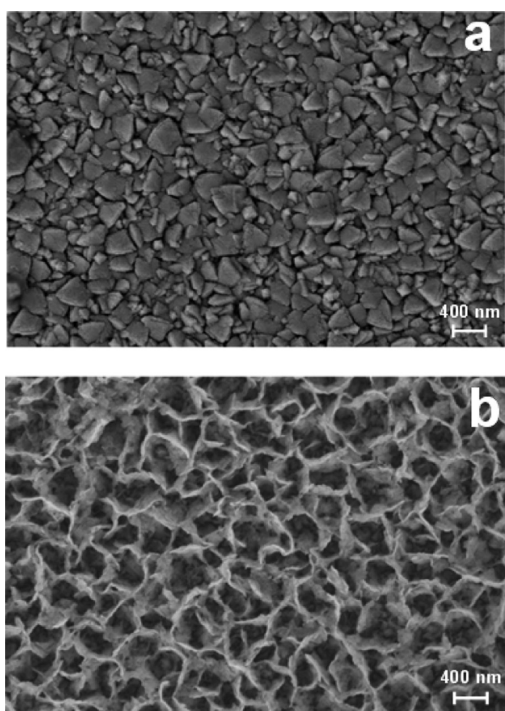
Figure 6. SEM images of NiO(15 min) films deposited on FTO/glass: (a) as-deposited and (b) following 3500 voltammetric cycles in aqueous KOH (0.1 mol dm^{-3}).

cathodic peak (A$_2$), for the reduction process. For all sets of such CVs, an increase in anodic current after +0.60 V (B) is observed that corresponds to the beginning of the oxygen evolution reaction (OER). These CV features are similar to those obtained for NiO thin films initially prepared by electrodeposition[13] and chemical bath deposition[39] techniques. The anodic and cathodic peak currents increase (Figure 7) with
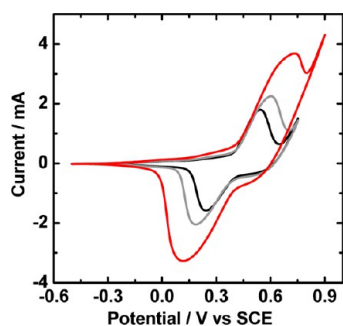

Figure 7. 100th CV (at 50 mV s^{-1}) in aqueous KOH (0.1 mol dm^{-3}) of films prepared from as-deposited NiO(10 min) (black), NiO(15 min) (gray), and NiO(20 min) (red).

an increase in deposition time, with more electroactive material being available. XRD data collected on this sample showed NiO still to be present (Figure 2e), but the relative intensities were now different to the original deposited film, with the (200) reflection especially reduced in intensity. This agrees with the morphology changes shown in the SEM images (Figure 6).

Electrochromic Properties. Table 1 gives in situ spectral data and calculated electrochromic performance parameters for square-wave potential switching between the "bleached" and colored forms after the as-deposited NiO films (prepared by AACVD for 10, 15, and 20 min) had been subject to 50, 100,

and 500 continuous conditioning oxidative voltammetric cycles in aqueous KOH (0.1 mol dm^{-3}) electrolyte. Figure 8 shows example visible region in situ transmittance spectra, in this case for the as-deposited NiO(15 min) film, and in the oxidized NiOOH colored state, following increasing numbers of conditioning cycles. For such a film, it is noted from Table 1, that after 500 cycles the change in optical transmittance between the "bleached" and colored forms increased from 21.4 to 54.8% when measured at 550 nm. This increase in transmittance change between the "bleached" and colored state on continuous cycling is once again due to the gradual change in film morphology from octahedral-like grains to a high surface area of porous interconnecting flakes. Such porous morphology shows greater electrochromic performance because of increased contact between active material and electrolyte for facilitating hydroxide ion penetration.

Figure 9 shows the transmittance spectra of all the as-deposited NiO films in the "bleached" and colored states. Transmittances for both the "bleached" (T_b) and colored (T_c) states decrease as the deposition time increases (Table 1 and Figure 9). On increase of deposition time the extent of color change to the oxidized form increases but the films also appear less transparent in the reduced state (for photographs see Figure 3). The films deposited for 10, 15, and 20 min, followed by 500 voltammetric cycles, each present the largest contrast (Table 1), the transmittance change (~54% at 550 nm) between the "bleached" and colored states, being more than that of the films that were conditioned by only 50 and 100 cycles.

Spectral data were further used to calculate the electrical power consumption of each electrochromic film, expressed as the coloration efficiency (CE = $(\Delta A)_{\lambda/\text{nm}}/Q$), where ($\Delta A$) is the absorbance change between the "bleached" and colored states and Q is the charge density (C cm^{-2}) for each switching process. Each charge density was calculated by integration of the current—time transients, recorded on switching color states. Examples of current—time transients (see Figure S5 in the Supporting Information) and visible region absorbance spectra (Figure 10) are given for the reversible switching between the "bleached" and colored states of one of the films. On oxidation of the transmissive green "bleached" state, the visible region absorbance increases (Figure 10a) as the deep brown colored state forms. On reduction, the deep brown colored state reverts to the transmissive green "bleached" state, with a decrease in the visible region absorbance (Figure 10b). The absorbance change, ΔA, increases with increasing deposition time and the number of "bleached"/colored cycles (Table 1). The highest values (0.72 at 550 nm (Figure 11 and Table 1) and 0.88 at 450 nm (Figure 11)) were obtained for NiO(20 min) recorded at 500 cycles. The CE values (Table 1 and Figure 12) are comparable to those for films obtained by electrodeposition (50 cm^2 C^{1-}),[13] template-assisted electrodeposition (41 cm^2 C^{-1}),[14] CVD (44 cm^2 C^{-1}),[21] spray pyrolysis (30 cm^2 C^{-1}),[40] and vacuum evaporation (32 cm^2 C^{-1}).[41]

Absorbance vs time plots (not included) were used to calculate the response times (Table 1) for all the NiO thin films. Response time is defined as the time required for obtaining partial or total change in absorbance.[1] Here, response times are reported as the time taken for the absorbance to reach 90% of the total absorbance change for both coloration (t_c) and "bleaching" (t_b) process (Table 1). Response times for both coloration and "bleaching" increased with both increasing number of conditioning cycles and film thickness. Generally,

Table 1. In Situ Spectral Data and Electrochromic Performance Parameters on Square Wave Switching (0.00 V → +0.50 V → −0.20 V vs. silver wire) between the "Bleached" and Colored States after the As-Deposited NiO Films had been subject to 50, 100, and 500 Continuous Conditioning Oxidative Voltammetric Cycles in Aqueous KOH (0.1 mol dm-3)[a]

original film source	cycle no.	$\%T_b$	$\%T_c$	$\Delta\%T$	ΔA	CE ($cm^2\ C^{-1}$)	t_c/t_b (s)
NiO(10 min)	50	86.8	66.6	20.0	0.11	39.6	3.2/2.7
NiO(10 min)	100	85.6	55.4	30.2	0.19	40.3	3.4/2.9
NiO(10 min)	500	84.6	30.9	53.7	0.44	34.6	5.6/3.8
NiO(15 min)	50	75.3	53.9	21.4	0.15	43.2	3.2/2.8
NiO(15 min)	100	74.8	46.4	28.4	0.21	45.0	4.1/3.6
NiO(15 min)	500	74.4	19.6	54.8	0.58	39.8	5.7/5.6
NiO(20 min)	50	65.9	33.7	32.2	0.30	41.8	5.0/4.2
NiO(20 min)	100	65.5	24.0	41.5	0.44	41.8	5.0/4.2
NiO(20 min)	500	66.3	12.5	53.8	0.72	32.5	7.4/6.5

[a]T_b = transmittance of "bleached" form, T_c = transmittance of colored form, $\Delta\%T$ = change in transmittance between the "bleached" and colored forms, ΔA = change in absorbance, CE = coloration efficiency, t_c and t_b = switching times for coloration and bleaching. All measurements were taken at the wavelength for maximal absorbance change, 550 nm, which is also the wavelength where the human eye is most sensitive.
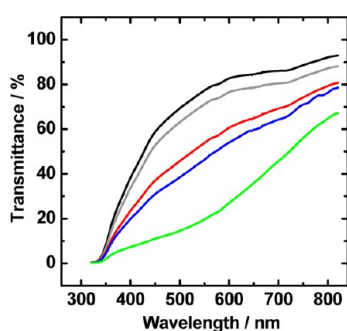

Figure 8. Visible region in situ transmission spectra recorded in the wavelength range 320−820 nm in aqueous KOH (0.1 mol dm^{-3}), showing the formation of the colored state with conditioning oxidative voltammetric cycle number. As-deposited NiO(15 min) film at 0.00 V vs silver wire (black). As-deposited NiO(15 min) film at +0.40 V vs silver wire (gray). NiO(15 min) film at +0.40 V vs silver wire, following 50 voltammetric cycles −0.50 V → +0.70 V → −0.50 V vs SCE (red). NiO(15 min) film at +0.40 V vs silver wire, following 100 voltammetric cycles −0.50 V → +0.70 V → −0.50 V (blue). NiO(15) film at +0.60 V vs silver wire, following 500 voltammetric cycles −0.50 V → +0.70 V → −0.50 V (green). All spectra were corrected for the transmittance of the uncoated FTO/glass substrate in aqueous KOH (0.1 mol dm^{-3}).
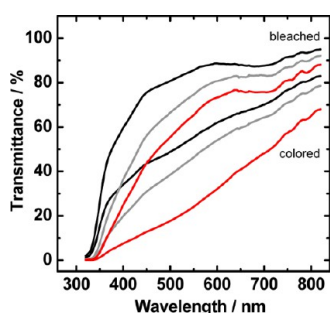

Figure 9. Visible region in situ transmission spectra for the "bleached" and colored states following 100 voltammetric cycles in aqueous KOH (0.1 mol dm^{-3}): NiO(10 min) (black), NiO(15 min) (gray), and NiO(20 min) (red). For each, the upper spectrum is that for the "bleached" form.

response times for the coloration process were longer than those for the "bleaching" process.

Cycle life is one of the key parameters for commercialization as it is an experimental measure of the film durability. Figure 13
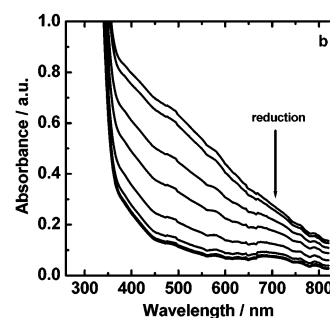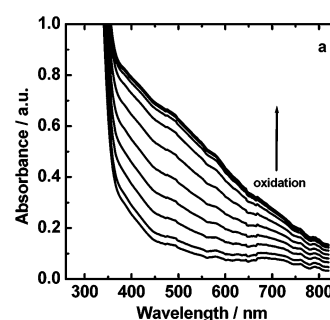

Figure 10. (a, b) Visible-region absorbance spectra (spectra recorded every 0.5 s), for the reversible switching of a NiO(10 min) film in aqueous KOH (0.1 mol dm^{-3}) between the transmissive green "bleached" state and the colored (deep brown) state. Electrochromic switching was conducted by application of potential steps (0.00 V → +0.50 V → −0.20 V) vs silver wire. The arrows indicate the direction of change in absorbance. The NiO(10 min) film had first been conditioned by 500 cycles (−0.50 → +0.70 → −0.50 V vs SCE) at 50 mV s^{-1}.

shows the visible in situ transmittance spectra of the as-deposited NiO(10 min) film following the 1000th and 10000th cycles. At 550 nm, the transmittance of the "bleached" state was 93.5 and 88.7% respectively, after the 1000th and 10000th cycles. The transmittance of the "colored" state was 49.3 and 47.6%, respectively, after the 1000th and 10000th cycles. The change in transmittance between the 1000th ($\Delta\%T$ = 44.2%) and 10000th ($\Delta\%T$ = 41.1%) cycle was minimal, indicating good adherence of the film and consistent color-switching properties. This shows that the NiO film deposited by AACVD is stable and suitable for electrochromic window applications. By way of comparison, in our laboratory, we have prepared NiO films by electrodeposition and on electrochromic
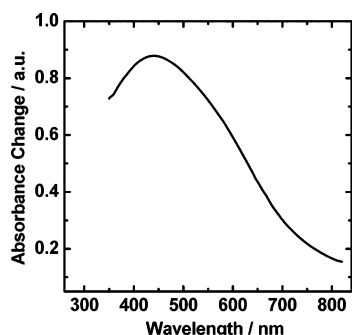
Figure 11. Change in absorbance of NiO(20 min) film recorded at cycle 500 in the wavelength range of 350−820 nm.
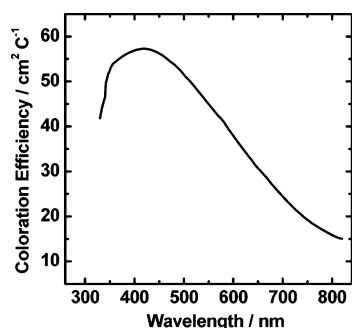

Figure 12. Coloration efficiency of NiO(15 min) film recorded at cycle 100 in the wavelength range of 330−820 nm.
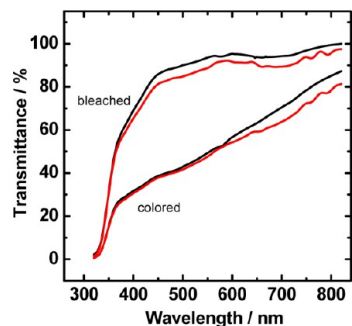

Figure 13. Visible region in situ transmission spectra for a NiO(10 min) film following the 1000th (black) and 10000th (red) CV in the "bleached" and colored states recorded in the wavelength range of 320−820 nm in aqueous KOH (0.1 mol dm^{-3}). The film had been cycled for 1000 and 10000 cycles (−0.50 → +0.70 → −0.50 V vs SCE) at 50 mV s^{-1}.

Table 2. Chromaticity Coordinates (CIE 1931%Y$_L$xy and CIELAB $L*a*b*$) for each of the NiO/NiOOH Films on FTO/Glass^a

original film source	x	y	%Y$_L$	$L*$	$a*$	$b*$
NiO(10 min) "bleached"	0.347	0.362	86.7	95	0	8
NiO(10 min) colored	**0.392**	**0.377**	**32.3**	**64**	**10**	**17**
NiO(15 min) "bleached"	0.361	0.376	77.1	90	1	16
NiO(15 min) colored	**0.420**	**0.391**	**21.3**	**53**	**12**	**23**
NiO(20 min) "bleached"	0.374	0.386	69.5	87	2	21
NiO(20 min) colored	**0.447**	**0.397**	**13.9**	**44**	**15**	**25**

^{a}Films were switched in aqueous KOH (0.1 mol dm^{-3}) between the "bleached" and colored states by application of potential steps (0.00 V → +0.50 V for 10 s and +0.50 V → −0.20 V for 10 s) vs silver wire.

Figure 14. (a) CIE 1931 xy chromaticity plots for each of the NiO/NiOOH films on FTO/glass. Films were switched in aqueous KOH (0.1 mol dm^{-3}) between the "bleached" and colored states by application of potential steps (0.00 V → +0.50 V for 10 s and +0.5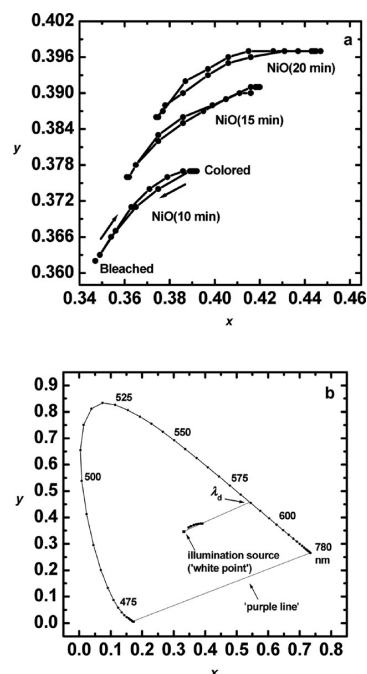0 V → −0.20 V for 10 s) vs silver wire. The arrows indicate the direction of the changes with the potential. (b) CIE 1931 xy coordinates for the NiO/NiOOH film on FTO/glass prepared from the as-deposited NiO(10 min). This Figure shows the locus coordinates, with labeled hue wavelengths, and the evaluation of the dominant wavelength (λ_d = 584 nm)) of the deep brown state.

switching we found the change in transmittance, $\Delta\%T$, to decrease from 84.8 to 56.0%, after just 50 electrochromic cycles.

Color Measurement of the NiO-Based Thin Films. Table 2 gives CIE 1931%Y$_L$xy and CIELAB $L*a*b*$ chromaticity coordinates for the various films as calculated from visible region absorbance spectra (such as Figure 10a, b).

Figure 14a shows the dynamic changes of the CIE 1931 xy coordinates as a hue and saturation track, on potential stepping between the "bleached" and colored states, as a function of the deposition time of the original NiO films.

At the initial applied potential (0.00 V), the "bleached" films appear by eye as transmissive light green. With an increase in film thickness, the x, y, and %Y$_L$ coordinates (Table 2) depart from those of the illumination source (the "white point", where

x = 0.332, y = 0.347, and %Y$_L$ = 100), as the light green color becomes slightly more intense. On stepping the applied potential to +0.50 V, films steadily turn to deep brown, with an increase in the x and y coordinates, and decrease in the luminance (%Y$_L$) (Table 2 and Figure 14a). In Figure 14b, the xy data for films prepared from as-deposited NiO(10 min) are overlaid onto the CIE 1931 color space template, showing the track of the xy coordinates between the "bleached" and colored states. In this representation, the line surrounding the horseshoe shaped area is called the spectral locus, giving the visible-light wavelength. The most saturated colors lie along the spectral locus. The line connecting the longest and shortest wavelength contains the nonspectral purples and is known as the purple line. Surrounded by the spectral locus and the purple

5680

dx.doi.org/10.1021/am401025v | ACS Appl. Mater. Interfaces 2013, 5, 5675−5682

line is the region known as the color locus, which contains every color that can exist. The location of any point in the *xy* diagram gives the hue and saturation of the color. The hue may be determined by drawing a straight line from the white point, through the point of interest to the spectral locus, thus obtaining the dominant wavelength (λ_d). The construction in Figure 14b gives an estimated value of 584 nm for colored (deep brown) state of the film prepared from as-deposited NiO(10 min). There is a small increase in λ_d values with increase in deposition time, with values being 585 and 587 nm for films prepared from NiO(15 min) and NiO(20 min), respectively.

In CIE theory, colors cannot be specifically associated with a given pair of *xy* coordinates, because the third dimension of color, lightness, is not included in the diagram. The relative lightness or darkness of a color is very important in how it is perceived, and is presented as the relative or percentage luminance, Y_L, of the sample, to that of the background, Y_o. Relative luminance values can range from 100% for white/transparent samples (no light absorbed) to zero for samples that absorb all the light. Figure 15 shows the graphical form of
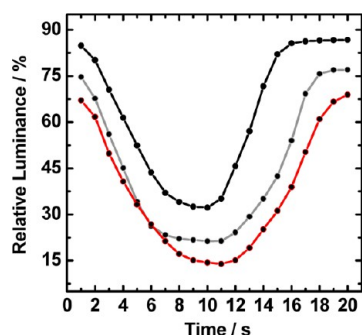

Figure 15. CIE 1931 relative luminance data vs time for each of the NiO/NiOOH films on FTO/glass. The films were prepared from the original as-deposited NiO films as indicated: NiO(10 min) (black), NiO(15 min) (gray), and NiO(20 min) (red). Films were switched in aqueous KOH (0.1 mol dm^{-3}) between the "bleached" and colored states by application of potential steps (0.00 V → +0.50 V for 10 s and +0.50 V → −0.20 V for 10 s) vs silver wire.

the changes in the %Y_L on potential switching between the "bleached" and colored state for all the NiO-based films. When the films are oxidized, the luminance dramatically decreases, as the deep brown color forms and steadily becomes more saturated.

The CIELAB *L*a*b** coordinates (Table 2) are a uniform color space defined by CIE in 1976 and offer a standard commonly used in the paint, plastic and textile industries. *L** is the lightness variable of the sample, while *a** and *b** correspond to the two antagonistic chromatic processes (red-green and yellow-blue). In a *L*a*b** chromatic diagram, +*a** is the red direction, −*a** is the green direction, +*b** is the yellow direction, and −*b** is the blue direction. The center (0, 0) of the chromaticity diagram is achromatic. As the *a** and *b** values increase, the saturation of the color increases. At the initial 0.00 V applied potential, the "bleached" state (*L** = 95, *a** = 0, *b** = 8) prepared from as-deposited NiO(10 min) is close to the achromatic "white point" (*L** = 100, *a** = 0, *b** = 0). For thicker films, there is a small decrease in the initial *L** value, and an increase in *a** and *b** (Table 2). As the potential is stepped to +0.50 V, *L** decreases and the saturation of the

brown color increases, both *a** and *b** values becoming more positive (Table 2). With increase in film thickness, the brown coloration becomes more saturated as quantified by a decrease in *L** when in its colored state and an increase in *a** and *b** (Table 2). Although it might be expected that a combination of positive *a** and *b** values would produce orange, in combination with low *L** values, the films are perceived as deep brown.

CONCLUSIONS

Aerosol-assisted chemical vapor deposition (AACVD) has been used for the first time to prepare thin films of NiO on FTO-coated glass. Following transfer to aqueous KOH (0.1 mol dm^{-3}) and conditioning oxidative voltammetric cycling, the films show good electrochromic properties with reversible switching between transmissive light green and deep brown states. Using a calculation method based on the integration of experimental spectral power distributions derived from in situ visible region spectra over the CIE 1931 color-matching functions, the color stimuli of the NiO-based films, and the changes that take place on reversibly switching between the "bleached" and colored forms have been calculated.

ASSOCIATED CONTENT

Ⓢ Supporting Information
EDS analysis, optical absorption spectra, an additional SEM image, and current−time transients are available. This material is available free of charge via the Internet at http://pubs.acs.org.

AUTHOR INFORMATION

Corresponding Author
*E-mail: r.j.mortimer@lboro.ac.uk.
Notes
The authors declare no competing financial interest.

ACKNOWLEDGMENTS

REFERENCES
(1) Monk, P. M. S.; Mortimer, R. J.; Rosseinsky, D. R. *Electrochromism and Electrochromic Devices*; Cambridge University Press: Cambridge, U.K., 2007.
(2) Mortimer, R. J. *Annu. Rev. Mater. Res.* **2011**, *41*, 241−268.
(3) Baetens, R.; Jelle, B. P.; Gustavsen, A. *Sol. Energy Mater. Sol. Cells* **2010**, *94*, 87−105.
(4) Byker, H. J. *Single-compartment, self-erasing, solution-phase electrochromic devices, solution for use therein and uses thereof.* U.S. Patent 4 902 108, 1990.
(5) Niklasson, G. A.; Granqvist, C. G. *J. Mater. Chem.* **2007**, *17*, 127−156.
(6) Nagai, J.; McMeeking, G. D.; Saitoh, Y. *Sol. Energy Mater. Sol. Cells* **1999**, *56*, 309−319.
(7) Zelazowska, E.; Rysiakiewicz-Pasek, E. *J. Non-Cryst. Solids* **2008**, *354*, 4500−4505.
(8) Xu, Y. Z.; Qiu, M. Q.; Qiu, S. C.; Dai, J.; Cao, G. J.; He, H. H.; Wang, J. Y. *Sol. Energy Mater. Sol. Cells* **1997**, *45*, 105−113.
(9) Yueyan, S.; Zhiyang, Z.; Xiaoji, Y. *Sol. Energy Mater. Sol. Cells* **2002**, *71*, 51−59.
(10) Conell, R. S.; Corrigan, D. A.; Powell, B. R. *Sol. Energy Mater. Sol. Cells* **1992**, *25*, 301−313.

5681

dx.doi.org/10.1021/am401025v | *ACS Appl. Mater. Interfaces* 2013, 5, 5675−5682

(11) Agrawal, A.; Habibi, H. R.; Agrawal, R. K.; Cronin, J. P.; Roberts, D. M.; Caron-Papowich, R.; Lampert, C. M. *Thin Solid Films* **1992**, *221*, 239−253.

(12) Scarminio, J.; Urbano, B.; Gardes, J.; Gorenstein, A. *J. Mater. Sci. Lett.* **1992**, *11*, 562−563.

(13) Carpenter, M. K.; Conell, R. S.; Corrigan, D. A. *Sol. Energy Mater.* **1987**, *16*, 333−346.

(14) Yuan, Y. F.; Xia, X. H.; Wu, J. B.; Chen, Y. B.; Yang, J. L.; Guo, S. Y. *Electrochim. Acta* **2011**, *56*, 1208−1212.

(15) Sharma, P. K.; Fantini, M. C. A.; Gorenstein, A. *Solid State Ionics* **1998**, *113−115*, 457−463.

(16) Dalavi, D. S.; Devan, R. S.; Patil, R. S.; Ma, Y.-R.; Patil, P. S. *Mater. Lett.* **2013**, *90*, 60−63.

(17) Dalavi, D. S.; Suryavanshi, M. J.; Patil, D. S.; Mali, S. S.; Moholkar, A. V.; Kalagi, S. S.; Vanalkar, S. A.; Kang, S. R.; Kim, J. H.; Patil, P. S. *Appl. Surf. Sci.* **2011**, *257*, 2647−2656.

(18) Zhang, E.; Tang, Y.; Zhang, Y.; Guo, C.; Yang, L. *Mater. Res. Bull.* **2009**, *44*, 1765−1770.

(19) Dalavi, D. S.; Devan, R. S.; Patil, R. S.; Ma, Y.-R.; Kang, M.-G.; Kim, J.-H.; Patil, P. S. *J. Mater. Chem. A* **2013**, *1*, 1035−1039.

(20) Patil, R. A.; Devan, R. S.; Lin, J.-H.; Ma, Y.-R.; Patil, P. S.; Liou, Y. *Sol. Energy Mater. Sol. Cells* **2013**, *112*, 91−96.

(21) Maruyama, T.; Arai, S. *Sol. Energy Mater. Sol. Cells* **1993**, *30*, 257−262.

(22) Hou, X.; Choy, K. L. *Chem. Vap. Deposition* **2006**, *12*, 583−596.

(23) Choy, K. L. *Prog. Mater. Sci.* **2003**, *48*, 57−170.

(24) Tahir, A. A.; Ehsan, M. A.; Mazhar, M.; Wijayantha, K. G. U.; Zeller, M.; Hunter, A. D. *Chem. Mater.* **2010**, *22*, 5084−5092.

(25) Dharmadasa, R.; Tahir, A. A.; Wijayantha, K. G. U. *J. Am. Ceram. Soc.* **2011**, *94*, 3540−3546.

(26) Tahir, A. A.; Wijayantha, K. G. U. *J. Photochem. Photobiol., A* **2010**, *216*, 119−125.

(27) Bloor, L. G.; Manzi, J.; Binions, R.; Parkin, I. P.; Pugh, D.; Afonja, A.; Blackman, C. S.; Sathasivam, S.; Carmalt, C. J. *Chem. Mater.* **2012**, *24*, 2864−2871.

(28) Wyszecki, G.; Stiles, W. S. *Color Science: Concepts and Methods, Quantitative Data and Formulae*, 2nd ed.; John Wiley and Sons: New York, 1982.

(29) Mortimer, R. J.; Varley, T. S. *Displays* **2011**, *32*, 35−44.

(30) *CIE Technical Report: Colorimetry*, 3rd ed.; Commission Internationale De l'Eclairage: Vienna, Austria, 2004.

(31) Kawar, R. K.; Chigare, P. S.; Patil, P. S. *Appl. Surf. Sci.* **2003**, *206*, 90−101.

(32) Patil, P. S.; Kadan, L. D. *Appl. Surf. Sci.* **2002**, *199*, 211−221.

(33) Garcia-Miquel, J. L; Zhang, Q.; Allen, S. J.; Rougier, A.; Blyr, A.; Davies, H. O.; Jones, A. C.; Leedham, T. J.; Williams, P. A.; Impey, S. A. *Thin Solid Films* **2003**, *424*, 165−170.

(34) Bouessay, I.; Rougier, A.; Beaudoin, B.; Leriche, J. B. *Appl. Surf. Sci.* **2002**, *186*, 490−495.

(35) Bouessay, I.; Rougier, A.; Tarascon, J.-M. *J. Electrochem. Soc.* **2004**, *151*, H145−H152.

(36) Bouessay, I.; Rougier, A.; Poizot, P.; Moscovici, J.; Michalowicz, A.; Tarascon, J.-M. *Electrochim. Acta* **2005**, *50*, 3737−3745.

(37) Huang, H.; Tian, J.; Zhang, W. K.; Gan, Y. P.; Tao, X. Y.; Xia, X. H.; Tu, J. P. *Electrochim. Acta* **2011**, *56*, 4281−4286.

(38) Lampert, C. M.; Omstead, T. R.; Yu, P. C. *Sol. Energy Mater.* **1986**, *14*, 161−174.

(39) Xia, X. H.; Tu, J. P.; Zhang, J.; Wang, X. L.; Zhang, W. K.; Huang, H. *Sol. Energy Mater. Sol. Cells* **2008**, *92*, 628−633.

(40) Arakaki, J.; Reyes, R.; Horn, M.; Estrada, W. *Sol. Energy Mater. Sol. Cells* **1995**, *37*, 33−41.

(41) Velevska, J.; Ristova, M. *Sol. Energy Mater. Sol. Cells* **2002**, *73*, 131−139.

■ NOTE ADDED AFTER ASAP PUBLICATION

This paper was published on the Web on June 10, 2013. Additional text corrections were implemented throughout the paper, and Figure 1 was revised. The corrected version was reposted on June 12, 2013.